Characterization of lasers based on self-organized In(Ga)As quantum dots

von

Dipl.-Phys. Dongxun Ouyang

aus Dongzhi, Anhui, China

Von der Fakultät II – Mathematik- und Naturwissenschaften

der Technischen Universität Berlin

zur Verleihung des akademischen Grades

Doktor der Naturwissenschaften

- Dr. rer. nat. -

Genehmigte Dissertation

Berichter:

Prof. Dr. D .Bimberg

Prof. Dr. N. N. Ledentsov

Vorsitzender:

Prof. Dr. D. Zimmermann

Tag der wissenschaftlichen Aussprache:

22.12.2003

Berlin 2003

D 83

ABSTRACT

In this thesis work, we characterize lasers based on self-organized In(Ga)As quantum dots (QDs). Intrinsic static and dynamic lasing properties of QD lasers are surveyed in high performance devices with a variety of device geometry, cavity loss and QD gain system.

At first, the carrier and gain processes are analyzed that affect the temperature dependence of QD lasers. The characteristic temperature and spectral characteristics are correlated in the analysis to pin down the major processes that determine various temperature dependent behaviors in different temperature ranges and in devices with varied cavity losses. The laser design strategy for extended temperature stability in QD lasers are addressed.

In the next, the waveguide effects in QD lasers are investigated. The spectral hole burning effects due to the cavity resonances modes are found to be responsible for the spectral intensity modulations in ridge waveguide QD lasers. High performance narrow stripe QD lasers with deep etched through waveguide are demonstrated. These results indicate that laser waveguide design is critical for both spectral and spatial mode control in QD lasers, and novel design elements can be incorporated in the active region without incurring deleterious effects to the laser performance, due to the strong carrier localization effect in QDs. Potentially a variety of QD devices can be realized in a cost-effective way by using novel fabrication techniques that are not suitable for the devices with conventional gain media.

The spectral dynamics of QD lasers are surveyed in a wide range of devices with different QD systems and at various temperatures. Antiphase mode dynamics feature all the investigated QD lasers, no matter if the mode spectrum is modulated by the waveguide effect and in both single- and multi-longitudinal-mode cases. Other than the vanishing mode oscillation amplitude in the quantum well lasers with current, the QD lasers show persistent strong oscillation intensity and are characterized by the frequency damping effects. Both stable and chaotic mode oscillation regimes are observed without changing the former oscillation frequency and amplitude characteristics. These spectral dynamic features are related to the mode cross-saturation mechanism in Fabry-Perot lasers, i.e. the

dynamic grating effect, and the QD carrier and gain dynamic properties, particularly the gain nonlinearity and various gain suppression mechanisms in QD gain.

For the dominance of multi-stacked QD gains, the basic lasing properties are characterized for the multi-stacked QD lasers. The effects of multiple dot layers and bimodal dot distributions on the temperature dependence are addressed. For multi-stacked QD lasers, the low temperature lasing properties are strongly affected by the carrier transport effect. The peculiar spectral features are surveyed with respect to a variety of device parameters and are attributed to the gain inhomogeneity as induced by the bottlenecked carrier transport across the multiple dot layers. The time-resolved study helps reveal the underlying laser dynamics. Self-organization processes in this specific laser system are analyzed to reproduce the dynamics. The transient lasing characteristics of narrow stripe gain-guided QD lasers are also investigated concerning the dynamic instability processes. The transient junction heating and the lateral spatial hole burning are found to be critical for the triggering of destabilization processes.

Finally the emission properties of four-sided QD lasers are studied. The mode properties specific to these near-square-shaped laser cavities are analyzed. The lasing characteristics are related to the different lasing mechanisms for both the total-internal-reflection modes and the leaky modes. The selection mechanisms for spectral and azimuthal modes are addressed, and the results of ray optical analysis support the corner diffraction loss as the major factor that determines the azimuthal mode structure.

Publication list:

Long-wavelength (1.3-1.5 μm) quantum dot lasers based on GaAs
A. R. Kovsh, N. N. Ledentsov, A. E. Zhukov, D. A. Livshits, N. A. Maleev, M. V. Maximov, V. M. Ustinov, J.-S. Wang, J. Y. Chi, D. Ouyang and D. Bimberg
Photonics West, LASE 2004, Proceedings of SPIE, vol. 5349, (2004). (invited).

Dynamics of a semiconductor quantum dot lasers
D. Ouyang, E. A. Viktorov, D. Bimberg, N. N. Ledentsov, and P. Mandel
Submitted to Phys. Rev. Lett., December 2003

Impact of the Mesa Etching Profiles on the Spectral Hole Burning Effects in Quantum-Dot Lasers
D. Ouyang, N. N. Ledentsov, R. L. Sellin, I. N. Kaiander, F. Hopfer and D. Bimberg
Submitted to Semicond. Sci. Technol. (Letter to the Editor), October 2003

High performance narrow stripe quantum-dot lasers with etched waveguide
D. Ouyang, N. N. Ledentsov, D. Bimberg, A. R. Kovsh, A. E. Zhukov, S. S. Mikhrin and V. M. Ustinov
Semicond. Sci. Technol. 18, L53-L54, December 2003

Self-induced transparency in InGaAs quantum-dot waveguides
S. Schneider, P. Borri, W. Langbein, U. Woggon, J. Förstner, A. Knorr, R. L. Sellin, D. Ouyang, and D. Bimberg
Appl. Phys. Lett. 83 (18), 3668 (2003)

Unique Properties of Quantum Dot Lasers (Invited)
N. N. Ledentsov, A. R. Kovsh, D. Ouyang, A. E. Zhukov, V. M. Ustinov, M. V. Maximov, Yu. M. Shernyakov, N. V. Kryzhanovskaya, I. N. Kaiander, R. Sellin and D. Bimberg
in IEEE-NANO 2003 Technical Program, WK: Nano-optics, Nano-optoelectronics and Nanophotonics II.

Temperature dependent homogeneous broadening and gain recovery dynamics in InGaAs quantum dots
P. Borri, W. Langbein, S. Schneider, U. Woggon, R. L. Sellin, D. Ouyang, D. Bimberg
SPIE Proceedings of the 10th International Symposium on Nanostructures: Physics and Technology vol. 5023 p. 334 (2003) (invited).

Alternative-precursor metalorganic chemical vapor deposition of self-organized InGaAs/GaAs quantum dots and quantum-dot lasers
R. L. Sellin, I. Kaiander, D. Ouyang, T. Kettler, U. W. Pohl, D. Bimberg, N. D. Zakharov, and P. Werner
Appl. Phys. Lett. **82** (6), 841 (2003)

Dephasing of biexcitons in InGaAs quantum dots
P. Borri, W. Langbein, S. Schneider, U. Woggon, R. L. Sellin, D. Ouyang, and D. Bimberg
Phys. stat. sol. (b) 238, 593 (2003). (invited)

Self-induced transparency in InGaAs quantum dot waveguides
S. Schneider, P. Borri, W. Langbein, U. Woggon, J. Förstner, A. Knorr, R. L. Sellin, D. Ouyang, D. Bimberg
Phys. stat. sol. (b) 238, to appear (2003).

Relaxation and dephasing of multiexcitons in electrically-pumped quantum dots
P. Borri, W. Langbein, S. Schneider, U. Woggon, R. L. Sellin, D. Ouyang, D. Bimberg
in Quantum Electronics and Laser Science Conference, QELS'2003, 2003 OSA Technical Digest.

Linewidth enhancement factor in InGaAs quantum-dot amplifiers
S. Schneider, P. Borri, W. Langbein, U. Woggon, R. L. Sellin, D. Ouyang, D. Bimberg
in Conference on Lasers and Electro Optics CLEO'2003, 2003 OSA Technical Digest.

Optical Rabi Oscillations in an InGaAs Quantum Dot Ensemble
W. Langbein, P. Borri, S. Schneider, U. Woggon, R. L. Sellin, D. Ouyang, D. Bimberg
in Quantum information processing in condensed media I, (DPG Spring conference, Dresden, 2003) SYQI 1.2.

Exciton Dephasing in InGaAs Quantum Dots
P. Borri, W. Langbein, S. Schneider, U. Woggon, R. L. Sellin, D. Ouyang, D. Bimberg
in Quantum Decoherence in Solid State Physics II, (DPG Spring conference, Dresden, 2003) SYQD 2.4.

Lateral-cavity spectral hole burning in quantum-dot lasers
D. Ouyang, R. Heitz, N. N. Ledentsov, S. Bognár, R. L. Sellin, Ch. Ribbat, and D. Bimberg
Appl. Phys. Lett. 81 (9), 1546-1548 (2002)

Rabi oscillations in the excitonic ground-state transition of InGaAs quantum dots
P. Borri, W. Langbein, S. Schneider, U. Woggon, R. L. Sellin, D. Ouyang, D. Bimberg
Phys. Rev. B. 66, 081306 (R) (2002).

Exciton relaxation and dephasing in quantum-dot amplifiers from room to cryogenic temperature
P. Borri, W. Langbein, S. Schneider, U. Woggon, R. L. Sellin, D. Ouyang, D. Bimberg
IEEE J. Sel. Topics Quan. Electron. 8, 984-991 (2002).

Relaxation and dephasing of multiexcitons in semiconductor quantum dots
P. Borri, W. Langbein, S. Schneider, U. Woggon, R. L. Sellin, D. Ouyang, D. Bimberg
Phys. Rev. Lett. 89, 187401 (2002).

Ultrafast processes in quantum dot devices
P. Borri, W. Langbein, S. Schneider, U. Woggon, R. L. Sellin, D. Ouyang, D. Bimberg
Proceedings of the 14th Indium Phosphide and Related Materials Conference IPRM'02, IEEE Catalog 02CH37307 p. 59 (invited).

Dephasing Processes in InGaAs Quantum Dots
P. Borri, W. Langbein, S. Schneider, U. Woggon, R. L. Sellin, D. Ouyang, D. Bimberg
Proceedings of the 26th International Conference on the Physics of Semiconductors (Institute of Physics Publishing, 2002) p. 205 (invited).

Temperature Dependent Time-Resolved Four-Wave Mixing in InGaAs Quantum Dots
P. Borri, W. Langbein, S. Schneider, U. Woggon, R. L. Sellin, D. Ouyang, D. Bimberg
Phys. stat. sol. (a) 190, 517 (2002).

Non-Lorentzian homogeneous lineshape in semiconductor quantum dots
W. Langbein, P. Borri, S. Schneider, B. Patton, U. Woggon, R. L. Sellin, D. Ouyang, D. Bimberg, K. Leonardi and D. Hommel
Quantum Electronics and Laser Science Conference QELS´2002, 2002 OSA Technical Digest, QWD5 p. 159.

Rabi oscillations of the excitonic ground-state transition in InGaAs quantum dots
P. Borri, W. Langbein, S. Schneider, U. Woggon, R. L. Sellin, D. Ouyang, D. Bimberg
Proceedings of the 26th International Conference on the Physics of Semiconductors (Institute of Physics Publishing, 2002).

Ultraschnelle Ladungsträgerdynamik in InGaAs Quantenpunktverstärkern
S. Schneider, P. Borri, W. Langbein, U. Woggon, R. L. Sellin, D. Ouyang, D. Bimberg
in Ultrakurzzeitphänomene I, (DPG Spring conference, Regensburg, 2002) HL 24.1.

Coherent Light-Matter Interaction in InGaAs Quantum Dots: Dephasing Time and Optical Rabi Oscillations
P. Borri, W. Langbein, S. Schneider, U. Woggon, R. L. Sellin, D. Ouyang, D. Bimberg
Phys. stat. sol. (b) 233, 391 (2002).

Ultralong dephasing time in InGaAs quantum dots
P. Borri, W. Langbein, S. Schneider, U. Woggon, R. L. Sellin, D. Ouyang, D. Bimberg
Phys. Rev. Lett. 87, 157401 (2001).

Ultrafast carrier dynamics and dephasing in InAs quantum dot amplifiers emitting near 1.3 μm-wavelength at room temperature
P. Borri, S. Schneider, W. Langbein, U. Woggon, A. E. Zhukov, V. M. Ustinov, N. N. Ledentsov, Zh. I. Alferov, D. Ouyang, D. Bimberg
Appl. Phys. Lett. 79, 2633 (2001).

Quantum dots for ultrafast amplifiers
P. Borri, S. Schneider, W. Langbein, U. Woggon, R. L. Sellin, D. Ouyang, F. Heinrichsdorff, M.-H. Mao, D. Bimberg and J. M. Hvam (invited)
in Integrated Photonics Research, OSA Technical Digest (Optical Society of America, Washington DC, 2001), IMF1.

Ultrafast gain dynamics and dephasing times in quantum-dot amplifiers from room to cryogenic temperature
P. Borri, W. Langbein, S. Schneider, U. Woggon, R. L. Sellin, D. Ouyang, D. Bimberg
Alaska Meeting on Fundamental Optical Processes in Semiconductors AMFOPS'01, (August 5-10 Alaska 2001) (invited) Abstract Book.

TABLE OF CONTENTS

5. Carrier transport effects in MQD lasers

6. Four-sided lasers

Acknowledgement

Biography

CHAPTER 0 INTRODUCTION

Contents:

0.1 Brief history of semiconductor quantum dot lasers

Since the first reports of working semiconductor lasers in 1962 by almost simultaneously 4 groups in USA,[1-4] the physics and device concepts of semiconductor lasers[5,6] has been continually innovated. Up to the second millennium in the human history, the semiconductor laser development has reached the climax in its short history, as highlighted by the advancement in quantum dot (QD) lasers[7] and the Noble prize for physics in the year 2000 for two pioneers in the area of semiconductor heterostructure devices.

The first generation of semiconductor laser are based on degenerately doped p+-n+ homojunction.[8] These devices are characteristic of high current density and low temperature operation, and remain only a curiosity in the laboratory. The introduction of heterostructures in the laser waveguide leads to the second generation of semiconductor lasers.[9-12] The double-heterostructure (DHS) laser has reduced current density and its continuous-wave operation at RT signals the beginning of practical application of semiconductor lasers. Since the introduction of DHS laser, the active region has changed from bulk to thin layer, in order to reduce further the current density and internal loss. In the separate-confinement laser waveguide, the carrier and optical confinement is decoupled, greatly facilitating the optimization of laser performance. Finally comes the third generation of semiconductor lasers, which are characterized by the use of semiconductor quantum heterostructures in the active region. Quantum well (QW) lasers seem to be a natural extension of the DHS laser with thin active layers. But the quantum size effect brings QW lasers significant advantage and potentials, compared to the conventional lasers.

The envision of semiconductor QW lasers could be traced to the patent[13] of Dingle and Henry, in which they proposed that size quantization effects, resulting in a strong

modification of the density of states (DOS), are very advantageous when used for the active media of semiconductor lasers, as they allow suppression of the states at high energies. These states are responsible for degradation of the device performance at high temperatures, as the carriers effectively populate high energy states with temperature increase, reducing the population of the near-band-edge states that are responsible for lasing. Moreover, in size-quantized heterostructures also the DOS at the band edge is strongly increased. This makes it possible to realize high performance lasers with high gain/differential gain, extremely low threshold current density, high slope efficiency and high modulation speed. The successful development of QW lasers[14] prove the concept of size quantization. To date, high performances QW lasers dominate the semiconductor laser market.

However, the transition from the bulk DHS lasers to the QW lasers is the first step in the application of size quantization concept to semiconductor heterostructure lasers. As was stressed by Dingle and Henry, size quantization in more than one direction would cause a singularity in the DOS near the band edge. The advantage of using 1- or 0-dimention quantum structures, i.e. quantum wires and QDs as laser media over the QWs was analyzed in the 80´s,[15,16] and it is predicted that compared to the bulk and QW lasers, the QD lasers could have further reduced transparency current, increased material gain and differential gain, high temperature stability, and last but not the least, decreased line enhancement factor and frequency chirp. The QD lasers represent an ultimate case of application of size quantization concept to semiconductor heterostructure lasers.

The predicted superior laser performance stimulated many courageous efforts towards the device realization of a QD laser. With a QW laser subject to a perpendicularly oriented strong magnetic field, the 2D carriers confined in the QW layer can be further localized, that mimics the 3D quantum confinement in ideal QDs. This experiment demonstrates clearly the improved temperature stability of threshold current density,[15] testifying a principal aspect of the potentials of the QD lasers. To fabricate the QDs for integration into the semiconductor heterostructure lasers, the QW structures are patterned in the lithographical process.[17] Artificially very high density and regular array of etched QDs can be obtained with the only limitation set by the precision of the lithography and etching processes. However, the performances of these etched QD lasers are inevitably frustrated by large scattering losses and defect/surface-related nonradiative recombination, as introduced by the specific fabrication methods. The threshold current density kept high

above 7.5 kA/cm^2 (77K, pulsed operation),[18] and there is little hope to reduce it further without a dramatic improvement in the existing technological routine. Albeit the genuine QDs are still not in scene that can be integrated in the semiconductor heterostructure lasers, researches on the electronic and optical properties of semiconductor nanostructures start to take off. Semiconductor nanocrystals are intensively studied with respect to their exciton gain mechanisms.[19] The seminar work by Zrenner et al[20] on the exciton localization by interface fluctuations in the QW eventually turned over the case, and lit the interests on "QD heterostructure" study particularly.

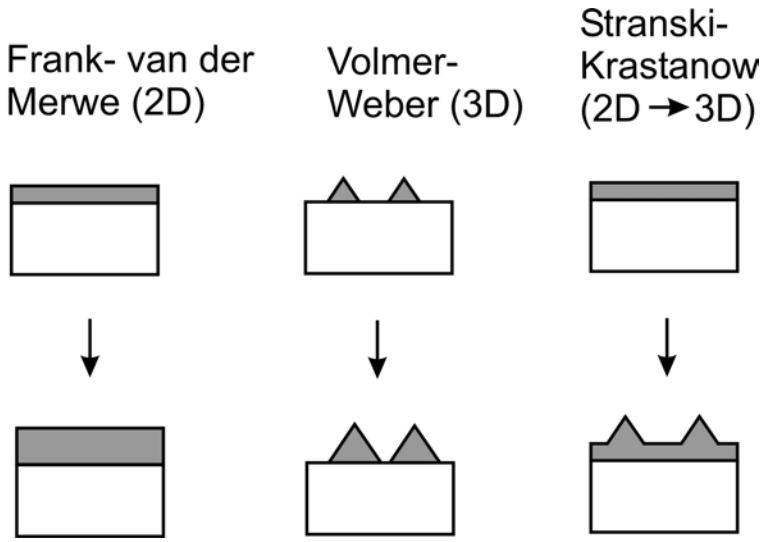

Fig. 0-1 Various epitaxi growth modes on semiconductor crystal surfaces.

In the meantime, epitaxial growth of coherent semiconductor nanostructures is becoming possible owing to the remarkable progress in the understanding of universal phenomena of self-organization of epitaxial nanostructures on semiconductor crystal surfaces.[7,21] Principally there are three possible growth modes, as shown in Fig. 0-1. In Frank-van der Merwe mode, the substrate surface energy γ_1 is larger than the sum of the epilayer surface energy γ_2 and the interface energy γ_{12}, so only the thin film can be formed. In Volmer-Weber mode, $\gamma_1 < \gamma_2 + \gamma_{12}$, and 3D islands can be formed. In comparison, the Stranski-Krastanow (S-K) mode is a rather special growth mode. With the deposition of layer above the critical thickness, the thick layer can self organize into the array of 3D islands that are seated on a thin wetting layer. The S-K growth mode requires stringent control of growth conditions, so generally only a small growth window in parameters is available. But it can be implemented in the otherwise deleterious lattice-mismatched material system, like InGaAs/GaAs, to grow QD heterostructures. This bottom-up approach takes advantage of self-organization formation of 3D islands, and the relaxation of strain energy in the

small islands can help reduce greatly the possibility of defect formation. This is particularly advantageous for the device application. The outcome of the self-organized growth is well beyond the expectation, and the naturally formed rather regular array of pyramid- or lens-shaped islands is shown to be the genuine QDs that emit in discrete sharp luminescence lines corresponding to δ function DOS.[22] The further development of the self-organized growth technique brings about almost defect free dense arrays of In(Ga)As QDs. Based on the self-organized QDs grown by Molecular Beam Epitaxy (MBE), the first optically pumped QD laser,[23] and then the first QD injection laser are realized in 1994.[24] Large material gain and differential gain are measured in these QD lasers.[25] The later QD growth by Metalorganic Chemical Vapor Deposition (MOCVD) provides better quality, and the InGaAs capping technique is applied to improve the luminescence efficiency and tailor the QD emission wavelengths. To decouple the dot size and density control, the dot seeding approach is devised. That uses a layer of high density small dots as the seeding layer to trigger the growth of large dots of the same high density on the upper layers. Lasers based on the optimized InGaAs QDs show dramatically improved performances and RT CW operation of a MOCVD InGaAs QD laser is demonstrated.[26] In Fig. 0-2, the TEM pictures of the high quality MOCVD grown InGaAs QD array (a) and a single dot cross section (b) are shown. The dot density is about 6.3 x 10^{10} /cm^2, and the base size of the lens-shaped dot is around 30 nm. To increase the saturation gain and differential gain, multi-stacked QDs are generally required in the QD lasers. In Fig. 0-3, the cross section STM of 3 vertically coupled QDs (a) is shown, along with the cross section TEM of InGaAs/GaAs short period superlattice (b). These pictures demonstrate coherent growth of multi-stacked QDs and the spatial correlation of QDs.

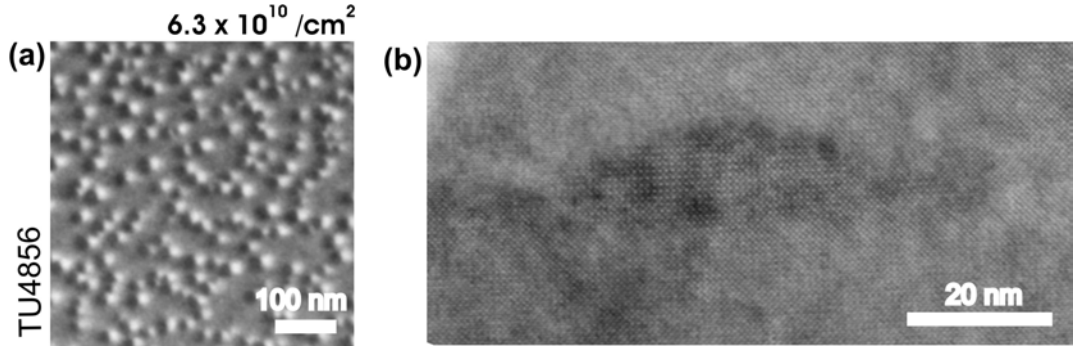

Fig. 0-2 TEM pictures of MOCVD grown InGaAs QDs. (a) plan view, (b) cross section view.

The promising results in GaAs based material system have triggered the survey of similar effects in other material systems, like InAs on Si, InP,[27] Si(Ge),[28] and GaSb[29] etc.

Particularly, it is realized that in the newly developed InGaN QW lasers[30] the exciton localization in the nanoscale fluctuations of indium content helps overcome the deleterious effect of nonradiative recombination from the high density misfit dislocations, which are currently deemed in the GaN based material system. This leads to the subsequent development of (In)GaN-based QD lasers.[31]

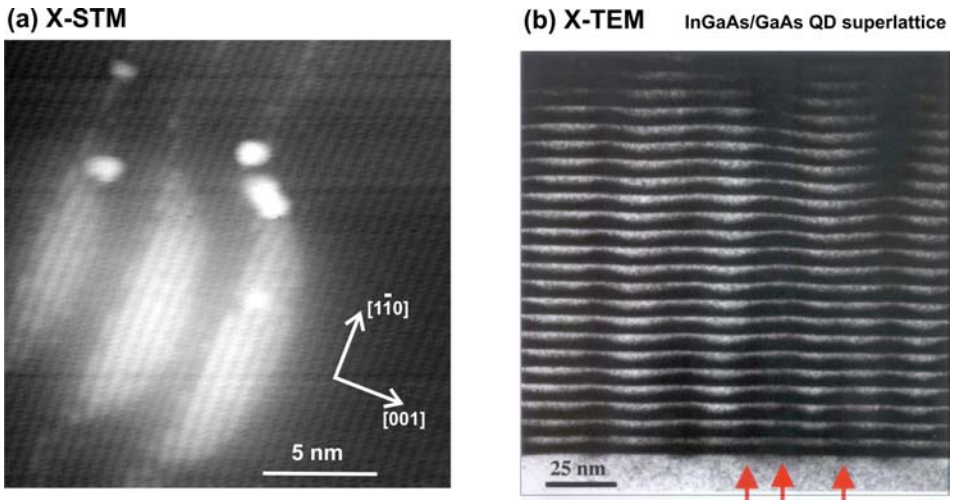

Fig. 0-3 (a) Cross section STM of 3-fold stacked InGaAs QDs with vertical correlation. (b) Cross section TEM of InGaAs/GaAs superlattice.

0.2 Recent development of QD lasers

While the original predictions of QD laser properties were based on simplified assumptions:

- infinite barriers
- ideal quantum dots of identical shape
- temperature-insensitive homogeneous broadening
- one confined electron and hole level
- bimolecular e-h-recombination
- ultrafast energy relaxation of injected carriers
- quasi-equilibrium carrier distribution
- lattice matched heterostructures and similar confinement volumes for electrons and holes

the laser properties of actual QD lasers are generally based on the more realistic assumptions:

- finite barriers
- size and shape dispersion of QDs

- many electron and hole levels and the impact of the continuum states of wetting layers and barriers
- excitonic recombination
- nonequilibrium carrier distribution
- strained heterostructures with completely different potential wells for electrons and holes

Since 1994, the overwhelming part of potential advantages of QDs has been verified on actual devices,[7,32] and new previously unexpected advantages are also demonstrated. It appears that the use of QDs in diode lasers has several decisive technological advantages:[33]

Largely extended tunability of emission wavelength by QD size and composition on a given substrate. Lasing wavelengths from 1.3 – 1.6 μm, important for telecom and free-space applications, can be realized on GaAs substrates.[34]

- Very low threshold current densities (< 6 A/cm^2 per dot layer) and, simultaneously, very low internal losses (~1-3 cm^{-1}) and high quantum efficiencies (~100%) are demonstrated.

- Carrier confinement in narrow gap QDs placed in a wide gap matrix can prevent nonequilibrium carrier spreading and nonradiative recombination. This improves radiation hardness and suppresses the facet overheating, increasing the catastrophic optical mirror damage (COMD) level for the high power lasers. The suppression of filamentation in QD lasers[35,36] will benefit the high power operation in narrow stripe lasers.

- For future metropolitan area networks the demand for cost-effective ultrafast amplifiers can exceed that of lasers. Semiconductor optical amplifiers (SOAs) are expected to play a decisive role in this area. SOAs based on self-organized In(Ga)As QDs show gain recovery times of 130 fs,[37,38] 4-7 times faster than the InGaAsP bulk and QW SOAs. Additional advantages of QD SOAs can be reduced chirp, larger saturated gain, no cross gain modulation, etc.

In addition, the GaAs-based QD lasers are conceived as the most cost-effective solutions for the massive telecommunications market, compared to the current InP-based QW lasers. This economic concern provides a strong impetus to the recent rapid development of long wavelength InAs QD lasers emitting in the 1.3 – 1.5 μm spectral range.[32,34,39]

Specifically for the growth of large sized dots emitting in 1.3 μm range, the growth technique incorporates both the Dot-in-a-well (DWELL) scheme and activated alloy phase separation.[40] As shown schematically in Fig. 0-4(a-c), at first the S-K mode is used to grow the small InAs QDs, next a thin InAlGaAs alloy QW layer is deposited above the QDs, and then the temperature is increased to activate the alloy phase separation process. In the latter process, the Indium atoms segregate to the top of QDs due to strain gradient, and the effective dot size is increased. The cross section TEM of the enlarged InAs QDs can be seen in Fig. 0-4d, along with the plan view TEM of the 1.3 μm QD array in Fig. 0-4e. These pictures demonstrate the potential in tailoring the QD size, shape and composition by advanced growth technique. This flexibility would facilitate the application of QD media in different area.

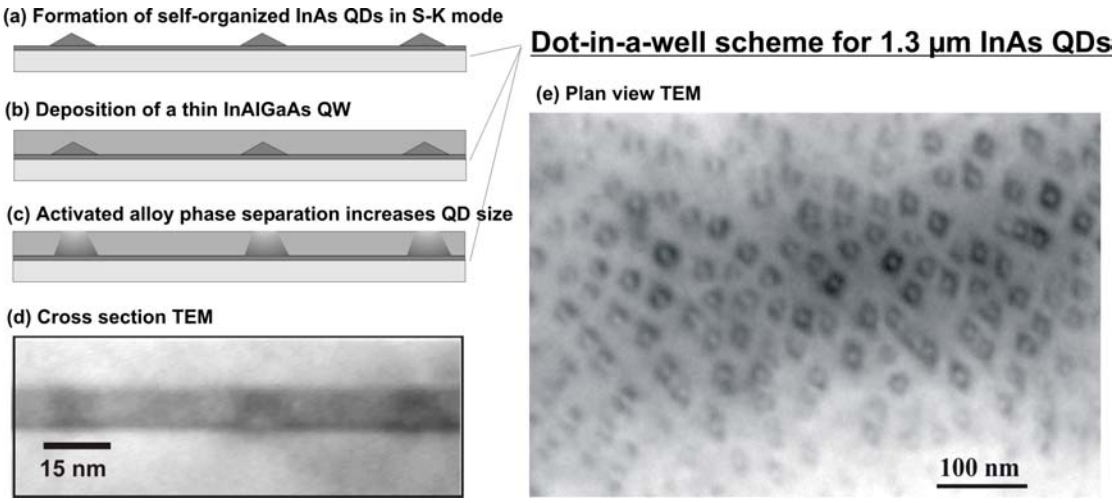

Fig. 0-4 (a-c) Schematic illustrations of DWELL and activated alloy phase separation technique. (d) and (e) TEM pictures of MBE grown 1.3 μm InAs QDs.

Besides edge emitting lasers, vertical-cavity-surface-emitting lasers (VCSEL) can benefit from the specific QD properties.[32] The reduced carrier spreading in the small aperture VCSEL can be rather advantageous for decreasing the threshold current density, improving the laser modulation properties and enhancing the lasing stability. The use of AlGaAs/GaAs Distributed Bragg reflectors (DBR) along with the InAs QDs also leads to a system advantage over that based on InP material system.[41]

QDs can be incorporated in a variety of special laser structures. The much reduced carrier diffusion length due to carrier localization in QDs allows fabricating open waveguides cost-effectively by direct etching through the active region.[42] Laterally coupled distributed feedback (DFB) laser [43-45] and ultra short edge emitting lasers with etched DBR mirrors[46]

have been realized with reasonable single mode performance. Electrically pumped InGaAs QD ring and cylindrical cavity lasers[47] could replace the QW counterpart in the gyroscopic application. Microdisk QD lasers[48-51] are important devices for exploring the strong coupling regime between the high-Q cavity modes and QDs. Optically pumped photonic crystal QD lasers[52] is also demonstrated recently, but there is still a long way to go towards the realization of the first electrically pumped thresholdless laser ever.

In the device design area, there are certain developments that are worth to note. For example, in *tunnel injection* QD lasers, the QW adjacent to the QD layer is used to inject carriers (i.e. electrons) in the dot ensemble through LO-assisted tunneling,[53] that helps eliminate the hot carrier effect and greatly enhances the modulation bandwidths.[54] In *p-type modulation doped* QD lasers, the crowded hole energy levels of QDs are intentionally filled to avoid the hole redistribution effect under temperature change or in high speed modulations. As a return, high characteristic temperature T_0 of ~ 200K (from 0°C to 80°C) is obtained in the 1.3 μm QD lasers,[55] and this approach improves the high-speed laser performance as well.[56] Above all, these innovative developments are based on the improved understanding of the laser principles in QD lasers. It is believed that new concept QD lasers may herald the development of powerful lasers that include more unprecedented design elements. Just as formulated by one of the semiconductor laser pioneers, the QD lasers and their variations will be developed in width and in depth.[57]

Accompanied by the rapid technological development, the QD lasers are also prepared to enter the commercial market. The successful development of 1.3 μm InAs QD lasers[39] in University of New Mexico, USA, has lead to a spin-off. The company, named *Zia Laser, Inc.*, was founded in Albuquerque, NM, in May 2000, aiming to develop and commercialize the long wavelength QD lasers for the communications networks market. The company's product development list includes ultra broadband QD gain blocks, ultra wide tunable external cavity QD lasers, and the recent debuted uncooled DFB lasers, among others. This signifies that, after near a decade R&D, the QD devices are beginning to erode the market occupancy of the QW ones and even prepared to take on new markets. Another company named NSC-*Nanosemiconductor GmbH*, situated in Dortmund, Germany, is recently spun out of the Ioffe Physico-Technical Institute in St Petersburg, Russia, and the solid state physics institute of Technical university of Berlin, Germany. It aims to offer semiconductor wafer nanoepitaxy services for solutions in optoelectronic and microelectronic applications. The high performance QD edge emitting and VCSEL laser

wafers head the company's portfolio. One noteworthy point is the QD laser wavelength range from 0.85 to 1.5 μm, which are all based on GaAs substrate. With the high performance QD laser wafer available in the market, it can be expected that the pace will be accelerated for the QD lasers to replace the QW lasers in the major laser market sections.

Finally it is noted that, besides the semiconductor QD heterostructure lasers, lasers based on semiconductor nanocrystals[58] are making advances as well. The synergetic effect in the development of different types of QD lasers could facilitate their implementation in widespread application areas, and help explore the advantages of QD media in distinct device configurations.

0.3 Potentials and challenges for QD lasers

In fact, the epitaxial growth of QD heterostructures has experienced great advances in the last decade, with a wide range of material systems being tested. This early stage of development gave birth to high quality, dense, coherent QD arrays applicable in a variety of devices. Owing to many newly developed material systems, QD lasers now can emit from near ultraviolet to near infrared by interband transition, and mid-infrared by intersubband transition. We have already high power laser diodes, datacom and telecom lasers and VCSELs,[59,60] all based on self-organized QDs. The QD lasers are delivering superior performance in many of the basic laser characteristics than ever before. To date, the QD lasers have proved to be advantageous all around over their QW counterpart.

However, the potentials of QD lasers are still not fully explored. The major potential of QD active media lies in the flexibility of tailoring the QD properties[40,61-63] by the adapted growth technique for the intended application. Currently, many growth techniques for the QD heterostructures have been developed, but the control on the QD size and composition dispersion is still at large. With the currently achievable dot area density ~ $10^{11}/cm^2$, the modal gain is limited to ~ 10 /cm per dot layer. The large dot dispersions, though potentially advantageous in certain application areas, mount up a waste of injected carriers in most cases, which cuts the lead that QD lasers otherwise could provide over the conventional lasers.

On the other hand, with improved dot uniformity, the saturation gain/differential gain can be enhanced, which increase the dynamic range of laser operation and the thermal stability by avoiding the gain saturation effect. High degree of spatial order in QD arrays is essential

for the realization of QD superluminescent devices, and for the exploration of novel electro-optic nonlinear effects and electromagnetic diffraction and interference effects in QD superlattices.[64] Ideal QD array is particularly attractive in optic and electronic storage,[65] for it enables massive parallel processing, and facilitates individual addressing. Moreover, the vertical stacking and electronical coupling of QDs are unique aspects worthy of exploration for engineering the QD properties.[66] The electronically coupled QD pairs are potentially useful for quantum computing,[67,68] and in spintronic devices.[69] The polarization anisotropy associated with the stacked QDs affects the performance of QD amplifiers. The electron tunneling between stacked QD layers is critical for the development of QD unipolar quantum cascade devices, which could greatly advance the performance of the quantum cascade lasers and cause widespread impact on the related technological field. Recently, the shape engineering of truncated pyramid shaped InAs QDs is shown to enhance the thermal stability.[70] Lateral coupling[71] of QDs is also intensively addressed, because it is critical for reaching long wavelength range (1.5 – 1.7 μm) based on GaAs substrate, and provides efficient carrier coupling among QDs that may help engineer the carrier thermal redistribution and gain properties.[72,73] The abovementioned potential and apparent benefits may provide a strong impetus for the advance of QD growth technique. The surging nanotechnology revolution let us in hope that these expectations are not far away from the reality in the near future.

Besides the challenge in the QD heterostructure growth area, the design, fabrication and characterization of QD devices are facing challenges as well, and they are critical for the full exploitation of the potential advantages pertaining to QD media. The multifaceted electronic and optical properties of QD gain media can bring new phenomena and effects into play, which demand novel concept to take advantage of the benign and useful aspects but meanwhile to avoid the possible deleterious side effects. Wide ranges of device configuration are usually needed to have a full characterization of particular device properties, in order to glean the intrinsic roles of QD media. This is reflected in the present case in the study of waveguide effect in the QD lasers. In the early stage of study, many uncertainties evolve due to the limited device and QD quality and disparate device geometry pertaining to the weirdly varied fabrication technique. These facts make the reported results too device-specific. In addition, certain basic QD parameters, like the homogeneous linewidth, are less understood. Only after these problems are solved, a systematic study becomes possible, that help reveal the intrinsic effects. The understanding of intrinsic waveguide effects, in turn, feedback the laser design, and lead to potentially

important spectral or wavelength control mechanisms. The fabrications of laser waveguide then can be directed to make use of or avoid the spectral intensity modulation in the emission spectrum of QD lasers. The study of temperature effect in QD lasers shows a similar pattern. A number of temperature dependent effects exist in QD media, and the temperature dependence of lasing characteristics also depends on the device parameters, like the cavity loss that determines the threshold gain. With high quality QD devices of extremely low internal loss, we can approach the lowest limit of device loss in the high reflection coated lasers, thus a wide range of gain can be probed. In this way, the roles of ground state (GS) gain saturation, excited states (ES) gain and bimodal dot distribution can be revealed, along with the intrinsic temperature dependence in the low linear gain region just above transparency. These general temperature effects form the base for the understanding of temperature dependence in a variety of particular QD lasers. They can be reckoned on in the laser design to obtain extended temperature stability in QD lasers.

The grasp of basic lasing characteristics and device character paves the way for the exploration of high-level device properties of QD lasers. Like in the present study of the spectral dynamics of QD lasers, the intrinsic multimode dynamics are revealed along with the peculiar spectral and dynamic features as induced by the carrier transport across the QD multilayers. Laser dynamics are basically dependent on the nonlinear gain properties. The intrinsic dynamic features thus help understand the nonlinear gain processes in QD lasers, and refine the laser modeling, especially concerning the gain suppression and saturation mechanisms. This knowledge will benefit the study of laser dynamics in all semiconductor lasers. Except the fundamental aspect, the intense antiphase dynamics in QD lasers are attractive features that may be exploited in the future generation of optical processing unit as self-generating and self-pacing multichannel sources. Because the multi-stacked QD (MQD) media are indispensable in the current generation of high power and high-speed QD lasers, the present study of lasing properties in MQD lasers is particularly important. Other than the basic characteristics, the carrier transport effect is still at large in MQD lasers. However, it is critical for the high-speed properties of MQD lasers. The present study of low temperature dynamics in MQD lasers should provide a first sign of the impact of carrier transport effect on the laser dynamics. In the future, the carrier transport effect in MQD lasers needs be investigated at ambient temperature and high-speed regime. This would require a good modeling of carrier and gain dynamics in MQD waveguide, and could be a rather challenging step towards optimized high-speed MQD devices.

Above all, the design, fabrication and characterization of high performance QD lasers are becoming highly integrated processes, not only for the optimization of certain device properties, but also for the exploration of novel properties provided by QD devices.

0.4 Organization of the thesis

In this thesis, we present the characterization study of high performance laser diodes based on self-organized In(Ga)As QDs, in an effort to explore the static and dynamic properties in width and in depth.[57]

In Chapter 0, after a brief introduction of the semiconductor laser history, the recent development of semiconductor QD lasers are overviewed, in addition to a short discussion of the potential and challenges. In Chapter 1, the basic carrier and gain processes and laser parameters of QD lasers are described in detail. They are then explored for a general understanding of the temperature dependent aspects in the basic characteristics of QD lasers.

Chapter 2 is devoted to the waveguide effects on the light-current and spectral characteristics of ridge waveguide QD lasers. A systematic study with varied waveguide parameters helps resolve the so-called mode-grouping problem. Specifically the lateral-cavity spectral hole burning effect[74] is shown to be responsible for the frequently observed spectral intensity modulation features in the longitudinal mode spectra. The impact of mesa etch profiles on the lasing spectra is studied to demonstrate the spectral hole burning effect of cavity resonance modes in different types of laser cavities. The potential spectral control mechanisms for QD lasers are discussed in this context. In addition, high performance narrow stripe QD lasers with deep etched waveguide are demonstrated, testifying one of the major advantages induced by the strong carrier localization in QD media.

In Chapter 3, we turn to multimode dynamics in QD lasers. Antiphase mode fluctuations are observed in all the investigated QD lasers, and they are attributed to the dynamic grating effects in Fabry-Perot lasers. The spectral and spatial cross relaxation processes in QD and QW gain are compared to explain the different dynamic characteristics and their dependence on the current. Specifically, the weak spatial cross relaxation is identified as the main factor that keeps the dynamic grating effect strong in QD gain. A modeling taking account of Auger capture in QD gain and dynamic grating effect is discussed. Besides the antiphase character, the mode oscillation frequency is observed in damping in laser

transients, and this is exclusively associated with QD lasers, as it is absent in the comparative study with the QW lasers of similar laser structures. The frequency-damping effect is discussed with respect to the experimental signature of the synchronization process of low relaxation oscillation frequencies. In addition, some typical transient spectral behaviors of QD lasers are discussed concerning the waveguide effects and the gain suppression effect of homogeneous broadening.

In Chapter 4, lasers based on multi-stacked electronically uncoupled QDs are studied. The multilayer effect and bimodal dot distribution effect on the basic lasing characteristics are analyzed. The lasers based on different QD systems are compared in their temperature dependence with regard to the different carrier confinement energy. The laser properties are characterized as a function of device losses to reveal the intrinsic temperature dependence.

In Chapter 5, we continue to study the spectral dynamics in multi-stacked QD lasers. The analysis of spectral characteristics shows the impact of bottlenecked carrier transport on the low temperature lasing spectra. The related peculiar spectral features are associated with the gain inhomogeniety induced by the carrier transport effect. The followed time-resolved studies help clarify the spectral peculiarity by resolving the transient dynamic aspects. Particular dynamic features, like the spectral waving pattern formation and phase-shifted collective mode relaxation oscillations, are observed. They are discussed concerning the underlying carrier and gain dynamics processes in multi-stacked QDs. A self-organization mechanism involving the carrier transport and lasing processes is proposed to explain the gain adaptation processes in the laser transient. In the next, we also studied the transient dynamic instability in narrow stripe QD lasers. The transient junction heating effect and transverse spatial hole burning effect are shown to be responsible for the dynamic destabilization process in the narrow stripe gain-guided devices. The dynamic variations at low temperature of the narrow strip QD lasers are discussed by taking account of both the carrier transport effect and the transient mode-guiding dynamics.

In the end, as a special topic, we investigate the emission properties of the four-sided lasers in Chapter 6. The far field emission profiles and light-current characteristics are measured, and they are discussed with regard to the mode confinement properties and lasing mechanisms in the square laser cavity. The spectral characteristics of four-sided lasers are specifically addressed, including the true spontaneous emission background and the

resolution-limited lasing peaks. The far-field-resolved emission spectra are measured to reveal the spatial and spectral lasing mode structures. The observed strong selection of azimuthal modes is attributed to the corner diffraction loss effect, as confirmed in the followed ray-tracing analysis. Concerning the spectral mode selection, the role of discrete ray dynamics in the four-sided laser cavity is emphasized, and the mode scattering and gain suppression are discussed as two possible selection mechanisms.

References:

[1] R. N. Hall, G. E. Fenner, J. D. Kingsley, T. J. Soltys, and R. O. Carlson, Phys. Rev. Lett. **9,** 366 (1962).

[2] N. Holonyak and S. F. Bevacqua, Appl. Phys. Lett. **1,** 82 (1962).

[3] M. I. Nathan, W. P. Dumke, G. Burns, J. F. H. Dill, and G. Lasher, Appl. Phys. Lett. **1** (1962).

[4] T. M. Quist, R. H. Rediker, R. J. Keyes, W. E. Krag, B. Lax, A. L. McWhorter, and H. J. Zeiger, Appl. Phys. Lett. **1,** 91 (1962).

[5] G. H. B. Thompson, *Physics of Semiconductor Laser Devices.* (Wiley, New York, 1980).

[6] G. P. Agrawal and N. K. Dutta, *Semiconductor lasers*, 2nd ed. (Van Nostrand Reinhold, New York, 1993).

[7] D. Bimberg, M. Grundmann, and N. N. Ledentsov, *Quantum Dot Heterostructures* (Wiley, Chichester, 1998).

[8] N. G. Basov, O. N. Krokhin, and Y. M. Popov, JETP **40,** 1320 (1961).

[9] Zh. I. Alferov, V. M. Andreev, D. Z. Garbuzov, Y. V. Zhilyaev, E. P. Morozov, E. L. Portnoi, and V. G. Trofim, Sov. Phys. Semiconductor **4,** 1573-1575 (1970).

[10] I. Hayashi, M. B. PAnish, P. W. Foy, and S. Sumski, Appl. Phys. Lett. **17,** 109-111 (1970).

[11] Zh. I. Alferov and R. F. Kazarinov, Double heterostructure lasers, Authors certificate no. 27448, Application no. 950 840, Priority from March 30, 1963 (1963).

[12] H. Kroemer, Proc. IEEE **51,** 1782-1784 (1963).

[13] R. Dingle and C. H. Henry, in *U. S. Patent 3982207* (1976).

[14] P. S. Zory, *Quantum well lasers* (Academic Press, Boston, 1993).

[15] Y. Arakawa and H. Sakaki, Appl. Phys. Lett. **40,** 939-941 (1982).

[16] M. Asada, M. Miyamoto, and Y. Suematsu, IEEE J. Quantum Electron. **22,** 1915-1921 (1986).

[17] Y. Miyamoto, M. Cao, Y. Shingai, K. Furuya, Y. Suematsu, K. G. Ravikumar, and S. Arai, Jpn. J. Appl. Phys. **26,** L225-227 (1987).

[18] H. Hirayama, K. Matsunaga, M. Asada, and Y. Suematsu, Electron. Lett. **30,** 142-143 (1994).

[19] L. Banyai and S. W. Koch, *Semiconductor Quantum Dots* (World Scientific, Singapore, 1993).

[20] A. Zrenner, L. V. Butov, M. Hagn, G. Abstreiter, G. Böhm, and G. Weimann, Phys. Rev. Lett. **72,** 3382-3385 (1994).

[21] V. Shchukin, N. N. Ledentsov, and D. Bimberg, *Epitaxy of Nanostructures* (Springer-Verlag, Heidelberg, 2003).

[22] M. Grundmann, J. Christen, N. N. Ledentsov, J. Böhrer, D. Bimberg, S. S. Ruvimov, P. Werner, U. Richter, U. Gösele, J. Heydenreich, V. M. Ustinov, A. Y. Egorov, A. E. Zhukov, P. S. Kop'ev, and Zh. I. Alferov, Physical Review Letters **74,** 4043-4046 (1995).

[23] N. N. Ledentsov, V. M. Ustinov, A. Y. Egorov, A. E. Zhukov, M. V. Maximov, I. G. Tabatadze, and P. S. Kop'ev, Semiconductors **28,** 832– 834 (1994).
[24] N. Kirstaedter, N. N. Ledentsov, M. Grundmann, D. Bimberg, V. M. Ustinov, S. S. Ruvimov, M. V. Maximov, P. S. Kop'ev, Zh. I. Alferov, U. Richter, P. Werner, U. Gosele, and J. Heydenreich, Electron. Lett. **30,** 1416-1417 (1994).
[25] N. Kirstaedter, O. G. Schmidt, N. N. Ledentsov, D. Bimberg, V. M. Ustinov, A. Y. Egorov, A. E. Zhukov, M. V. Maximov, P. S. Kop'ev, and Zh. I. Alferov, Appl. Phys. Lett. **69,** 1226-1228 (1996).
[26] F. Heinrichsdorf, Thesis, Technical University Berlin.
[27] T. Riedl, E. Fehrenbacher, A. Hangleiter, M. K. Zundel, and K. Eberl, Appl. Phys. Lett. **73,** 3730-3732 (1998).
[28] O. G. Schmidt, C. Deneke, S. Kiravittaya, R. Songmuang, H. Heidemeyer, Y. Nakamura, R. Zapf-Gottwick, C. Muller, and N. Y. Jin-Phillipp, IEEE J. Select. Topics Quantum Electron. **8,** 1025- 1034 (2002).
[29] L. Müller-Kirsch., Thesis, Technical University of Berlin, 2002.
[30] S. Nakamura, M. Senoh, S.-i. Nagahama, N. Iwasa, T. Yamada, T. Matsushita, Y. Sugimoto, and H. Kiyoku, Appl. Phys. Lett. **70,** 616 (1997).
[31] Y. Arakawa, in *Nano-Optoelectronics*, edited by M. Grundmann (Springer-Verlag, Heidelberg, 2002), p. 391-410.
[32] N. N. Ledentsov, IEEE J. Select. Topics Quantum Electron. **8,** 1015-1024 (2002).
[33] D. Bimberg, in *Quantum Dots: Lasers and Amplifiers*, Tokyo, Japan, 2002 (IOP Publishing Ltd), p. 485-492.
[34] N. N. Ledentsov, A. R. Kovsh, A. E. Zhukov, N. A. Maleev, S. S. Mikhrin, A. P. Vasil'ev, E. S. Semenova, M. V. Maximov, Y. M. Shernyakov, N. V. Kryzhanovskaya, V. M. Ustinov, and D. Bimberg, Electron. Lett. **39,** 1126- 1128 (2003).
[35] S. Fathpour, P. Bhattacharya, S. Pradhan, and S. Ghosh, Electron. Lett. **39,** 1443 - 1445 (2003).
[36] C. Ribbat, R. L. Sellin, I. Kaiander, F. Hopfer, N. N. Ledentsov, D. Bimberg, I. P. Kaminow, R. S. Tucker, A. R. Kovsh, V. M. Ustinov, A. E. Zhukov, and M. V. Maximov, Appl. Phys. Lett. **82,** 952–954 (2003).
[37] K. Kim, J. Urayama, T. B. Norris, J. Singh, J. Phillips, and P. Bhattacharya, Appl. Phys. Lett. **81,** 670-672 (2002).
[38] P. Borri, W. Langbein, J. M. Hvam, M.-H. Mao, F. Heinrichsdorff, and D. Bimberg, IEEE Photon. Technol. Lett. **12,** 594-596 (2000).
[39] A. Stintz, G. T. Liu, H. Li, L. F. Lester, and K. J. Malloy, IEEE Photon. Technol. Lett. **12,** 591-593 (2000).
[40] M. V. Maximov, A. F. Tsatsul'nikov, B. V. Volovik, D. S. Sizov, Y. M. Shernyakov, I. N. Kaiander, A. E. Zhukov, A. R. Kovsh, S. S. Mikhrin, V. M. Ustinov, Zh. I. Alferov, R. Heitz, V. A. Shchukin, N. N. Ledentsov, D. Bimberg, Y. G. Musikhin, and W. Neumann, Phys. Rev. B **62,** 16671-16680 (2000).
[41] N. N. Ledentsov, IEEE J. Select. Topics Quantum Electron. **36,** 1272-1279 (2002).
[42] D. Ouyang, N. N. Ledentsov, D. Bimberg, A. R. Kovsh, A. E. Zhukov, S. S. Mikhrin, and V. M. Ustinov, Semicond. Sci. Technol. **18,** L53 - L54. (2003).
[43] Y. Qui, P. Gogna, R. Muller, P. Maker, D. Wilson, A. Stintz, and L. Lester, in *NASA Tech Briefs, NPO30503* (2003), p. 15a.
[44] M. Müller, M. Kamp, A. Forchel, and J.-L. Gentner, Appl. Phys. Lett. **79,** 2684-2686 (2001).
[45] R. Krebs, F. Klopf, S. Rennon, J. P. Reithmaier, and A. Forchel, Electron. Lett. **37,** 1223 -1225 (2001).

[46] S. Rennon, F. Klopf, J. P. Reithmaier, and A. Forchel, Electron. Lett. **37,** 690 -691 (2001).
[47] K. M. Groom, L. R. Wilson, D. J. Mowbray, M. S. Skolnick, G. Hill, M. J. Steer, and M. Hopkinson, Electron. Lett. **37,** 1220 -1222 (2001).
[48] B. Gayral, J. M. Gérard, A. Lemaître, C. Dupuis, L. Manin, and J. L. Pelouard, Appl. Phys. Lett. **75,** 1908-1910 (1999).
[49] H. Cao, J. Y. Xu, W. H. Xiang, Y. Ma, S.-H. Chang, S. T. Ho, and G. S. Solomon, Appl. Phys. Lett. **76,** 3519-3521 (2000).
[50] P. Michler, A. Kiraz, L. Zhang, C. Becher, E. Hu, and A. Imamoglu, Appl. Phys. Lett. **77,** 184-186 (2000).
[51] L. Zhang and E. Hu, Appl. Phys. Lett. **82,** 319-321 (2003).
[52] T. YOSHIE, O. B. SHCHEKIN, H. CHEN, D. G. DEPPE, and A. SCHERER, Electron. Lett. **38,** 967-968 (2002).
[53] P. Bhattacharya, in *Advances in semiconductor lasers and applications to optoelectronics*, edited by M. Dutta and M. A. Stroscio (World Scientific, Singapore, 2000), p. 1.
[54] S. Ghosh, S. Pradhan, and P. Bhattacharya, Appl. Phys. Lett. **81,** 3055-3057 (2002).
[55] O. B. Shchekin and D. G. Deppe, IEEE Photon. Technol. Lett. **14,** 1231-1233 (2002).
[56] O. B. Shchekin and D. G. Deppe, Appl. Phys. Lett. **80,** 2758-2760 (2002).
[57] Zh. I. Alferov, in *Nano-Optoelectronics*, edited by M. Grundmann (Springer-Verlag, Heidelberg, 2002), p. 3-22.
[58] A. V. Malko, A. A. Mikhailovsky, M. A. Petruska, J. A. Hollingsworth, H. Htoon, M. G. Bawendi, and V. I. Klimov, Appl. Phys. Lett. **81,** 1303-1305 (2002).
[59] J. A. Lott, N. N. Ledentsov, V. M. Ustinov, A. Y. Egorov, A. E. Zhukov, P. S. Kop'ev, Zh. I. Alferov, and D. Bimberg, Electron. Lett. **33,** 1150 -1151 (1997).
[60] J. A. Lott, N. N. Ledentsov, V. M. Ustinov, N. A. Maleev, A. E. Zhukov, A. R. Kovsh, M. V. Maximov, B. V. Volovik, Zh. I. Alferov, and D. Bimberg, Electron. Lett. **36,** 1384 -1385 (2000).
[61] S. Fafard, Z. R. Wasilewski, C. N. Allen, D. Picard, M. Spanner, J. P. McCaffrey, and P. G. Piva, Phys. Rev. B **59,** 15368–15373 (1999).
[62] L. Rebohle, F. F. Schrey, S. Hofer, G. Strasser, and K. Unterrainer, Appl. Phys. Lett. **81,** 2079-2081 (2002).
[63] M. Gurioli, S. Testa, P. Altieri, S. Sanguinetti, E. Grilli, M. Guzzi, G. Trevisi, P. Frigeri, and S. Franchi, Physica E **17,** 19-21 (2003).
[64] G. Y. Slepyan, S. A. Maksimenko, V. P. Kalosha, J. Herrmann, N. N. Ledentsov, I. L. Krestnikov, Zh. I. Alferov, and D. Bimberg, Phys. Rev. B **59,** 12275-12278 (1999).
[65] H. Pettersson, L. Baath, N. Carlsson, W. Seifert, and L. Samuelson, Appl. Phys. Lett. **79,** 78-80 (2001).
[66] M. Colocci, A. Vinattieri, L. Lippi, F. Bogani, M. Rosa-Clot, S. Taddei, A. Bosacchi, S. Franchi, and P. Frigeri, Appl. Phys. Lett. **74,** 564-566 (1999).
[67] A. Imamolu, D. D. Awschalom, G. Burkard, D. P. DiVincenzo, D. Loss, M. Sherwin, and A. Small, Phys. Rev. Lett. **83,** 4204 (1999).
[68] G. Burkard, G. Seelig, and D. Loss, Phys. Rev. B **62,** 2581-2592 (2000).
[69] M. Ouyang and D. D. Awschalom, Scienceexpress **301,** 1074-1078 (2003).
[70] V. Tokranov, M. Yakimov, A. Katsnelson, M. Lamberti, and S. Oktyabrsky, Appl. Phys. Lett. **83,** 833-835 (2003).
[71] Y. I. Mazur, W. Q. Ma, X. Wang, Z. M. Wang, G. J. Salamo, M. Xiao, T. D. Mishima, and M. B. Johnson, Appl. Phys. Lett. **83,** 987-989 (2003).
[72] B. Shi and Y. H. Xie, Appl. Phys. Lett. **82,** 4788-4790 (2003).

[73] C.-F. Lin, Y.-S. Su, D.-K. Yu, C.-H. Wu, and B.-R. Wu, Appl. Phys. Lett. **82,** 3403-3405 (2003).
[74] D. Ouyang, R. Heitz, N. N. Ledentsov, S. Bognar, R. L. Sellin, C. Ribbat, and D. Bimberg, Appl. Phys. Lett. **81,** 1546-1548 (2002).

CHAPTER 1 TEMPERATURE DEPENDENT CHARACTERISTICS OF QD LASERS

Contents:

1.1 Introduction

Temperature effect on the basic lasing properties has been a traditional issue haunting the research and development of semiconductor lasers. Thermal heating in the active region not only effects the carrier thermal redistribution and subsequent loss, but also induces thermal optical guiding effect. The laser threshold and slope efficiency suffer deterioration, and the emission properties, such as lasing modes and wavelengths, can also vary significantly with temperature. The high power performance will be limited, and the cost soars for the sophisticated thermal management in keeping the high current or stable wavelength operation of laser diodes. Strong temperature sensitivity of lasing characteristics would inhibit cost-effective solutions for applications in ambient environment with widely varied temperature. In this context, the temperature stability has been recognized as an important index in evaluating the comprehensive performance of

laser diodes. For the threshold current, the characteristic temperature T_0 is introduced as the index for the temperature stability, as in $I(T) = I'(T') \cdot \exp((T-T')/T_0)$. High absolute value of T_0 indicates a high degree of temperature stability, vice versa.

In the past few decades, the performance of laser diodes have been dramatically improved, especially since the introduction of semiconductor quantum structures as gain media. Lasers based on the quantum wells[1] (QWs) demonstrate much lower threshold current, higher external efficiency and temperature stability than any of the conventional semiconductor lasers. These superior characteristics are attributed to the modified DOS in the QWs, which enhances the gain capacity and increases the carrier confinement and thermal activation energy. However, the temperature stability of the QW lasers is still limited in the temperature range (-50 to 80°C) critical for communications application. Especially the long wavelength laser operation in the communications waveband (1.3-1.6 μm) is inevitably accompanied with strong threshold current contributions from Auger recombination, free carrier absorption and intersubband absorption, which are all temperature sensitive and severely reduce T_0. To counter these temperature effects, lasers based on the strained-layer QWs have been introduced to take advantage of the modified valence band structures in reducing further the threshold current and enhancing the temperature stability.[2,3]

The advent of self-organized QD lasers brings a breakthrough in the laser diode performances, with some important parameters being pushed to the ideal limits, such as internal quantum efficiency ~ 100%, internal loss ~ 1-3 /cm. The clear advantages of QD lasers over conventional lasers increase also the expectation level for a much higher degree of temperature stability in QD lasers. This is heralded by the prediction of an infinite T_0 for the quantum-box lasers.[4] While such a prediction is nothing wrong by itself, it should not be taken for granted as suitable for the analysis of the actual QD lasers. In the simplified model that generates such an optimistic prediction, the δ-function DOS of idealized QDs is emphasized, but apparently some important intrinsic properties of QDs are ignored, like the homogeneous broadening linewidth and its temperature dependence, the complex energy structure, among others. In addition, the inhomogeneous broadening effect is inevitable in the self-organized QDs, so the temperature change could induce variations in the gain maximum level and spectral profile, due to the carrier and gain redistribution. We can assort all these ignored parameters as non-ideal QD ones, as compared to the ideal ones considered in the simple model. In fact, theoretically, a part of these non-ideal

parameters have been treated[5-9] somewhat quantitatively to estimate the gain and laser performance. Experimentally, in the actual QD lasers, strongly varied T_0 values have been measured in different temperature sections, with typical negative T_0 at low temperature and positive T_0 at high temperature, and persistent temperature sensitivity near RT. In certain cases, temperature insensitivity is observed in medium and low temperature range, and this has sometimes been misinterpreted as a proof of the formerly discussed infinite T_0 prediction, causing a confusion on the actual mechanisms underlying this phenomenon. With many aspects of the QD laser performances approaching the ideal limits, it becomes a subtle issue to estimate the significance of each individual temperature relevant laser parameter on the T_0, for apparently an otherwise trivial temperature dependent perturbation can mean a great impact on, for example, an extremely low threshold. With in mind many other superior performances of QD lasers, the temperature stability issue becomes even critical in promoting the QD lasers for applications in many technically challenging areas, such as communications and high power application.

Taking account of the realistic parameters of QD lasers and understanding their temperature dependent aspects can be the first step in order for the interpretation of the widely varied T_0 values in different temperature range and device conditions. The eventuality of the temperature stability issue of QD lasers would rely on the use of this knowledge in the laser design and optimization to achieve a high T_0, with the other advantageous performances of QD lasers maintained.

In the following, we first introduce the basic aspects of QD gain media in relation to the carrier and gain processes in QD lasers and their temperature dependence. Then we analyze the temperature dependent lasing characteristics of typical devices based on the self-organized InGaAs QDs grown by Metalorganic chemical vapor deposition (MOCVD). For the temperature effect is deeply involved and prevailingly relevant in the present work, we refer to the later chapters for detailed analysis of other featured QD lasers, like those based on 1.3 μm InAs QDs grown by Molecular Beam Epitaxy. We conclude with considerations for the laser design issue in getting high temperature stability.

1.2 Basic properties of QD gains and their temperature dependences

In this section, the basic properties of QD gains are discussed, and the related temperature dependent aspects are addressed.

1.2.1 Electronic properties of the QDs

As can be seen in Fig. 1-1, QDs are 0D electronic systems characterized by their discrete DOS. Compared to the continuum DOS characteristic of the QW and the bulk, the discrete energy levels of the QD enforce a much reduced thermal broadening effect, which would mean a constant linewidth when the carrier thermal energy kT is smaller than the thermal activation energy, that is the energy level splitting. Actually this is the main point that leads to the prediction of infinite T_0 for the idealized QD lasers with only one confined energy state.[4] However, for the actual QDs, we have to consider their finite confining potentials and the realistic energy structures, important for a consistent understanding of the temperature stability issue in QD lasers.

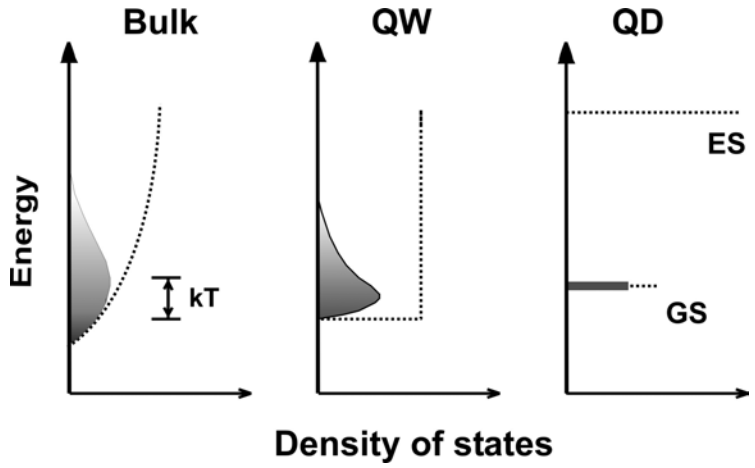

Fig. 1-1 DOS schematics for the bulk, QW and QD.

The band diagram and the schematics of the QD energy level system are shown in Fig. 1-2. Here we take the example of the InGaAs/GaAs QDs system, as studied in this work. Apparently, the electron energy splitting is generally larger than that of holes, due to the larger hole effective mass. Considering the exciton notion and with the ambipolar approximation active (or charge neutrality condition), the exciton confinement energy would be the sum of the confinement energy for the electron and hole. The ground state (GS) excitons have the largest confinement energy among others and they provide the gain for the desired GS lasing. To the advantage of QDs, much larger exciton confinement energy can be realized in self-organized QDs than in the QWs for a similar materials system. The growth of QWs with large band offsets will inevitably meet the problem associated with the large lattice mismatch, and the resulting incoherent growth is characterized by defect and dislocation formation that inhibits the possible lasing action with these QWs. In contrast, the standard QD growth technique, in the Stranski-Krastanow mode, takes advantage of the large lattice mismatch and its associated strain

energy to activate the nanoscale dot formation. The faceted dots help relax the large portion of strain energy, and reduce or practically eliminate the possibility of defect formation. The ability in growth of device quality QDs with deep confining potential enables a large exciton confinement energy that is unachievable in the QW system, and opens the window to the long wavelength range within the GaAs-based materials system.

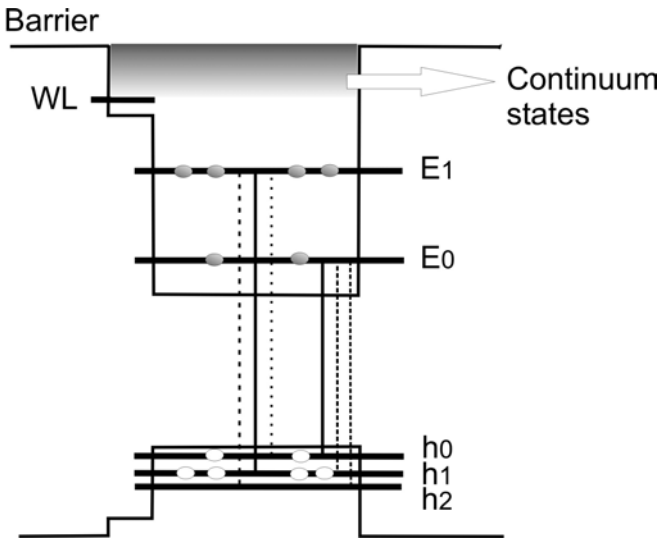

Fig. 1-2 Band diagram and energy level scheme of QD heterostructure.

The wetting layer (WL)/barrier states generally have large DOS, so thermal distribution on these states can cost a great amount of carriers, and carrier radiative/nonradiative recombination thereupon can severely quench the QD GS emission,[10] and suppress the maximum gain levels.[11] Large exciton confinement energy can help suppress the thermal population in the high-lying 2D/3D states, thus reduce the threshold and the strengthening of internal efficiency at elevated temperature, for the thermal activation energy of the carriers is increased and the adverse thermal effects are shifted to higher temperature range. It is noted that concerning the temperature stability of QD lasers, the GS-ES splitting[12] is as important as large exciton confinement energy.

The large confinement energy makes the QDs efficient carrier traps. Carriers on the WL or barrier are captured into the QDs, and relax to the lowest available energy states. The carrier capture processes rely on the emission of multiple optical phonons, and the capture rate increases with temperature for the apparent role of phonon scattering. Near RT the capture time is found < 8 ps.[13] With increasing dot-filling factors, the carrier-carrier scattering helps further increase the capture rate. Depending on the dot-filling factor, the carrier relaxation rate can be quite different. For long it has been speculated that the

phonon bottleneck effect occur to the electron relaxation processes in the QDs, because the energy separation between the discrete energy levels may not match well with the LO phonon energy such that phonon emission or absorption is inhibited. Experimentally the phonon bottleneck effects[14,15] are actually observed. However in these few cases, a very low dot-filling factor (smaller than one exciton per dot) is found as the necessary condition, with non-geminate electron capture[14,15] or weakened LO phonon-exciton coupling[14,15] also emphasized. When the QDs are filled with one exciton or more carriers in average, the carrier-carrier scattering will ensure efficient carrier relaxation, which is the generally observed case. The electron relaxation time in a InGaAs QD laser is found to increase with temperature for the Auger relaxation process involving hot electron and cold hole.[16] So the electron-hole scattering can be the dominant mechanism for the relaxation of hot carriers.[17] At higher dot-filling factors, other carrier scattering processes will hasten further the carrier relaxation. Because the transparency condition of QD lasers is fulfilled at a dot-filling factor of one exciton per dot, the operation of QD lasers is borne immune to the phonon bottleneck effect, which would otherwise be very deleterious to the laser performance. Recently ultrafast intraband pump-probe spectroscopy experiments show that in InAs QDs both the carrier capture and relaxation occur on the ps scale and the stepwise relaxation through the QD ES is the most efficient relaxation pathway.[18]

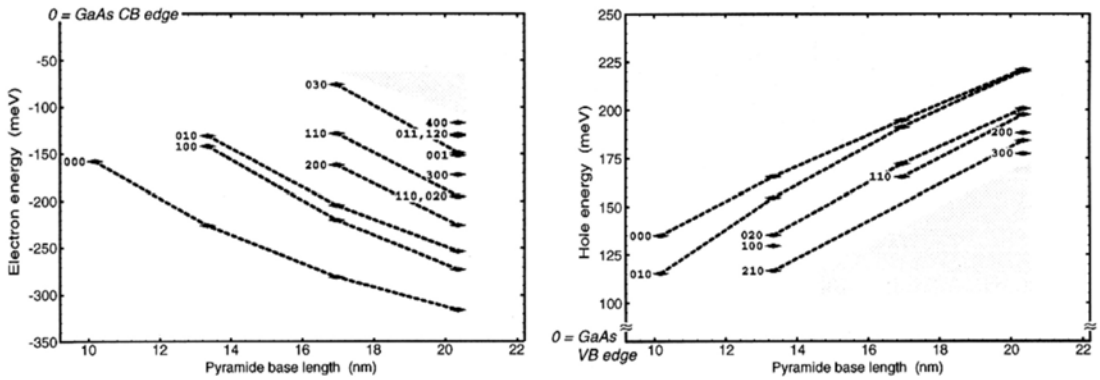

Fig. 1-3 Size dependence of electron and hole energy levels of pyramidal InGaAs QDs. After Ref. 19.

Compared to the simplified energy level scheme in Fig. 1-1, the actual QD energy structure can be much complex. One example of the static QD electronic structures is shown in Fig. 1-3, which is calculated within the 8-band k·p scheme.[19] With the varied dot base size, the energy of single particle states shows systematic shifts, so that both the confinement energy and energy splitting change significantly. In general, the QD energy structure is a sensitive function of the dot size, shape, strain, and composition, and so is the oscillator strength

distribution. This property makes QDs a name as artificial atoms, and provides great flexibility in QD engineering through refined growth technique.[20,21]

The exciton recombination lines observed in the single dot spectroscopy[22,23] possess a complex of fine structures impacted by few-particle effects and many-particle effects.[24] The whole set of exciton lines can be sorted by their energy shell structure.[25] Specific in the InGaAs QD system, the hole energy state separation is much lower than that of electrons. The electron or hole levels may be denoted in a similar way as for the atom levels. So the transitions between the electron GS (1s) and the first few hole states (1s, 2s, 2p…) form the so-called s-shell, those starting from the electron 1st ES belong to the p-shell, and so on. As for QD filling, the s-shell is filled at first. When the dot-filling factor is higher than 2 excitons per QD, the carriers will fill up the p-shell and higher ones due to the Pauli blocking effect. So the QD emission spectrum shows typical state filling effect.[20]

In the energy shells other than the s-shell, the exciton lines can be rather crowded, due to the large degeneracy of the electron ES and their possible splitting caused by symmetry breaking. Importantly, for the s-shell, there is one dominant exciton line originating from the electron and hole GS, which contributes the most to the GS exciton gain. From the consideration of the symmetry property of wave functions, this GS exciton line would be the only dipole allowed transition in the s-shell for the otherwise symmetrical QD confining potential. However, in the actual self-organized QDs, their QD shape, composition and strain are all imposing symmetry breaking in the QD confining potential. Perturbation to the symmetry property of wave functions and possible In-Ga intermixing makes those originally forbidden transitions assume finite transition probability. It is estimated, based on the actual dot parameters,[26] that these sidelines may gain an intensity ratio of about 1 - 20% to the dominant GS exciton line. The sidelines with sizable intensity ratio would increase the complexity of the GS gain composition, especially when the inhomogeneous broadening is considered. That may induce only a slight quantitative change in the gain level, and affect little the basic laser properties, like threshold and efficiency. But its implication to the coherent optical properties of the QDs can be significant and may manifest itself in the dynamics of QD lasers.

Assuming the QD confining potential is affected little by temperature change, as is the case in InGaAs QD system, the exciton transition energy of the QDs will decrease with temperature, following the trend of the band gap reduction as common to the bulk and

QWs. The temperature effect on the electron and hole energy distribution in the QDs is closely related to their energy structure. In the usually surveyed temperature range (50 K < T < 300 K), the holes are thermally distributed on their close-lying energy states with typical energy splitting ~10-20 meV. In comparison, the electron energy splitting can range from typically 25 meV up to 108 meV[20,27] for various InGaAs QDs, as realized by tailoring the growth technique. The electron thermal distribution on the ES and higher energy states is quenched at low temperature, and only takes up at relatively high temperature. So the thermal distribution effect of electron and hole could have a pivotal role in determining T_0 for different temperature ranges.[12]

1.2.2 QD ensemble effects

In the last section, we discussed the main electronic properties of singular QDs. In the following, the main ensemble effects are introduced, knowing that it is an ensemble of QDs being used as gain media in the current generation of QD lasers.

a) Inhomogeneous broadening

An ensemble of self-organized QDs are characterized by their dispersion in size, shape, strain and composition, so the discrete energy states are generally inhomogeneously broadened. Due to the inhomogeneous broadening effect, the fine structure of single QD spectra is smeared out in the QD ensemble. For the desired GS lasing, the GS spectral gain then possesses an inhomogeneous broadened profile. Depending on the specific dot dispersion characters, the gain profile can be single-modal or multi-modal, which usually can be approximated by one or more Gaussian peaks.[28,29] When the inhomogeneous broadening becomes comparable or goes beyond the GS-ES energy splitting, the overlap of the GS and ES gain can greatly enlarge the gain bandwidth. Therefore, while the inhomogeneous broadening property of QD gain definitely reduces the otherwise achievable levels of saturated gain and differential gain, it actually gives the QD lasers a lead in the applications like widely tunable lasers or wide band sources.[30] A wide band and flattop gain profile will provide a rather stable laser tuning property.

Interestingly, the time-resolved single QD spectroscopy shows that the QD exciton recombination energy is often experiencing random fluctuations[31] reminiscent of telegraphic signals. This perturbation is attributed to the quantum confinement stark effect, as induced by the dynamic electronic environment, which can be impurity- or defect-related electric field fluctuations. The energy jitter patterns are characteristic to every single

QD, so this effect is another inhomogeneous property of the QDs, though its broadening effect is almost negligible compared to the former static inhomogeneous broadening effects.

For the inhomogeneous broadening leads to a distributed GS exciton confinement energy in a wide range, this makes possible the carrier redistribution among the QDs with different confinement energy. The following gain redistribution can be strongly temperature dependent, because it is the thermionic emission process that limits the carrier shuffling[23] between the QDs, and the exciton confinement energy is directly related to the thermal activation energy. In the spectral range of the nominal GS exciton gain, the contribution from the 1st ES will be present if the inhomogeneous broadening is large enough to cause the GS and ES overlap.[32,33] The 1st ES may contribute gain or loss, depending on the dot-filling factor. The temperature sensitivity of the 1st ES contribution can thus lead to strong temperature dependence of threshold and lasing wavelength. With multi-modal QD dispersion, the carrier distributions among the different QD groups can show quite complex temperature dependent behaviors, as determined by the ratio of QD numbers in different groups and their respective confinement energy.[29] The impact of inter- and intra-dot carrier and gain redistribution on the laser properties and their temperature dependence will be addressed frequently in this work for its pertinent importance. By the way, the notion of energy states here has a one-to-one correspondences with that of the energy shell structure, that is, the GS refers to the s-shell, the 1st ES the p-shell, and so on.

b) Carrier statistics

Besides the inhomogeneous broadening effect, the QD ensemble is characterized by its specific carrier statistical property. The ensemble statistical effect exists even in the ensemble composed of uniform QDs, but in the self-organized QDs, it is coupled with the inhomogeneous broadening effect.

In a single or multiple layers of electronically uncoupled self-organized QDs, the QDs are spatially isolated. In this situation, carrier capture into individual QDs can be justified to be a stochastic process. At the typical area dot density, ~ $10^{11}/cm^2$, there is no tunneling possible between the neighboring QDs, and the carrier thermalization processes among the QDs are mediated by the carrier escape (through thermionic emission) and recapture processes. Inside every QD, carrier relaxation and scattering processes work together to

reach an internal thermal carrier distribution.[34] Thus the random capture and weak link of carriers in isolated QDs distinguish the carrier statistics in QDs from those in conventional gain media. Taking account of the entire carrier processes and treating the different carrier distribution configurations in the individual QDs as microstates, the carrier statistics problem of the QD ensemble in principle can be solved. Apparently in single QDs, the dot filling is in digital format, for example, in the GS, 0, 1, or 2 excitons are the only possible filling states (ambipolar approximation). So one of the main conclusions on the carrier statistics in QDs is that for any average dot-filling factor, there exists a distribution of probability for various digitally filled QD microstates. With current, the dominating microstates in the distribution shift from the lowly filled states to the highly filled states. The sound effect following the microstate distribution is that at even low carrier density the ES of a reasonable number of QDs can be filled with more excitons than expected from the thermal distribution on the ES at the average dot-filling factor.

The basic aspects of carrier statistics in the QDs have been revealed in the ultrafast coherent optical experiments, which confirmed the existences of QD microstates composed of digital numbers of excitons.[33,35] Photoluminescence and electroluminescence of the QDs have been widely studied as a function of temperature and excitation intensity. For the interpretation of these emission spectra, microstate master equations are solved for the carrier statistics, which turn out to agree well with the QD state filling spectra.[36] In general, the correct handling of the carrier statistics in the QD ensemble is important for understanding the separate roles of Pauli blocking effect, the temperature effect and the microstate statistics characteristic of the QD ensemble.

The carrier statistics of the QDs essentially determine the QD gain properties, which are fundamental in understanding the static and dynamic properties of QD lasers. The solution of microstate master equation[37] shows that the resulting carrier radiative recombination current depends strongly on the choice for the carrier capture mode, that is, either exciton capture or separate electron and hole capture. However, it is noted that in QD lasers the carrier filling is intrinsically violating the charge neutrality in QDs due to electrostatic field effect.[6] This intrinsic effect affects the radiative recombination current and thus the threshold current. Its temperature dependence also contributes to the temperature sensitivity of QD lasers.[6]

1.2.3 Homogeneous broadening

The discrete density of state is the main characteristics of the QD media. However, in rare cases the line shapes of the discrete QD energy levels can be approximated by the δ functions. Besides the inhomogeneous broadening, the QD energy levels can have finite homogeneous broadening linewidth. In the following we discuss the homogeneous broadening mechanisms and the implication to the QD gain.

a) Homogeneous linewidth

The homogenous linewidth is related to the decay time of the exciton polarization, as formulated in the general relation $\Gamma \cdot \tau = h/2\pi$, with Γ and τ being the homogeneous linewidth and the dephasing time, respectively.

For the QDs, a basic linewidth broadening mechanism originates from the radiative recombination. It leads to a natural lifetime broadening of the discrete energy levels. The natural linewidth amounts to a few μeV, for the spontaneous emission lifetime lies at ~1 ns. The radiative recombination rate may vary with temperature and current, causing a slight increase in the natural linewidth.[35]

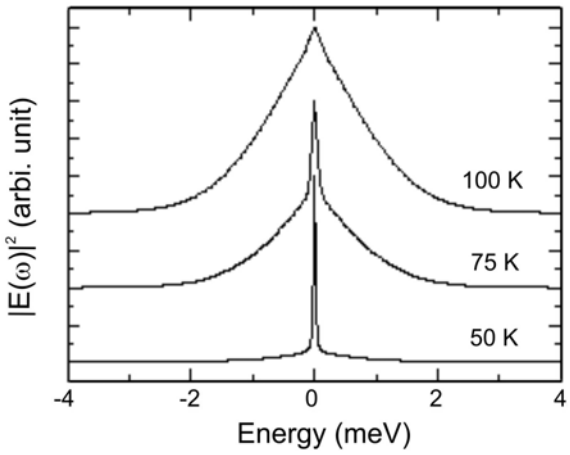

Fig. 1-4 Power spectra of time-integrated four-wave mixing field at various temperatures. After Ref. 41.

Besides the natural lifetime broadening, the exciton-scattering-induced dephasing process makes another important linewidth broadening mechanism. The QD GS excitons can interact with other carriers, such as those on the ES or the 2D/3D carriers in the WL/barrier, and they can also couple with the crystal vibrations, i.e. phonons. Much work has been done both theoretically[38-40] and experimentally[33,41,42] in exploring the roles of these different scattering processes. In the following we discuss the main experimental results obtained from the InGaAs QDs system.

The transient four-wave mixing spectroscopy has been used to measure directly the dephasing time and line shape of the GS exciton transitions of the InGaAs QDs embedded in a QD amplifier structure without electrical injection.[41] As can be seen in Fig. 1-4, at T < 100 K, the line shape is characterized by a sharp Lorentzian zero-phonon line (ZPL) with a broad band. The ZPL is broadened due to inelastic processes, such as radiative recombination and phonon-assisted activation into higher energy exciton states. The broad band is attributed to the pure dephasing originating from the elastic scattering with acoustic phonons. Below 50 K, the sharp ZPL dominates the line shape that has negligible broadband component. A linewidth of 2 μeV was measured for the ZPL at 7 K, which corresponds to an ultralong dephasing time of 630 ps. The ZPL width changes marginally with temperature, at a rate of 0.22 μeV/K. In contrast, the broadband part broadens nonlinearly with temperature at a greater rate than that of the ZPL, and its weight in the line shape also grows up. The resulting non-Lorentzian line shape in total has a dominant broadband part above 75 K, with the linewidth reaches the meV range at 100 K. The situation above 100 K looks much simple. Ultrashort dephasing times < 1 ps were generally measured for 125 K < T < 300 K. The homogeneous linewidth increases linearly at a rate of 0.02 meV/K, reaching 6 meV at RT. With temperature, it is natural to have intensified elastic scatterings with acoustic phonons, due to the increased phonon population. However, compared to that of acoustic phonon broadband below 100 K, the change of the homogeneous linewidth with temperature has a higher rate above 100 K. This indicates that at high temperatures additional dephasing processes set in. For example, the LO optical phonons can be involved in the elastic scattering processes, thus enhancing the whole dephasing rate.

In the InGaAs QD amplifier under electrical injection, the complex dephasing mechanisms of the multiexciton states are investigated using differential transmission spectroscopy and four-wave mixing.[33,35] The microstates associated with different multiexciton configurations are characterized by their distinct dephasing times. For example, at 10 K,

Microstates with only GS carriers have a typical decay time from 1 ns to 200 ps for I = 0 to high current, determined by the interplay between radiative recombination and capture;

Microstates with only one ES carrier have slow time constants of 4 ps and 35 ps, attributed to the relaxation of a hole or an electron;

Microstates with more than one ES carrier have a much fast relaxation time of 0.33 ps, due to the high number of final states available for the phonon-assisted relaxation.

Note that up to 200 K, the multiexciton excited states (b, c) are current independent in their dephasing times. But above 200 K, their dephasing times show a current dependence that increases also with temperature. The homogeneous linewidths are shown in Fig. 1-5 for different temperatures and currents. At RT, the corresponding homogeneous linewidth goes up from 6 meV at I = 0 mA to 20 meV at high current. This strong current and temperature dependence is attributed to the elastic coulomb scattering with carriers thermally populating the wetting layer. A further study shows that such current and temperature dependence of the dephasing time is suppressed in the deep confined InAs QDs emitting at 1.3 μm. This supports the elastic scattering with the carriers in the wetting layer as an efficient dephasing process in less-confined InGaAs QDs, due to the thermal population in the wetting layer, which is quenched in deep confined InAs QDs.[43]

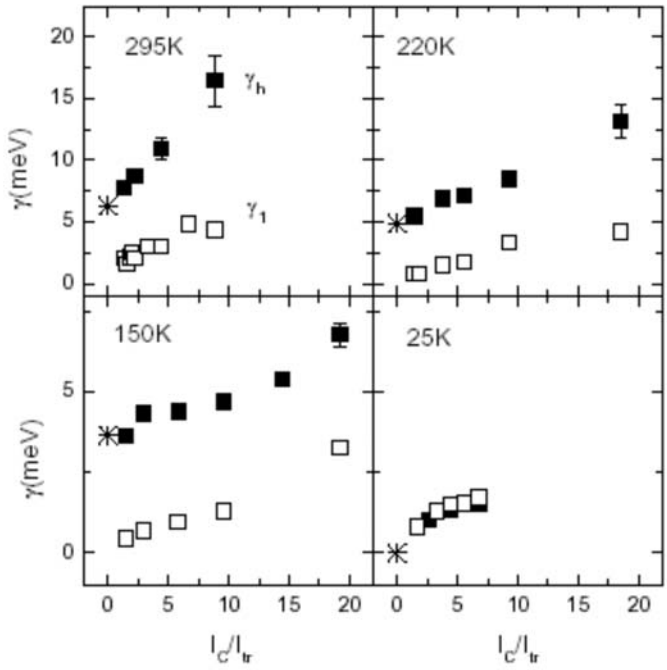

Fig. 1-5 Homogeneous linewidths (solid) and lifetime broadening (open) at various temperatures and as a function of current. After Ref. 35.

It is noted that the homogeneous linewidth measured by the four-wave mixing technique is inevitably a characteristic value for the relevant QD ensemble. In reality, each QD may have its distinct homogeneous linewidth due to the different energy structure and the environment.[42] In deed, the homogeneous linewidths of single QDs have been studied by near field optics. The experimental results under weak excitation confirm that every single

QD has a distinct linewidth, which mainly originates from the electron-LO phonon interaction and increases slightly with the GS-ES splitting, indicating the existence of strongly coupled electron-phonon modes in QDs.[44] The strong excitation density dependence of the linewidths is attributed to the Auger-type scattering between the electron and hole via coulomb interaction in the highly excited QDs.[45]

b) Homogeneously broadened gain

Homogeneous linewidth of QD exciton transitions is one of the fundamental aspects in the optical and electronic properties of QDs. It defines the linewidth of absorption and gain spectrum of single QDs. In the following, we give an overview on the gain properties affected by the homogeneous broadening effects.

The homogeneous line shape determines the spectral gain profile when the inhomogeneous linewidth is smaller than the homogeneous linewidth. In this case, the change of homogeneous linewidth affects the spectral gain at most. The maximum gain level will decrease and the gain linewidth increase, when the homogeneous linewidth increases with temperature or other factors. In the opposite case, when the inhomogeneous linewidth becomes comparable to or larger than the homogeneous linewidth, the change of homogeneous linewidth will not only affect the maximum gain level but also have edge effects on the inhomogeneously broadened gain profile. Currently this opposite case represents the reality in the self-organized QDs for the overwhelming dot dispersion.

Whether large or small inhomogeneous linewidths, finite homogeneous linewidths mean that the light can interact with the QDs whose energy levels lie within the homogeneous linewidth. For a compulsory single mode operation, a large homogenous linewidth would be rather advantageous in making full use of the gain source dispersed by the inhomogeneous broadening. In free running lasers without mode selection, a large inhomogeneous broadening would enforce multimode lasing. With homogeneous linewidths varied with temperature, the evolution of multimode lasing width with current could show distinct behaviors, and this aspect has been speculated for long in the literature.[46,47] The related spectral characteristics of QD lasers will be one of the main issues explored in this thesis work.

The notable facts about the homogeneous linewidths in the QDs are not only their temperature dependence, but also their variation in individual QDs according to the

specific energy level scheme and dot-filling factors. The QD ensemble effect dictates the existence of the dispersed homogeneous linewidths at any temperature and current. To date it is difficult to appreciate this specific property, but it would be certainly relevant when fewer QDs are used in the lasers and therefore the fluctuation in the dot-filling factors becomes significant.

1.2.4 QD gains

a) Materials gain of QDs

Compared to the conventional gain media, such as the bulk and QWs, the QDs have much reduced effective volume. Transparency condition will be met by filling the QD GS with one exciton per dot in average. Therefore, the transparency current density for a QD laser can be extremely low. A further filling of QD GS would provide gain. Due to the discrete energy levels and enhanced DOS, the material gain of QDs is much stronger than that of conventional gain media, and a value of 6.8 x 10^4 /cm has been obtained in lasers based on the self-organized InGaAs QD.[48] These QDs also show enhanced differential gains.

As discussed in the above three sections, the actual QD gains are not a simple multiplication of the gain of single QDs. The inhomogeneous and homogeneous broadening effects would broaden the gain spectral width and reduce the maximum gain level severely. They also lead to the possible gain mixing or overlap effect, which can be the GS-ES overlap, or the overlap between two QD groups in a bimodal dot distribution,[28,29] as documented in Chapter 4. The QD ensemble statistics increase further the complexity of gain compositions. The nominal gain is actually a combined result of gain and absorption originating from many QD sub-ensembles that have characteristic dot-filling factors distributed in a wide spectrum. Here we see the big difference between QD gain and those of QWs or the bulk in their gain compositions.

The QD gain spectral is determined by the carrier distribution in the QD ensemble. In single QDs, the efficient relaxation and scattering processes ensure a thermal carrier intra-dot distribution. For the hole energy separation is much lower that that of electron, the hole thermal distribution at high energy states becomes significant from medium to high temperature. This greatly reduces the gain capacity at high temperature, and has been conceived as the one of the main hurdles towards high T_0 at RT.[49] In the inhomogeneously broadened QD ensemble, the carrier distribution is far from settled as can be described by a global quasi-Fermi level like in the bulk or QWs. The lack of efficient inter-dot carrier

relaxation mechanisms makes nonequilibrium distribution among QDs prevail. With little carrier shuffling among QDs, the carrier distribution is simply determined by the detailed balance of carrier capture and radiative recombination, and the varied confinement energy among QDs makes no difference. At the typical dot area density (~10^{11}/cm^2), QDs are spatially isolated without tunneling channels. So the only possible way for the carrier redistribution among QDs is through the carrier escape and recapture processes. This kind of local carrier exchange will take the wetting layer or barrier states as the medium station and is delineated somehow in its spatial range by the carrier diffusion length in the wetting layer and barrier. The carrier escape process is strongly temperature dependent, and its thermal activation energy is directly related to the carrier confinement energy. So with temperature, the carrier shuffling among QDs becomes frequent, and the carrier distribution among QDs can gradually assume a partial thermalization status. In general, the thermal redistribution favors the filling of deeper confined QDs. It is important to note that, even at RT, a pure exciton thermal distribution model is not suitable for QD lasers, and a partial free carrier thermal distribution is needed to account for the lasing characteristics properly.[50] This compromised model implies the intrinsic nonequilibrium nature of carrier distribution in QD lasers. Thus the usually claimed quasi-Fermi carrier distribution inferred from the RT gain measurement is rather a coincidence than the intrinsic carrier distribution characteristic of QDs.[51]

With temperature and current, the contribution of QD ES becomes significant. This is most pronounced when the inhomogeneous broadening is comparable or larger than the GS-ES splitting. It could result in asymmetry in an otherwise symmetrical GS gain profile.[32,33]

b) Modal gain of QD lasers

The modal gain of the QD laser is still limited by the finite dot area density per layer, with a typical value ~10 /cm.[52] Using multiple layers of QDs can make up the gain deficiency. The more QD layers, the higher the transparency current. This is still affordable for QD lasers due to the extremely low transparency current. While the introduction of multi-stacked QDs can reduce the carrier density, it could lead to gain inhomogeneity due to the carrier transport effect across the QD heterostructure. The deep confined QDs act as efficient carrier traps, so carriers can be trapped in the transport across multiple QD layers. The carrier transport effect in multi-stacked QD lasers are addressed in Chapter 4 and 5.

c) Temperature effects in long wavelength QD lasers

As the main temperature dependent aspects of QD gains have been discussed, there are still certain concerns with other temperature effects typical in long wavelength lasers, like free carrier absorption, intersubband absorption, and Auger recombination. These effects are closely related to the valence band structure, and responsible for the temperature sensitivity of long wavelength QW lasers. Strained-layer QWs have been taken advantage to help reduce the temperature sensitivity through the modified valance band structure, such as the splitting of the previous degenerate uppermost valence bands and the reduced hole effective mass.[2] Self-organized QDs are generally strained for their large lattice mismatch with the matrix materials, so their modified valance band structure could help suppress the related temperature sensitive effects. Actually the extremely low internal losses, achieved thus far, reflect the much-reduced loss contribution from free carrier and intersubband absorption in QD lasers. With very low threshold carrier density, Auger recombination component in the threshold can be much reduced as well. Experimentally it has been shown in one InGaAs QD laser that Auger recombination coefficient decreases with temperature.[16] Therefore, for long wavelength QD lasers, these temperature effects are much reduced or even have reversed temperature dependence. However, as emphasized, the role of these effects on the final temperature stability of QD lasers should not be underestimated, for the extremely low threshold can be more susceptible to the residual temperature effects, not to say, for high threshold current density the Auger recombination current can sour up[53] due to its exponential dependence on the carrier density.

d) Gain nonlinearity in QDs and QD lasers

Finally, it can be emphasized that QD gains possess strong nonlinear effects. One simple nonlinear gain effect is related to the dot-filling factors. Like for GS, it can contain maximal two excitons. So with current, QD GS gain naturally saturates.[33,54] The differential gain is also current dependent, and retreats to zero when the saturated gain is approached. The beginning of carrier population on the ES and higher energy state would lead to a more complicated situation. These thermal population will suppress the GS gain,[11,49] meanwhile the addition of ES gain would disguise the saturation effect from the GS gain. The GS-ES gain overlap thus makes the temperature dependence of maximum gain levels vary with the dot-filling factor.

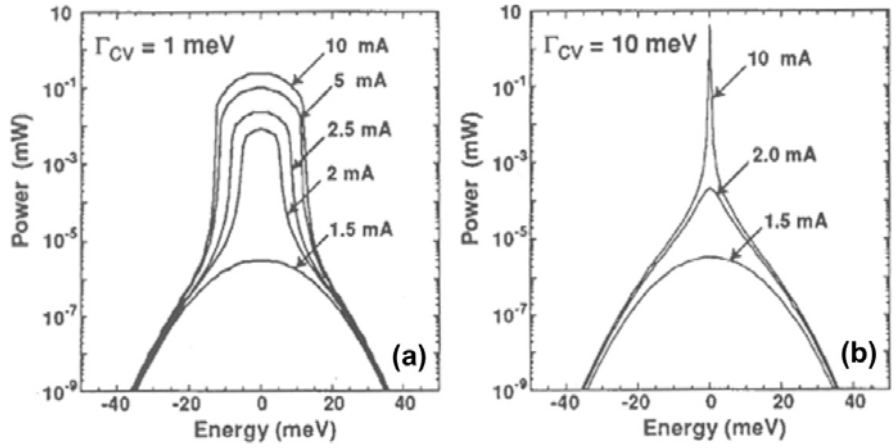

Fig. 1-6 Simulated lasing spectra for QD lasers with different homogeneous broadening. The inhomogeneous broadening is kept the same in both cases (a) and (b). After Ref. 46.

Another nonlinear gain effect comes from the gain suppression effect, as phenomenally called in semiconductor lasers. This effect can be of a vast variety of origins. Among many others, carrier heating, free carrier or valence intersubband effect, and Auger effect can lead to a suppressed linear gain capacity. However for the lasing process, the most significant gain suppression effects are those that cause gain cross saturation. Spectral hole burning effect associated with the finite intraband relaxation time[55,56] has been analyzed theoretically to get the related gain suppression coefficient. The so-called dynamic grating effect, which originates from the spatial and spectral hole burning effect due to the longitudinal mode standing wave pattern, is also incorporated in the calculation of gain suppression coefficient, in order to account for properly the experimental spectral characteristics.[56] Although these theoretical works consider only the bulk semiconductor lasers, the principal concepts of gain suppression are applicable to the QW and QD lasers. According to these theoretical analyses, both the linear gain and the gain suppression terms are necessary for the description of multimode lasing process. The gain suppression terms in the multimode rate equation contribute mostly to the mode coupling.

We note that, in an effort to account for certain peculiar spectral characteristics of QD lasers, multimode rate equations have been written that take account of the homogeneous linewidths and inhomogeneous broadening of QD gain.[46,57] Apparently these equations use reasonable values for the laser parameters, specifically the homogenous and inhomogeneous linewidth and other device parameters. But the model failed in describing the actual laser spectrum. In Fig. 1-6, one simulation result from such a model is shown. The low temperature spectra, in Fig. 1-6a, are not so much different from the experiments, but the high temperature spectra, i.e. for large homogeneous linewidth, deviate from the

features in real spectra, and especially for high currents, this model predicts a spectral splitting behavior, which is never observed in QD lasers in the actual sense (refer to Chapter 2). We perceive that the fateful misconception in this model is to use the homogeneous and inhomogeneous broadened QD gain to represent both the linear gain and gain suppression terms. This makes the model count nominally only the mode optical coupling through stimulated emission process for the modes within the homogenous linewidth, even if it can contain explicitly the gain suppression due to spectral hole burning effect. It is equivalent to distributing the QD gains to different lasing modes simply based on the mode optical powers. This optical mode coupling model may be suitable for the laser system with weak gain nonlinearity and mode coupling, such as the glass lasers,[58] but not for semiconductor QD lasers. In QD lasers, the mode couplings are rather complex nonlinear processes, which include not only the direct optical coupling, but also the couplings through carrier modulation, such as the dynamic grating effect. The specific carrier processes can lead to unique characteristics of spectral and spatial cross relaxation. For these additional mode-coupling mechanisms, different forms of mode coupling terms are needed in the rate equation to account for the various mechanisms of gain nonlinearity. It is suggested that in QW lasers the carrier diffusion can wash out the pattern effect of dynamic grating. But in QD lasers, the much reduced carrier diffusion can be responsible for a stronger dynamic grating effect. In this context, the inclusion of strong gain suppression terms in the multimode rate equation becomes even critical for QD lasers. Furthermore, the dynamic grating effect has been raised to be responsible for the antiphase dynamics in the multimode semiconductor lasers. So the proper modeling of this effect in QD lasers is important for understanding the spectral dynamics. We refer to the later chapters for detailed analysis of the spectral characteristics and their relation to the various gain suppression effects, including a direct comparative study between QD and QW lasers.

1.3 Temperature dependent characteristics of InGaAs QD lasers

In this section, we analyze certain basic characteristics of InGaAs QD lasers, such as the light-current (L-I) and spectral characteristics.

The laser structure --- TU 4819 --- is grown by MOCVD. It has 3-fold stacks of self-organized InGaAs QDs in the center of waveguide. A detailed waveguide description can be found in Chapter 2. The preliminary characterization based on broad area devices (w = 100 μm) shows an internal quantum efficiency η_{int} ~ 97%, internal loss α_I ~ 5.3/cm, and

transparency current density J_{tran} ~ 57 A/cm^2. Another laser structure --- TU 5447 --- is also grown in MOCVD, but has 6-fold stacks of InGaAs QDs and an improved internal loss. Its close-to-ideal device characteristics has been reported by Sellin et al.[59] Note that the QDs in both laser structures are designed to have a GS emission wavelength of ~1.14 μm at RT. Ridge waveguide laser diodes are processed from these laser structures.

Before analyzing the laser characteristics, it is necessary to get some basic information about the QDs, like their energy levels, inhomogeneous broadening and carrier distribution. The true spontaneous emission spectrum can provide this valuable information. In addition, for the QDs, it is shown[7] that the true spontaneous emission spectrum matches the gain spectrum by a general factor, if a quasi-Fermi distribution can be assumed for the carrier distribution among the QDs.

1.3.1 True spontaneous emission spectrum

Electroluminescence from laser diodes can be (a) edge emission; (b) side emission. The edge emission is actually amplified spontaneous emission (ASE), for the gain and self-absorption distort the spectrum from the true spontaneous emission. The side emission avoids the gain and self-absorption effect, so it is the true spontaneous emission. Here we take the side emission from a small window on the backside contact of the devices, which are mounted p-side-down.

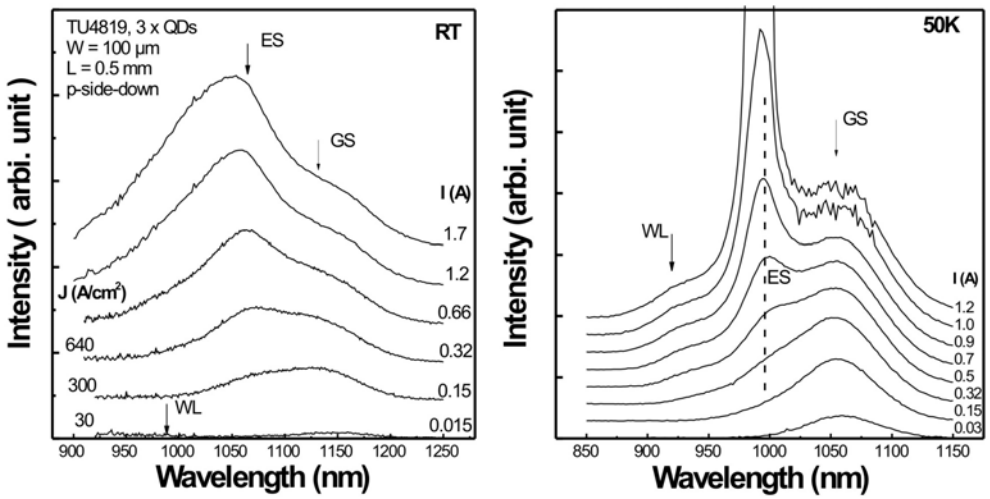

Fig. 1-7 True spontaneous emission spectra of the 1.14 μm InGaAs QDs.

Fig. 1-7 shows the backside emission spectra as a function of injection current. As can be seen at 50K and low current, the GS peaks are inhomogeneously broadened with a FWHM

of ~60 meV. With current, new peaks appear on the high energy side, and they are denoted as ES and WL. Here we see the typical state filling effects in QD emission spectra. The GS-WL separation amounts to ~130 meV, a rather large confinement energy. The GS-ES splitting is estimated to be ~60 meV, similar to the GS inhomogeneous broadening, so we can see the strong overlap between GS and ES.

The temperature dependence of these emission spectra is evident. At the same current, like I = 0.15 A, the integrated emission intensity at 50 K is much stronger than at RT. As striking as is for I = 0.32 A, there is only a small shoulder from ES emission at 50 K, but at RT the ES peak intensity already surpasses the GS one. So we see two different scenarios at different temperatures. At RT, the thermal population of ES occurs for the finite GS-ES splitting, whereas at 50 K, such a thermal population is quenched, and the ES population occurs in the state filling spectra mainly due to the Pauli blocking effect in the GS. The saturation of GS emission at 50 K begins before the ES emission takes up, but at RT, well before the saturation level is approached, the GS emission is strongly suppressed by the thermal effect. This GS emission suppression implies a reduced GS gain and differential gain at high temperature, compared to those at low temperature and similar current. The GS saturated gain may never be reached at RT in the practical current range, or the ES gain will take over it at relatively lower current.

The general reduction of integrated emission intensity at RT indicates that the carrier thermal escape takes up and quenches the emission. This reduces further the GS gain and differential gain for a certain carrier density. In Fig. 1-7, we can see that the WL emission intensity is most pronounced at low temperature and high current. The evident WL emission results from the high WL DOS that increases the carrier occupation probability. The weak WL emission at RT and at low current implies that the thermal carriers in the wetting layer are subject to nonradiative recombination, which is again quenched at 50 K.

Compared to the thermal energy kT ~ 26 meV for RT, the GS-WL separation (~ 130 meV) of these deeply confined QDs is more than 3 times larger. If the QDs have only one confined state, then the thermal agitation from the GS to the WL and above is totally quenched. This would imply a temperature insensitivity of GS emission efficiency. However in the actual QDs, a complex of confined ES exist as well. In the current QDs, the GS-ES splitting is as large as ~60 meV, but the ES can be of rather complicated structure, as properly descried as a jungle of ES that extend to the wetting layer states. So

the critical carrier confinement energy is determined by the GS-ES splitting (actually the electron GS-ES splitting). At RT, the thermal carriers on 1st ES can escape the QDs through the jungle of ES. The detailed balance in the QDs thus strongly suppresses the carrier population on the GS. Here we appreciate the importance of GS-ES splitting to the carrier thermal effects, so it is necessary to strive to increase this splitting by adequate growth and post processing technique, in order to make the device emission less temperature sensitive.

As can be seen in Fig. 1-7, the 0.5 mm long device is lasing at high current, with I_{th} ~ 1 A (J_{th} ~ 2 kA/cm2). The threshold gain equals the total loss ~ 29 /cm, with α_{mirror} = 24 /cm and α_I ~ 5 /cm. Apparently the GS saturated gain cannot afford the threshold gain, so the device is lasing on the ES instead of the GS. The GS gain here makes no contribution to the lasing process, but rather a burden that increases dramatically the threshold current. This is the main reason why the ES lasing is not desirable in the practical devices, though the ES saturated gain can be much higher than that of GS for the high degeneracy of ES. Note that the spectral noise around the GS at high currents is the artifact from the optical filter that is used in attenuating the strong ES laser emission.

1.3.2 Amplified spontaneous emission spectrum

The edge emission of laser diodes driven below threshold is the amplified spontaneous emission. Its deviation from the true spontaneous emission can be attributed to the gain and self-absorption along the longitudinal direction of devices. In the following we analyze the edge emission spectra to get the information about the spectral profiles of gain and self-absorption in addition to their evolution with current.

Usually the spectral profile of gain is not coincident with that of self-absorption, like in the bulk and QWs. This can be traced back to their continuum DOS. In continuous energy bands, carriers can thermalize to quasi-Fermi distributions through the efficient intraband relaxation, and the resulting carrier distribution is sensitive to temperature and current. Consequently, the spectral profiles of gain and absorption also vary with temperature and current, leading to ASE spectra of varied spectral profile and position. In comparison, the situation in QDs is quite different. In the QD ensemble the carrier shuffling processes among the QDs are rather inefficient as compared to the carrier-carrier scattering processes in the bulk and QWs. So the carrier distribution in the QD ensemble is somehow confined to the inhomogeneous broadening profile. In fact, the carriers on the

GS, for example, can redistribute among the QDs with different confinement energy through carrier shuffling. The resulting partially thermalized carrier distribution thus would deviate from the inhomogeneous broadening profile. But this deviation is only significant at low currents. At high currents when the average dot-filling factors are higher than one exciton per QD, the Pauli blocking effect damps the redistribution effect of carrier shuffling process. In this case, the spectral profile of gain coincides approximately with that of self-absorption if any, and both conform to the inhomogeneous broadening profile.

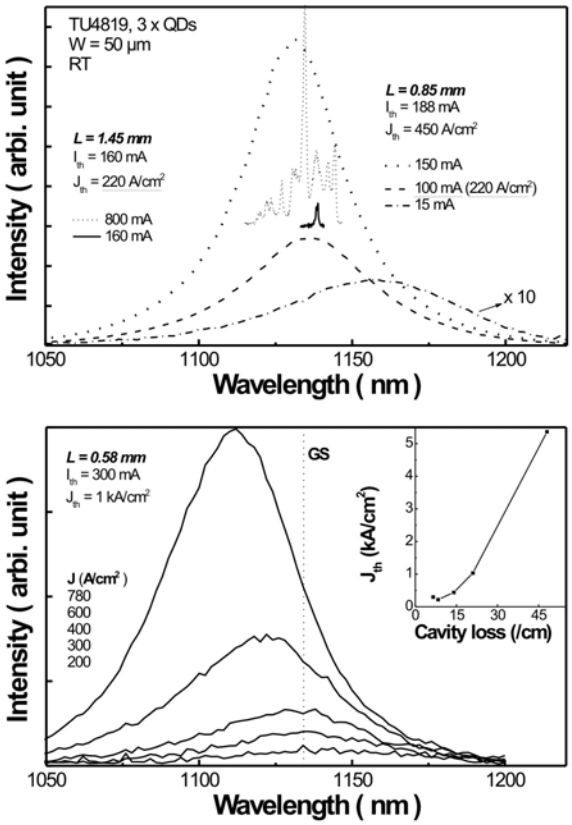

Fig. 1-8 (Top) Emission spectra of 1.14 μm InGaAs QD lasers with different cavity lengths. (Bottom) ASE spectra of a short cavity QD laser. The inset shows the dependence of threshold on the cavity loss.

Fig. 1-8 shows the edge emission spectra as a function of current and the device length. The three devices differ only in the length, equivalently the mirror loss. Among them, the shortest device (L = 0.58 mm) has the highest cavity loss and threshold current density J_{th}~ 1 kA/cm^2. So we can get its ASE spectra up to very high current density without extreme gain amplification near or above threshold. It can be seen that from J = 200 to 400 A/cm^2, the spectral intensity increases with little spectral shift. The spectra centered on the supposed GS center position. These stable spectra demonstrate the case of the coincident spectral profiles of gain and self-absorption in QDs. Above J = 400 A/cm^2, continuous

blue shifts occur due to the strong ES overlap. Here we refer to the RT spectra in Fig. 1-7, where the large inhomogeneous broadening and less pronounced GS gain lead to a continuous transition of maximum gain from GS to ES. The inserted plot of J_{th} vs. cavity loss in Fig. 1-8 shows also a consistent picture of continuous transition. In contrast, in the case with small inhomogeneous broadening, there will be a dip between the peaks of GS and ES, and then the transition would be a jump from the GS maximum to that of ES. In addition, note the high emission ratio of ES to GS in Fig. 1-7 compared to the negligible ratio in Fig. 1-8. This indicates a strong self-absorption at ES that leaves little edge emission out of the device, presumably due to the high degeneracy of ES that requires more carriers to meet transparency condition than GS. Except the side emission, the ES emission is self-absorbed and transformed into heat energy.

For $J < 200$ A/cm^2, the edge emission spectra have deviated spectral profiles. For example, for the 0.85 mm long device, as shown in Fig. 1-8 (bottom), the spectrum at I = 15 mA (J = 33 A/cm^2) has its maximum red shifted far away from the supposed GS center position. Here the spectral intensity at the high energy side may be partly affected by the strong absorption of the ES, but the red shift is mainly originated from the thermal redistribution of carriers among the QDs. The QDs with deeper confinement energy are favored in the redistribution process, so the maximum of absorption bleaching is red shifted, noting that no gain is available at this current density for $J < J_{tran}$~57 A/cm^2. With current, the maximum of the emission spectra will gradually shift back to the GS center position with the gain maximum shifting simultaneously.

Finally, for the two devices with L = 0.85 mm and 1.45 mm, as in Fig. 1-8 (top), we compare their spectra at the same current density J = 220 A/cm^2, which is also the threshold current density for the 1.45 mm long device. The longer device starts lasing near the maximum emission wavelength of the shorter device. At a higher current density of 1.1 kA/cm^2, the lasing width increases around the GS center position, indicating a rather symmetric gain/differential gain profile.

1.3.3 Lasing characteristics

In the following, we analyze the L-I and spectral characteristics, and their temperature dependence.

a) Light-current characteristics

Fig. 1-9a shows the L-I curves for a broad area device at different temperatures. Above 150 K, the external quantum efficiency remains constant with temperature. Below 150 K, the transition to the linear lasing region is prolonged, as shown in the 50 K L-I curve.

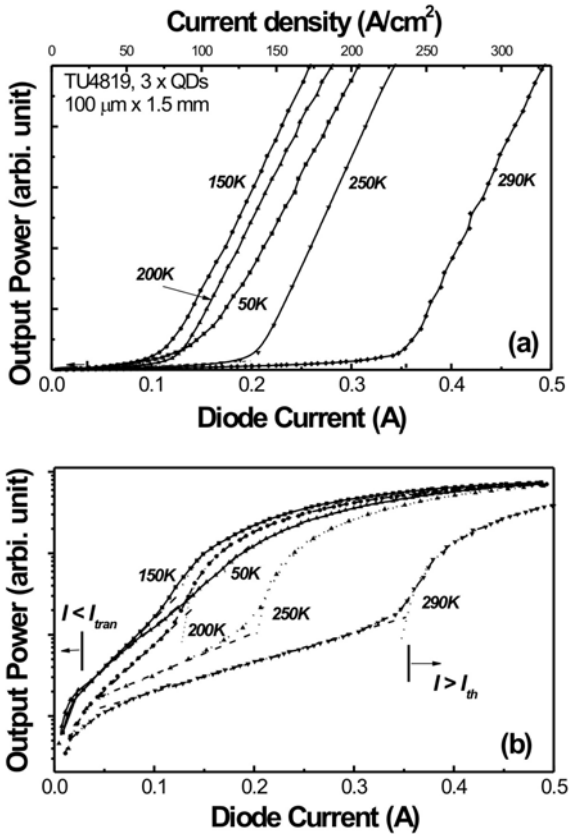

Fig. 1-9 L-I curves of the 1.14 μm InGaAs QD laser. Note the different scales for the power axis.

In Fig. 1-9, we re-plot these L-I curves in semi-logarithmic scale to facilitate the analysis. Now each L-I curve actually shows 3 distinct sections: (A): $I<I_{tran}$; (B): $I_{tran}< I < I_{th}$; (C): $I>I_{th}$.

- Section A

  This part of L-I curve features an exponential increase of emission power followed by the gradual saturation. Since the injection turn-on, the QDs begin to be filled with carriers, and the emission starts, but is limited by self-absorption. With more QDs being filled and joining the emission process, the emission power increases. When most QDs are somehow filled, the emission starts saturation and the transparency condition is approached.

- Section B

This section begins when I_{tran} is reached, and ends when I_{th} is approached. With current, gain appears and ASE power increases exponentially as gain increases. However, the modal gain is below the cavity loss in this section. When the gain meets the loss, the L-I curve experiences a super-exponential transition, then entering the linear region.

- Section C

  This region is characterizes by the linear L-I curve, as shown by the fit lines (dotted line) in the semi-logarithmic plots in Fig. 1-9b.

Above all, the L-I characteristics are strongly temperature dependent. In section A and B, the emission power is clearly suppressed above 150 K, due to the thermal activation of carrier distribution on the higher energy states and possible nonradiative recombination channels thereupon; while below 150 K, the L-I curves coincide well with each other, indicating the quenching of thermionic emission. So above 150 K, both I_{tran} and I_{th} increase with temperature, while I_{tran} changes little below 150 K. However below 150 K, I_{th} decreases with temperature. As can be seen in Fig. 1-9b, in the transition region between section B and C, there is a big reduction of output power from 150 K to 50 K and the transition region is prolonged at 50 K. We know that in this temperature range, the carrier shuffling among QDs is being quenched, so the carriers will be distributed in the QD ensemble just as they are captured. The lower the temperature is, the larger the carrier distribution width will be, and the spectral gain profile is also broadened with decreasing temperature. So at 50 K, the carriers will fill more QDs outside the lasing spectral region in the rather broad spectral gain profile, leading to an effective increase in threshold and enhanced amplified spontaneous emission near the threshold, which smears the transition into the linear region of the L-I curve, i.e. section C.

The temperature dependence of the threshold current density is shown in Fig. 1-10a. There exist generally three temperature regions with distinct features:

- Above 200 K, J_{th} increases exponentially with temperature. This behavior is typical in semiconductor lasers, and can be attributed to the onset of thermionic emission and/or thermal broadening effect. In QD lasers, the carriers can be excited to the ES or just escape from the QDs onto the wetting layer and barrier, where the carriers spill over the cladding layer of the waveguide. The carrier escape/spillover and the following nonradiative recombination make the most of dark and leak

current. They are thermally activated processes that depend strongly on the QD confinement energy and the barrier energy of cladding layers. Fitting this temperature section, we get T_0 = 80 K.

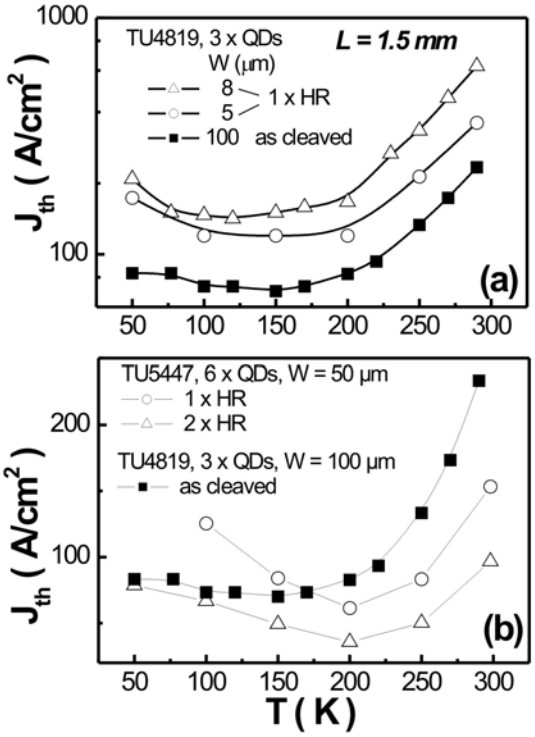

Fig. 1-10 Temperature dependence of threshold current density for various device geometries.

100 K< T <200 K. In this temperature region, J_{th} goes through the minimum, where the nominal T_0 can be infinite. Because the main carrier loss mechanism – thermionic emission and the following nonradiative recombination – is quenched below 200 K, the carrier distribution then is mainly determined by the carrier interdot redistribution (carrier accumulation) and intradot thermalization (carrier dispersion) processes. As denoted, apparently these two processes function reversely in affecting the carrier distribution, so with temperature their effects will cancel each other partly. This in turn helps stabilize the threshold current in certain temperature region. However, for the different thermal activation energy, the carrier intradot thermalization is quenched at relatively lower temperatures than the interdot redistribution does. So with decreasing temperature, the quenching effect of the carrier interdot redistribution at first takes advantage, resulting in enhanced carrier dispersion, which leads to the increase of threshold. Only when the carrier intradot thermalization is also becoming quenched at even lower temperature, both the carrier processes then become comparable again and the tendency of threshold increase is damped. In Fig. 1-10b, the temperature dependence of J_{th} of the 6-fold stacked QD lasers is compared with that of the 3-fold one. The effect of the carrier interdot

redistribution becomes stronger for the increased effective QD area density brought by more QD layers. As a benefit, this may help reduce the threshold at high temperature, but with the quenching of carrier interdot redistribution at low temperature, the benefit turns into a burden, with more QDs consuming carriers without contributing to lasing processes in a broadened spectral gain profile. The result is an enhanced tendency of threshold increase at low temperature. This is of similar physical mechanism as revealed in a simulation study of vertically coupled QD lasers.[60] Note that the higher loss help further enhance this tendency, if comparing the two 6-fold devices with different mirror losses. The negative T_0 region is more evident here than for the 3-fold device.

Below 100 K, the threshold is not so clearly defined for the smeared threshold transition region in the L-I curve, and we get a nominal threshold by extrapolating the good linear part, though this method will overestimate the threshold somehow. Below 100 K, both carrier interdot redistribution and intradot thermalization processes will be strongly quenched, leaving a broad spectral gain profile.

In Fig. 1-9a, we see that the slope efficiency changes rarely with temperature, so the internal quantum efficiency and internal loss (note the RT values of η_{int} ~ 97% and α_i ~ 5.3/cm for the laser structure TU4819) remains constant in the whole temperature range. This indicates a negligible amount of recombination current from thermally activated defect or impurity in the laser active region, and may be interpreted as the merit of QD gain, for the strong carrier localization effect of QDs reduces the chance of carriers being captured in the defect or impurity. In turn, we can also exclude the effect of nonradiative recombination[61] on the T_0 at high temperature. The observed low T_0 (= 80 K) shows rather that both thermionic emission and the hole thermal distribution are working in leading to severe gain saturation at high temperature.[49] As to the smeared threshold transition regions, we observed that for higher threshold gain this peculiar L-I behavior appears at higher temperature. This indicates that at the saturated gain regime, the spectral gain profile is characterized by the inhomogeneous broadening.

b) Spectral characteristics

The center lasing wavelengths near threshold are shown in Fig. 1-11 as a function of temperature. For comparison, the QD GS and ES center wavelengths, drawn from the backside emission spectra, are also shown. The temperature dependence of the GS center wavelengths and the lasing wavelength of the broad area device shows similar trends,

which are typical for this QD ensemble as shown in temperature dependent photoluminescence study on the similar QDs.[34] The red shift of the lasing wavelength from the GS center wavelength can be generally the effect of ES loss, but at high temperature, the effect of thermal gain redistribution among the QDs can be another reason for the red shift, especially at low threshold gain. In Fig. 1-11, the results from two narrow stripe devices show that the lasing wavelengths blue shift with increasing threshold gain. Note that the comparison of threshold current density is shown in Fig. 1-10a for these wide and narrow stripe devices. In Fig. 1-11, the blue shift is particularly strong at high temperature, indicating the reduced thermal redistribution effect with increasing carrier density and specifically the enhanced role of ES gain due to the carrier intradot thermalization.

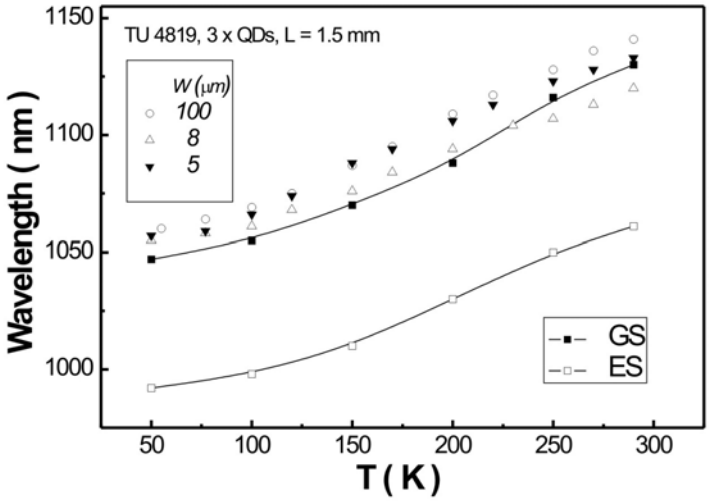

Fig. 1-11 Temperature dependence of lasing wavelengths for the 1.14 μm QD lasers with various stripe widths. The GS and ES emission wavelengths are taken from the backside emission.

Fig. 1-12 shows the lasing spectra at the same injection current I = 1 A (J = 666 A/cm^2) as a function of temperature. The current ratio to threshold ranges from 2.5 at RT to near 10 at low temperature, so the current is well above threshold. It is notable to observe that the lasing width increases continuously from RT, even when the threshold begins to increase below 150 K. This result supports that the spectral gain profile broadens monotonously with temperature decrease, presumably due to the reducing carrier interdot redistribution processes. In Fig. 1-12, the steeper spectral border region at higher temperature implies also a stronger gain suppression effect due to the intense carrier shuffling capability at high temperature.

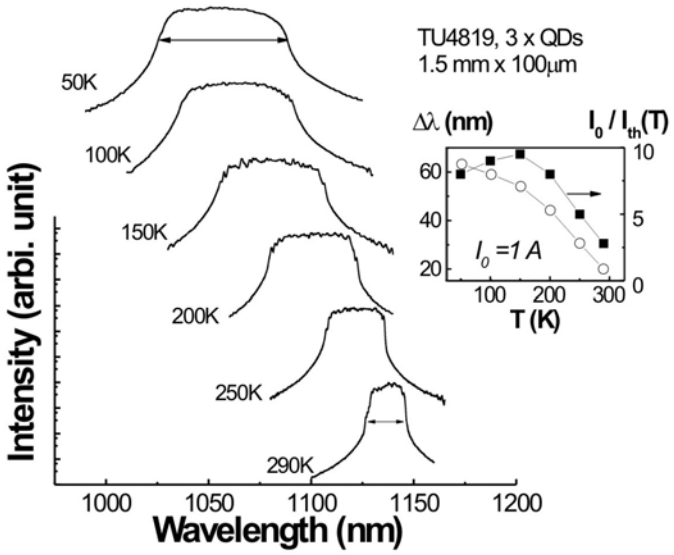

Fig. 1-12 Lasing spectra of the wide stripe QD laser for the same current and at various temperatures. The inset shows the lasing widths and current ratio.

Fig. 1-13 shows the lasing spectra from another wide stripe device that is fabricated in a different process run. These spectra are measured using the photon-counting technique without switching optical filters, and the spontaneous emission is left out. It is clear that the spectra of QD lasers are not necessarily smooth as they are in Fig. 1-12. Note that the low temperature spectra in Fig. 1-13b are slightly affected by the movement of the device, which is cooled in the continuous flowing He cryostat by blowing with temperature-stabilized He gas. For the spectra in Fig. 1-12 and in later chapters of this work, we switch to the Micro cryostat (He) from Oxford Instruments, and mount the sample on the cooling finger to achieve high mechanical stability. Furthermore, we use the Lock-in technique with LN_2 cooled Ge detector and switching optical filters to enhance the detection dynamic range.

In Fig. 1-13, the lasing width varies greatly with temperature. Specifically near threshold, the lasing width at 77 K amounts to ~ 20 nm, but only ~ 1 nm at RT. This broad lasing width at low temperature can be attributed to the broadened gain profile and the weak gain suppression originating from the quenched carrier shuffling, as similar to the case with Fig. 1-12. In addition, the spectral intensity modulations found in Fig. 1-13, sometimes called mode-grouping effects, look rather periodic, with a period ~ 3- 4 nm. The origin of such mode grouping effects will be explored in the next chapter concerning the waveguide effect.

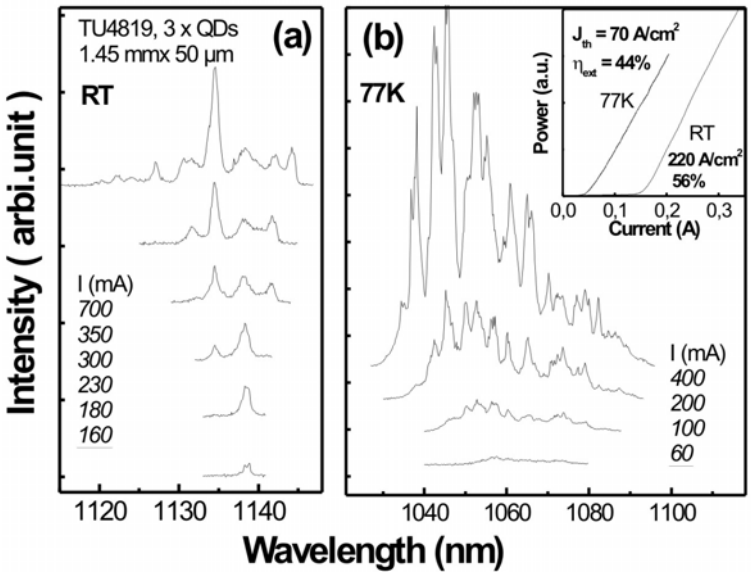

Fig. 1-13 Lasing spectra of the wide stripe QD laser. In (a) the spectra are offset for clarity. The L-I curves for the laser are shown in the inset of (b)

1.4 Laser design for extended temperature stability

Achieving high level of temperature stability will make QD lasers promising for many technically demanding applications. However, the laser design in this respect can be rather involved.

Firstly, the main factors determining T_0 vary in various temperate ranges[62] and they also vary with the threshold gain levels. At high temperatures up to RT or above, the carrier thermionic emission and spillover are the most familiar thermal activated carrier loss processes.[9] Their effects can be shifted to higher temperature by increasing the carrier confinement energy, including both the confining potential in the active layer and the barrier potential of the cladding layer. The carrier confinement can be further enhanced by applying the carrier-reflecting short-period superlattice as barriers.[21,62] As for the threshold gain levels, the gain saturation effects should be avoided or reduced as much as possible, for otherwise they would result in high threshold current density that then cause severe carrier thermal emission losses and significant Auger recombination. To counter the strong GS gain saturation effect originating from the carrier thermal populating on ES and higher energy states, specifically for the holes in InGaAs QDs, p-type modulation doping of the QD active region has been employed to increase the maximum GS gain and differential gain.[63] This approach helps improve T_0 to 232 K (0 – 80 °C) for the 1.3 μm devices while keeping still reasonable low threshold current density.[64] However, a more basic approach to

increase carrier confinement and saturated gain level, is of course to engineer the QD properties within the growth steps. This approach has been intensively studied, though it is still in the early stage. It needs a fundamental understanding of not only the QD parameters with relation to the electronic properties, but also the QD growth mechanisms and the possibility of taking control of them. One example has shown that this approach can be rather promising, and it has produced 1.22 μm InGaAs QD lasers with T_0 = 380 K up to 55°C.[21]

Secondly, there exist indirect factors affecting the temperature stability. For example, we have discussed the canceling effect of carrier interdot redistribution and intradot thermalization processes on the temperature dependence of carrier and gain distribution. This effect could result in temperature stability or negative T_0 at low temperature; however, it is overshadowed at high temperature by the thermionic emission effect. As the hole intradot thermal distribution causes GS gain saturation effect from medium temperature on, the electron thermal distribution would have similar effect at relatively higher temperature due to the larger GS-ES electron energy splitting. Therefore, increasing the QD GS-ES splitting would be advantageous to shift the gain saturation effect of electron thermal distribution to higher temperature. As to the effect of carrier interdot redistribution on the temperature dependent spectral gain, it is the electron side that makes the main contribution, because the electron energy dispersion is much large than that of hole. So to suppress the electron energy dispersion is then a proper way to reduce the temperature dependent effect from carrier interdot redistribution. The growth of more uniform QDs naturally provides less electron energy dispersion, but can be rather demanding on the growth technique. In this context, another hybrid approach is rather direct and effective, that is using tunnel injection scheme.[65] The tunnel injection of cold electrons from the adjacent QW into the QD GS selects only the QDs in a narrow energy range. This reduces dramatically the electron energy dispersion and meanwhile maintains a quasi-Fermi carrier distribution. The originally large amounts of nonequilibrium carriers, not only hot carriers, that make no contribution to lasing process are saved. Actually this injection scheme also eliminates the intradot thermal distribution simultaneously. So double benefits are achieved by one and the same scheme, which has created a record high T_0 of 363 K (5 – 60 °C) in QD lasers.[66] This example shows that the non-ideal parameter effect in actual QD lasers can be overcome by careful design of carrier processes in the active region, and the advantageous aspect of ideal QD properties may be realized, like here ultra high T_0.

Above all, the understanding of raw carrier and gain processes in QD lasers provides the base for advanced design concept. Innovative growth technique will help realize the design concept and also enlarge the design space. It should be noted that, for certain laser applications, the goals of laser design and optimization can be more than only the temperature stability of threshold current. For example, the lasing wavelengths need be stabilized against temperature change, but that may require a different set of design criteria[67] from those for a high T_0. So it remains a big challenge for laser design to achieve a comprehensive temperature insensitive performance in QD lasers. Great flexibility in growth technique would be one prerequisite.

1.5 Summary

In summary, the QD gain properties and their temperature dependent aspects are overviewed. Temperature dependent characteristics of InGaAs QD laser are analyzed. Some considerations on the laser design towards high level of temperature stability are given with examples.

Compared with idealized uniform QDs that have a single confined exciton energy state and δ-function DOS, the self-organized QDs are impacted in their gain properties by many non-ideal QD parameters. The saturated gain levels are lowered due to the finite inhomogeneous broadening and homogeneous broadening effect of exciton transitions, despite the fact that benefiting from the discrete DOS of 3D quantum confinement energy states, the actual QD lasers have demonstrated extremely high materials gain and low internal cavity loss. The carrier thermal populating ES and higher energy states further reduces the GS maximum gain and differential gain levels. The carrier distribution in the QD ensemble is determined by the carrier statistics and thermal redistribution, so the QD spectral gain depends on both temperature and current. The comprehensive action of these carrier and gain processes in the QD ensemble is responsible for the widely varied T_0 in different temperature range and the significant dependence on the cavity loss. In addition to the former discussed linear gain and its nonlinear effect, the gain suppression effects are the gain nonlinearity active in the lasing processes, especially in the multimode lasing case. Both the homogeneous broadening and dynamic grating effect are contributing to the gain suppression coefficient, which is necessary for the modeling of multimode lasing in QD lasers. The strong carrier localization effect by QDs could enhance the gain suppression effect in QD lasers as compared to QW lasers.

Experimentally, true spontaneous emission spectra and ASE spectra are studied as a function of temperature and current. The basic QD parameters are drawn from the low temperature spectra. The temperature effects on the emission spectra help reveal the temperature dependence of carrier distributions and the related QD spectral gain. The analysis of the current dependent spectral profiles of gain and self-absorption shows the influence of dot-filling factors on the result of carrier interdot redistribution. Large inhomogeneous broadening and the suppressed GS gain at high temperature lead to a continuous transition of gain maximum from GS to ES with current.

The L-I characteristics and spectral characteristics are investigated for lasers based on 1.14 μm InGaAs QDs. Three consecutive sections of the L-I curve are recognized as (a) before the transparency; (b) amplified spontaneous emission; (c) above threshold --- lasing. The temperature dependent laser emission power shows clearly the thermal quenching effects above 150 K. Below 150 K, the output power in section (a) and (b) is temperature independent, indicating the quenching of thermionic emission and dark current. However, the section (c) shows that the threshold current increases below 150 K, implying that the spectral gain width increases continuously at low temperature. As to the temperature dependence of threshold current, the carrier thermionic emission and spillover lead to positive T_0 above 200 K; whereas below 200 K, these carrier losses are quenched, and the canceling effect of carrier interdot redistribution and intradot thermalization processes could result in a temperature insensitive region in the medium temperature range. Due to the different thermal activation energy, the quenching temperatures of carrier interdot redistribution and intradot thermalization processes are different, and the carrier distribution effects from these two carrier processes only partially cancel each other, resulting in a negative T_0 at low temperature. As to the spectral characteristics, the lasing width increases continuously with decreasing temperature, confirming the broadening of spectral gain profile at low temperature, due to the quenched carrier shuffling among the QDs.

Advanced laser design concept is desirable for achieving high level of temperature stability in QD lasers. High T_0 (up to 380 K) QD lasers have been obtained in a variety of examples based on different approaches, such as p-type modulation doping[64], tunnel injection[66], and QD shape engineering[21]. These promising results demonstrate that QD lasers have great potential for further improvement in their laser performance. The next big challenge for laser design is to achieve a comprehensive temperature insensitive performance in QD

lasers. For that goal, great flexibility in growth technique would be one prerequisite, and it is necessary to develop innovative QD growth technique.

References:

[1] P. S. Zory, *Quantum well lasers* (Academic Press, Boston, 1993).

[2] M. O. Manasreh, *Strained-Layer Quantum Wells and Their Applications* (Gordon and Breach science publishers, Amsterdam, 1997).

[3] J. P. Loehr and J. Singh, IEEE J. Quantum Electron. **27,** 708-716 (1991).

[4] Y. Arakawa and H. Sakaki, Appl. Phys. Lett. **40,** 939-941 (1982).

[5] L. V. Asryan and R. A. Suris, Semicon. Sci. Technol. **11,** 554-567 (1996).

[6] L. V. Asryan and R. A. Suris, IEEE J. Select. Topics Quantum Electron. **3,** 148-157 (1997).

[7] L. V. Asryan, M. Grundmann, N. N. Ledentsov, O. Stier, R. A. Suris, and D. Bimberg, IEEE J. Quantum Electron. **37,** 418-425 (2001).

[8] L. V. Asryan, M. Grundmann, N. N. Ledentsov, O. Stier, R. A. Suris, and D. Bimberg, J. Appl. Phys. **90,** 1666 (2001).

[9] L. V. Asryan and R. A. Suris, IEEE J. Quantum Electron. **34,** 841-850 (1998).

[10] M. Gurioli, S. Testa, P. Altieri, S. Sanguinetti, E. Grilli, M. Guzzi, G. Trevisi, P. Frigeri, and S. Franchi, Physica E **17,** 19-21 (2003).

[11] D. R. Matthews, H. D. Summers, P. M. Smowton, and M. Hopkinson, Appl. Phys. Lett. **81,** 4904 (2002).

[12] O. B. Shchekin, G. Park, D. L. Huffaker, and D. G. Deppe, Appl. Phys. Lett. **77,** 466-468 (2000).

[13] J. Feldmann, S. Cundiff, M. Arzberger, G. Böhm, and G. Abstreiter, J. Appl. Phys. **89,** 1180-1183 (2001).

[14] J. Urayama, T. B. Norris, J. Singh, and P. Bhattacharya, Phys. Rev. Lett. **86,** 4930-4933 (2001).

[15] R. Heitz, H. Born, F. Guffarth, O. Stier, A. Schliwa, A. Hoffmann, and D. Bimberg, Phys. Rev. B **64,** 241305 (2001).

[16] S. Ghosh, P. Bhattacharya, E. Stoner, J. Singh, H. Jiang, S. Nuttinck, and J. Laskar, Appl. Phys. Lett. **79,** 722-724 (2001).

[17] P. Bhattacharya, T. B. Norris, J. Singh, and J. Urayama, in *Proceedings of SPIE*, 2002 (SPIE--The International Society for Optical Engineering), p. 25-32.

[18] T. Müller, F. F. Schrey, G. Strasser, and K. Unterrainer, Appl. Phys. Lett. **83,** 3572-3574 (2003).

[19] O. Stier, *Electronic and Optical Properties of Quantum Dots and Wires, PhD Thesis* (Wissenschaft und Technik Verlag, 2002).

[20] S. Fafard, Z. R. Wasilewski, C. N. Allen, D. Picard, M. Spanner, J. P. McCaffrey, and P. G. Piva, Phys. Rev. B **59,** 15368–15373 (1999).

[21] V. Tokranov, M. Yakimov, A. Katsnelson, M. Lamberti, and S. Oktyabrsky, Appl. Phys. Lett. **83,** 833-835 (2003).

[22] E. Dekel, D. Gershoni, E. Ehrenfreund, D. Spektor, J. M. Garcia, and P. M. Petroff, Phys. Rev. Lett. **80,** 4991-4994 (1998).

[23] H. Htoon, H. Yu, D. Kulik, J. W. Keto, O. Baklenov, J. A. L. Holmes, B. G. Streetman, and C. K. Shih, Phys. Rev. B **60,** 11026–11029 (1999).

[24] H. C. Schneider, W. W. Chow, and S. W. Koch, Phys. Rev. B: Condens. Matter **64,** 115315 (2001).

[25] M. Lomascolo, A. Vergine, T. K. Johal, R. Rinaldi, A. Passaseo, R. Cingolani, S. Patanè, M. Labardi, M. Allegrini, F. Troiani, and E. Molinari, Phys. Rev. B **66,** 041302(R) (2002).

[26] A. Schliwa, private communication.
[27] Y. Q. Wei, S. M. Wang, F. Ferdos, J. Vukusic, A. Larsson, Q. X. Zhao, and M. Sadeghi, Appl. Phys. Lett. **81,** 1621-1623 (2002).
[28] S. Anders, C. S. Kim, B. Klein, M. W. Keller, R. P. Mirin, and A. G. Norman, Phys. Rev. B **66,** 125309 (2002).
[29] T. K. Johal, G. Pagliara, R. Rinaldi, A. Passaseo, R. Cingolani, M. Lomascolo, A. Taurino, M. Catalano, and R. Phaneuf, Phys. Rev. B **66,** 155313 (2002).
[30] P. M. Varangis, H. Li, G. T. Liu, T. C. Newell, A. Stintz, B. Fuchs, K. J. Malloy, and L. F. Lester, Electron. Lett. **36,** 1544 -1545 (2000).
[31] V. Türck, S. Rodt, O. Stier, R. Heitz, R. Engelhardt, U. W. Pohl, D. Bimberg, and R. Steingrüber, Phys. Rev. B **61,** 9944-9947 (2000).
[32] H. C. Schneider, W. W. Chow, and S. W. Koch, Phys. Rev. B **66,** 041310(R) (2002).
[33] P. Borri, W. Langbein, S. Schneider, U. Woggon, R. L. Sellin, D. Ouyang, and D. Bimberg, Phys. Rev. Lett. **89,** 187401 (2002).
[34] R. Heitz, I. Mukhametzhanov, A. Madhukar, A. Hoffmann, and D. Bimberg, J. Electron. Mater. **28,** 520-527 (1999).
[35] P. Borri, W. Langbein, S. Schneider, U. Woggon, R. L. Sellin, D. Ouyang, and D. Bimberg, QELS (2002).
[36] M. Grundmann and D. Bimberg, Phys. Rev. B **55,** 9740 (1997).
[37] M. Grundmann, R. Heitz, and D. Bimberg, Physics of the solid state **40,** 772-774 (1998).
[38] A. V. Uskov, I. Magnusdottir, B. Tromborg, J. Mørk, and R. Lang, Appl. Phys. Lett. **79,** 1679-1681 (2001).
[39] A. Uskov, A. Jauho, B. Tromborg, J. Mørk, and R. Lang, Phys. Rev. Lett. **85,** 1516-1519 (2000).
[40] E. Tsitsishvili, R. v. Baltz, and H. Kalt, Phys. Rev. B **66,** 161405(R) (2002).
[41] P. Borri, W. Langbein, S. Schneider, U. Woggon, R. L. Sellin, D. Ouyang, and D. Bimberg, Phys. Rev. Lett. **87,** 157401 (2001).
[42] C. Kammerer, C. Voisin, G. Cassabois, C. Delalande, P. Roussignol, F. Klopf, J. P. Reithmaier, A. Forchel, and J. M. Ge´rard, Phys. Rev. B **66,** 041306(R) (2002).
[43] P. Borri, S. Schneider, W. Langbein, U. Woggon, A. E. Zhukov, V. M.Ustinov, N. N. Ledentsov, Z. I. Alferov, D. Ouyang, and D. Bimberg, Appl. Phys. Lett. **79,** 2633-2635 (2001).
[44] K. Matsuda, K. Ikeda, T. Saiki, H. Tsuchiya, H. Saito, and K. Nishi, Phys. Rev. B **63,** 121304(R) (2001).
[45] K. Matsuda, K. Ikeda, T. Saiki, H. Saito, and K. Nishi, Appl. Phys. Lett. **83,** 2250-2252 (2003).
[46] M. Sugawara, K. Mukai, Y. Nakata, H. Ishikawa, and A. Sakamoto, Phys. Rev. B **61,** 7595-7603 (2000).
[47] M. Sugawara, K. Mukai, and Y. Nakata, Appl. Phys. Lett. **74,** 1561-1563 (1999).
[48] N. Kirstaedter, O. G. Schmidt, N. N. Ledentsov, D. Bimberg, V. M. Ustinov, A. Y. Egorov, A. E. Zhukov, M. V. Maximov, P. S. Kop'ev, and Z. I. Alferov, Appl. Phys. Lett. **69,** 1226-1228 (1996).
[49] O. B. Shchekin and D. G. Deppe, IEEE Photon. Technol. Lett. **14,** 1231-1233 (2002).
[50] A. Dikshit and J. M. Pikal, Appl. Phys. Lett. **82,** 4812-4824 (2003).
[51] J. D. Thomson, H. D. Summers, P. M. Smowton, E. Herrmann, P. Blood, and M. Hopkinson, J. Appl. Phys. **90,** 4859-4861 (2001).
[52] E. Herrmann, P. M. Smowton, H. D. Summers, J. D. Thomson, and M. Hopkinson, Appl. Phys. Lett. **77,** 163-165 (2000).

[53] I. P. Marko, A. D. Andreev, A. R. Adams, R. Krebs, J. P. Reithmaier, and A. Forchel, Electron. Lett. **39,** 58 -59 (2003).
[54] S. Schneider, P. Borri, W. Langbein, U. Woggon, R. L. Sellin, D. Ouyang, and D. Bimberg, CLEO (2002).
[55] M. Asada and Y. Suematsu, IEEE J. Quantum Electron. **QE-21,** 434-442 (1984).
[56] M. Yamada and Y. Suematsu, J. Appl. Phys. **52,** 2653-2664 (1981).
[57] H. Jiang and J. Singh, J. Appl. Phys. **85,** 7438 (1999).
[58] B. Peters, J. Hünkemeier, V. M. Baev, and Y. I. Khanin, Phys. Rev. A **64,** 023816 (2001).
[59] R. L. Sellin, C. Ribbat, M. Grundmann, N. N. Ledentsov, and D. Bimberg, Appl. Phys. Lett. **78,** 1207-1209 (2001).
[60] B. Shi and Y. H. Xie, Appl. Phys. Lett. **82,** 4788-4790 (2003).
[61] M. Sugawara, K. Mukai, and Y. Nakata, Appl. Phys. Lett. **75,** 656-658 (1999).
[62] F. Schäfer, B. Mayer, J. P. Reithmaier, and A. Forchel, Appl. Phys. Lett. **73,** 2863-2865 (1998).
[63] O. B. Shchekin and D. G. Deppe, Appl. Phys. Lett. **80,** 2758-2760 (2002).
[64] O. B. Shchekin, J. Ahn, and D. G. Deppe, Electron. Lett. **38,** 712-713 (2002).
[65] L. V. Asryan and S. Luryi, IEEE J. Quantum Electron. **37,** 905-911 (2001).
[66] S. Pradhan, S. Ghosh, and R. Bhattacharya, Electronics Letters **38,** Page(s): 1449 - 1450 (2002).
[67] F. Klopf, S. Deubert, J. P. Reithmaier, and A. Forchel, Appl. Phys. Lett. **81,** 217-219 (2002).

CHAPTER 2 WAVEGUIDE EFFECTS IN QD LASERS

Contents:

2.1 Introduction

A semiconductor laser structure is composed of three necessary elements: the active medium (gain), the waveguide and the optical feedback mechanism (mirror). The waveguide is the critical part that determines the laser output. It is designed to: (1) maximize the overlap of the spatial mode profile with the gain medium, and minimize the overlap with the lossy region, such as the highly doped cladding layers; (2) control the near field profile for the desired far field emission property; (3) control the mode threshold spectrum for desired spectral mode output. The first design criterion is important for keeping low threshold current density and high efficiency. The second criterion facilitates the collection of laser output, for example, for efficient coupling into the optical fiber. Normally in edge emitting lasers, the fundamental mode is the only confined mode when the cutoff property of waveguide is properly designed. The separate confinement laser structure provides the best solution for the fundamental transverse mode confinement and carrier confinement, whereas in the lateral direction, it is difficult to have the optical confinement decoupled from the carrier and current confinement. There are a variety of waveguide forms for the lateral confinement.[1] Among them, ridge waveguides are the most flexible and cost-effective ones. The etched mesa stripe helps define the current injection

area, and provide gain guiding mechanism for the lateral modes. The mesa depths can be varied to suppress the current spreading effect, and induce index guiding for the lateral modes. For sufficiently narrow stripe widths, a single spatial mode laser can be realized, that is, with the fundamental modes being the only existing modes in both the transverse and lateral directions. In a shallow mesa waveguide, the single mode requirement on the stripe widths may be loosed up to 8 μm due to the gain guiding effect.[2,3] The higher order lateral modes are excluded for their higher modal losses. In practice, a weak index guiding mechanism is preferred for a better mode stability, like against the mode hopping effect.

The last design criterion, i.e. spectral control, is rather critical but is also the most demanding one. The extreme case is to have a single longitudinal mode lasing. This generally requires sophisticated fabrication steps to incorporate Distributed Bragg reflector (DBR) or Distributed feedback (DFB) structure in the waveguide and active region. Etching into the gain region usually causes strong nonradiative recombination, and the DFB lasers even need re-growth. These processes deteriorate the laser performance and increase the cost. On the contrary, in the free-running case, there are no such extra processes, and particularly in the conventional lasers such as the bulk and QW ones, the lasing spectra have rather narrow widths, so the spectral characteristics is rarely affected by the ridge waveguide parameters, except for the imperfection or non-uniformity.[4]

The advent of QD lasers changes the situation dramatically. The carrier localization effect makes the QD gain resistant to the surface/defect nonradiative recombination as induced by the etching process. This potentially lifts the technological and cost barrier in engineering the waveguide, including the active region. More significantly, the lasing width of a free-running QD laser is much wider than that of conventional lasers, thus the lasing spectrum is vulnerable to the perturbation of large period modulation structure in the mode threshold gain/loss spectrum, like that originating from the substrate leaky mode.[5] This effectively couples the waveguide parameters with the spectral characteristics in QD lasers. The spatial modal control is no longer irrelevant to the spectral control. The waveguide parameters may have great impact on the longitudinal mode spectrum. In turn, there are more possibilities for realizing the spectral control. Moreover, the large inhomogeneous broadening of QD media not only helps increase the gain width, but also facilitate the spectral hole burning (SHB) effect and increase the sensitivity of gain spectrum to any optical perturbations that may originate from the waveguide effects. Thus

the QD gains provide a unique opportunity to survey the optical properties of laser waveguides, especially those with complex multi-layered heterostructures.

In this chapter, we study the effects of waveguide parameters on the spectral characteristics and other basic laser properties in ridge waveguide QD lasers. The lateral-cavity SHB effects are found to be responsible for the generally reported mode-grouping effects in the lasing spectra of QD lasers. The impact of mesa-etch profiles on the SHB effects is studied with implication for a possible spectral control mechanism in QD lasers. High performance narrow stripe QD lasers with deep etched waveguides are demonstrated, which indicate a cost-effective way for realizing various types of QD devices through direct deep etching technique.

2.2 Lateral-cavity spectral hole burning effects

2.2.1 Background

The spectral characteristics of QD lasers have been intensely studied both experimentally[6-14] and theoretically.[11,14-16] It was observed that the envelope of the longitudinal mode spectrum may exhibit strong intensity modulations despite a smoothly peaking inhomogeneous gain profile. This spectral modulation can be related to the interaction of a QD ensemble with the cavity modes. Detailed understanding of this interaction may provide potentially important information for optimizing of the devices, for instance, improving wavelength control of the lasing spectrum of QD lasers. Several effects have been proposed to explain such modulations. Leaky modes, propagating into the substrate, were claimed as the most probable origin of modulations with a quasi-periodicity of ~ 3-5 nm for a substrate thickness of 100 to 200 μm.[8,12] Alternatively, the peak-to-peak energy separation in the intensity-modulated lasing spectra was related to the homogeneous linewidth of QD transitions at room temperature.[14]

Here a comprehensive study of injection lasing spectra of ridge waveguide QD lasers is present as a function of stripe width, temperature, and excitation density. It is demonstrated that *lateral cavity resonances* causing spectral intensity modulations through SHB, explain the present results as well as may shed extra light on the previously reported data. It is proposed to apply *lateral cavity engineering* to control the emission spectra of QD lasers, e.g., to get wavelength-stabilized narrow spectrum lasers and possibly single-mode injection lasers.

2.2.2 Experiments

The laser structures (TU 4819) studied in this work were grown on GaAs (001) Si-doped substrate using metal-organic chemical vapor deposition (MOCVD).[17] Three layers of In(Ga)As QDs separated by 30 nm GaAs spacers were centered in a 200 nm thick waveguide, which was confined by 1.19 μm thick, p- and n-doped $Al_{0.6}Ga_{0.4}As$ cladding layers. A 350 nm thick p+-doped contact layer completed the growth. The schematics of the laser structure are shown in Fig. 2-1. Ridge waveguide lasers were fabricated by 1.3 μm deep wet etching and covered with 100 nm SiN_x using plasma-enhanced-sputtering. The laser facet SEM picture in Fig. 2-1 shows the etch profile. The wafers were polished down to a thickness of 100 μm from the substrate side. Narrow stripe lasers (stripe width w = 8 and 5 μm) were cleaved and HR coated on one facet, while the facets of wide stripe laser (w = 24, 50 and 100 μm) were left uncoated. The cavity length was 1.5 mm for all devices.

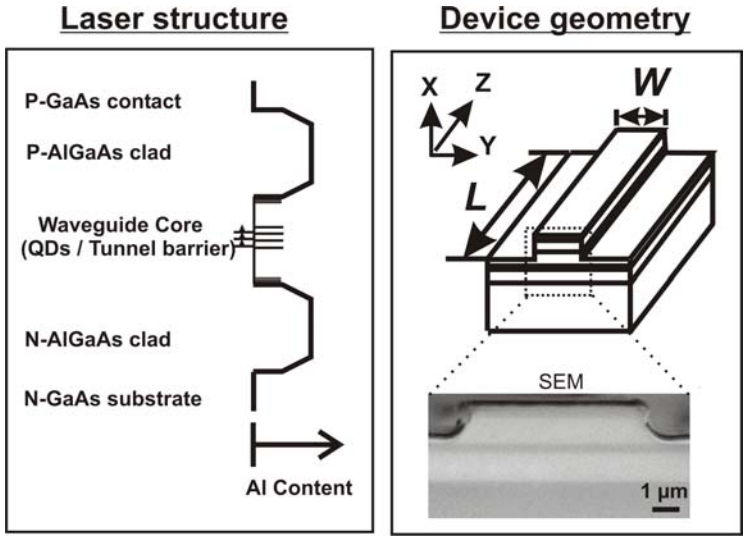

Fig. 2-1 Schematics of the laser structure and ridge waveguide. The SEM picture shows the mesa profile.

Electroluminescence (EL) spectra were taken for temperatures between 50 K and 290 K in a quasi-continuous-wave pulsed mode (500 ns pulse width, 5 kHz repetition frequency) to avoid heating. EL from the uncoated facet was spectrally dispersed by a half-meter monochromator, with the slit oriented parallel to the junction plane, and detected by a cooled Ge diode. Spontaneous EL was measured on a 100 μm long reference device from the substrate side through windows in the back metal contact (refer to the last chapter). The temperature dependence of the ground state (GS) and excited state (ES) transition energies is similar to previously reported PL results showing thermal redistribution within the QD ensemble.[18] For the investigated devices, the GS-ES splitting (~ 60 meV) is of similar size as the inhomogeneous broadening.

2.2.3 Spectral analysis

The spontaneous EL spectra taken from the reference device indicate a conventionally smooth, single-peaked, inhomogeneously broadened transition between the electron GS and several hole states of the QDs (refer to the last chapter). EL spectra taken at 290 K are shown in Fig. 2-2a for lasers of different stripe widths. It is evident that characteristic periods exist, which increase steadily with narrowing stripe widths. The modulation period vs. stripe width dependence is shown in Fig. 2-2b by solid dots. In all the devices threshold current densities were similar, thus one can exclude the effect of homogeneous broadening[14] on the spectral features.

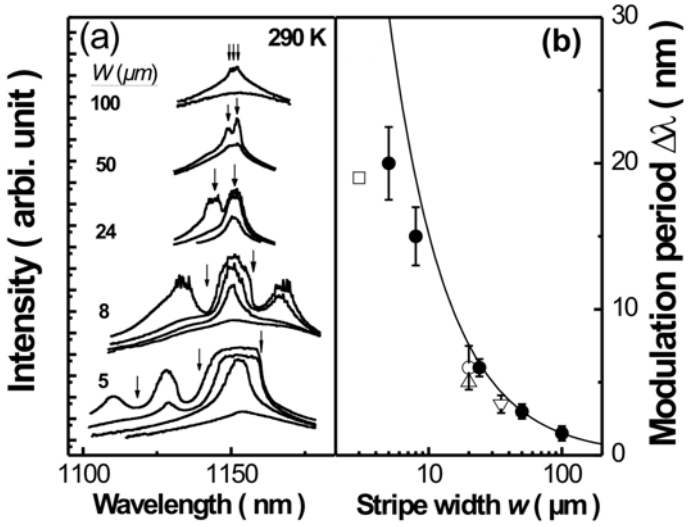

Figure 2-2 (a) EL spectra for different stripe widths. The distance between neighboring arrows present the modulation periods. (b) Modulation period $\Delta\lambda$ in dependence of the nominal stripe width *w*. The solid data points are from this work; other data points from literature (see Ref. 23). The solid line shows the calculated lateral cavity resonance period for λ_0 = 1 μm and n_{eff} = 3.3.

In Fig. 2-3a, lasing spectra at 100 K are compared for two devices (w = 100 μm and 5 μm). For the 100 μm wide stripe device, lasing spectra taken well above the threshold current density show a generally featureless intensity profile. The observed broadband lasing at low temperature is typical for weakly interacting QDs with negligible homogeneous linewidth.[14] Multimode lasing action is observed already at threshold. Lasing of one spectral part of the QD ensemble does not necessarily clamp the gain of the rest of the QDs. In consequence more and more QDs reach the lasing threshold, allowing for lasing in an increasing wavelength range, with increasing drive current. Due to gain saturation and broad size distribution of QDs, the lasing spectrum assumes the observed broad profile at high excitation density. As opposite, the lasing spectra of the 5 μm wide stripe device show strong intensity modulations, with valleys separated by ~ 15-20 nm. For the present substrate thickness of 100 μm, the substrate-leaky-mode related modulation quasi-period

would be ~ 3-5 nm,[8] much smaller than the period found in the experiment. Furthermore, the substrate thickness is the same for all the processed devices, which would imply a constant modulation period in contradiction to our experiments. As can be seen in Fig. 2-2a and Fig. 2-3a, the intensity modulations appear already in the edge emission spectra taken near lasing threshold, and the spectral positions of the valleys do not depend on the drive current. The depth of the valleys also decreases with widening stripes and decreasing temperature (Fig. 2-3b).

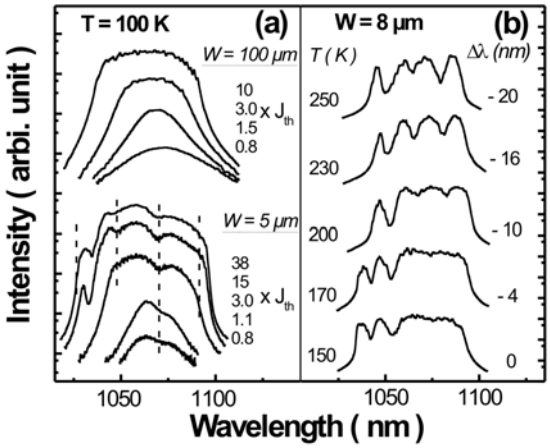

Figure 2-3 (a) Lasing spectra for w = 5 and 100 μm. The dash lines denote the supposed modulation valleys. (b) Lasing spectra for J = 3.8 kA/cm² and different temperatures. For more spectra, see Fig. 2-4.

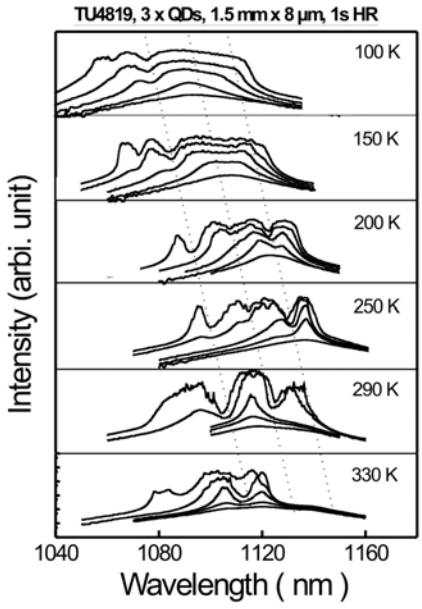

Fig. 2-4 Lasing spectra for the stripe width w = 8 μm. The 3 slanted dotted lines indicate approximately the temperature dependence of spectral valley positions.

The full range of lasing spectra for the stripe width w = 8 μm are shown in Fig. 2-4. The spectral positions of the valleys as a function of temperature are plotted in Fig. 2-5 for the two narrowest devices. With increasing temperature, a collective redshift is observed with periods of ~15 nm and 20 nm for 8 μm and 5 μm stripe width, respectively. The redshift

is, however, much weaker than that of the bandgap. For comparison, the GS emission energy as observed in the backside EL spectra is shown in Fig. 2-5 (open circles).

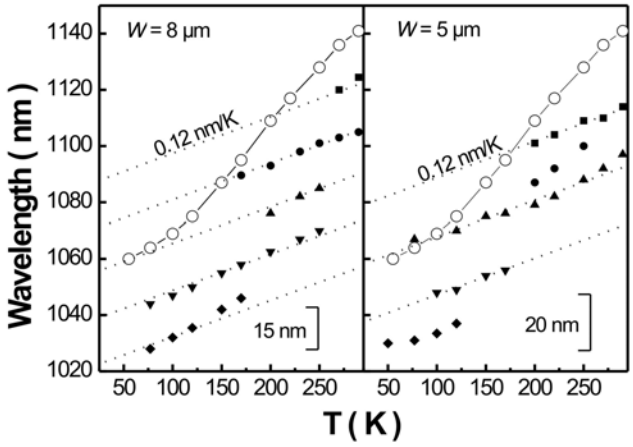

Figure 2-5 Spectral intensity modulation valley wavelengths of narrow-stripe QD lasers as a function of temperature. Fitted are the dotted lines with gradient of 0.12 nm/K, and offset of 15 nm and 20 nm for the stripe width w = 8 µm and 5 µm. The GS energy positions are plotted in open circles.

2.2.4 Discussion

In the following, a mechanism is proposed to explain the observed spectral intensity modulations.

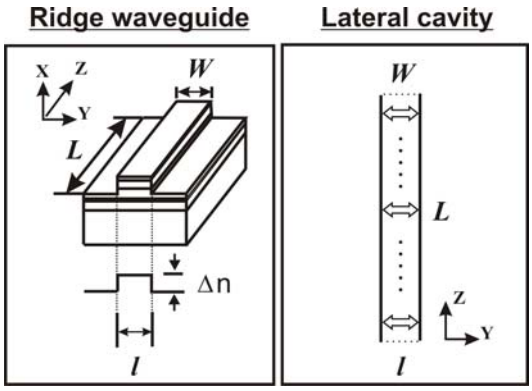

Fig. 2-6 Schematics of ridge waveguide laser and the lateral cavity.

As shown in Fig. 2-6, the steps of the effective refractive index of the ridge waveguide structure introduce lateral waveguiding[19] in the junction plane along the y-axis for the *longitudinally propagating wave* (along the z-axis). However, the ridge stripe also forms a lateral Fabry-Pérot resonator (along the y-axis in Fig. 2-6). The large external losses in such a short cavity prohibit lasing in the lateral direction, but light waves propagating in the waveguide in this same direction, still form standing waves and experience gain, which is sufficient to generate amplified spontaneous emission (ASE) with the lateral-cavity-resonance pattern. Note that this ASE competes for the same gain medium as the longitudinal modes, thus burning holes in the otherwise smooth spectral gain profile of the

longitudinal modes. The resulting suppression of longitudinal modes in these spectral regions causes the intensity valleys in the envelope of the longitudinal mode spectrum. For lateral cavity resonances $n \cdot l \cdot \cos\theta = m \cdot \lambda/2$ must be satisfied, with *n* the effective index, *l* the lateral cavity length, *m* the order of the resonance, λ the light wavelength in vacuum, and $\cos\theta$ ~1. For stripe widths w = 8 μm and 5 μm, n = 3.3, λ = 1 μm, the resonance period ($\Delta\lambda = \lambda^2/(2n \cdot w)$) would be ~18.8 nm and 30 nm, respectively. The nominal stripe width, however, underestimates the lateral gain width in such a shallow-stripe hybrid gain/index-guided laser. Indeed, these periods are slightly larger than the experimental ones. From the experimental periods, effective lateral cavity lengths of ~10 μm and 7.5 μm respectively are derived. This relative large cavity length may be also related to the near normal lateral cavity resonance. With the same parameters as above and dn/dT ~ 4x10^{-4} /K,[20] the temperature coefficient of the resonance wavelengths can be calculated ($d\lambda/dT = \lambda/n \cdot dn/dT$), to be ~ 0.12 nm/K. As shown in Fig. 2-5, the redshift of the valleys with increasing temperature is well described by the calculated temperature coefficient, supporting the modulation to originate from lateral cavity resonances. The periods for devices with wider stripes (w = 100 μm, 50 μm and 24 μm) are also in good agreement with the estimated periods for the lateral cavity. Fig. 2-2b summarizes the present and published results on the modulation period in dependence on the nominal stripe width. The solid line represents the period for an ideal lateral cavity defined by the nominal width of the shallow stripe as shown in the schematics of Fig. 2-2b. The agreement is remarkable, considering the large diversity of devices and processing parameters. Our results thus suggest the *spectral hole burning* effect by lateral cavity resonances to be a general property of ridge waveguide QD lasers. Note that the effect relies on the particular properties of QDs as active medium. Even at room temperature, coupling between the QDs via the wetting layer by thermal emission and recapture is weak compared to the coupling of light with the QDs, enhancing nonlinear effects and allowing for the *spectral hole burning* effect.

The width of the intensity valleys (Fig. 2-2) may be linked to the finesse *F* of the lateral cavity. The full-width-at-half-maximum of the resonances is given by $\delta\lambda = \Delta\lambda/F$. For the current devices the effective refractive index step is small, providing only a low finesse. The modulation depth increases with increasing temperature (see Fig. 2-3b and Fig. 2-4), and that can be attributed to the gain saturation effects. Note that the modulation depth observed at RT is sufficient to turn off lasing. This effect might be valuable for possible

applications. Thus a specific design of the lateral cavity may provide an effective means to control the lasing spectrum of QD lasers. The cavity finesse can be increased, e.g., by etching deeper ridges or introducing etched Bragg mirrors for the lateral cavity, etc. The effective resonance bandwidth can be tuned by gradually tapering the ridge width along the stripe length. Moreover, aperiodic Bragg mirrors and etched antireflection multilayer interference filters can be used to suppress lateral cavity resonances at one particular wavelength. With these methods wavelength-stabilized narrow spectrum QD lasers may be realized. Adapting the narrow spectrum to a particular pump band may provide a simple and cost-efficient way to fabricate high-power narrow band pump lasers with high reliability and low temperature sensitivity. It might even be, probably, possible to obtain wavelength-stabilized single-mode lasing in QD devices with ultra short cavity and deeply etched Bragg mirrors, as recently demonstrated for a quantum well laser. [21] It is interesting to observe that the substrate leaky wave effect is negligible in the investigated laser structures, which make the present study possible. In principle, the substrate leaky wave effect can be thought of as a vertical cavity effect. It is perceptible that the lateral and vertical cavity effects, if combined, would provide a versatile tool for design of QD lasers.

Concerning the speculation on the relation of homogeneous linewidth with the peak-to-peak separation in the lasing spectra of QD lasers,[14] and the relevant simulation work, we refer to the part of discussion on the QD gain nonlinearity in Chapter 1 to resolve this confusing issue.

2.2.5 Conclusion

Spectral intensity modulation in the longitudinal mode spectrum of ridge waveguide QD lasers is shown to result from the SHB effect associated with the lateral cavity resonances. This relevance of the waveguide parameter with the spectral output has profound impact on the waveguide design for the devices based on QD gains, and specifically the lateral cavity effect can be employed as a spectral control mechanism in ridge waveguide QD lasers.

2.3 Impact of mesa etch profiles on the SHB effects

In the last section, the stripe widths of the ridge waveguides are varied, and it happens that the lateral cavity effects are rather strong at the used mesa etch depth (see the SEM picture in Fig. 2-1). In this section, the mesa etch profiles of ridge waveguides are varied, and we

investigate their impact on the lateral-cavity SHB effects and the L-I characteristics of QD lasers.

2.3.1 Experiments

The laser epiwafers are grown on GaAs (001) Si-doped substrate using MOCVD[17]. The GaAs waveguide totals 380 nm thick, centered with 6 (TU 5447) or 3 (Np305I) layers of In(Ga)As QDs separated by 25 nm GaAs spacers. P- and *n*-doped $Al_{0.3}Ga_{0.7}As$ cladding layers in 1 μm thick, and *p*+-doped contact layer in 0.3 μm thick completed the growth. Ridge waveguide lasers are fabricated by direct wet etching mesa into different depths, and other processing steps are the same as in the previous section. In addition, chemically assisted ion beam etching (CAIBE) with Cl_2 is used to fabricate the devices with deep-etched vertical sidewalls. All the devices are HR coated (R ~ 90%) on one facet with another facet left as cleaved (R ~ 30% assumed in the device characterizations below). The cavity length is kept at 1.5 mm for all devices (w = 5-50 μm).

The EL measurement condition is the same as in the previous section. RT photoluminescence spectra of the reference QD samples demonstrate inhomogeneously broadened QD GS emission around 1.14 μm for 6 layer dot sample and 1.1 μm for 3 layer dot sample, with the full-width at half-maximum of 60 meV. The first ES appears at ~ 50 meV higher photon energies.

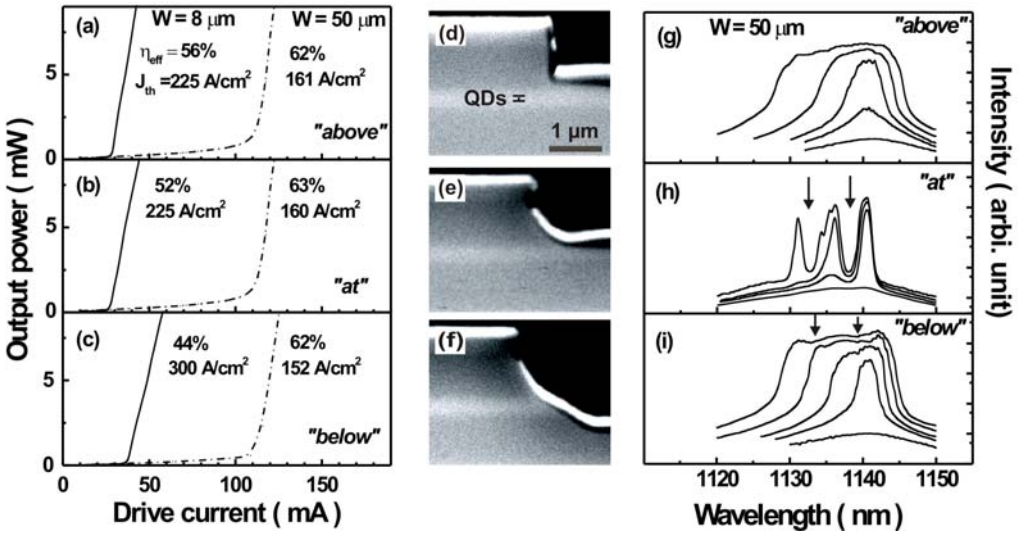

Fig. 2-7 (a-c) L-I curves for lasers with the etching profiles shown in (d-f), respectively; The etching depths are 1.1 μm (d), 1.3 μm (e), and 1.9 μm (f), respectively; (g-i) Lasing spectra of the former lasers with the same stripe width (w = 50 μm). The arrows indicate the modulation valley positions.

2.3.2 Results and discussions

In Fig. 2-7 (a-c, g-i) we show the lasing characteristics of the devices fabricated by the wet-etching approach. These devices are based on 6 layer QDs emitting at 1.14 μm. The secondary electron microscopy (SEM) images of the as-cleaved facets from the devices processed with three different etching depths are shown in Fig. 2-7 (d-f). In one case (Fig. 2-7d), the etching was stopped at about 200 nm above the GaAs waveguide layer ("above"). In the second case, (Fig. 2-7e) the etching was terminated at the waveguide ("at"). In the third case (Fig. 2-7f), the etching was stopped well below ("below") the waveguide layer resulting in extended tilted mesa sidewalls.

We found no significant difference in the L-I characteristics in all three cases. For broad stripe devices (w = 50 μm) all the three different mesa types show similar threshold current density J_{th} (~161 A/cm^2, if using the corrected effective stripe width) and similar differential quantum efficiency η_{eff} as high as 62%. This situation doesn't change down to the stripe widths as narrow as 10 μm. Thus the exposed waveguide layer in the deep mesa case doesn't introduce significant carrier loss due to the nonradiative recombination in surface states. This is consistent with the fact that in the QD active region, the carriers are effectively localized by the deep confinement potential in QDs. It has been shown experimentally that the carrier confinement may help reduce the effective carrier diffusion length at RT down to 0.5 μm in InGaAs QD devices.[22]

In spite of the similarity in the L-I characteristics of the devices fabricated with different mesa etching profiles, their spectral characteristics appear to be completely different. In Fig. 2-7 (g-i), the lasing spectra of the devices with the same stripe width (w = 50 μm) are shown. In the range of comparable injection current density, the sample with shallow etching ("above") profile shows no mode grouping effect. The sample with the "at"-type etching profile shows a remarkable (two orders of magnitude) modulation of the intensity of the lasing spectra. The sample with the "below"-type etching profile shows also a significant intensity modulation. The modulation depth is strong, (about 50 %, note the logarithmic scale in Fig. 2-7 (g-I)), even though it is less pronounced as compared to that of the "at"-type.

The lasing spectra from the devices with the "at"-type mesa geometry are shown in Fig. 2-8a for different stripe widths. The spectral intensity modulation period for w = 50 (24) μm is about 4.7 (8.4) nm, respectively, as can be estimated from the spectral valley separation.

These values are consistent with the lateral-cavity SHB effect[23]. We also estimated the temperature dependence of the valley wavelengths. The temperature gradient is about 0.075 nm/K, the value consistent with that given in the previous study[23], and the temperature dependence of the effective refractive index of the waveguide. For w = 8 μm, the supposed period is expected to be around 30 nm and the second valley can't be resolved even at the highest injection currents (~8 x I_{th}) for the narrow spectral range. The cavity resonances observed in the previous study[23] for the same stripe width and mesa profile can be attributed to the much broader emission spectrum in that case, due to the pronounced modal gain saturation effect caused by a smaller number of QD stacks (3 vs. 6) used therein.

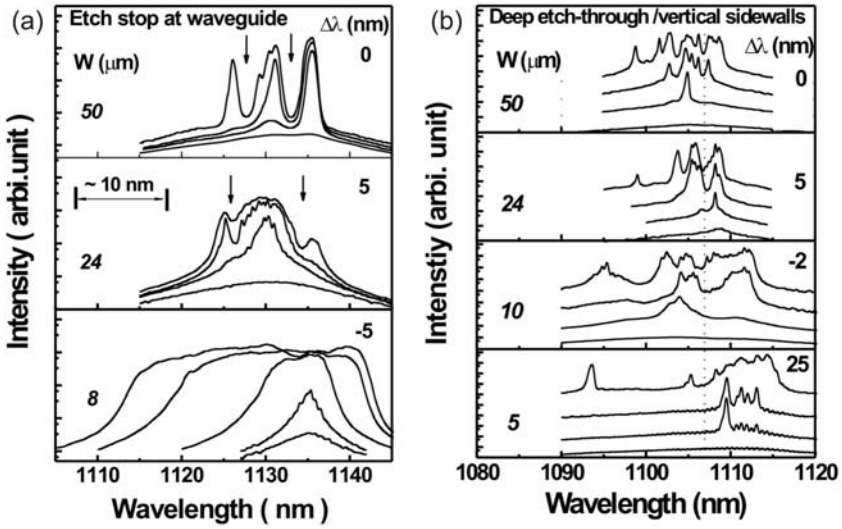

Fig. 2-8 Lasing spectra of lasers with various stripe widths. Note that the spectra are shifted in Δλ for clarity. (a) Mesa etch stopped at waveguide. The arrows indicate the actual or expected modulation valley positions. (b) Deep etched through waveguide with vertical sidewalls.

As to waveguide analysis[24], the shallow mesa ("above"-type) geometry can be treated perturbatively in the frame of the effective refractive index method. We conducted guided mode simulations with the actual waveguide parameters (Beam propagation method). The effective index for the full waveguide structure without any etching is found to be n_{eff} = 3.34, and the corresponding effective refractive index step Δn_{eff} = 1.3 x 10^{-3} for the "above"-type mesa profile. This index step is sufficient for lateral optical confinement of the lasing modes.[19] Using this value, we can calculate the quality factor Q for the lateral FP cavity resonances as follows[25]:

$$Q = 2\pi c/\lambda \cdot t_p = 2\pi n_{eff}/(\lambda \cdot \alpha) \qquad (2\text{-}1)$$

with c, λ the light velocity and wavelength in vacuum, t_p the photon lifetime, and α the total cavity loss of the lateral cavity. To get the total cavity loss, we use the following formulas:

$$\alpha = \alpha_i + \alpha_{mirror} \approx \alpha_{mirror}, (\alpha_{mirror} >> \alpha_i \sim 2\ cm^{-1}) \quad (2\text{-}2)$$

$$\alpha_{mirror} = -\ln(R_1 \cdot R_2)/(2w) = -\ln R/w, (R1 = R2 = R) \quad (2\text{-}3)$$

$$R = ((n_1-n_2)/(n_1+n_2))^2 \approx 1/4(\Delta n_{eff}/n_{eff})^2. \quad (2\text{-}4)$$

with α_i the internal loss, α_{mirror} the mirror loss, and R the reflectivity due to the effective index step. By taking w = 50 μm and λ = 1.1 μm, the quality factor Q is calculated to be ~ 60, and the corresponding resonance line width $\delta\lambda = \lambda/Q \sim 18$ nm for the lateral FP cavity in the "above" -type device. This resonance line width is much larger than the resonance period (~ 5 nm) or the free spectral range $\Delta\lambda$ of a 50 μm long FP cavity, consistent with the absence of the resonance structure in Fig. 2-7g.

We consider another extreme case, that is a deep etched through waveguide mesa with vertical sidewalls. Take the mode reflectivity at the mesa edge R ~ 0.3, similar to that of as-cleaved facets, we get Q ~ 600, $\delta\lambda$ ~ 1.8 nm with other parameters the same as used above. So in this case, the resonance structures could be well pronounced in the lasing spectra with sharp features as narrow as 1.8 nm. We will discuss this case later. However, the "at"-type mesa profile presents an intermediate case between the shallow mesa geometry ("above"-type) and the deep etched through waveguide with vertical sidewalls. The deep etch reached the waveguide layer, so it prevents us from calculating the reflectivity by considering any effective index step unambiguously. But we may estimate the Q factor from the resonance feature in Fig. 2-7h. The apparent line width amounts to about ~ 2-3 nm, so the Q factor can be estimated to be less than ~ 360 - 540, if considering the nonlinear nature of the SHB effect.

For the tilted sidewall mesas (see Fig. 2-7f), the refractive index step is even larger than for the "at"-type mesa geometry. This causes a significant intensity modulation. However, due to the tilting of the sidewalls, the effective reflectivity is reduced, similar to the case of the tilted facets in the analysis by Iga et al.[26] This reduces the intensity modulation to ~ 50 %.

In Fig. 2-9a we show L-I characteristics of the devices with deep etched through waveguide featuring vertical sidewalls. These devices are based on 3 layer QDs emitting at

1.1 μm. Threshold current density and differential efficiency are a weak function of the stripe width. For w = 5 μm, (not shown here) the threshold current density increases to ~200 A/cm^2, due to the switching to the QD ES lasing, the effect we attribute to the increased scattering losses, which may originate from the dry etching process and the non-uniformity at the mesa edge introduced by the photolithography step for narrow stripes (w ≤ 8 μm in our case) causing extra scattering loss. As it is shown recently, threshold current density (~ 100 A/cm^2) and differential efficiency of dry-etched-through ridge waveguide QD lasers may remain unaffected down to the stripe width of 4 μm.[27]

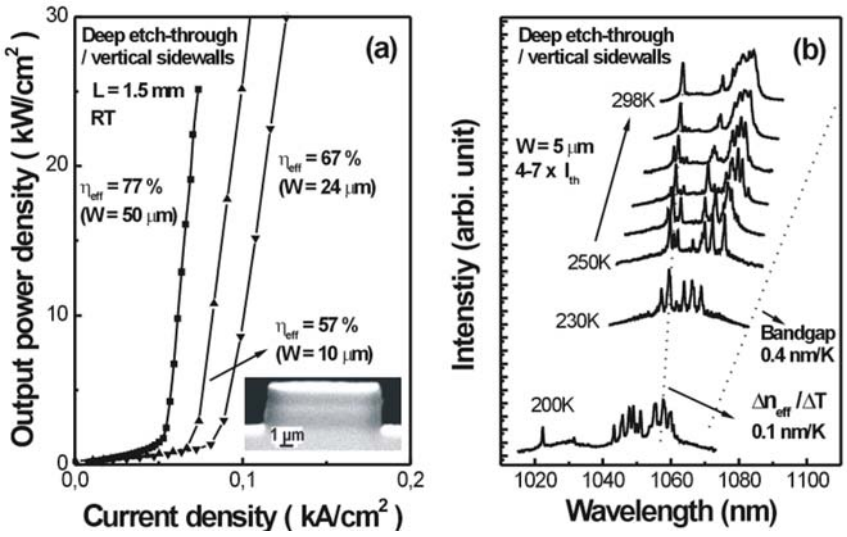

Fig. 2-9 (a) L-I curves of lasers with deep etched through waveguide and vertical sidewalls. The inset shows the SEM of the typical mesa profile. (b) Lasing spectra of the narrow stripe laser. The dotted lines indicate the temperature dependence for the band gap and the effective refractive index.

In spite of the good L-I characteristics, these vertical-sidewalled devices show a spectral behavior completely different from that for the devices with the "at"-type mesa etch profile as well as for those with tilted sidewalls. As can be seen in Fig. 2-8b, the lasing spectra feature strong intensity modulation, exceeding 2-3 orders of magnitude. Meanwhile, the characteristic valley separation appears to be much smaller as compared to that from the lateral cavity resonances. In addition, it is observed (Fig. 2-9b) that with temperature, the well-reproducible sharp spectral features exhibit a wavelength shift defined by the temperature dependent refractive index change. From the last point, we may pin down that these spectral features also originate from the cavity resonance effect. Compared to the previous estimated quality factor (Q ~ 600) and the resonance line width (δλ ~ 1.8 nm) for a 50 μm wide device, the spectra in Fig. 2-8b show even sharper features, indicating even higher Q factors. It is comprehensible that, in the present case, the devices with deep-etched vertical sidewalls may form modes specific to rectangular

resonators. High Q-factor resonance modes in such resonators are formed via the total internal reflection (TIR) at all the resonator boundaries. For example, these modes in rectangular resonators have attracted much interest for add-drop filter applications in dense wavelength-division multiplexing.[28] These TIR modes have ray trajectories tilted with respect to the direction of the lateral FP cavity, leading to reduced spectral separations as compared to the lateral FP modes. Superimposed to the normal lateral FP cavity resonances, they contribute to extra SHB features of shorter modulation periods in the gain spectra, causing more complicated intensity modulation pattern in the lasing spectra. At the same time, as it follows from Fig. 2-8b, there is a general trend of increased modulation periods with reduced stripe widths. This supports the interpretation of the spectral features as related to the SHB effect induced by the rectangular cavity. Concerning the rectangular waveguide, we refer to Chapter 6 for the detailed study.

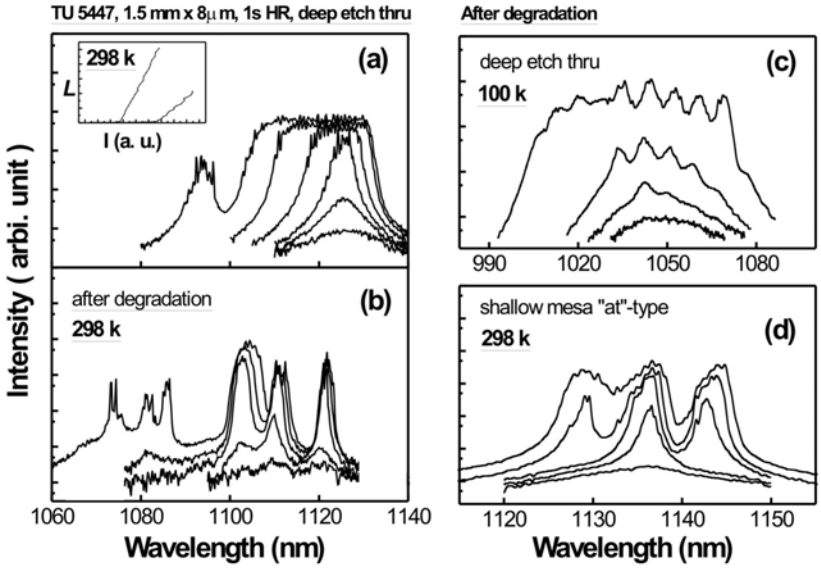

Fig. 2-10 (a-c) Lasing spectra of one QD laser with deep wet-etched through waveguide. The inset shows the L-I curves before and after degradation. (b, c) measured after the device breaks down at high currents. (d) Lasing spectra after the degradation of the shallow mesa 8 μm wide device as in Fig. 2-8a.

Finally it is emphasized that certain unintentional perturbations can cause the spectral intensity modulations as well. Like in Fig. 2-10a, for one narrow stripe device with a deep wet-etched mesa profile as in Fig. 2-7f, the lasing spectra show only one valley at high current, consistent with the large modulation period ~ 30 nm for the stripe width w = 8 μm. However, the laser breaks down at very high currents, as evidenced by the deteriorated L-I characteristics shown in the inset of Fig. 2-10a. Correspondingly the lasing spectra change dramatically. Now the spectra move to higher energy, presumably due to the high loss caused by the degradation process. The open waveguide of this deep mesa laser can be rather vulnerable to the high voltage impact, though covered by a 100 nm thick SiN_x

dielectric layer. We attribute the rare breakdown case to the imperfections or non-uniformity in the dielectric layer or waveguide. From the periodic modulation structures as clearly seen in the low temperature spectra (Fig. 2-10c), it may be inferred that the characteristic length of the waveguide region as affected by the breakdown lies at around 50 μm. In Fig. 2-10b, the high energy groups of peaks in the RT spectra originate from the QD ES. We found there some valleys are inconsistent with the supposed periodic modulation structures. This reflects the complex energy level structures of the QD ES, and also helps explain the inconsistent valley positions at high energy regions in Fig. 2-3, 4, and 5. We note that the electrical breakdown in waveguide is not a necessary condition for the change of spectra. In Fig. 2-10d, the lasing spectra of the same 8 μm wide laser as in Fig. 2-8a show again spectral modulations. But in this case, the L-I characteristics show only a slight degradation after applying very high current to the device. The cavity loss seems remain constant because the threshold lasing wavelengths ~ 1135 nm are the same before and after the degradation. This different laser degradation behavior can be related to different material variations under the electrical impact. Above all, these spectrum variations testify that the waveguide is responsible for the spectral intensity modulations in the lasing spectra of QD lasers. The lateral cavity effect indirectly induces the spectral modulation, but the degradation-related waveguide variations directly modulate the mode threshold gain/loss spectrum, just like in the coupled cavity lasers.

2.3.3 Conclusion

The present study demonstrates the crucial impact of the mesa etching profiles on the spectral characteristics of ridge waveguide lasers based on self-organized In(Ga)As QDs, with identical L-I characteristics. In addition to the general lateral-cavity SHB effect, we found extra spectral intensity modulation features in the emission spectra of deep-etched-through devices with vertical sidewalls. These features are related to the SHB effect induced by the high Q-factor TIR resonance modes in the rectangular resonators. The present results will help extend the possibility for the spectral engineering in QD lasers.

2.4 High performance narrow stripe QD lasers with deep etched waveguide

2.4.1 Introduction.

Long-wavelength GaAs-based QD lasers[29] offer unique advantages for applications in data- and telecommunications[30]. Lasers based on self-organized InAs QDs have demonstrated very low threshold current density (16 A/cm^2)[31] and a transparency current density of 6 A/cm^2 per dot layer[32], high efficiency and high temperature stability of the threshold

current[33]. An important advantage of QD-based structures is suppressed spreading and surface recombination of nonequilibrium carriers in deep mesa structures down to submicrometer sizes[34]. Suppressed role of nonequilibrium carrier spreading also follows from realization of ultralow threshold current densities in oxide-confined narrow-stripe devices[35], and is important for the recently observed suppression of filamentation of the fundamental mode[36]. These advantages lead us to raise the question whether high-quality deep-mesa QD lasers with open waveguide suitable for high refractive index contrast distributed feedback (DFB) and photonic crystal QD lasers can be realized.

2.4.2 Experiments

The laser structures (Ioffe 4924) were grown by solid source molecular beam epitaxy (MBE) in a Riber 32P machine. Ten layers of 2.5 ML InAs QDs covered by 5 nm-thick $In_{0.15}Ga_{0.85}As$ QW in the GaAs matrix were formed in the active region. The spacer layer thickness between the QD planes was 30 nm. Detailed description of the MBE growth and properties of such QDs is presented elsewhere[37]. An $Al_{0.13}Ga_{0.87}As$ waveguide of 0.6 μm thickness and 1.5 μm-thick *Si*- and *Be*-doped $Al_{0.7}Ga_{0.3}As$ cladding layers were used. In the following laser diodes based on these 10-fold stacked QDs were investigated. They were processed into shallow or deep mesa stripes of different widths and a cavity length of 1.5 mm. The L-I characteristics are measured in the same condition as in the former sections.

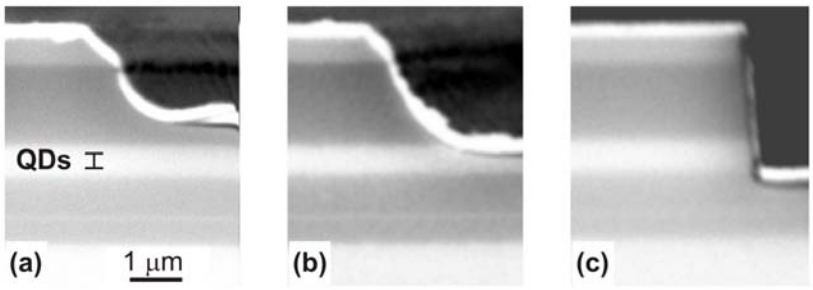

Fig. 2-11 SEM images of various mesa etch profiles. (a, b) wet etching. (c) dry etching

2.4.3 Results and discussion

In Fig. 2-11 we show the SEM images of the mesa structures investigated. In two cases (Fig. 2-11a, 11b) a wet etching technique was applied to define the laser stripe. In one case the etching was stopped at about 0.4 μm above the waveguide (Fig. 2-11a). In the other case, the etching profile entered the $Al_{0.13}Ga_{0.87}As$ waveguide region (Fig. 2-11b). Deep-mesa structures were processed using a dry etching technique (CAIBE with Cl_2), and the process was stopped after 0.4 μm of the bottom $Al_{0.7}Ga_{0.3}As$ cladding layer was etched-off.

We refer to these designs as to "shallow", "medium" and "deep" mesa lasers. Devices with stripe widths of 8 μm, 10 μm, 24 μm, 50 μm and 100 μm were fabricated and tested. The cavity length was fixed at 1.5 mm. A high reflectivity coating (R ~ 90%) was deposited on the rear facet, while the front facet remained not coated (R ~ 30% assumed in the following characterization). Broad area devices (50-100 μm) demonstrated comparable threshold current densities of 80-100 A/cm^2, being slightly lower (~20%) for medium and deep-etched mesa. Internal quantum efficiency and waveguide losses for broad area devices were close to 100% and 1.5 cm^{-1}, respectively[33], as drawn from the measurements on the devices with different lengths. Characteristic temperature was 150 K in the temperature range 20-55°C. The emission wavelength ranges between 1.28 – 1.3 μm[33].

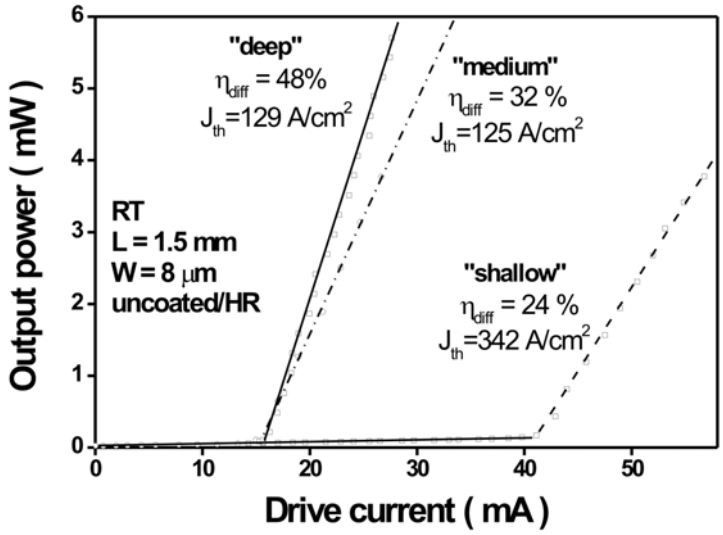

Fig. 2-12 L-I curves for lasers with etching profiles as in Fig. 2-11: (a) shallow, (b) medium, (c) deep.

For narrow stripe widths (8-30 μm), a remarkable difference in the performance of the devices processed with different approaches was found. In Fig. 2-12 we show the L-I characteristics of the devices. Maximum external differential efficiency 50% (note all the external differential efficiency values in this work refer to the output from both facets) was observed for a deep mesa laser, even though the threshold current densities were fairly close in the cases of "deep" and "medium" mesa devices (129 A/cm^2 and 125 A/cm^2, respectively). Lower external differential efficiency of the "medium" mesa laser may be related to a higher scattering loss due to slightly inferior uniformity of the wet-etching process. The performance of the shallow mesa device was significantly worse in the case of the narrow stripe widths. The typical threshold current density of the devices was higher (>300 A/cm^2) and the external differential efficiency was lower (24%) for 8 μm-wide devices. We attribute these observations to the current spreading resulting in effectively broader stripe width on one side, and less uniform carrier injection on the other.

2.4.4 Conclusions

Realization of low-threshold high-efficiency deep mesa QD lasers open unique opportunities in device engineering. Fabrication of DFB lasers by single-step direct dry etching through lithographic masks becomes possible. Integrated diode laser based systems involving photonic crystals become possible using QDs[38] as active media of the devices.

2.5 Summary

In this chapter, we address the waveguide effects in QD lasers. The spectral intensity modulations in the lasing spectra are related to various waveguide parameters. In ridge waveguide lasers with mesa etched near to or in the waveguide, the lateral cavity resonances associated with the ridge widths cause periodic modulations through spectral hole burning in the spectral gain spectrum of longitudinal modes. In lasers with mesa etched through waveguide, the spectral characteristics are impacted by more cavity resonance modes including high-Q TIR modes in the virtually open rectangular laser cavity. Importantly the laser performance is found not being affected by the open waveguide surface that usually can induce strong surface/defect recombination in conventional lasers. Moreover, narrow stripe QD lasers with deep etched open waveguide are demonstrated to have better laser performance than those with shallow or medium mesa etch depth. These experimental results indicate that optical waveguide design in QD devices can be exploited for the spectral or wavelength control, and various waveguide structures can be realized in a cost-effective way by using novel techniques, such as direct etching through waveguide without inducing deleterious effects on the device performances. Different application area of QD lasers could benefit from such flexibility in laser design, fabrication and spectral property control. The QD amplifiers can benefit from the easier light coupling and overlap with the well-defined gain region confined in the deep etched waveguide. The design of laser waveguide and QD gain can be coupled to provide a unique way to realize a QD laser with desirable spatial and spectral output profiles.

Finally, Note that in Section 3.3 of Chapter 3, the nonlinear dynamics origin of the waveguide effects is revealed in the time-resolved study of the spectrum intensity modulations. This supports the spectral hole burning effect of cavity resonances modes as being responsible for the spectral modulations.

Reference:

[1] L. A. Coldren and S. W. Corzine, *Diode Lasers and Photonic Integrated Circuits* (Wiley, New York, 1995).

[2] N. Chinone and M. Nakamura, in *Part C, Secmiconductor injection lasers, II / Light-emitting diodes*, edited by W. T. Tsang (Academic press, Orlando, 1985), p. 61-91.
[3] R. J. Nelson and N. K. Dutta, in *Part C, Secmiconductor injection lasers, II / Light-emitting diodes*, edited by W. T. Tsang (Academic press, Orlando, 1985), p. 1-59.
[4] F. H. Peters and D. T. Cassidy, Appl. Phys. Lett. **57,** 330-332 (1990).
[5] E. V. Arzhanov, A. P. Bogatov, V. P. Konyaev, O. M. Nikitina, and V. I. Shveikin, Quantum Electronics **24,** 581-587 (1994).
[6] Q. Xie, A. Kalburge, P. Chen, and A. Madhukar, IEEE Photon. Technol. Lett. **8,** 965 -967 (1996).
[7] S. V. Zaitsev, N. Y. Gordeev, V. M. Ustinov, A. E. Zhukov, A. Y. Egorov, M. V. Maksimov, A. F. Tsatsul´nikov, N. N. Ledentsov, P. S. Kop´ev, Z. I. Alferov, and D. Bimberg, Semiconductors **31,** 455-459 (1997).
[8] E. P. O'Reilly, A. I. Onischenko, E. A. Avrutin, D. Bhattacharyya, and J. H. Marsh, Electron. Lett. **34,** 2035-2037 (1998).
[9] L. Harris, D. J. Mowbray, M. S. Skolnick, M. Hopkinson, and G. Hill, Appl. Phys. Lett. **73,** 969-971 (1998).
[10] A. Patanè, A. Polimeni, M. Henini, L. Eaves, P. C. Main, and G. Hill, J. Appl. Phys. **85,** 625 (1999).
[11] D. Bhattacharyya, E. A. Avrutin, A. C. Bryce, J. H. Marsh, D. Bimberg, F. Heinrichsdorff, V. M. Ustinov, S. V. Zaitsev, N. N. Ledentsov, P. S. Kop'ev, Z. I. Alferov, A. I. Onischenko, and E. P. O'Reilly, IEEE J. Select. Topics Quantum Electron. **5,** 648-657 (1999).
[12] A. Patanè, A. Polimeni, L. Eaves, M. Henini, P. C. Main, P. M. Smowton, E. J. Johnston, P. J. Hulyer, E. Herrmann, G. M. Lewis, and G. Hill, J. Appl. Phys. **87,** 1943-1946 (2000).
[13] D. J. Mowbray, L. Harris, P. W. Fry, A. D. Ashmore, S. R. Parnell, J. J. Finley, M. S. Skolnick, M. Hopkinson, G. Hill, and J. Clark, Physica E **7,** 489-493 (2000).
[14] M. Sugawara, K. Mukai, Y. Nakata, H. Ishikawa, and A. Sakamoto, Phys. Rev. B **61,** 7595-7603 (2000).
[15] H. Jiang and J. Singh, J. Appl. Phys. **85,** 7438 (1999).
[16] H. Huang and D. G. Deppe, IEEE J. Quantum Electron. **37,** 691-698 (2001).
[17] R. L. Sellin, C. Ribbat, M. Grundmann, N. N. Ledentsov, and D. Bimberg, Appl. Phys. Lett. **78,** 1207-1209 (2001).
[18] R. Heitz, I. Mukhametzhanov, A. Madhukar, A. Hoffmann, and D. Bimberg, J. Electron. Mater. **28,** 520-527 (1999).
[19] I. P. Kaminow and R. S. Tucker, in *Guided-Wave Optoelectronics*, edited by T. Tamir (Springer-Verlag, Berlin, 1988), p. 211-315.
[20] S. Adachi, J. Appl. Phys. **58,** R1-R29 (1985).
[21] M. Kamp, J. Hofmann, A. Forchel, and S. Lourdudoss, Appl. Phys. Lett. **78,** 4074-4075 (2001).
[22] J. K. Kim, T. A. Strand, R. L. Naone, and L. A. Coldren, Appl. Phys. Lett. **74,** 2752-2754 (1999).
[23] D. Ouyang, R. Heitz, N. N. Ledentsov, S. Bognar, R. L. Sellin, C. Ribbat, and D. Bimberg, Appl. Phys. Lett. **81,** 1546-1548 (2002).
[24] G. P. Agrawal and N. K. Dutta, *Semiconductor lasers*, 2nd ed. (Van Nostrand Reinhold, New York, 1993).
[25] A. Yariv, *Quantum Electronics*, 3rd ed. (John Woley & Sons, New York, 1988).
[26] K. Iga, K. Wakao, and T. Kunikane, Appl. Opt. **20,** 2367-2371 (1981).
[27] M. Kuntz, M. Lämmlin, A. R. Kovsh, and D. Bimberg, private communication (2003).
[28] A. W. Poon, F. Courvoisier, and R. K. Chang, Opt. Lett. **26,** 632 (2001).

[29] D. L. Huffaker, G. Park, Z. Zou, O. B. Shchekin, and D. G. Deppe, Appl. Phys. Lett. **73,** 2564-2566 (1998).
[30] N. N. Ledentsov, IEEE J. Select. Topics Quantum Electron. **36,** 1272-1279 (2002).
[31] G. T. Liu, A. Stinz, H. Li, T. C. Newell, A. L. Gray, P. M. Varngis, K. J. Malloy, and L. F. Lester, IEEE J. Quantum Electron. **36,** 1272-1279 (2000).
[32] D. Bimberg, in *Quantum Dots: Lasers and Amplifiers*, Tokyo, Japan, 2002 (IOP Publishing Ltd), p. 485-492.
[33] A. R. Kovsh, N. A. Maleev, A. E. Zhukov, S. S. Mikhrin, A. P. Vasil´ev, Y. M. Shernyakov, M. V. Maximov, D. A. Livshits, V. M. Ustinov, Z. I. Alferov, N. N. Ledentsov, and D. Bimberg, Electron. Lett. **38,** 1104-1105 (2002).
[34] N. N. Ledentsov, M. V. Maximov, P. S. Kop'ev, V. M. Ustinov, M. V. Belousov, B. Y. Meltser, S. V. Ivanov, S. V. A., Z. I. Alferov, M. Grundmann, D. Bimberg, S. S. Ruvimov, W. Richter, P. Werner, U. Gösele, U. Heidenreich, P. D. Wang, and C. M. Sotomayor Torres, Microelectronics Journal **26,** 871-879 (1995).
[35] G. Park, O. B. Shchekin, D. L. Huffaker, and D. G. Deppe, IEEE Photon. Technol. Lett. **12,** 230-232 (2000).
[36] C. Ribbat, R. L. Sellin, I. Kaiander, F. Hopfer, N. N. Ledentsov, D. Bimberg, I. P. Kaminow, R. S. Tucker, A. R. Kovsh, V. M. Ustinov, A. E. Zhukov, and M. V. Maximov, Appl. Phys. Lett. **82,** 952–954 (2003).
[37] M. V. Maximov, A. F. Tsatsul'nikov, B. V. Volovik, D. S. Sizov, Y. M. Shernyakov, I. N. Kaiander, A. E. Zhukov, A. R. Kovsh, S. S. Mikhrin, V. M. Ustinov, Z. I. Alferov, R. Heitz, V. A. Shchukin, N. N. Ledentsov, D. Bimberg, Y. G. Musikhin, and W. Neumann, Phys. Rev. B **62,** 16671-16680 (2000).
[38] D. Bimberg, M. Grundmann, and N. N. Ledentsov, *Quantum Dot Heterostructures* (Wiley, Chichester, 1998).

CHAPTER 3 TIME-RESOLVED LASING SPECTRA OF QD LASERS

Contents:

3.1 Introduction

In the previous part of this thesis work, we only pay attention to the spectral characteristics of QD lasers in time averaged format. Since this chapter, we also take account of their temporal aspects, and the time-resolved studies of the lasing spectra of QD lasers are presented. Time-resolved studies reveal dynamic information of spectral modes that are complementary to time-averaged studies. Thus the manifold dynamic behaviors of QD lasers can be surveyed, and the underlying dynamic aspects of QD gain properties can be examined. On the other hand, the transient behavior of lasing instability could have profound implication for possible applications of QD lasers.

In the following, we investigate multimode dynamics of InGaAs QD lasers. The spectral transient dynamics are analyzed in the frequency regime from ~ 100 kHz to 0.5 GHz, as limitations set by the detection system. Distinct dynamic features, such as antiphase mode dynamics and transient frequency damping are observed at frequencies from a few MHz up to the detection limit. These features are found to be robustly present for all the investigated QD devices, within most of the range of the examined laser parameters, including waveguide parameters, temperature and injection current density. Comparative study with QW lasers shows that different gain suppression properties are responsible for the different forms of antiphase dynamic outputs of QD and QW lasers. We also analyze the laser transient spectra for different devices, mainly concerning the temporal evolution

and stability of their spectral characteristics. This analysis not only helps clarify the specific spectral features, but also provides insight on the nonlinear dynamics aspect of the QD gain properties, which may shed light on the proper modeling of QD lasers. Finally, we refer to the next chapter for more peculiar spectral dynamic features in multi-stacked QD lasers, where it is found that the laser dynamics are disturbed by the carrier transport effect in the multiple QD layers.

3.2 Multimode dynamics in QD lasers

3.2.1 Introduction

The present status of QD lasers indicates that they are generally lasing in multiple longitudinal modes if without special mode selection mechanisms applied. The multimode feature results from both the broad spectral gain due to finite inhomogeneous broadening, and the spatial hole burning effect[1] characteristic of QD gain media that greatly reduces the multimode threshold. From the viewpoint of fundamental research, the study of multimode dynamics in QD lasers is of great curiosity for the underlying complex QD physics. In comparison with the conventional multimode lasers, QD lasers have much broad dimensions in the carrier and gain dynamics. Their nonlinear dynamics in laser processes could provide an important platform for the nonlinear system research. In particular, the multimode features of QD lasers are significant for they are very flexible in the numbers of lasing modes. From some modes just above threshold to hundreds of modes well above threshold, the lasing width can span a spectral range from some nm to near 100 nm if properly designed. Thanks for the very low threshold current density and high slope efficiency, large numbers of modes can be attainable at relatively low injection currents, compared to that it is practically impossible in QW lasers. Thus QD lasers are particularly suitable for exploring multimode dynamics in semiconductor lasers with enlarged mode parameter space. Moreover, the exceptional lasing performances achievable in QD lasers[2] contrast those in the conventional semiconductor lasers, providing many unprecedented possibilities and conditions for the dynamic study, such as ultra low threshold and ultra high power. It could be expected that the specific gain properties of QD media would expand the dynamic parameter spaces, and their great tunability through enabling nanotechnology will make QD lasers rather viable test beds for many fundamental concepts in nonlinear dynamics and cavity dynamics. The multimode dynamic studies will not only enrich the basic understanding of the roles of various dynamic variables in lasing process, but also provide more facilities for the possible applications of QD devices as sources and sensors. In this respect, QD lasers with well-behaved

multimode dynamics could become unique sources when multi-wavelength operation is preferred. The control on the spectral dynamics of QD lasers, either passive or active, is highly desirable in the future when multiplexing optical processing and computing is concerned.

On the other hand, currently single-mode lasers are highly desirable as coherent emitters for practical applications in optical communication and spectroscopy, so the mode selection mechanisms like DFB or DBR need be introduced in the otherwise multimode emitting QD lasers to make them emit in single mode. Nevertheless, the multimode QD lasers can still find their place in some critical application areas. For example, as pump laser diodes, the high power capability of QD lasers is enhanced by the reduced carrier diffusion and self-absorption. Though, in certain cases, the broad lasing widths mean a low pumping efficiency due to the overflow from the pumping spectral window, they definitely help make full use of the QD spectral gains, in favor of high power capacity. For pumping purpose, it would be all right if the pump laser diodes are emitting in steady state and not sensitive to the perturbations such as optical feedback. It is also desirable to minimize the hazardous effect due to electrical spikes introduced in the laser diode drivers. This would require a fast damping transient behavior with asymptotic stable state. For otherwise, any dynamic variations of the output power or spectral-temporal instability of the pump lasers will be transferred to the functional elements (e.g. amplifiers or other lasers such as fiber lasers.) being pumped, incurring in these elements unexpected effects that may be detriment to their functions or performances. In this sense, the multimode dynamic behaviors of QD lasers become indispensable lasing characteristics that are critical for the seamless implementation of QD lasers in these practical application areas.

Multimode laser dynamics have been studied in many types of solid-state lasers including microchip lasers, fiber lasers and conventional semiconductor lasers, [3-5] in addition to dye lasers[6,7] and CO_2 lasers[8]. For these Class B lasers,[9] relaxation oscillation phenomena are commonly observed in the laser transients. In the pioneering work of McCumber[10], the relaxation oscillations in single mode Class B lasers are related to the noise peak in power spectra that reflects the intensity fluctuation in the laser output. Then the Tang-Satz-deMars (TSD) multimode laser equations[11] are formulated that take account of spatial hole burning effect, and they are applied for the analysis of relaxation oscillations in multimode solid-state lasers. Based on the linear stability analysis of TSD multimode laser equations, it is shown that, as a universal property, a free-running N-mode lasers with spatial hole

burning exhibits self-organized collective mode oscillation behavior, in which an individual mode shows antiphase oscillation featuring N relaxation oscillation frequency $f_1 > f_2, \cdots f_N$, while the total intensity exhibits a unique predominant relaxation oscillation frequency, f_1, just like in a single-mode laser.[12] Those relaxation frequencies other than f_1 are generally lower than the main frequency f_1. Actually the (N-1) low frequencies may be degenerate in all or partly, depending on the lasing parameters of modes. The amazing effect of such low frequency dynamics is that all the (N-1) low frequency components of one individual mode are canceled out by those of the other modes, so leaving the ideal single relaxation oscillation at f_1 for the total intensity. The main frequency f_1 can be seen as resulting from the dynamic coupling between photons and gain medium, so it is the same for single mode lasers and for the total output of multi mode regime. Meanwhile the low frequency components and their antiphase character evolve directly from the cross-saturation dynamics. It has been proposed and proved in many cases that, in a Fabry-Perot laser, the spatial hole burning of the laser gain by the longitudinal modes provides the necessary nonlinear mode coupling mechanisms.[5,13-16] The longitudinal mode spatial hole burning effect is often called the dynamic grating effect, for the standing wave pattern looks like a diffractive grating. In semiconductor Fabry-Perot lasers, the dynamic grating effect is one of the most important mode cross-saturation mechanisms, along with the spectral hole burning effect due to homogenous broadening.[17,18] It has been shown that the dynamic grating effect is responsible for a specific multimode dynamics --- Low frequency fluctuation (LFF) --- that is frequently observed in semiconductor lasers with optical feedback.[16] In conventional semiconductor lasers, carrier drift and diffusion is believed to smear out the dynamic grating effect, so it can be difficult to observe the antiphase dynamics in these lasers. As opposite, the dynamic grating effect keeps strong in the QD lasers for the rather limited carrier diffusion in the QD layers.[19] Moreover, the spatial isolation of QDs and the weak link of their confined carriers help enhance the cross-saturation strength of dynamic grating effect.[1] Therefore, it is expected that QD lasers could show significant cross-saturation dynamics, like antiphase dynamics. If considering other nonlinear QD gain properties, new forms of multimode dynamics may well emerge from QD lasers. For example, the spectral hole burning effect due to the homogeneous broadening of QD gains may behave quite differently from that of QW or bulk gains, just because different spectral cross relaxation and spatial cross relaxation mechanisms ensue for the gain media based on different quantum structures.

To date, there is still lack of a systematic study on multimode dynamics of QD lasers, though some ps-resolved short pulse transients (pulse duration up to 8 ns) have been reported.[20-22] In these previous works, the total output traces show either strongly damped relaxation oscillation with only two resolved oscillation peaks, or damped relaxation oscillation with irregular transient envelopes, but they all indicate that the main relaxation oscillation frequency f_1 lies in GHz range. These damped relaxation oscillation phenomena indicate strong nonlinear gain effects taking place in QD lasers due to the complicated carrier and gain dynamics in QD layers, which may induce also strong low frequency multimode dynamics. In the following, we first present the result of experimental study on such low frequency multimode dynamics in InGaAs QD lasers, and then make a comparative study on QW lasers with similar laser structures. The ns-resolved spectral mode transients lasting a few μs are recorded, and we observed antiphase mode dynamics with sustained oscillation amplitude. Especially for QD lasers, the transients of individual modes show distinct frequency damping effect, leaving rather stable but intense low frequency periodic oscillation only after many cycles of quasi-periodic oscillations. Even though a wide range of mode oscillation frequencies are measured at various temperatures and in different device geometry, the maximum frequency components of the typically wide and continuous power spectrum show a consistent linear dependence on the injection current density. In contrary to QD lasers, the QW lasers with similar laser structures show rather low mode oscillation amplitudes that even decay with the injection current. This effect and other spectral characteristics of QW lasers are discussed in the context to help clarify the role of different nonlinear gain properties in determining the distinct dynamic features of QD and QW lasers.

3.2.2 Experiments

The QD lasers studied in this work are fabricated from the laser structure (Np305I) that has 3 stacks of 1.1 μm InGaAs QDs in the waveguide layer. The QW lasers are made from the laser wafer (Np306I) with one InGaAs QW in the similar waveguide. All the devices have shallow mesa ridge waveguides, except for the narrow stripe QD laser (w = 5 μm) that has deep-etched-through ridge waveguide for single transverse mode lasing. We refer to the previous chapter for the detailed description of this laser structure and the processing steps.

The laser diode is bonded on a SMA male submount, which is then plugged into a female SMA connector at the end of a superfine HF coaxial cable. The SMA part and cable are

attached to the cold finger of a continuous flow Helium cryostat --- MicrostatHe from Oxford Instruments. The HF cable passes a throughput on the cryostat and is connected to a HP 8116A pulse generator (< 6 ns rise time). The detection system includes a Hamamatsu InGaAs fast pin photodiode (ϕ300μm), a wideband amplifier and an Infinium digital oscilloscope with 2G Sa/s sampling rate. The time resolution of the whole detection system reaches 1 ns. For the spectral filtering, we use a BM50 0.5-meter monochromator that has a maximum resolution of 0.1 nm. An electronic shutter is used to block the photodiode between the sampling intervals, in order to avoid any bleaching effect from strong laser emission. For laser pumping, we use electrical square pulses with repetition frequency of 10 kHz, and the current pulse amplitude uncertainty is monitored far below 1%. The pulse duration is chosen below 3 μs to avoid the effect of significant pulse drooping. The laser diode is temperature stabilized to 0.1 K. The spectrally resolved time traces are averaged for every consecutive set of 1024 pulses to get a better Signal/Noise ratio, noting that the main noise source is the white noise from the wideband amplifier.

3.2.3 Transient behavior of QD lasers

a) Wide stripe devices

We first analyze the time-resolved spectra of wide stripe (w > 8μm) QD devices. In Fig. 3-1, the 3D spectra are shown for various temperature and currents. Note that these spectra are color-mapped in intensity for better view on the dynamic perspectives. Evidently all the lasing modes show rather regular intensity oscillations, and in each of these four cases, the modes have similar oscillation frequencies. For the same current, in Fig. 3-1(a-c), the frequencies are almost the same despite the different temperatures and spectral mode profiles, and the frequency decreases at lower current as in Fig. 3-1d. Pay attention to the different wavelength scale for the lasing widths depend strongly on temperature and current. At 290 K, in Fig.3-1a, the two mode groups at the high energy side switch their intensities in the 1 μs pulse duration, besides the quasi-periodic mode oscillations; but at lower temperatures, in Fig. 3-1(b-d), we see only regular mode fluctuations around rather constant mode mean intensities. The intensity switching indicates weak mode interactions, and that may be related to the wide gap existing between these switching mode groups as in Fig. 3-1a. Here the clustering effect of spectral modes is presumably attributed to the waveguide effects as discussed in Chapter 2. Note that in Chapter 2 we use the logarithmic intensity scale for time-averaged spectra instead of linear one here. This is due to the much lower dynamic range of the fast detecting system than that of slow detecting one with

Lock-in technique, as used for time-averaged spectrum measurement, and the waveguide-induced spectral intensity modulation would be better recognizable in semilogarithmic plots because the mode intensities can span large dynamic range as the intrinsic property of lasing spectra.

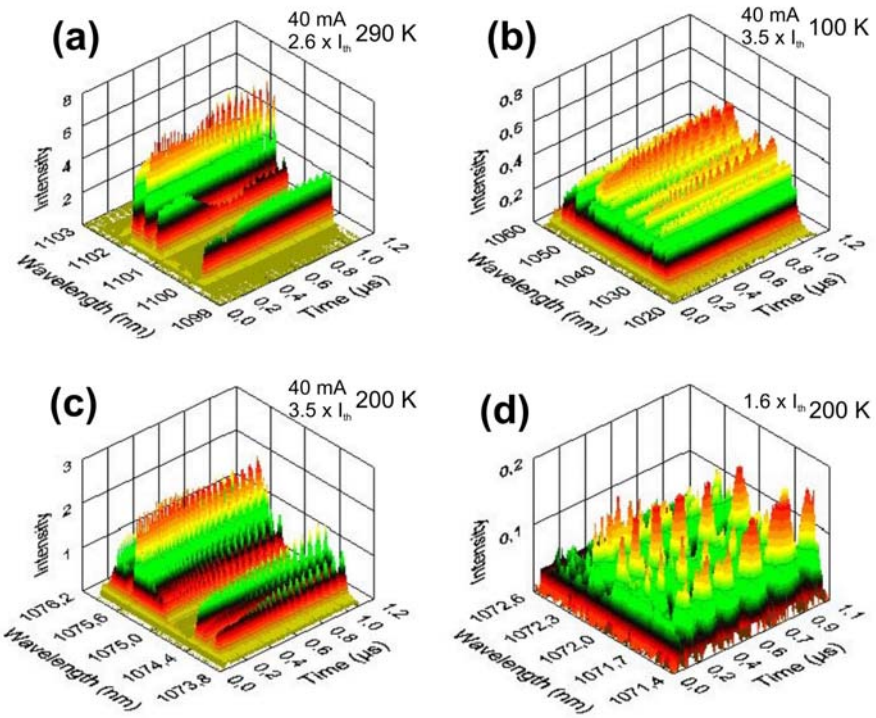

Fig. 3-1 Time-resolved lasing spectra of the 1.1 μm InGaAs QD laser (Np305I, 3 x QDs, 1.5 mm x 24 μm, 1s HR) at various temperatures and currents.

To look into the details of mode dynamics, we turn to the time traces of longitudinal modes as shown in Fig. 3-2a. Note that the mode distance for 1.5 mm devices lies near 0.12 nm, so it is still lower than the peak intervals of the time-integrated spectrum in the inset of Fig. 3-2a. The shown 6 time traces are selected mostly near the peak positions. The strong mode intensity fluctuations feature quasi-periodic oscillations at time scales of tens ns, and slow chaotic fluctuations in the μs period. Three remarkable features are apparent:

The fast intensity oscillations are fully correlated among the modes, with either in phase or antiphase relations. This relation exists not only for the 6 shown modes, but for all the modes we observed clear antiphase relations between every pair of most neighboring modes.

The frequency of the fast intensity oscillations slow down along the time traces, as happening to all the modes.

Despite the fiercely fluctuating individual mode intensities, the time trace of total output conforms firmly to the square shape of the driving current pulse. This indicates that the modes are actually compensating each other in intensity, a clear signature of antiphase dynamics.

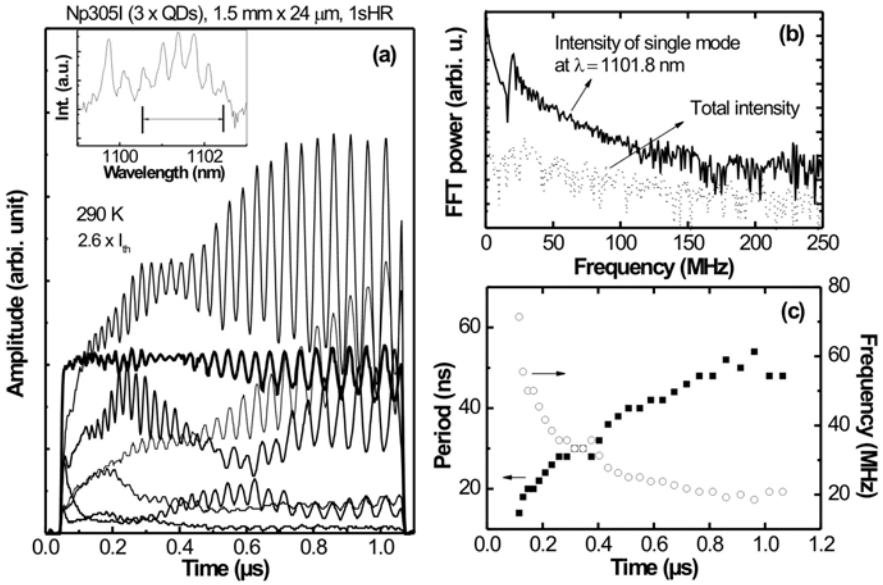

Fig. 3-2 (a) Time traces for different modes in the spectral range as indicated in the inset. (b) FFT power spectra. (c) Temporal behavior of mode oscillation period and the equivalent frequency.

In Fig. 3-2b, the Fast-Fourier-Transformation (FFT) power spectra are shown for both the time traces of one individual mode and the total output. Here we apply no windowing in the FFT process, so the power spectra include all the frequency components appearing during the 1 μs pulse duration. The broad peak near the low frequency limit can be attributed to the mode fluctuations at large time scale, while the second peak and its long tail at high frequency is related to the fully correlated fast mode oscillations. The wide frequency range in the peak tail reflects the frequency damping effect, but this second peak also shows a clear cutoff low frequency at the cliff of the peak. To understand this, we plot in Fig. 3-2c the peak intervals of the fast oscillations. The frequency curve shows clearly that the major oscillation frequency is damping with time and approaches a stable low frequency limit (~20 MHz), which can be readily related to the cutoff frequency in FFT power spectrum. The mode fluctuations at long time scales result in much higher FFT power below the cut-off frequency, compared to that of the integrated trace. Now go back to Fig. 3-2b, and we see the power spectrum intensity of the total intensity time trace is much lower than that of the individual mode. At the cutoff frequency the oscillation suppression ratio of the total output reaches about 40 dB. We note that the basic shape

and amplitude of the power spectra of all modes are rather similar, and the minor difference is mainly originating from the large-scale slow mode fluctuations that are somehow intense at RT. In contrast, we have seen in Fig. 3-1 that the slow fluctuations become weak at lower temperatures.

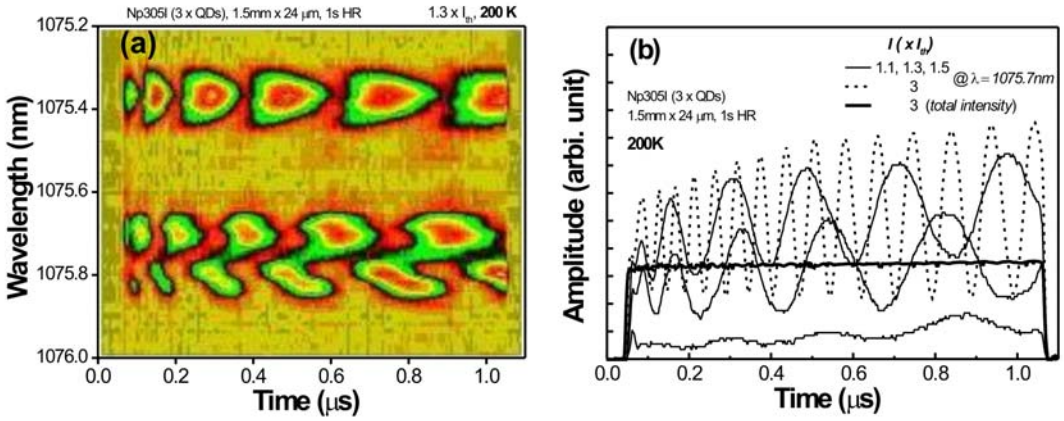

Fig. 3-3 (a) Time-resolved lasing spectrum with longitudinal mode structure resolved. (b) Typical modal time traces at increasing currents. The square-pulse-shaped thick line shows the total output intensity trace.

At low temperatures, the multimode dynamics are of similar antiphase character and show frequency damping as well, except the mode number increases and the mean mode intensity decreases correspondingly, as clearly demonstrated in Fig. 3-1(b, c) for the same current and even the same threshold at different temperatures. The absence of slow chaotic fluctuations makes it easier to analyze the tendency of the regular mode oscillations. In Fig. 3-3a, a 3D spectrum is zoomed in and projected to the λ-t plane for a clear view of resolved modes. The 3 strong longitudinal modes are well resolved in an interval ~0.12 nm for such a device. In the gap between the two strong modes there can be only two extremely weak modes if recognizable. It is apparent that the phase relations in all the modes are determined by the two strong modes that are in antiphase oscillation. The broad mode widths here are due to the finite spectral resolution (~0.1 nm) and it is also possible that high order modes exist for the wide stripe device. In Fig. 3-3b, we present also the time traces of one fixed spectral mode at various currents. These rather regular oscillating modes show clear frequency dependence on current, and that can be also seen in the comparison between the two 3D spectra in Fig.3-1b and 1c for different current at 200K. In Fig. 3-3b, at low currents, only few cycles of quasi-periodic oscillations occur within the 1 μs pulse, and the frequency damping extends beyond the 1 μs pulse duration. But at the highest current as shown, the cutoff low frequency is approximately reached within the pulse duration. So we can say that the rate of frequency damping approximately

scales with the oscillation frequency. As to the mode oscillation amplitudes, they amount to ~ 50% of mean mode intensity, but it can reach 70% in some cases, so no apparent dependence on current exists. The total intensity trace in Fig. 3-3b is as expected a flat square pulse, so the fast oscillations are completely canceling each other, a beautiful character of antiphase dynamics. In Fig.3-1d, the 3D zoom-in spectrum indeed has antiphase mode relations though the modes are not seen as resolved.

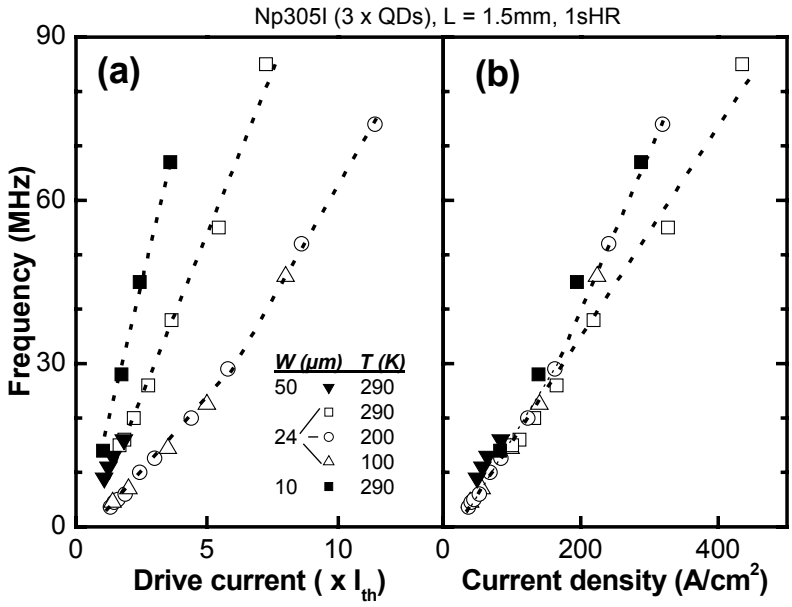

Fig. 3-4 The injection intensity dependence of the major mode oscillation frequency for devices with different stripe widths and at various temperatures, as plotted in different ways in (a) and (b).

As we have studied the time-resolved spectra from the QD devices of varied stripe widths with w > 8 μm, their dynamic features are rather similar. The relation between the oscillation frequency and injection intensity is summarized in Fig. 3-4 for various devices and different temperatures. Due to the ubiquitous frequency damping effects, the power spectra of typical time traces contain broad frequency components, and the cutoff frequency is even not available for those traces with few oscillation cycles in the finite pulse duration. To facilitate the comparison between these traces, we use the Hanning window in the FFT analysis to draw the frequency components mainly in the middle of time traces. The frequencies of the maximum in the power spectra are shown in Fig. 3-4. Clearly at low frequency regime the frequencies thus obtained are overestimated compared to the expected cutoff frequency, but this happens equally irrespective of different devices or temperatures. In Fig. 3-4a, the frequency is higher for narrower devices and higher temperatures when plotted in respect to the current ratio I/I_{th}. However, if considering the different thresholds and injection areas in these devices and temperatures, it is reasonable

to normalize these factors by using the current density in comparison. So the frequencies are plotted vs. J_{th} in Fig. 3-4b. As can be seen, the frequencies now fall onto each other, suggesting a general linear dependence on the current density. The apparent deviation at high current density is a little beyond the frequency reading error of a few MHz, but we note that there are still other factors not normalized. For example, the actual mode number can be quite different in each case and will be also affected by the additional transverse modes. On the other hand, depending on the cavity loss, the linear gain margin between the threshold and the saturated gain varies in different devices and temperatures, and that could affect the mode self- and cross saturation strengths as well. A detailed study on the dynamic effects from these factors would need a survey on a wide range of device parameters. That may be done in the future.

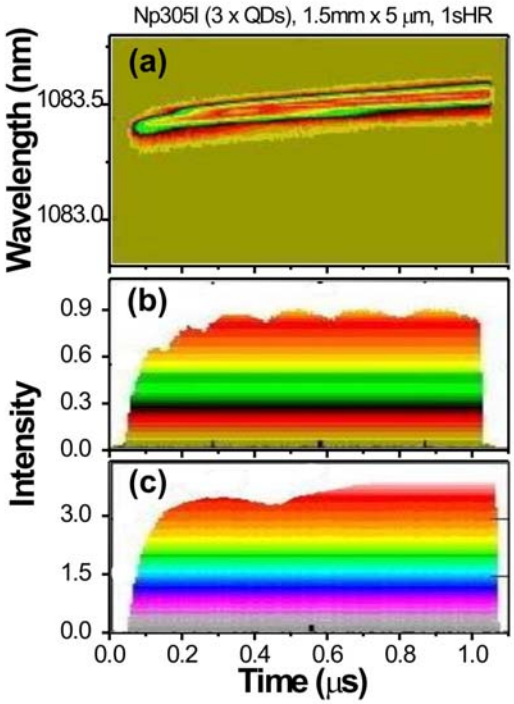

Fig. 3-5 (a) Time-resolved single longitudinal mode lasing spectrum of the narrow stripe QD laser at RT and 35 mA (1.1x I_{th}). (b) and (c) Time traces of the mode in (a). The spectral resolution is reduced for (c).

b) Narrow stripe devices

After analyzing the wide stripe devices that emit in multiple transverse modes, we may ask what happens in a single mode laser? We fabricated a narrow stripe (w = 5 μm) QD laser with deeply dry-etched mesa geometry. The narrow stripe helps suppress the role of transverse modes if still present, and the deep mesa induces strong modulation in the lasing spectrum that makes it possible to realize lasing action in a single longitudinal mode. For

the latter waveguide effect, we refer to Chapter 2. In this narrow stripe device, we realize single longitudinal mode lasing for $I < 1.6 \times I_{th}$, and the side mode suppression ratios amount to 20-30 dB, as can be measured in the time-averaged spectra with high dynamic range. For RT and $1.1 \times I_{th}$, the 3D time-resolved mode spectrum is projected on the λ-t plane in Fig. 3-5a. As compared to the case in Fig. 3-3a, here the mode wavelength strongly red shifts along the trace. This is a typical junction heating effect due to the relatively large thermal resistance of the narrow stripe device. Now that it is not possible to get the mode time trace at a fixed wavelength, we turn to Fig. 3-5b, where the projection on the intensity-time plane is shown. The envelope again shows low frequency mode oscillation with frequency damping effect. This effect is rather contradictive for it seems that these typical multimode dynamic features even present in a single mode case where there should be no mode interaction at all. Actually the single mode laser problem has been intensively studied concerning their noise properties.[23-26] These studies show that the interaction between the main mode and weak side modes is critical for the understanding of excess intensity and phase noise of a single mode free-running laser, and for noise and amplitude squeezing the side modes need be suppressed. Similarly in the present case, we have to consider the mode coupling effect from weak side modes. To show that effect, we measured the single mode spectrum in a course resolution that would integrate more neighboring side modes. As can be seen in Fig. 3-5c, the mode oscillation originally seen in Fig. 3-5b is now averaged out, leaving only an envelope with much slow fluctuation. So the fast fluctuations in side modes are actually anticorrelated with that of the main mode. This explains also why the oscillation amplitude in single mode case is much lower than in multimode case.

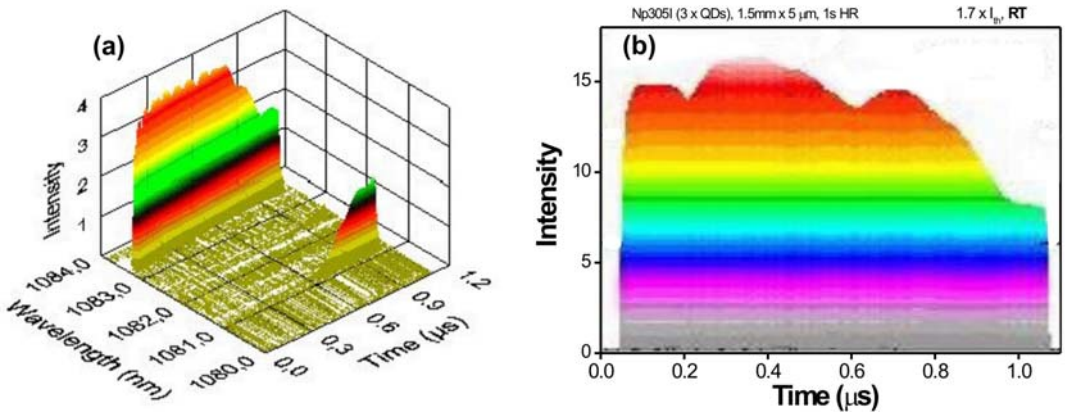

Fig. 3-6 (a) Time-resolved spectrum of the narrow stripe QD laser as in Fig. 3-5, at RT and $1.7x\ I_{th}$. (b) The time trace for the main mode in (a).

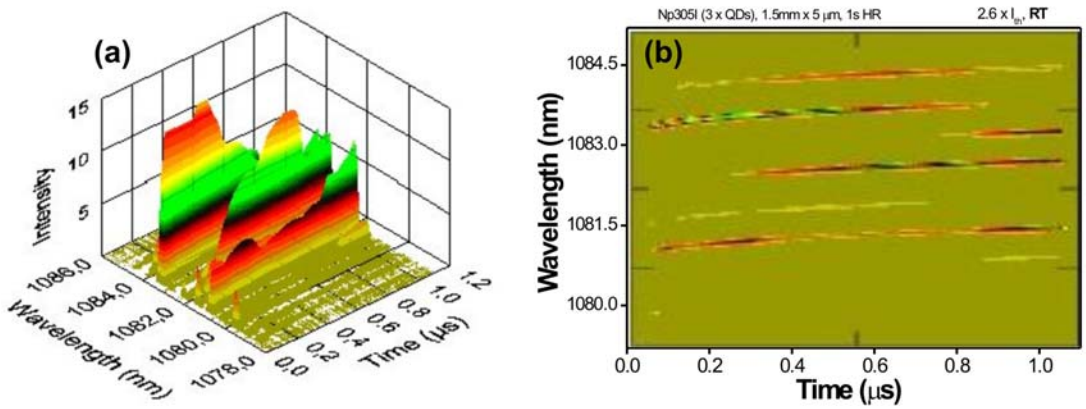

Fig. 3-7 Time-resolved spectrum of the narrow stripe QD laser at high current, in different plots.

In Fig. 3-6a, at 1.7 x I_{th}, the oscillation frequency increases as compared to that at 1.1 x I_{th}, and a second strong mode appears in the form of intensity switching. The fast oscillations are again smoothed to some extent in the coarse spectrum as shown in Fig. 3-6b. For even higher current 2.6 x I_{th}, much more modes come out, as the coarse spectrum in Fig. 3-7a shows. We can see in Fig. 3-7b that there exist certain regular mode distances ranging in 2-4 nm, and the mode red shift is clearly demonstrated that argues strongly against its attribution to the mode hopping effect. As discussed in Chapter 2, the sparsely peaked feature of the mode spectrum originates indirectly from the complex resonance mode structure in the deep mesa waveguide. These resonance modes inside waveguide would interact with each other when they share gain in parts of their trajectories, so this type of mode coupling mechanism can also affect the mode dynamics indirectly, though it is somewhat different from that of the dynamic grating effect. We attribute the rather chaotic oscillations to this special mode coupling effect, while the mode coupling from the dynamic grating effect is responsible for the fast quasi-periodic oscillations as in usual cases.

Compared to the ground state (GS) emission of the QD laser structure, we can see that at RT this narrow stripe device lases at much shorter wavelengths with a difference of ~30 nm from the GS maximum. This is mainly due to the large cavity loss incurred by the scattering on the nonuniform deep mesa sidewalls. So at RT, the threshold current density reaches 200 A/cm^2 for the ES lasing, compared to a low value of ~70 A/cm^2 for the GS lasing in the shallow mesa wide stripe device (w = 50 μm). At such a high current density, the excited states (ES) gain becomes larger than the GS gain, which is depressed relative to its saturated level due to the thermal escape and the intradot thermal distribution at high temperatures. In contrast, at low temperatures, these thermal gain depression effects are greatly reduced, so for the same current the GS gain is enhanced while the ES gain is

reduced. In Fig. 3-8, we can see that the lasing wavelengths actually move back to the GS maximum for 180 K. This shows that the cavity loss is lower than the GS saturated gain level. We note that with temperature decrease, the threshold current of this narrow device decreases continuously with minor change below 200 K, but the otherwise constant slope efficiency at high temperatures halves since 200 K. Such a strong reduction in efficiency indicates a reduced differential gain, which occurs when the saturated GS gain is approached. The gain saturation is known to have a damping effect on the relaxation oscillation at the main frequency (i.e., in the GHz range).[27] Here we would see it also have impact on the low frequency dynamics. At 180 K, the mode resolved spectra show almost no sign of fast oscillations, or the oscillation amplitudes are too weak to perceive. So we only show the coarse resolution spectra with ~3 modes integrated. In Fig. 3-8a, at 3 x I_{th}, the integrated modes start intensity fluctuations with small amplitude. In strong contrast to the wide stripe cases, the fluctuations are still extremely slow up to 14 x I_{th}, as in Fig. 3-8b, but the perceivable fluctuations apparently show antiphase character and even frequency damping effect. These integrated mode behaviors suggest the underlying individual mode dynamics, though extremely weak in oscillation amplitude, still possess the typical low frequency dynamic features as observed for wide stripe devices. The gain saturation actually damps the fast oscillations both in amplitude and frequency. The similar spectral dynamic behaviors persist at lower temperatures. In Fig. 3-8c, the 3D spectrum from Fig. 3-8b is projected on the λ-t plane. Again there appear rather regular mode distances around 1.5 – 3 nm. For all these devices have a cavity length of 1.5 mm, so their normal longitudinal mode distance is 0.12 nm. We found also some rather regular mode distances of ~ 0.2 nm and 0.45 nm for the stripe width w = 10 μm, 0.38 nm for w =24 μm, and 0.12 nm for w = 50 μm Based on these observations, it strongly recommends that the open waveguide of this deep-dry-etched narrow stripe device is responsible for the mode selection, as in Chapter 2.

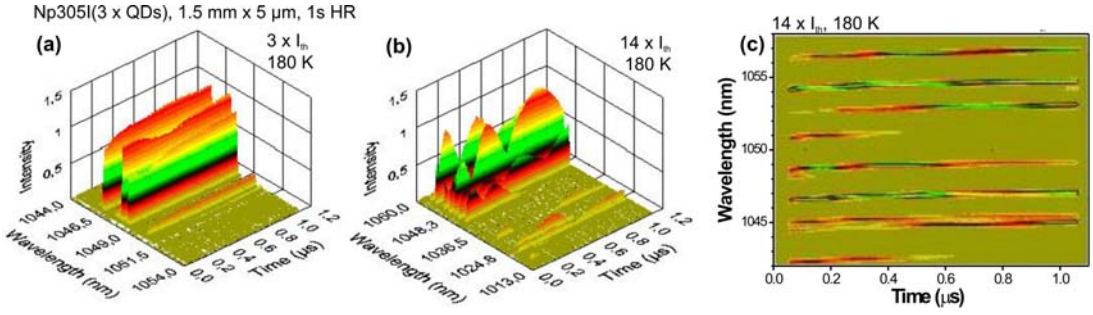

Fig. 3-8 Time-resolved spectra of the narrow stripe QD laser at high current.

c) Comparative study with QW lasers

To help understand the role of different gain media in laser dynamics, we make a direct comparison between the QD lasers and their QW counterparts. The QW laser structure (Np306I) possesses the same waveguide design as the former 1.1 μm InGaAs QD laser wafer (Np305I). In particular the InGaAs QWs are tuned to emit at a similar wavelength ~1.12 μm as the QD GS. We fabricated QW devices with shallow mesa geometry. As deduced from the test with broad area devices (w >100 μm), the QW laser structure has similar internal quantum efficiency and internal loss (~97%, 2.8 /cm) as the QD laser one (~97%, 2.2 /cm), but has much higher transparency current density (50 A/cm^2) compared to ~9 A/cm^2 for the QD lasers. The QW devices with a cavity length of 1.5 mm are high reflectivity (HR) coated on both facets. The HR coatings help lower the threshold current density to be comparable to those of QD lasers, and they also help get rid of possible external optical feedbacks that are known to have significant effects on the dynamics of conventional semiconductor lasers.[15,27,28] In the following, we first discuss the lasing characteristics of these QW lasers, and then analyze their dynamics in comparison with those of QD lasers.

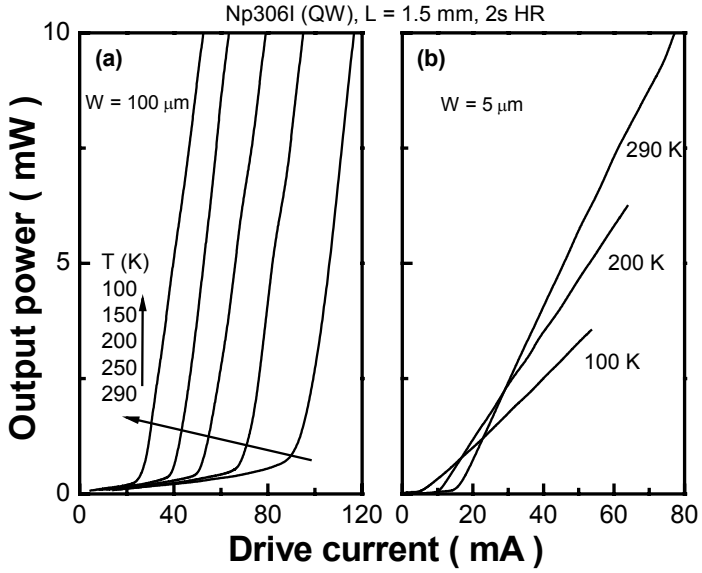

Fig. 3-9 L-I curves at various temperatures for the 1.1 μm QW lasers with different stripe widths.

I. Basic characteristics of QW lasers

The L-I curves of the QW lasers are shown in Fig. 3-9. With temperature decrease, the threshold currents of both devices continuously decrease, and while the slope efficiency of the wide stripe (w = 100 μm) device keeps almost constant, the narrow stripe (w = 5 μm) device has continuously decreasing slope efficiency. In comparison to the wide stripe

device, the narrow stripe one has higher threshold current density (~ 3 times) and lower efficiency (less than 50%). This deterioration of laser characteristics can be attributed to the current spreading and high scattering loss in the narrow stripe laser, and the gain saturation is responsible for the low slope efficiency. Finally the lasing wavelengths of both devices share the same temperature dependence, ~ 0.36 nm/K.

The lasing spectra are shown in Fig. 3-10 for the wide stripe QW laser. For all temperatures the GS lasing spectra expand into the low energy side with current, and a weak peak always appears about 10 nm on the high energy side for high current. Considering the low threshold gain condition in this low loss device, the spectral expansion into low energy side corresponds to a low excitation case in the QW. The evolution of the linear spectral gain profile with current depends on the specific carrier distribution in the QW subbands. So the weak peak on the high energy side can be associated with the transition between the GS electron subband and the GS light-hole subband. The lasing widths are not so much temperature dependent as the case of QD lasers. As can be seen in Fig. 3-10b, at 200 K, the spectrum at 1.2 x I_{th} shows more than one peak. This peak splitting effect happens only for a narrow current range, and is most probably due to the minor unevenness of the spectral gain profile near the gain peak region.

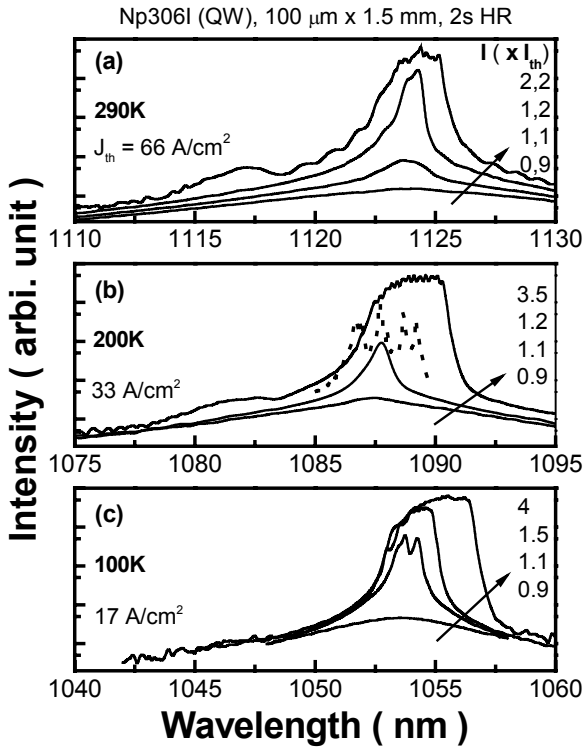

Fig. 3-10 Lasing spectra of the wide stripe QW laser at various temperatures.

In contrast to the former spectra of the wide stripe device, the spectra of the narrow stripe QW laser show totally different scenarios. As shown in Fig. 3-11a for RT, the lasing peaks red shift continuously with current, much significant than expected from possible junction heating effect. So the lasing modes are actively adapting to the gain profile that varies with current. For the high threshold gain in this narrow device, the gain margins of the spectral modes are rather limited, as the gain saturation sets in. In this case, the lasing processes experience dramatic self-organization through the mode competitions, with the most stable lasing configuration winning out. This self-organization process is also responsible for the spectral shift seen in the lasing spectra of very short QD lasers with high mirror loss. The gain saturation facilitates the self-organization process, and if the gain margin is much larger, the formerly established lasing modes will not be easily changed for their strong coupling to the gain.

At lower temperatures, the self-organization phenomena are more apparent. At 200 K, in Fig. 3-11b, the lasing peak first blue shifts, then stays there, but on the low energy side, another peak appears about 4 nm away. In Fig. 3-11c, at 100K, the peak splitting occurs as well, and it looks more symmetric, which may be related to the spectral gain profile that is more symmetric due to the gain consolidation at lower temperature.

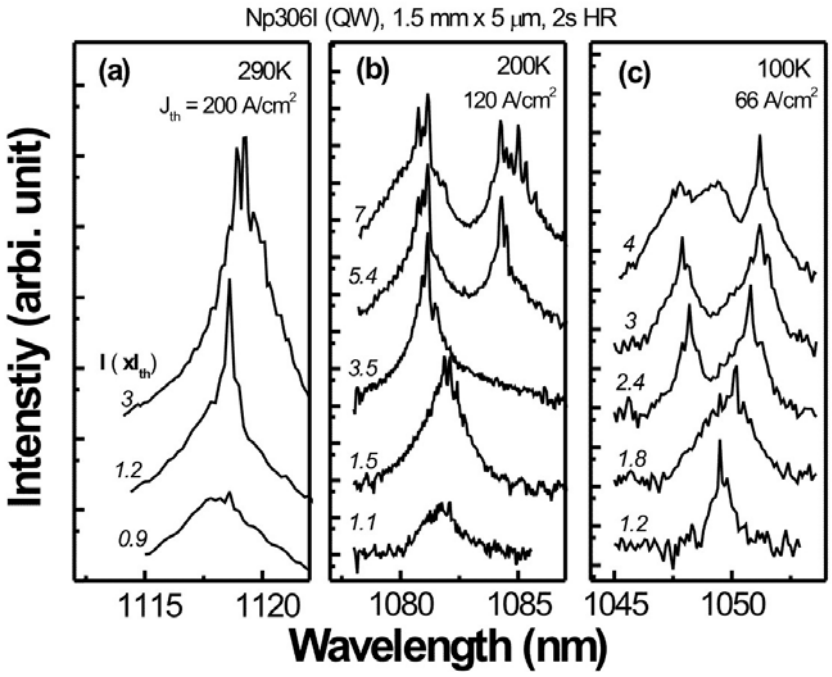

Fig. 3-11 Lasing spectra of the narrow stripe QW laser at various temperatures. The spectra are offset for clarity.

As shown in Fig. 3-11c, the evolution behavior of lasing spectra with current particularly resembles the results of simulation based on a simple rate equation model, though the model is supposed for use with the QD gains.[29] That model takes account of the homogeneous broadening as the only mode coupling mechanism, but no other nonlinear gain effects are considered. So it is not possible to make a direct comparison between the present experimental results and the simulation. Nevertheless, the homogeneous broadening of QW gains may play a significant role in the above peak splitting effects, especially considering the large spectral range of energy transfer. The QW has a finite homogeneous linewidth originating from the fast intraband carrier scattering processes. It is found that the QW homogeneous linewidth varies little with current but increases toward lower temperatures.[30] The homogeneous linewidth is generally larger than the inhomogeneous linewidth. So one of the mode interaction mechanisms can be the spectral hole burning effect associated with the homogenous linewidth.

Note that the homogeneous linewidth of QD gains is measured up to tens of meV, but no such peak splitting effects are observed in QD lasers. This may be attributed to the different spectral cross relaxations in QD and QW gains. The QWs have continuum density of states, and the fast intraband carrier scatterings result in efficient spectral cross relaxation. For the carriers beyond a certain lasing state can be efficiently transferred to that lasing state through intraband carrier relaxation, the gain compression effect of the lasing state significantly affects the differential gain of neighboring energy states, thus enhances the mode competition effect in QW lasers. On the contrary, the spatial isolation of QDs makes the spectral cross relaxation only possible through the interdot carrier shuffling, which is mediated by thermionic emission (carrier escape) and recapture processes in addition to carrier drift or diffusion in the wetting layer (WL) or barriers. So the spectral cross relaxation in QDs is hampered by the weak carrier links between different energy states. The lasing states drain the carriers from the reservoir in the WL/barrier region, but that does not affect the differential gains of neighboring states sufficiently as done by intraband carrier relaxation in QWs, because the fast carrier consumption rate in the lasing QDs needs be balanced by a comparable carrier capture rate that can be increased only when the carrier density is raised. The insufficient gain suppression means weak mode competitions that may explain the absence of peak splitting effects in QD lasers. Note again that there are many types of gain suppressions that have quite different physical origins. Here the discussed gain suppression is related to the spectral cross relaxation,

different from that of spatial cross relaxation as discussed before concerning the role of dynamic grating effect in the antiphase dynamics of QD lasers.

In the homogeneously broadened QW gain, the spectral hole burning effect associated with the homogeneous linewidth would otherwise ensure a single mode lasing. But under lasing conditions, the spatial hole burning effect becomes important. The dynamic grating effect leads to multimode lasing and incomplete clamping of carrier density. In the narrow stripe lasers, the lateral spatial hole burning effect strongly couples the carrier profile with the mode power and mode index profile, thus leading to continuous variation of mode gains with current. Carrier heating also contributes to the incomplete carrier clamping that results in continuous increase of lasing widths with current. The spectral features of lasing spectra in Fig. 3-10 and Fig. 3-11 conform to the above considerations.

II. Transient analysis of QW lasers

In the following we investigate the multimode dynamics in the QW lasers, and discuss the role of dynamic grating effect in QW lasers as compared with QD lasers.

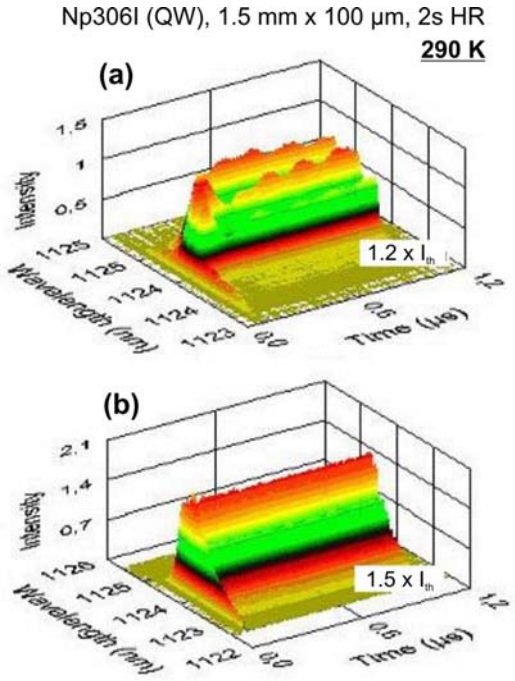

Fig. 3-12 Time-resolved lasing spectra of the wide stripe QW laser.

For the wide stripe QW laser, the 3D time-resolved spectra are shown in Fig. 3-12 for RT. Mode oscillations can be seen at 1.2 x I_{th}, but there are almost no perceivable oscillation at 1.5 x I_{th} and above. In Fig. 3-12a, the mode oscillations are actually in antiphase relations, as confirmed in the mode resolved spectrum. The typical time traces are shown in Fig. 3-

13a as a function of current. The oscillation frequencies increase with current, but the oscillation amplitudes decrease quickly with current, and above 1.5 x I_{th}, it is not possible to observe any oscillation beyond the noise level. It is interesting here to compare the time traces from both the QW laser and the QD laser. In Fig. 3-12b, the trace from the QW laser is shown together with another trace from a QD laser (TU5447, 6 x QDs, 1.5 mm x 50 μm, 1s HR), which has almost the same threshold current density ~ 66 A/cm^2 as the QW laser and is recorded at 200 K. As can be seen, the mean periods of both time traces are rather similar, but the apparent frequency damping effect in the QD trace is absent in the QW trace.

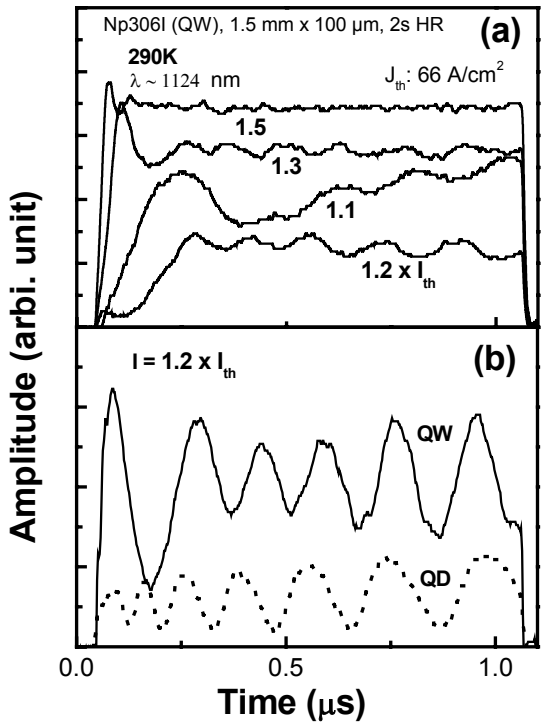

Fig. 3-13 (a) Time traces of the wide stripe QW laser at increasing currents, (b) Comparison of time traces from QD and QW lasers at a similar current density.

We observed similar dynamic features at lower temperatures. The time traces become already totally flat for the current a little bit higher than threshold. The oscillation amplitudes are generally weak and decrease with current. The antiphase dynamic nature of the mode oscillations is evidently reflected in the square pulse shape of the total intensity trace. It is noted that, the spectral dynamics of the narrow stripe QW laser features too much instabilities characterized by frequent mode switching, which may be related to the strong junction heating effect in the narrow stripe device and the irregular mode spectra

that change continuously with current, as shown in Fig. 3-11. The gain saturation may also result in weak mode coupling that inhibits possible mode oscillations.

The above transient analysis shows that the mode interaction in the QW laser can induce low frequency antiphase mode dynamics. The frequency similarity of QD and QW lasers at the same current density, as shown in Fig. 3-13b, strongly recommends a common mode coupling mechanism that is responsible for multimode dynamics in both types of lasers. As in many previous experimental and theoretical studies, the longitudinal spatial hole burning effect, i.e. dynamic grating effect, has been raised as the mode cross-saturation mechanism behind the antiphase dynamics. [4,5,13,14,16] The antiphase dynamics in the QW and QD lasers thus can be treated within the same framework of laser dynamics by taking account of the dynamic grating effect in different element spaces of the relevant dynamic variables. The different dynamic characteristics in both lasers may result from their distinct nonlinear gain properties.

Due to the quantized energy structure, QW gain shows stronger nonlinearity than bulk gain.[31] For example, the QW shows strong spectral hole burning effect due to the finite intraband relaxation time. As have been discussed concerning the peak splitting effect in narrow stripe QW lasers, the QW gain also shows more efficient spectral cross relaxation than QD gain. The spectral cross relaxation helps couple modes locally in the energy space, so it is important for mode competition. The spectral hole burning effect is more or less related to the mode self- and cross-saturation if not considering the homogeneous linewidth. Thus for QW lasers, their strong nonlinear gain effects are supposed to enhance the mode cross-saturation dynamics, which is excited by dynamic grating effect. However, the efficient spectral cross relaxation in QW lasers is accompanied with efficient smoothing of dynamic gratings, because the fast intraband carrier relaxation and the in-plane carrier transport in the QW ensure efficient spatial cross relaxation. The intricate anti-correlation relation between spectral and spatial cross relaxation in the QW may well explain the reduction of oscillation amplitudes with current as observed in Fig. 3-13a.

In contrast, the spectral cross relaxation in QD gains is not as efficient as that in QW gains, but the spatial cross relaxation in QD gains is also not so efficient as being able to smoothing out the dynamic gratings. The carriers in different lasing states are kept in spatially isolated dots, without direct connection except sharing one carrier reservoir. The carrier transport in the longitudinal direction of QD lasers is only possible through the

carrier diffusion in the WL/barrier and the carrier exchange between the QDs and the WL/Barrier. But the large confinement energies of QDs greatly reduce the "effective" carrier diffusion length. Therefore, these specific carrier processes ensure that the dynamic grating effect in QD lasers is not killed by the carrier diffusion, even with the increased carrier density. It should be noted that the spectral hole burning effect (without considering the homogeneous broadening) in QDs is even larger than that in QWs,[31] and this aspect definitely helps enhance the mode cross-saturation dynamics originating from the dynamic grating effect. So with persistent dynamic grating effect and strong spectral hole burning, the mode dynamics in QD lasers keep strong with current. At low temperature, the QD homogeneous linewidth should become negligible with the very low threshold, but we see no significant attenuation in oscillation amplitude. This fact indicates that the homogeneous broadening is not critical for the mode coupling in the currently observed multimode dynamics. This is opposite to the viewpoint expressed in some previous published works,[29,32,33] where the rate equations have the homogeneous broadening as the main mode coupling mechanism. So even these rate equations may generate certain dynamics, they are incorrect in describing the physical situation in QD lasers.

The above comparative study with QW lasers proves that the specific QD properties, like the large carrier confinement energy and weak carrier links between confined carriers in QDs, can actually help break the limit pertaining to the conventional semiconductor lasers, leading to an enlarged parameter space for the multimode dynamics study in semiconductor lasers.

3.2.4 Further discussion

For the inhomogeneous broadening of QDs is larger than their typical homogeneous linewidths, it is reasonable to compare the multimode dynamics of the QD lasers with that of the Nd-doped glass laser,[5] which has also strongly inhomogeneously broadened gain consisting of spatially dispersed gain units. Though the glass laser is operated in continuous wave (cw) regime in the study by Peters et al,[5] whereas the QD lasers are excited with quasi-cw pulses, both types of lasers show antiphase dynamics, with low frequency relaxation oscillations at 10-500 kHz for the glass laser and above MHz for QD lasers. The difference in the frequency range is due to the different time constants in the respective laser systems, such as the carrier or excited state lifetime and the photon lifetimes.

In the glass laser, the Fourier transformation power spectrum of each mode shows only a small number of many existing low frequency components, because strong correlation exists only in the group of neighboring modes of the same amplitude.[5] But in QD lasers, the mode power spectra are similar for all individual modes and thus all of them show similar low frequency components. Nevertheless, there are also common features in the two types of lasers. For example, in few-mode cases, the compensation of low frequency oscillations is incomplete and there exists residual oscillation in the total intensity; and in many-mode cases, the compensation is rather complete and the total intensity keeps constant.

In the glass laser, the frequency of antiphase oscillations is found to depend linearly on the mean mode intensity but not the total intensity. Whereas, in QD lasers, for example as shown in Fig. 3-3b and Fig. 3-4, the oscillation frequency increases almost linearly with the current density, and so is the mean mode intensity of those central modes for not so high current density. Thus the frequency of antiphase oscillations in the QD lasers is a linear function of both the mean modal intensity and the total intensity.

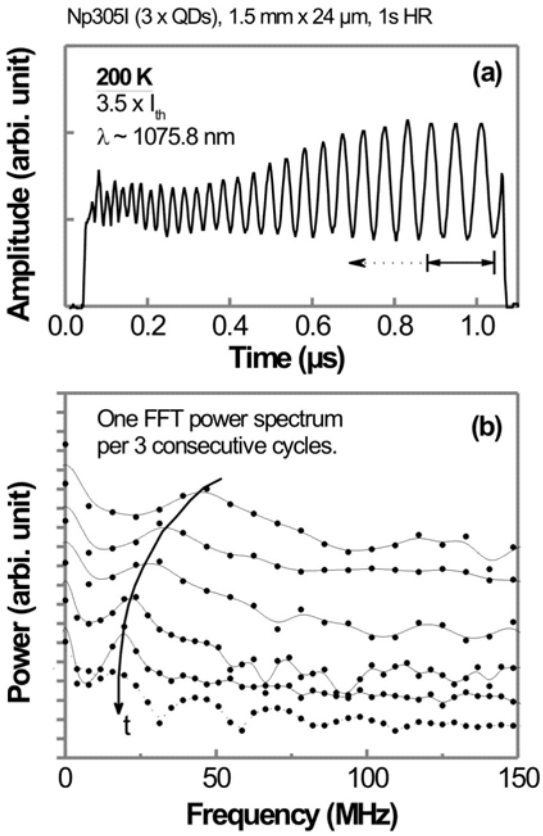

Fig. 3-14 (a) Typical time trace of a 1.1 μm QD laser. (b) FFT power spectra of the consecutive 3-cycle sections of the time trace in (a). The arrows indicate the corresponding time orders.

The above comparison suggests that the multimode dynamics of QD lasers have some fundamental characteristics that cannot be deduced from the simple inhomogeneous broadened gain. This is appreciable because the QD gain properties are actually so complex that this before we have considered only a few of them in discussing the dynamic features. There are many other aspects of QDs-specific gain properties still not explored, as discussed in Chapter 1. Are the effects of these gain properties possible to be renormalized in certain existing effective parameters? and how? or if they need new parameters to describe? To elucidate these effects, many comparative studies may be done in the future on lasers with different QD media. The perspective relies on the better understanding of carrier and gain processes in the QDs and the progress in QD growth technique that could eventually lead to dense, well-ordered and less dispersed dot arrays. At present, these jungles of effects defy the inclusion of them in a detailed modeling of the multimode dynamics in QD lasers.

The present study is limited to laser transient analysis with duration less than 3 μs, so we do not know for sure if the low frequency oscillations are damping out to steady state or keep periodic oscillations in the CW regime. However, in all devices investigated, for high enough oscillation frequency, we did always observe the frequency damping effects featuring asymptotically stable frequency components. For example, in Fig. 3- 14, the time evolution of power spectra is shown for one typical mode time trace. Clearly with time, the frequency components condense into narrow range while the main frequency (i.e. the maximum frequency component in the power spectrum, but not the main frequency f_1 in GHz range.) decreases and approaches a stable frequency. This type of frequency asymptotic behavior is common to all the lasing modes, implying that the observed dynamics in QD lasers is not simply a frequency damping, but indeed a *synchronization of relaxation oscillation frequencies*. In general at the beginning of the transient, the number of relaxation oscillation frequencies is about the number of lasing modes, but through the transient this array of relaxation oscillations relaxes into one or few frequencies. As the mode oscillations at the main frequency are fully correlated in the apparent antiphase dynamics along the trace, phase locking finally occurs. Such a phase locking behavior as suggested for the CW operation of QD lasers reflects strong nonlinear couplings among the non-optical relaxation oscillation modes of QD lasers. It is worth to note that the phase locking behavior is also observed for the collective modes in the closely packed vertical-cavity-surface emitting laser arrays.[34] This implies that the oscillating modes in QD lasers can be treated as an array of globally coupled oscillators. Thus the multimode

dynamics in QD lasers may well serve as a test bed for the study of specific nonlinear system dynamics.[35]

The fascinating dynamic features of QD lasers stimulate the theoretical interest in modeling of semiconductor laser dynamics above all and QD lasers specifically. As a preliminary effort to account for the observed antiphase dynamics, a phenomenological model is built that includes spectral and spatial hole burning effects.[36] Rate equations are used that couple the modal intensities to the nonlinear modal free carrier averages, via the grating created by the field. Identical modal gains and losses are assumed because the gain bandwidth is one to two orders of magnitude larger than the frequency separation among the modes. Following Agrawal[37], we model the spectral hole burning as an additional weak contribution to the gain saturation in the modal field equations. The parameters used for the numerical simulations are chosen to match the experimental results, for example a strong cross-coupling parameter is used. The antiphase oscillation can be reproduced. So physically, this confirms that the appearance of antiphase dynamics results from spatial and spectral hole burning effects, which is common in QD and QW lasers. Further efforts are under way to address the QD specific carrier processes. For example, Auger carrier capture[38] is considered to effectively describe the spectral and spatial cross relaxations in QD gains, and it may have potentials to handle the nonlinear gain effect that would be important for the modeling of damped relaxation oscillation at the main frequency f_1 and the present antiphase dynamic results.[39]

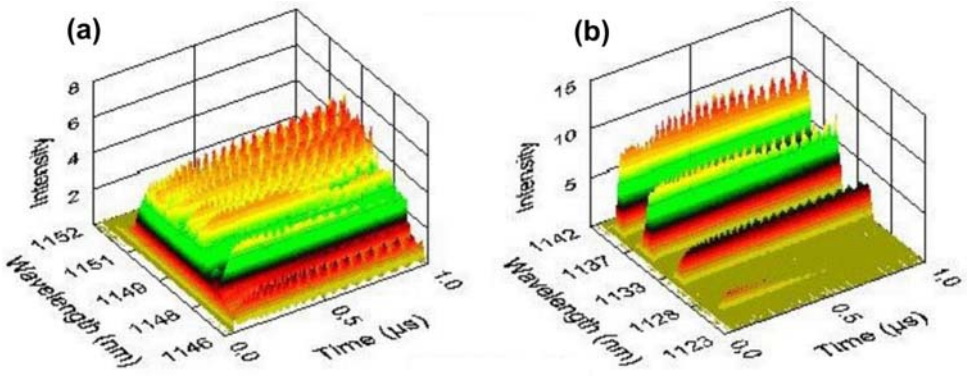

Fig. 3-15 Time-resolved spectra of the 6-fold stacked 1.14 μm InGaAs QD lasers at 1.4 x I_{th} and RT. (a) Shallow mesa device. (b) Deep mesa device. The cavity lengths are 2.5 and 1.5 mm, and the current densities are 100 and 150 A/cm², for (a) and (b) respectively.

3.3 Transient spectral characteristics of QD lasers

In the last section, we show the multimode dynamics of QD lasers fabricated from the specific laser wafer Np305I, which is grown by MOCVD and has 3 stacks of ~1.1 μm InGaAs QD layers. It needs be emphasized that the finding of antiphase dynamics and frequency damping effects in the synchronized multimode oscillations is not limited to the specific QD systems. We investigated in addition lasers based on the MOCVD grown 1.14 μm InGaAs QDs and the MBE grown 1.3 μm InAs QDs. And for all types of these QDs, the lasers may consist of up to 10 stacks of QD layers. The abovementioned dynamic features are present in all of these lasers under vastly varied conditions, suggesting that these low frequency multimode dynamics are characteristic of the QD gains. In this section, we show some transient spectral results obtained from the investigations on these additional lasers, and discuss specifically the transient spectra and spectral hole burning effects. For a dedicated study of those multi-stacked QD lasers, especially 1.3 μm InAs QD lasers, we refer to the next chapter that addresses their peculiar properties.

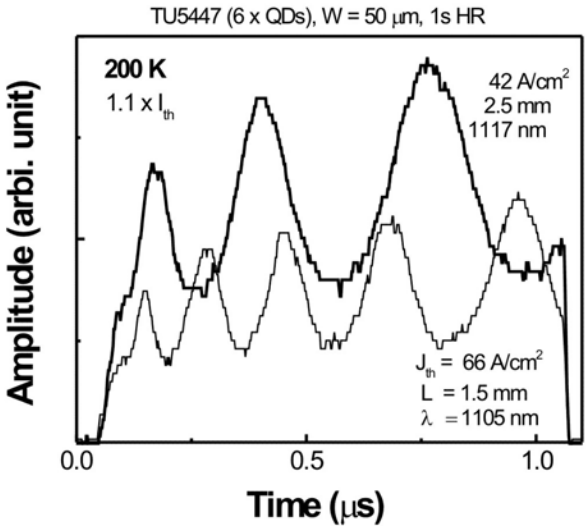

Fig. 3-16 Time traces with the lowest oscillation frequencies.

For the MOCVD grown 1.14 μm InGaAs QDs (TU5447), Fig. 3-15 shows the 3D time-resolved spectra of two lasers with different mesa etch depths and cavity lengths. The longer device (Fig.3-15a) has lower mirror loss and threshold current density, and it emits at longer wavelengths. The deep mesa device shows strong mode spectrum modulation, as in Fig. 3-15b, though both lasers have similar external efficiencies. The different spectra seem not affect the mode dynamic features at all. In Fig. 3-16, time traces recorded at 200 K are shown for both lasers. Note that the longer device keeps the low oscillation frequency record (~3 cycles in the 1 μs pulse duration), as the minimum number of

oscillation periods ever observed in the semiconductor QD lasers. This record is achieved by virtue of the low threshold current density (7 A/cm^2 per dot layer), and at a low mode power for just above threshold.

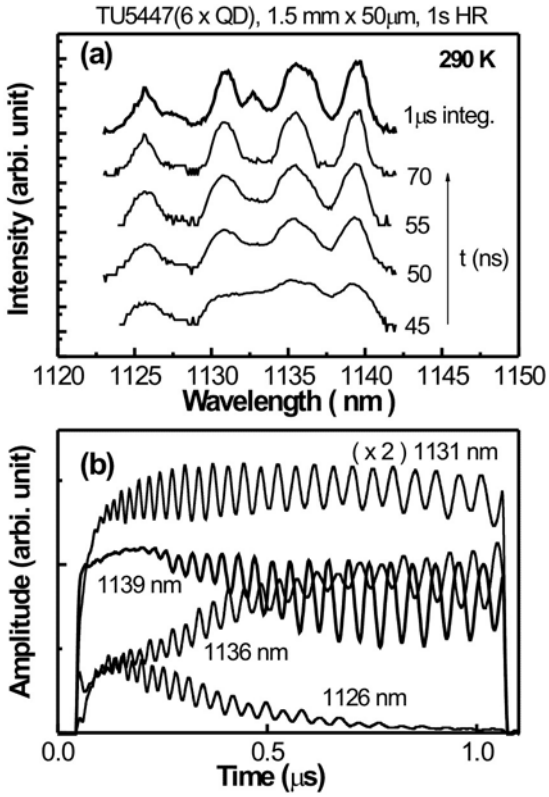

Fig. 3-17 (a) Transient spectra at 1.6 x I_{th}. The spectra are offset for clarity. (b) Time traces for peaks in (a).

The spectral intensity modulation, as seen in Fig. 3-15b, is just the lateral-cavity spectral hole burning effect as effected by the deep mesa ridge waveguide. This has been discussed in Chapter 2. The present time-resolved spectrum shows that this waveguide effect is rather stable temporally and the typical mode dynamic features are not affected by the corrupted spectral profiles. In Fig. 3-17, we show the transient spectra and time traces of this deep mesa device. Note that the denoted time is not corrected for the electronic delay of the detection system. The time traces in Fig. 3-17b show again synchronized mode oscillations and other dynamic features as referred before. In Fig. 3-17a, it can be seen that the spectral intensity modulation appears in all these spectrum transients. Indeed we observed even weak modulation patterns from the very beginning of laser turn-on. Because we observe no spectral intensity modulations in the amplified spontaneous emission spectra, this indicates that the spectral intensity modulation is indeed a kind of nonlinear laser dynamic effect.

As in Fig. 3-17a, before reaching the stable oscillation state, the emission peaks continue narrowing without peak shifts, and the valleys are deepening as well. In fact, this spectral dynamic behavior is generally observed in the QD lasers specific at high temperatures, and it is also present in the QW lasers (see the expanded spectral widths in the beginning of pulse, in Fig. 3-12).

A more general form of the above spectral feature is illustrated by the transient turn-on spectra (in 2 ns step) as shown in Fig. 3-18. Since the laser turn-on, the spectrum narrowing occurs, but only at high temperature like in Fig. 3-18b for 290 K. At low temperature, the transient spectra continuously broaden with time before the maximum spectral intensity is established. This temperature dependent spectrum effect can be related to the spectral cross relaxation in laser gain under lasing condition. For inhomogeneously broadened gain, all the modes will have a take-off in their optical powers since the laser turn-on, and those modes that reach their own specific thresholds earlier can build up power much quicker and lase. The optical modes induce spectral hole burning effects through spectral cross relaxation in laser gain, in favor of the modes with stronger intensity. The weak modes are then depressed. The homogeneous linewidth of the laser gain[18] may help define the working range of this gain compression effect, though there are other gain suppression mechanisms. The spectral narrowing behavior varies for different spectral gain profiles. In Fig. 3-18b, the spectral gain profile at RT is rather smooth and the gain width is comparable to the homogeneous linewidth that is at least 6 meV for the current studied QDs, so a global spectral narrowing occurs. In contrast, for the case in Fig. 3-17a, since laser turn-on the lateral-cavity spectral hole burning effect is also started, and its contribution adds to the above global spectral hole burning effect, leading to specifically local spectral narrowing. At low temperature, the spectral gain profile is much broader. So as can be seen in Fig. 3-18a for 50 K, a broad transient spectrum appears at the laser turn-on. Since the homogeneous linewidth is almost negligible (< 1 nm) at 50K, no spectral narrowing effect would be expected, and a spectral broadening effect is observed instead. Note that the rather weak transient emission spectrum just after the laser turn-on are in fact from lasing action, but not amplified spontaneous emission (ASE). We checked the steady state ASE spectra near threshold at both temperatures, and they are too weak compared to this transient turn-on spectrum. The intensity drop in the high energy tails, as in Fig. 3-18b, is another fact that argues against the origin of the spectral narrowing effects from the gain increment with current, as is the case for spectral narrowing in ASE spectra.

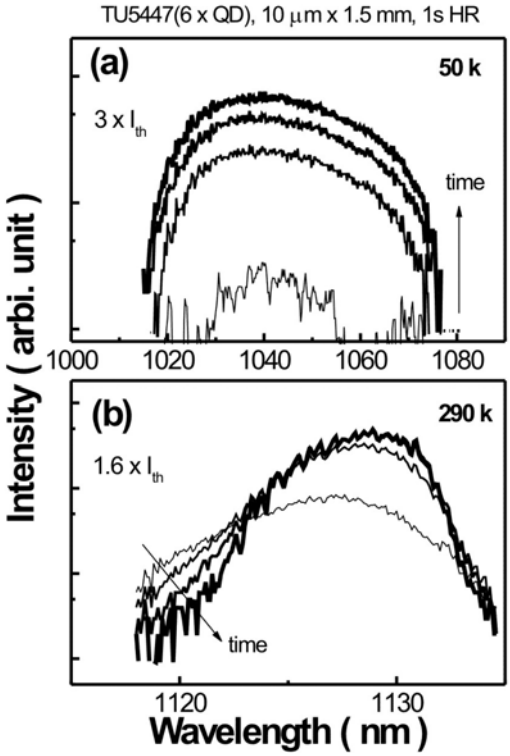

Fig. 3-18 Transient spectra of a narrow stripe 1.14 μm QD laser at various temperatures.

The extent of spectral narrowing effect could depend on sharpness of the spectral gain profile. In the QW lasers, the much narrow spectral profile and broad homogeneous linewidth of the QW gain result in a significant spectral narrowing effect, and so is the case for a QD laser at high temperature. In Fig. 3-17a, the lateral-cavity spectral hole burning effect helps modulate the gain spectrum so that the local spectral narrowing effect is enhanced. However, as shown in Fig. 3-18b, the spectral narrowing only plays a marginal second-order role in reducing the lasing width. The much smaller RT lasing width, as compared to that at 50 K, indicates a narrow gain width that results from the interdot carrier redistribution. The present result thus suggests that some previous published works.[29,32,33] overestimated the spectral hole burning effect associated with the homogeneous broadening in QD gains. The overestimation is presumably due to the roughness of the used rate equation models therein, as have been addressed in Chapter 1 concerning the nonlinear gain effects in QD lasers.

The less significant spectral hole burning effect also reduces the hope to achieve single mode lasing through gain suppression within the homogeneous linewidth. The narrowing of lasing width with temperature, as generally observed in QD lasers, is therefore mainly due to the reduction of gain width by thermal effect. In order to significantly narrow the lasing width in QD lasers, there are then two ways, either through the growth of more

uniform dots, or by sharpening the spectral gain profile by laser design. For the latter case, a mode selection mechanism can be introduced into the waveguide, such as in DFB or DBR lasers, and external cavity configurations can be taken like in the Fiber Bragg grating stabilized laser.[40] There are other novel methods, like lateral-cavity engineering as proposed in Chapter 2, or a tunnel injection scheme[41] that can be used to select a narrow range of dot energy.[40]

3.4 Summary

In the first part of this chapter, the time-resolved lasing spectra of QD lasers are investigated. We observed intense mode oscillations in the μs long time traces. The multimode dynamics show clear antiphase character, as evidenced by the complete compensation of mode oscillations in the total intensity time trace. The mode oscillation frequencies are generally higher and of a broad range at the beginning. Along the time trace, they relax to a subset of low frequencies. This frequency damping effect demonstrates the synchronization of relaxation oscillation frequencies. On the other hand, it indicates phase locking as the asymptotic behavior of mode dynamics. Comparative study with QW lasers shows that the dynamic grating effect is responsible for the antiphase mode dynamics both in QD and QW lasers. However the dynamics in QW lasers are weak and have different current dependence from that of QD lasers. We attribute these different dynamic characters to the distinct nonlinear gain properties. The characteristics of spectral and spatial cross relaxations are discussed in relation to the different carrier processes in QD and QW gains. The multifaceted dynamic features in QD lasers show that the QD lasers can be promising platforms for the study of nonlinear laser dynamics. The great flexibility of tailoring the QD structural and electronic properties would provide much possibility to explore nonlinear laser dynamics in a large space of laser parameters and dynamic variables. The specific carrier and gain processes in QDs also make the QD lasers attractive for the study of certain more general nonlinear effects in nonlinear dynamic systems, such as synchronization in globally coupled oscillator systems.

In the second part of this chapter, the transient spectral characteristics of various lasers are studied. Spectral transient narrowing effects are generally observed at high temperature in QD lasers and for all temperatures in QW lasers. The less significant narrowing of lasing widths in QD lasers suggests that the gain suppression plays a limited role in the temperature dependence of lasing width, which is attributed mainly to the narrowing of gain width with temperature due to the carrier thermal redistribution. In addition to the

global spectral narrowing effect, local spectral narrowing effects are observed in the transient spectra of the deep mesa QD lasers. The specific spectral dynamic features support the nonlinear dynamics origin of the spectral intensity modulation effects, which is related to the lateral cavity resonances in the deep mesa ridge waveguide devices. In the end, the means for significantly reducing the lasing widths of QD lasers are discussed.

References:

[1] L. V. Asryan and R. A. Suris, Appl. Phys. Lett. **74,** 1215-1217 (1999).

[2] D. Bimberg, in *Quantum Dots: Lasers and Amplifiers*, Tokyo, Japan, 2002 (IOP Publishing Ltd), p. 485-492.

[3] K. Wiesenfeld, C. Bracikowski, G. James, and R. Roy, Phys. Rev. Lett. **65,** 1749-1752 (1990).

[4] A. Uchida, Y. Liu, I. Fischer, P. Davis, and T. Aida, Phys. Rev. A **64,** 023801 (2001).

[5] B. Peters, J. Hünkemeier, V. M. Baev, and Y. I. Khanin, Phys. Rev. A **64,** 023816 (2001).

[6] L. A. Westling, M. G. Raymer, M. G. Sceats, and D. F. Coker, Opt. Commun. **47,** 212 (1983).

[7] *Optical Instabilities*; edited by R. W. Boyd, M. G. Raymer, and L. M. Narducci (Cambridge University Press, Cambridge, 1986).

[8] C. Lepers, V. Zehnle, D. Hennequin, D. Dangoisse, A. Barsella, and E. Arimondo, Opt. Commun. **125,** 121-127 (1997).

[9] C. O. Weiss and R. Vilaseca, *Dynamics of Lasers* (VCH, Weinheim, 1991).

[10] D. E. McCumber, Phys. Rev. **141,** 306–322 (1966).

[11] C. L. Tang, H. Satz, and G. deMars, J. Appl. Phys. **34,** 2289-2295 (1963).

[12] K. Otsuka, Progress in Quantum Electronics **23,** 97-129 (1999).

[13] P. Mandel, *Theoretical problems in cavity nonlinear optics* (Cambridge University Press, Cambridge, 1997).

[14] K. Otsuka, *Nonlinear Dynamics in Optical Complex Systems* (Kluwer Academic Publishers, Dordrecht, 1999).

[15] G. Vaschenko, M. Giudici, J. J. Rocca, C. S. Menoni, J. R. Tredicce, and S. Balle, Phys. Rev. Lett. **81,** 5536-5539 (1998).

[16] E. A. Viktorov and P. Mandel, Phys. Rev. Lett. **85,** 3157-3160 (2000).

[17] M. Yamada and Y. Suematsu, J. Appl. Phys. **52,** 2653-2664 (1981).

[18] G. Agrawal, IEEE J. Quantum Electron. **23,** 860- 868 (1987).

[19] J. K. Kim, T. A. Strand, R. L. Naone, and L. A. Coldren, Appl. Phys. Lett. **74,** 2752-2754 (1999).

[20] S. Ghosh, P. Bhattacharya, E. Stoner, J. Singh, H. Jiang, S. Nuttinck, and J. Laskar, Appl. Phys. Lett. **79,** 722-724 (2001).

[21] D. Bhattacharyya, E. A. Avrutin, A. C. Bryce, J. H. Marsh, D. Bimberg, F. Heinrichsdorff, V. M. Ustinov, S. V. Zaitsev, N. N. Ledentsov, P. S. Kop'ev, Z. I. Alferov, A. I. Onischenko, and E. P. O'Reilly, IEEE J. Select. Topics Quantum Electron. **5,** 648-657 (1999).

[22] M. Kuntz, N. N. Ledentsov, D. Bimberg, A. R. Kovsh, V. M. Ustinov, A. E. Zhukov, and Y. M. Shernyakov, Appl. Phys. Lett. **81,** 3846-3848 (2002).

[23] M. Travagnin, J. Opt. B: Quantum Semiclass. Opt. **2,** L25-L29 (2000).

[24] T.-C. Zhang, J. P. Poizat, P. Grelu, J.-F. Roch, P. Grangier, F. Marin, A. Bramati, V. Jost, M. D. Levenson, and E. Giacobino, Quantum Semiclass. Opt. **7,** 601-613 (1995).
[25] S. Inoue, S. Lathi, and Y. Yamamoto, J. Opt. Soc. Am. B **14,** 2761-2766 (1997).
[26] S. Lathi and Y. Yamamoto, Phys. Rev. A **59,** 819-825 (1999).
[27] K. Petermann, *Laser diode modulation and noise* (Kluwer Academic Publishers, Dordrecht, 1988).
[28] T. W. Carr, D. Pieroux, and P. Mandel, Phys. Rev. A **63,** 033817 (2001).
[29] H. Jiang and J. Singh, J. Appl. Phys. **85,** 7438 (1999).
[30] R. W. H. Engelmann, C.-L. Shieh, and C. Shu, in *Quantum well lasers*, edited by P. S. Zory (Academic Press, Boston, 1993), p. 131-188.
[31] T. Takahashi and Y. Arakawa, IEEE J. Quantum Electron. **27,** 1824-1829 (1991).
[32] M. Sugawara, K. Mukai, Y. Nakata, H. Ishikawa, and A. Sakamoto, Phys. Rev. B **61,** 7595-7603 (2000).
[33] M. Sugawara, K. Mukai, and Y. Nakata, Appl. Phys. Lett. **74,** 1561-1563 (1999).
[34] S. Riyopoulos, Phys. Rev. A **66,** 053820 (2002).
[35] Y. Kuramoto, *Chemical Oscillations, Waves and Turbulence* (Springer Verlag, Berlin, 1984).
[36] E. A. Viktorov and P. Mandel, private communication (2003).
[37] G. P. Agrawal, Phys. Rev. A **37,** 2488-2494 (1988).
[38] A. V. Uskov, Y. Boucher, J. L. Bihan, and J. McInerney, Appl. Phys. Lett. **73,** 1499-1501 (1998).
[39] D. Ouyang, submitted to PRL (2003).
[40] A. Ferrari, G. Ghislotti, S. Balsamo, V. Spano, and F. Trezzi, J. Lightwave Technol. **20,** 515-518 (2002).
[41] P. Bhattacharya, in *Advances in semiconductor lasers and applications to optoelectronics*, edited by M. Dutta and M. A. Stroscio (World Scientific, Singapore, 2000), p. 1.

CHAPTER 4 MULTI-STACKED QD LASERS

Contents:

4.1 Introduction

As in multiple-quantum-well (MQW) lasers,[1] multi-stacked QD (MQD) gain media are included in the waveguide to create lasers with larger maximum gain/differential gain, lower threshold current density, and higher output power. The high-speed laser performance can be also enhanced if the waveguide are properly designed.[2] Specifically for potential applications of QD lasers, multiple stacking of QD layers is perceived as essential to help get around the laser gain deficiency. Presently, the maximum modal gain (<10/cm) obtained from the single layer of QDs is still limited, due to the finite dot area density (~10^{10}-10^{11}/cm^2), low light confinement factor (~10^{-3}) and relatively large inhomogeneous broadening (~30-110 meV). MQD gain media also help reduce the effective carrier density per dot layer, making it possible to achieve the promising very low limit of optical loss inherent to QD gain system. By optimizing the number of QD layers and area density, the theoretically predicated low limit of threshold current density may be approached.[3,4] In practice, replicable layers of electronically uncoupled QDs now can be grown without much layer-by-layer variation in dot sizes and chemical compositions, and very low transparency current density per dot layer has been achieved with these MQDs.[5,6] Such high performance MQD lasers prepare for the exploration of their intrinsic properties. It would be particularly interesting to characterize these lasers concerning the impact of multiple QD layers (N=3-10) on both the static and dynamic lasing properties. Comparative study with different types of QDs definitely helps define the roles of different structural and electronic properties in affecting laser properties. In this chapter, we discuss

the basic lasing properties of MQD lasers, taking account of specific dot properties in different types of QDs.

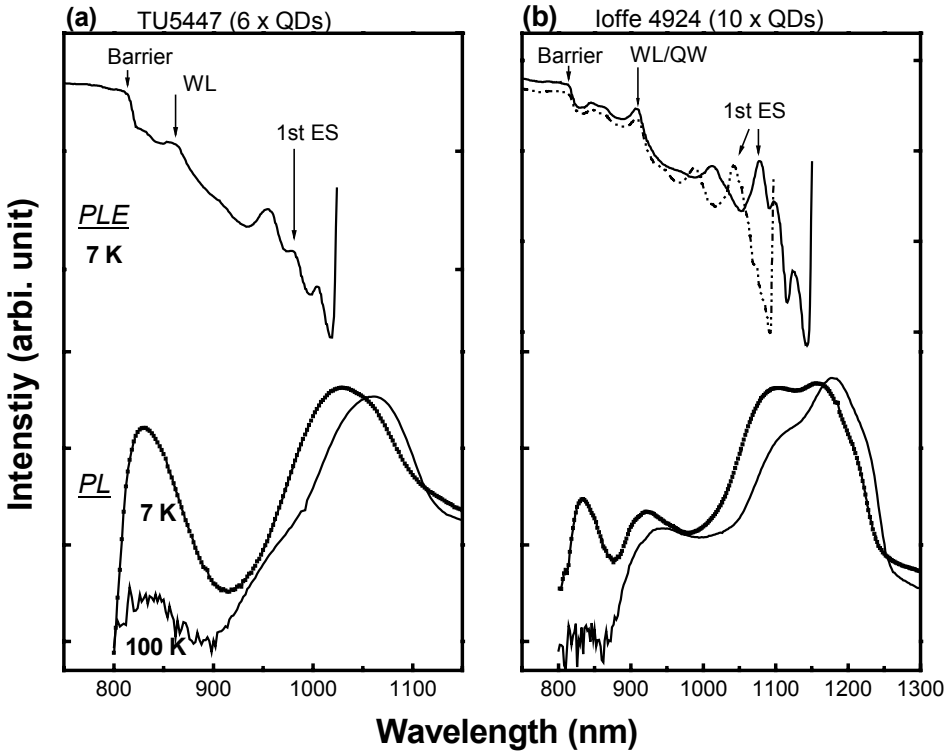

Fig. 4-1 PLE and PL spectra for (a) 6-stacked InGaAs QDs; (b) 10-fold stacked InAs QDs. The PLE spectra are detected at the GS maxima. The excitation density for PL is about 5 mW/cm².

4.2 Basic lasing properties of MQD lasers

The investigated lasers are based on 1.14 μm InGaAs QDs (TU5447 and 5430), and 1.3 μm InAs QDs (Ioffe 4914 and 4924). The detailed laser structures have been described in Chapter 1 and 2. In the following, we analyze the optical spectra of both types of QDs, to get some basic information about their electronic properties.

4.2.1 Optical properties of MQDs

The photoluminescence (PL) and excitation (PLE) spectra are shown in Fig. 4-1. Because both types of QDs are based on GaAs material system, their PL spectra share similar emission peaks for the barrier/cladding layers. The short wavelength QDs are grown in the standard Stranski-Krastanow mode, with self-organized QDs sitting on the wetting layer that consists of only a few monolayers. The PL peaks of the wetting layer and the barrier merge into one peak, as shown in Fig. 4-1a. The QD ground state (GS) peak shows typical Gaussian distribution with a FWHM of ~65 nm. In PLE spectrum, the QD 1st excited state (ES) absorption peak is accompanied with multiple LO-phonon-assisted resonance absorption peaks, and the GS-ES splitting amounts to 50 nm. In comparison, in Fig. 4-1b,

the long wavelength QDs show clearly separated PL peaks from the barrier and the wetting layer/QW respectively. This reflects the special QD growth scheme, the so-called QDs-in-a-QW (DWELL) scheme, for realizing large InAs QDs on the GaAs substrate for long wavelength emission.[7] Interestingly, the QD GS shows double peaks. Note that these PL spectra are all taken at extremely low excitation density. So the double peaks are not from the state filling effect. In the PLE spectra of both GS peaks, we can see that they share similar spectra at high energy. This indicates that these GS peaks are actually from two groups of QDs embedded in the same matrix. Both the GS peak splitting and the dispersions of each peak amount to 60 nm. In the DWELL growth scheme, a layer of seed InAs QDs is first grown on GaAs, and then the InAlGaAs QW of a few nm thick is deposited on the seed dots to increase the dot size through activated alloy phase separation. The seed dots have base sizes about tens of nm, much larger than the height and the overgrown QW thickness, so the QD quantization energy is mainly determined by the small dimensions, i.e. the dot height here. We may attribute the present bimodal dot distribution to two groups of QDs with different height that developed in the alloy phase separation step. For the same growth parameters, we expect the bimodal effect occurs for all the dot layers in this laser structure. The bimodal dot distributions have been studied in some previous works,[8,9] and there both the dot shape and In composition are suggested to affect the energy structure. Here for the dot groups with different dot height, we may expect the GS-ES splitting will be larger for the high energy group of dots. But contrarily, in the PLE spectra as in Fig. 4-1b, the GS-ES splitting can be estimated to be ~80 nm for the low energy group and ~ 60 nm for the high energy one. This reversed relation between the GS-ES splitting and the GS energy implies that the dot shape and In composition both may vary greatly in different dot groups. In the PL spectrum at 7 K, the two dot groups show comparable GS emission intensity, but at 100 K, the peak from the high energy dot group falls dramatically, indicating strong thermal distribution effects in the different dot groups. For the GS splitting is comparable to the characteristic GS-ES splitting, the thermal distribution effect in the two dot groups will add to that of thermal distribution on ES, and we would see later that the lasing characteristics and their temperature dependence will be affected by the presence of bimodal dot distribution.

In Fig. 4-2, the PL spectra are compared for the 1.3 μm InAs QDs in two laser structures with different QD layer numbers. Though the growth parameters are supposed the same in the two samples, the bimodal dot distributions still shows certain differences. The 5-fold

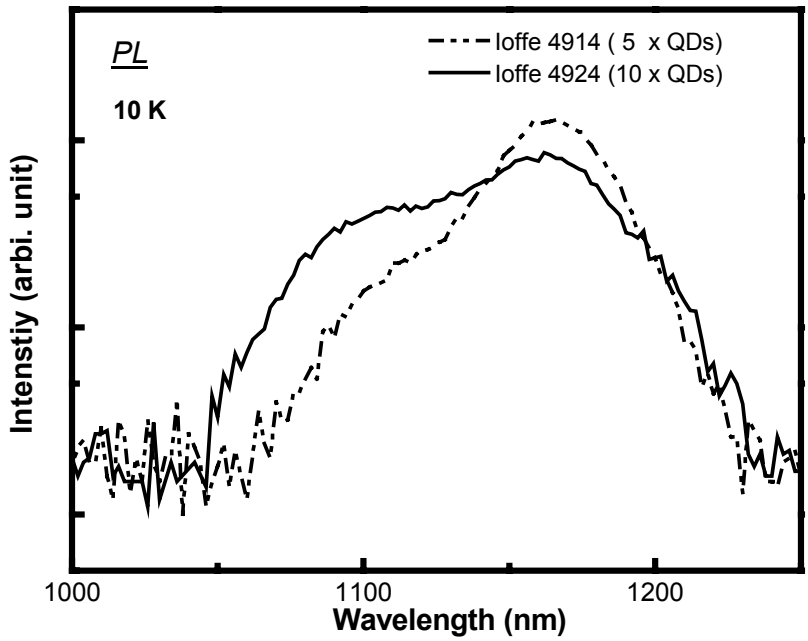

Fig. 4-2 PL spectra of 5- and 10-stacked InAs QDs. The excitation density is about 5 mW/cm².

stacked QDs show a dominant low energy group, compared to the comparable double peaks for the 10-fold stacked QDs. This may be related to different developing stages of the alloy phase separation step in the dot growth. In the 5-fold stacked QD sample, this step is developed to relatively full extent, so most of the seed dots have grown in size. This is supported by the small dispersion of the low energy dot group ~ 40 nm. In the DWELL scheme, the thickness of QW sets the limit for the growth of dot height, so a fully developed dot group will show reduced dispersion for the self-limiting effect, and the small residual dispersion can be originating from the dispersion in dot base size and possible composition variations. For the 5-fold stacked QDs, the GS-ES splitting is also reduced to 45 nm. This further supports the interpretation of the formation of bimodal distribution as due to different developing stages in the alloy phase separation step. The growth parameters are set the same for both QD samples, so the seed dot layer should have similar dot distribution. If the bimodal distribution comes from the seed dots, the double GS peaks would keep similar ratios for both samples, in contrary to the present result. The different results of alloy phase separation in these samples suggest that this growth step is rather sensitive to minor variations in growth conditions despite the same growth parameters set nominally.

4.2.2 Lasing characteristics of MQD lasers

Following the study of lasing characteristics of QD lasers in Chapter 1, we investigate the lasing properties of MQD lasers, especially their temperature dependence. Comparison is

made between lasers based on different QDs. The cavity loss is varied through using different cavity lengths and high reflection (HR) coatings. A full range of temperature from 50 K to RT is surveyed. As before, all the data are taken under pulse operation, if not otherwise noted.

a) Basic lasing characteristics

Because the investigated laser structures have very low internal losses (~2 /cm), the mirror loss becomes a significant part of the laser total loss. By using long devices and HR coatings, we can reduce the mirror loss and approach the transparency condition. The low loss operation also helps confine the lasing to the GS spectral region and to a great extent avoid the gain overlaps from ES that are of complicated energy structures.

I. Multiple dot layer effect

In Fig. 4-3, the lasing characteristics are shown for lasers based on 6- and 10-fold stacked 1.14 μm InGaAs QDs. These lasers are wide stripe devices with one side HR coating and ultralong cavity lengths, so the mirror loss (~2-3 /cm) is comparable to the internal loss.

We first discuss the multilayer effects, and compare the two devices with the same device geometry. For the laser structures (TU5447 and 5430) are of the same waveguide and dots except different layer numbers, their transparency current densities per dot layer can be assumed to be the same. The finite device loss will be matched by the gain contributed by all the dot layers. In Fig. 4-3, the difference of threshold current density is not as large as expected from the proportionality to the dot layer numbers. The threshold current and gain can be related to the layer number N as follows:

$$J_{th} = N \cdot j_{tr} + \Delta J = N \cdot J_{tr} + G_{th}/g' \qquad (4\text{-}1)$$

$$G_{th} = N \cdot g' \cdot \delta j \equiv g' \cdot \Delta J \qquad (4\text{-}2)$$

where j_{tr} is the transparency current density per dot layer, g' the differential gain coefficient, and δj the increment of current density per dot layer above the transparency level.

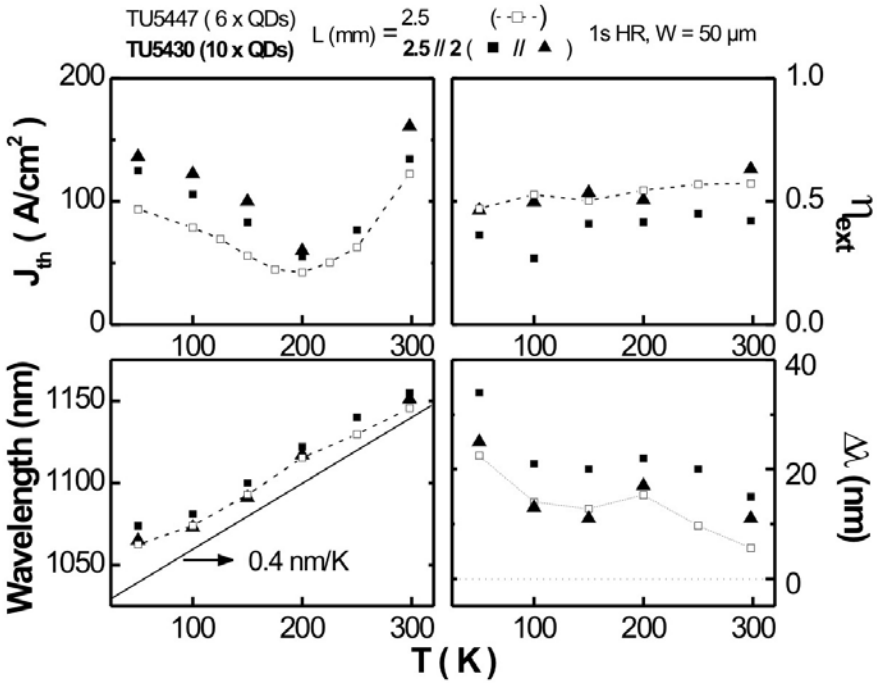

Fig. 4-3 Temperature dependences of 1.14 μm InGaAs QD lasers with different number of dot layers and cavity lengths. The solid line denotes the GS maximum wavelength λ_0 as the reference wavelength for $\Delta\lambda$.

Using the experimental data of J_{th}´s and G_{th} ~ 5 /cm, we can estimate j_{tr} and g´, which are assumed of the same value for both devices. For RT and 200 K, j_{tr} has a similar value of ~3 A/cm^2, but g´ is quite temperature dependent, with ~0.02 cm/A for RT and 0.2 cm/A for 200 K. The order of magnitude fall of differential gain coefficient g´ at RT indicates the serious gain attenuation effect due to thermionic emission and carrier thermal distribution on high energy states. Note that g´ could be current dependent, especially in high gain regime.

The external quantum efficiency η_{ext} of QD lasers can be defined in the relation:

$$\eta_{ext} = \eta_i \cdot \alpha_m/(\alpha_m+\alpha_i) \qquad (4\text{-}3)$$

where η_i is the internal quantum efficiency, α_m the mirror loss and α_i the internal loss.[10] With large carrier confinement energy and negligible nonradiative recombination in the defect-free QDs, η_i can in reality approach 100% for QD lasers with well-designed GRIN-SCH waveguide. In Fig. 4-3, both devices have η_{ext}´s around 50%, consistent with the fact that their α_m and α_i have comparable values. The 6-fold stacked QD laser structure has a measured η_i ~ 97%, vs. ~ 80% for the 10-fold stacked one. So the difference in η_{ext}´s originates from the different η_i´s.

The lasing wavelengths are related to the maximum of the spectral gain profile at threshold. In Fig. 4-3, the difference between the lasing wavelength and the GS center position λ_0 is shown as $\Delta\lambda = \lambda - \lambda_0$. Apparently both devices are lasing at the low energy side of GS, but the 10-fold stacked device is further away from λ_0. As shown in Eqn. 4-1 and Eqn. 4-2, δj is inversely proportional to the layer number N, so the threshold current density per dot layer in the 10-fold device is lower than in 5-fold one. The same is true for the carrier density per dot layer. Thus for the same device loss, the MQD gain media can help reduce the excitation density per dot layer. This explains the big difference ~ 10 nm between the lasing wavelengths of both devices in the total temperature range.

II. Temperature dependence

The temperature dependence of threshold current densities in QD lasers has been analyzed in Chapter 1, and we conclude that at low temperature the multi-stacked QDs would help enhance the negative characteristic temperature T_0. The QD layers in MQD lasers are separated by barrier layers about 30 nm thick, so the QDs are electronically uncoupled, but the interdot carrier exchange is facilitated due to the N-time increased effective dot area density. At high temperature, with the same *intradot thermal distribution*, the enhanced carrier exchange in MQD lasers would lead to efficient *interdot carrier redistribution* that may help condense the gain. But at low temperatures, the interdot redistribution processes are quenched, and leave a broad gain spectrum. At threshold, only the narrow central part of this gain spectrum contributes to the lasing action, and the outside parts of gain is totally wasted for spontaneous emission. Hence we can see that here the multiple layers do help amplify the negative effect, even though they may slightly reduce the carrier density. In Fig. 4-3, negative T_0 at low temperatures is evident for these MQD lasers. Above 200K, the thermionic emission and carrier thermal distribution on high energy states are responsible for the take-up of threshold and the resulting positive T_0.

As these devices have mirror losses α_m comparable to the internal losses α_i, their η_{ext}´s would be sensitive functions of α_i, but here in Fig. 4-3, the η_{ext}´s show only slight reduction with temperature decrease. This would indicate that the internal losses change little with temperature, if assuming η_i can only better at low temperature. But it should be noted that below 150 K, the gain inhomogeneity effect could set in for MQD lasers, as will be explored in the next chapter. So we may have to count on the variations of both η_i and α_i for the explanation of experimental results, especially at low temperatures.

In Fig.4-3, the lasing wavelength deviation from the GS center, i.e. $\Delta\lambda$, shows interesting temperature dependence. This corresponds to the temperature dependence of spectral gain profile with its maximum at threshold gain level. Generally, the interdot carrier redistribution process is expected to favor the filling of large dots, so it helps move the maximum gain to the low energy regime, i.e. positive direction in $\Delta\lambda$. Apparently, the ES could also have impact on the spectral gain profile by adding their contribution of gain or loss. This aspect is closely related to the intradot carrier distribution, and thus depends strongly on temperature and the dot-filling factor, with the latter one due to the Pauli blocking effect. The experimental results of $\Delta\lambda$ can be understood as resulting from the interplay of the abovementioned factors. As can be seen in Fig. 4-3, $\Delta\lambda$ decreases from 200 K to RT. This trend contradicts the expected if considering only the interdot carrier redistribution. So at high temperature the carrier thermal population on ES actually affects the spectral gain profile. Most probably at RT the ES gain adds to the relatively low GS one, helping match the threshold and also move the gain maximum position in the ES direction. This is possible for the GS-ES splitting amounts to ~50 nm, as compared to the GS dispersion ~65 nm. Below 200 K, the effect of ES gain is diminished for the reduced ES population and enhanced GS gain ratio to the ES one. Specifically for these devices with low threshold losses, the ES may contribute only loss at low temperature, so that $\Delta\lambda$ keeps positive for low temperatures. Again we emphasize here that the gain inhomogeneity effect may affect the apparent $\Delta\lambda$ at very low temperatures, see e.g. the excess $\Delta\lambda$ for 50 K.

Finally we compare the 10-fold stacked devices with different lengths. The mirror losses α_m amount to ~3.3 and 2.6 /cm for L = 2 mm and 2.5 mm. In Fig. 4-3, the short device shows higher threshold current density and η_{ext} for its higher α_m. Due to the increased carrier density per dot layer, its lasing wavelength blue shifts relative to that of the 10-fold long device. This is the case also for the 6-fold device compared to its 10-fold counterpart; though there is a little difference in their temperature dependence, especially at high temperatures where the 10-fold one shows relatively larger $\Delta\lambda$, reflecting the enhanced carrier exchange in the device with more dot layers.

Above all, in Fig. 4-3, the temperature dependence in these different devices shows strong similarity. This indicates that consistent results are obtained for the intrinsic lasing properties of these low loss devices with different dot layers, despite the reduced light confinement factor for those dot layers far away from the waveguide centre and the gain

inhomogeneity originating from the carrier transport effect in MQD lasers as will be explored in the next chapter.

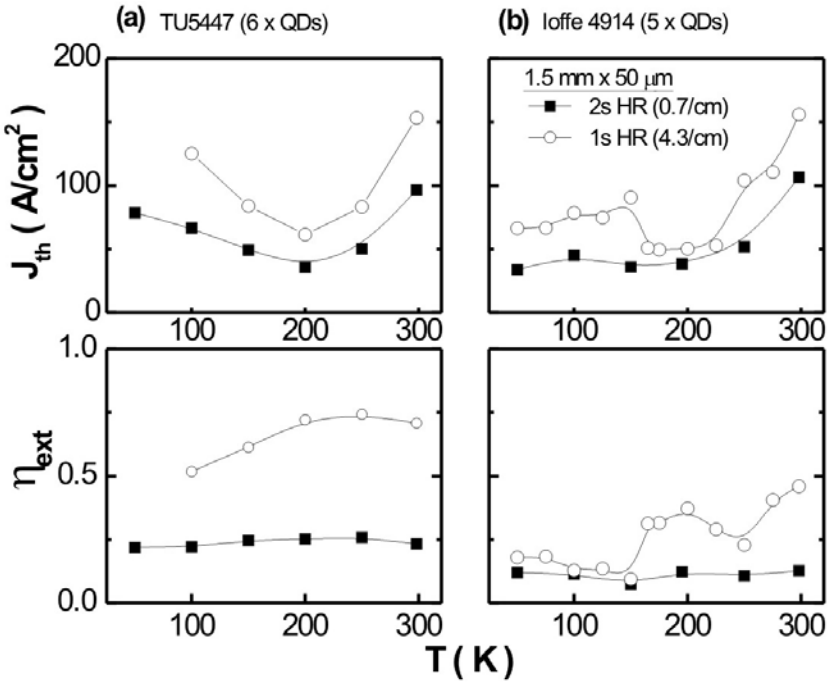

Fig. 4-4 Temperature dependence of lasers based on 1.14 μm InGaAs QDs (a) and 1.3 μm InAs QDs (b).

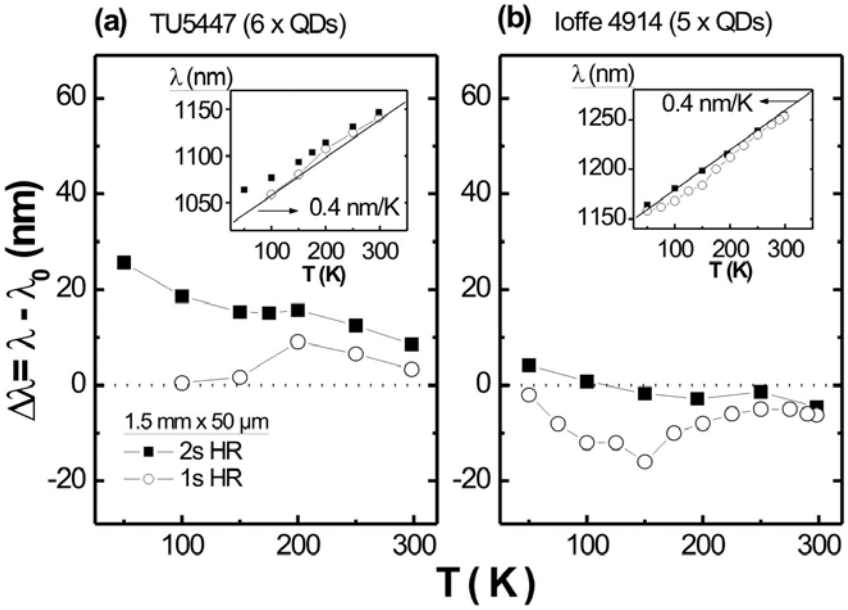

Fig. 4-5 The difference between lasing wavelength and the GS maximum wavelength λ_0 (the sold lines in the insets). The devices are the same as in Fig. 4-4.

b) Comparison with long wavelength MQD lasers

I. 1.14 μm InGaAs QDs vs. 1.3 μm InAs QDs

In this section, we compare the lasing characteristics of devices based on 1.14 μm InGaAs QDs and 1.3 μm InAs QDs. The dot area density per layer is similar for both QD laser structures, ~ 4 x 10^{10} /cm^2. The cavity lengths are fixed at 1.5 mm. The 5- or 6-fold stacked QD devices have one or two side HR coatings, and the center wavelength of the HR coatings is matched for different QDs to maintain similar reflectivity (~ 90%) at lasing wavelengths.

We first look at the two short wavelength devices. In Fig. 4-4a, J_{th}-T and η_{ext}-T relations are shown, with the corresponding $\Delta\lambda$-T relation plotted separately in Fig. 4-5a. Like those in Fig. 4-3, the short wavelength devices show similar temperature dependence. The low loss laser (2 side HR coated) shows almost constant η_{ext} but of low value due to the negligible out-coupling loss α_m. In contrast, the high loss device (1s HR) shows higher J_{th}, especially at low temperatures. The high loss also leads to significant reduction in η_{ext} below 200 K. However, the more significant low temperature effect appears in Fig. 4-5, where the lasing wavelengths blue shift to near the GS center position and strongly deviate from the temperature dependence for the low loss device. These low temperature effects are correlated, implying that the spectral gain width increases dramatically below 200 K, due to the quenching of interdot carrier redistribution process. A broadened gain spectrum needs much higher current to feed up to the threshold gain due to the low differential gain. With higher device loss, the broad gain spectrum at threshold also has a less steep top profile, so that the central lasing modes are always accompanied with strong ASE at both sides, leading to reduced η_{ext} below 200 K. Here both η_i and α_i are supposed to be constant with temperature, as suggested by the constant η_{ext} for the low loss device that is only different in the HR coatings. So Eqn. 4-3 apparently fails in this broad gain spectrum case, and an effective η_i may be used for this special case.

Next we turn to the long wavelength devices. As known in Fig. 4-2, this 5-fold stacked QD sample shows a bimodal dot distribution. From the integrated PL intensity ratio of the double GS peaks in Fig. 4-2, it can be estimated that the population of the high energy dot group amounts to about one tenth of that of the low energy one. In addition, the dispersion of low energy dot group ~ 40 nm is comparable to the GS peak interval ~ 45 nm, so the overlap of gain or loss is possible for the double dot groups. In Fig. 4-4b and

Fig. 4-5b, the low loss device (2s HR) shows rather simple temperature dependence. Above 200 K, the take-up of J_{th} is attributed to the thermionic emission and thermal distribution on high energy states. The J_{th}´s of this long wavelength device are comparable to those of the short wavelength counterpart, but below 200 K, the difference is apparent. This long wavelength laser shows almost constant J_{th} below 200 K, instead of a negative T_0 as in short wavelength devices (see Fig. 4-4a). So the ES gain can be excluded at low temperatures for this low loss device. We conclude that the low dispersion (~ 40 nm) of the dominant low energy dot group helps diminish the negative T_0 effect in the low loss case. In Fig. 4-4b, the η_{ext}´s keep almost constant but low values. This can be related to the large α_i in this 5-fold stacked QD laser structure. For the two 1.3 μm QD laser structures as in Fig. 4-2, they have exactly the same growth layer series except different dot layer numbers in the very central waveguide region. This leads to different waveguide thicknesses, with 420 nm for the 10-fold stacked QD sample and 245 nm for the 5-fold one. As these QDs emit in the 1.3 μm spectral range, the 245 nm thick waveguide is much thinner than a wavelength inside waveguide, i.e. ~ 1.3 μm/n_{eff} with n_{eff} ~ 3.4. So the confined mode profile penetrates deeply into the cladding layers, incurring high absorption loss. From the η_{ext} for the low loss device in Fig. 4-4b, we estimate the internal loss α_i amounts to ≤ 5 /cm for the 5-fold stacked QD laser structure. In Fig. 4-5b, the lasing wavelengths of the low loss device show similar temperature dependence as that of its counterpart in Fig. 4-5a, though the transition point moves to higher temperature (250 K) for the long wavelength device. This subtle difference may reflect the effect of two important aspects: (1) the low energy dot group has much reduced dispersion of ~ 40 nm as compared to the GS-ES splitting (> 60 nm), so the ES effect is minimized in the low loss case; (2) The long wavelength QDs have much deeper confinement energy than the short wavelength QDs, with ~ 260 nm for 1.3 μm InAs QDs and only 160 nm for 1.14 μm InGaAs QDs, as can be seen in Fig. 4-1 as the energy interval between the GS and the wetting layer. Finally we note that the reference wavelength in Fig. 4-5b is the GS center wavelength of the low energy dot group, rather than the total GS center wavelength as in Fig. 4-5a. Clearly if using the total GS center as the reference, the temperature dependence and the absolute value of $\Delta\lambda$ would be very similar for these two low loss lasers based on different QDs.

Now we look at the high loss (1s HR) 1.3 μm QD laser. In Fig. 4-4b and Fig. 4-5b, this device shows dramatic variations in the temperature dependence. We can recognize two

distinct temperature regions where anomalous changes take place. In Fig. 4-4b, J_{th}´s increase abnormally near 250 K and below 150 K, compared to those of the low loss device. In the same temperature regions, η_{ext}´s decrease dramatically. As such big variations have never been observed in the devices based on single-peak dispersed QDs, we attribute this abnormal temperature dependence to the bimodal dot distribution in this 5-fold stacked QD laser structure. As can be seen in Fig. 4-1b, the PL intensity ratio of the double GS peaks is very sensitive to the temperature change, indicating that the carrier thermal distribution is at least partly established in the two dot groups. The simple temperature dependence observed in the low loss device thus can be related to the low dot filling, which leads to a negligible effect from the high energy dot group that may contributes only loss in the low dot filling case. In the high loss device, the dot filling at threshold is increased. In this case, both dot groups can contribute to gain in the overlapping spectral region. Let us first see the η_{ext}-T relation. In Fig. 4-4b, the high loss device shows an η_{ext} near 50% at RT. This fits perfect to our former estimation for η_i (~ 100%) and α_i (~ 5/cm). However, below 150 K, the η_{ext}´s drop abruptly to 10 - 20%. The corresponding changes in the J_{th}´s and wavelengths are also abrupt. From the lasing wavelengths, it is apparent that at 150 K the maximum gain at threshold lies in the overlap region of both dot groups. But from the population ratio of both dot groups as in Fig. 4-2, we conclude that the gain contribution from the high energy dot group cannot move the maximum of the overlapped gain profile to the overlap region, simply due to the dominant population of the low energy dot group. Thus below 150 K, the ES gain contribution comes up to make up the GS gain deficiency, which is induced by the broadening of gain width due to the quenched interdot carrier redistribution. From 150 K to 50 K, the lasing wavelengths move back the GS center of the low energy dot group, indicating that the gain there is enhanced at lower temperatures. This contradicts the situation in single-peak distributed QD lasers as in Fig. 4-4a, where the gain would be dispersed for the continuous broadening of gain width at low temperatures. The possible explanation for this apparent contradiction can be traced to the bimodal dot distribution and the small dispersion of the dominant dot group. The trend of gain width broadening will be limited in the QDs with small dispersion. Meanwhile, the carrier thermal distribution in the bimodal dot groups induces the temperature dependence of the gain in the high energy dot group. At lower temperature, the reduced loss or enhanced gain contribution from the high energy dot group would add to that from the dominant dot group, thus help enhance the maximum gain at the low energy dot group. The quenching of intradot carrier distribution also helps

condense the gain at lower temperatures. In total, the enhanced GS gain requires less ES contribution to match the threshold gain, leading to the reduction of J_{th} and slight increase of η_{ext} at lower temperature. In Fig. 4-4b, near 200 K, high η_{ext}´s and low J_{th}´s are apparent. Here the ES contribution is still present, but the GS gain dominates the threshold gain. Above 200 K, the thermionic emission takes up. It is expected that the high energy dot group is more affected than the low energy one, for their different confinement energy. This may result in enhanced loss from the high energy dot group and lead to the reduction of η_{ext} and increase of J_{th} near 250 K. Above 250 K, both dot groups are strongly affected by the thermionic emission, and thermal distribution on ES and higher energy states takes up. The J_{th}´s dramatically increase, but due to the significant interdot carrier redistribution at high temperature, the gain width is greatly reduced and η_{ext} returns to normal value as defined by Eqn. 4-3.

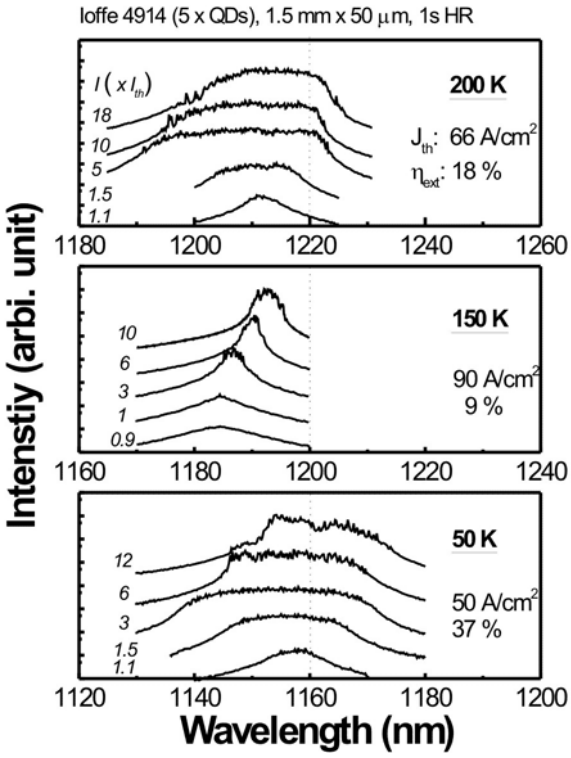

Fig. 4-6 Lasing spectra of the 5-fold stacked 1.3 μm InAs QD laser. The dotted lines denote the GS maximum positions of the low energy dot group in the bimodal dot distribution. The spectra are offset for clarity.

The above complicated temperature dependence is also reflected in the lasing spectra. In Fig. 4-6, the high loss device shows quite distinct spectral features at different temperatures. At 200 K, the spectra expand quickly to the high energy side, indicating a continuously growing strong ES gain contribution. Strikingly, the high energy side begins to retreat above 5 x I_{th}, and some sharp peak patterns appear there. Meanwhile, we can see

that the low energy part of the spectra continue increasing and expanding. This spectral feature is not a junction heating effect as all the spectra are taken under pulse operation. We attribute the retreating spectral part to the induced absorption in the high energy dot group. Above 5 x I_{th}, the strong lasing power begins to saturate due to the gain saturation. In this saturation stage, the gain renormalization may occur between the ES gain and that of high energy dot group. Through carrier depletion and competition, the carrier occupation in the high energy dot group may be drained out for the much less dot population in this group. The induced absorption effect is closely related to the gain saturation. As in Fig. 4-6, at 150 K, the lasing starts farther away at the high energy side with the help of ES gain contribution. Up to 10 x I_{th}, no lasing occurs at the GS center position of low energy dot group, indicating a saturated gain there due to the broadened gain spectrum. With current, the induced absorption leads to red shift, due to the carrier competition effect that favors the dot group with dominant population. At 50 K, the lasing starts near the GS center position, and the spectra expand in both directions comparably, indicating a strong GS gain presumably due to the quenched intradot thermal distribution. At high currents, similar spectral variations occur as those at 200 K. But in this case, the peculiar features appear rather near the GS center, showing that the ES contribution is less pronounced here than at 200 K.

Above all, the spectral characteristics as discussed are consistent with our former interpretation of lasing characteristics as in Fig. 4-4b and Fig. 4-5b, indicating that the bimodal dot distribution indeed affects the basic lasing properties significantly. The carrier distribution in the bimodal dot groups is strongly temperature dependent, and the resulting gain spectrum is also dependent on the relative population of different dot groups. So it would be interesting to compare the lasing properties of devices with different bimodal dot distributions. In the following, we investigate the 10-fold stacked 1.3 μm QD lasers that happen to possess comparable dot populations in the bimodal dot groups.

II. Bimodal dot distribution effect

Compared to the above 5-fold stacked 1.3 μm InAs QD lasers, the 10-fold ones have much more significant bimodal dot distribution, as in Fig. 4-2. In addition, as can be deduced from the PL and PLE spectra in Fig. 4-1b, the *dispersion* of the double GS peaks in the 10-fold stacked QD laser structure is similar to their peak interval, with both at ~ 60 nm. The *GS-ES splitting* amounts to ~ 80 nm for the low energy dot group and ~ 60 nm for the high energy one. This crowded energy structure and large inhomogeneous

broadening make it possible to have many complex overlapping possibilities among the double GS peaks and their ES. In the spectral range concerned in the following study, we may neglect the overlapping effect from the ES of the high energy dot group for it is too far away (~ 120 nm) from the low energy GS.

Table 1 Device parameters

Cavity length (mm)	HR coating (R ~ 90%)	Mirror loss (/cm)	Stripe width (μm)
1	2side	1	50
1.5	1side	4	50
1.5	none	8	100
0.7	none	17	100

To vary the device losses, we use a combination of cavity lengths and facet coatings as listed in Table 1. As discussed in last section, the 10-fold stacked 1.3 μm InAs QD laser structure has an optimal waveguide thickness, compared to the 5-fold one that has a much thinner waveguide. The latter one shows a high internal loss of ~5/cm, due to the field penetration into the highly doped cladding layers. It is expected that the present 10-fold QD laser structure has a lower α_i.

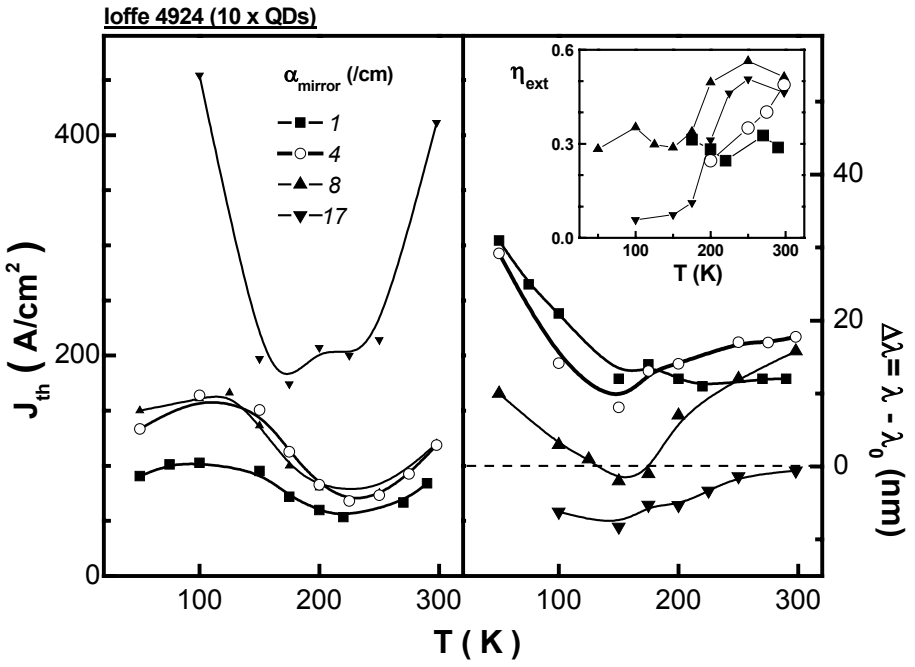

Fig. 4-7 Temperature dependence of 10-fold stacked 1.3 μm InAs QD lasers with various mirror losses.

In Fig.4-7, the lasing characteristics are shown for the 10-fold devices of various mirror losses. From the RT η_{ext} for the device with the lowest α_m ~ 1 /cm, α_i can be estimated to be ~ 2-3 /cm. This is also supported by the separate wafer test on broad area devices with varied cavity lengths and as-cleaved facets, and there η_i is found near 100 %.

We first compare the two devices with respective α_m ~1 and 4 /cm. In Fig. 4-7, we refer to the GS of the low energy dot group as the 1st GS and use its center wavelength as the reference wavelength λ_0. It can be seen that, for both devices in the total temperature range, the lasing wavelengths reside on the low energy side of the 1st GS center, indicating that the threshold gain is dominated by the GS gain from the low energy dot group. The low loss device (α_m ~1 /cm) shows shorter wavelengths than the high loss (α_m ~4 /cm) one. This is rather counter intuitive, for in the lasers based on single-peak distributed QDs the increase of the gain maximum level is generally accompanied by the blue shift of wavelength. So the bimodal dot distribution is causing an unusual λ - G_{th} relation in the low loss regime. The J_{th}´s still increase with threshold loss in a usual way, so with current, the 2nd GS is filled and its reduced loss or increased gain helps red shift the gain maximum wavelength. The low loss device shows almost constant lasing wavelengths down to 150 K, indicating that the thermal redistribution in the bimodal dot groups causes little change in gain maximum position. Its J_{th}´s increase only slightly above 200 K, showing the benefits of multiple layers of QD gain and the deep confinement energy of 1.3 μm QDs. Below 200 K, the J_{th}´s increase as the result of broadened gain width due to the quenching interdot carrier redistribution processes. However, from 150 K to 50 K, the J_{th}´s become stabilized somehow. We note that in this temperature range, the lasing behavior is strongly influenced by the gain inhomogeneity as caused by the carrier transport effect in MQDs. This effect is particularly reflected in the strongly red shifted lasing wavelengths and the abnormal slope characteristics of the light-current curves near the threshold current region. For the latter reason, no realistic η_{ext}´s can be drawn, so note that in the inset of Fig. 4-7 no η_{ext}´s are plotted for that temperature range. The gain inhomogeneity effect will persist for α_m up to 8 /cm. So for the three low loss devices, their low temperature lasing characteristics defy a normal reasoning based on the data as in Fig. 4-7. We refer to the next chapter for a detailed analysis of the peculiar spectral and dynamic characteristics that are related the carrier transport effect in MQDs. In the following we continue the discussion of high temperature lasing characteristics. In Fig. 4-7, from RT to 200 K, η_{ext}´s

of the high loss device (α_m ~4 /cm) decrease dramatically, with lasing wavelengths blue shifting. This suggests that η_i deteriorates with temperature decrease. We may exclude the contribution of any significant amount of nonradiative recombination centers like defects or impurity, because firstly the QDs are defect-free and secondly the devices already show excellent, almost ideal η_i (~100%) and α_i (~2-3 /cm) at RT. Here we propose a model to explain the observed reduction of η_i. The energy structure of the bimodal distributed 1.3 μm InAs QDs is illustrated in the following energy level schematics:

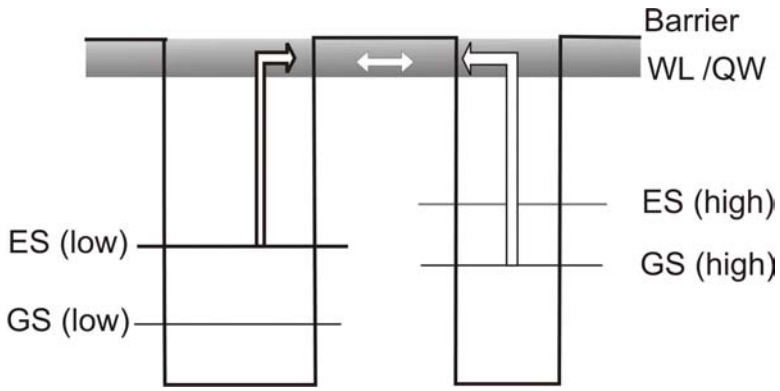

Here the energy intervals scale with the realistic ones as deduced from the PL and PLE spectra in Fig. 4-1b. The left represents the low energy dot group, and the right corresponds to the high energy dot group. Only GS and the 1st ES are shown and we ignore any higher ES of QDs. As can be seen, the low energy ES is a little bit higher than the high energy GS, and their energy interval (~ 20 nm) is much lower than the dispersion (≥ 60 nm). At high temperatures, the different dot groups can exchange carriers through the wetting layer/QW and barriers by thermal escape and recapture processes. When J_{th} is relatively low so that the ES is not filled, the carriers would shuffle between both GS. For its apparent deeper confinement energy, the low GS will be favored in the interdot carrier thermal redistribution. Now if J_{th} is increased so that the low ES is also being filled, the carrier shuffling will involve not only both GS but also the low ES. Here we assume that the high ES is not filled for the high energy dots are disadvantaged in the dot-filling factor in total. As the thermal escape process is temperature sensitive, the carrier direct escape from the low GS will slow down quickly with temperature decrease for its high thermal activation energy. When the role of the low GS wanes, we are left with the low ES and high GS. In this case, the thermal escape of the low ES is relatively faster than that of the high GS. The carrier shuffling between these two energy levels will favor the high energy dots, and lead to a relative loss of carriers in the low energy dots. Here we attribute the

formerly observed reduction of η_i to such a loss of carriers in the lasing low energy dots. Actually there is certain similarity between the function of the high GS here and the deep energy level usually associated with the impurity or defect. It is noted that the above described carrier competition scenario happens if only the above illustrated energy level arrangement exists. In the current studied 10-fold stacked QD lasers, it is the significant bimodal dot distribution that makes this carrier competition scenario more apparent for certain dot-filling conditions.

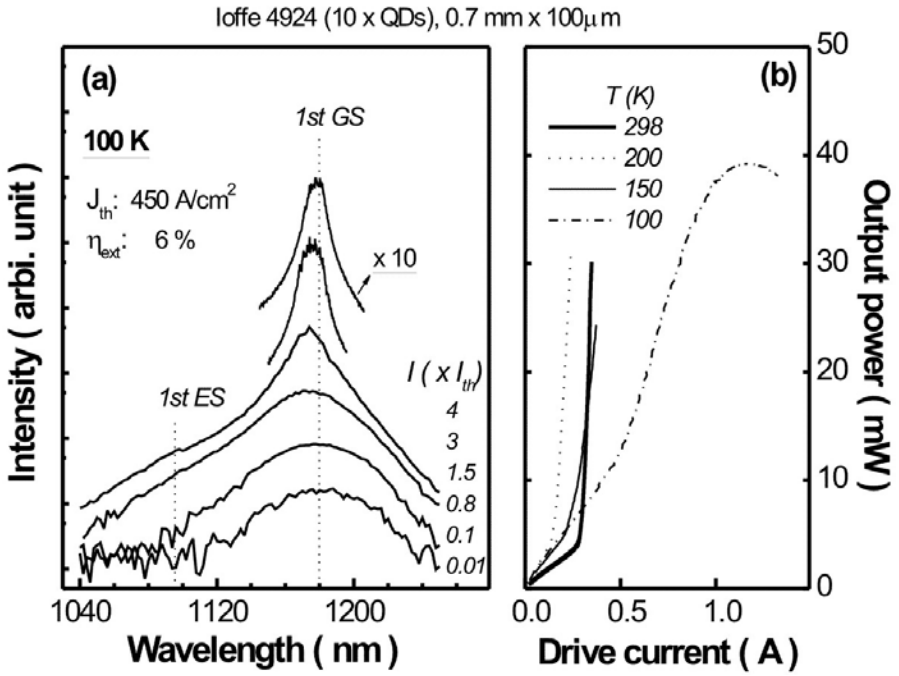

Fig. 4-8 (a) Emission spectra at 100K, and (b) L-I curves of the 10-fold stacked 1.3 μm InAs QD laser.

Next we examine the left two devices with highest losses (α_m = 8 and 17 /cm). In Fig. 4-7, the device with α_m = 8 /cm shows very similar J_{th} as that with 4 /cm. As listed in Table 4-1, the former device has a stripe width of 100 μm compared to 50 μm for the latter one. For the current spreading effect in these shallow mesa devices becomes less significant in the broad area device, this leads to the apparent reduction in its J_{th}´s. Nevertheless, even after taking account of the current spreading effect, the temperature dependence of J_{th}´s looks still very similar between the two devices. Significant difference appears in their lasing wavelengths. From RT to 150 K, the lasing wavelengths of the former device blue shift strongly back to the 1st GS center, indicating the increased gain contribution from the low ES and high GS. The η_{ext}´s of this device are generally lower than expected. From Eqn. 4-3 by using the known η_i and α_i for this laser structure, we would expect an η_{ext} near 80% for RT, as compared to the actual value of only 50%. This can be understood as

follows: At higher threshold loss, the dot-filling factors of the low energy dot group need be increased to match the threshold gain, but a part of the increased carriers will go to the low ES as thermal population. The increased population on the low ES will be lost to the high GS through the former illustrated carrier competition process, thus leading to a reduced effective η_i andη_{ext}. In Fig. 4-7, below 200 K, the η_{ext} of this device falls abruptly

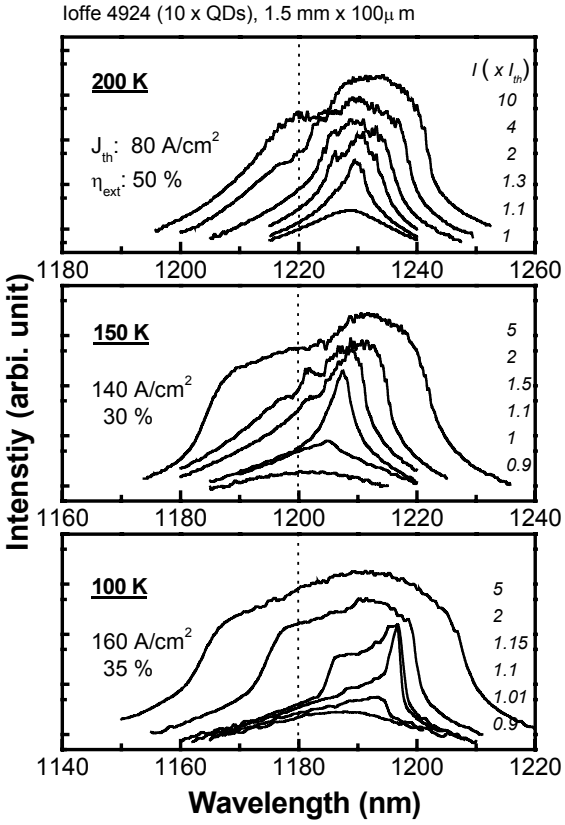

Fig. 4-9 Lasing spectra of a 10-fold stacked 1.3 μm QD laser. The dotted lines denote the GS maximum wavelengths of the low energy dot group in the bimodal dot distribution.

to 30%. We attribute this change to the gain width broadening that takes up below 200 K. The fall of η_{ext} becomes even more dramatic for the device with α_m = 17 /cm. Near 200 K, its η_{ext} drops from 50% to 10%. Apparently this device suffers strong gain saturation effect. Near 200 K, its J_{th} reaches 200 A/cm^2, compared to <100 A/cm^2 for other devices. Its lasing wavelengths reside at the high energy side of the 1st GS center. The even higher J_{th}´s of > 400 A/cm^2 at RT and below 100 K indicates the saturated gain has been reached. In Fig. 4-8a, the lasing spectra in this extreme case are shown for 100 K. With current, the lasing widths even decrease, showing extreme temperature sensitivity of the saturated low energy GS gain. As can be seen, the emission of the high energy GS is rather limited as compared to that from the low energy GS, indicating that at such high current density, the high energy dot group is filled insufficiently due to the thermal redistribution between the

two dot groups. In addition, the 1st ES (i.e. the low ES in the above bimodal QD energy schematics) can be seen as a shoulder of the GS peak, implying a strong ES filling, for otherwise the ES absorption should inhibit its appearance in the emission spectrum. In Fig. 4-8b, the light-current curves are shown for various temperatures. Below 200 K, strong nonlinear effects occur. The roll-off at high current and 100 K coincides with the high current saturation spectral features: reduced lasing widths and spectral red shift as in Fig. 4-8a.

In Fig. 4-9, a series of lasing spectra are shown for the device with α_m = 8 /cm. Above 200 K (not shown), the spectra are rather symmetric and smooth, with flattop profiles for I >2 x I_{th}. At 200 K, the spectra are still centered at the threshold lasing wavelength up to 2 x I_{th}, and at higher currents additional feature appears on the high energy side. The rather distorted profile may be attributed partly to the complex carrier redistribution processes under lasing condition that involve carriers from both GS and the low ES. At lower temperatures, the spectra are no longer centered at the threshold wavelength and they evolve to the extreme case at 100 K. As noted before, these peculiar features can be comprehensible only by taking account of the gain inhomogeniety effect, as to appear in the next chapter.

4.3 Summary

In summary, we investigate the lasing properties of MQD lasers and their temperature dependence. At first, the multiple dot layer effects on the basic lasing characteristics are demonstrated in 1.14 μm InGaAs MQD devices. The intrinsic lasing properties are revealed consistently in various low loss devices. In the next, lasers based on 1.14 μm InGaAs QDs and 1.3 μm InAs QDs are compared to show the effects of different dot confinement energy on their temperature dependence. In particular for the 1.3 μm InAs QD laser structures, various bimodal dot distributions are characterized by PL and PLE spectra. We found that the bimodal dot distribution has dramatic impact on the laser temperature dependence. In addition to the abnormal temperature dependence in lasers with a dominant dot group, the bimodal dot distribution also causes strong reduction of internal quantum efficiency in lasers with comparable bimodal dot groups. It is proposed that the reduced effective η_i results from carrier thermal redistributions between the bimodal dot groups with specific energy level arrangements. Finally the study of the 10-fold stacked 1.3 μm QD lasers with varied mirror losses indicates that their spectral characteristics are affected not only by the complex carrier redistribution processes

between the bimodal dot groups, but also by the gain inhomogeneity originating from the bottlenecked carrier transport in MQDs at low temperatures. The carrier transport effect will be treated in the next chapter.

References:

[1] R. W. H. Engelmann, C.-L. Shieh, and C. Shu, in *Quantum well lasers*, edited by P. S. Zory (Academic Press, Boston, 1993), p. 131-188.

[2] K. Y. Lau, in *Quantum well lasers*, edited by P. S. Zory (Academic Press, Boston, 1993), p. 217-275.

[3] L. V. Asryan and R. Suris, Semiconductor Science and Technology **11,** 554 (1996).

[4] L. V. Asryan and R. Suris, IEEE Journal of Quantum Electronics **34,** 841-850 (1998).

[5] G. T. Liu, A. Stinz, H. Li, T. C. Newell, A. L. Gray, P. M. Varngis, K. J. Malloy, and L. F. Lester, IEEE J. Quantum Electron. **36,** 1272-1279 (2000).

[6] D. Bimberg, in *Quantum Dots: Lasers and Amplifiers*, Tokyo, Japan, 2002 (IOP Publishing Ltd), p. 485-492.

[7] M. V. Maximov, A. F. Tsatsul'nikov, B. V. Volovik, D. S. Sizov, Y. M. Shernyakov, I. N. Kaiander, A. E. Zhukov, A. R. Kovsh, S. S. Mikhrin, V. M. Ustinov, Z. I. Alferov, R. Heitz, V. A. Shchukin, N. N. Ledentsov, D. Bimberg, Y. G. Musikhin, and W. Neumann, Phys. Rev. B **62,** 16671-16680 (2000).

[8] S. Anders, C. S. Kim, B. Klein, M. W. Keller, R. P. Mirin, and A. G. Norman, Phys. Rev. B **66,** 125309 (2002).

[9] T. K. Johal, G. Pagliara, R. Rinaldi, A. Passaseo, R. Cingolani, M. Lomascolo, A. Taurino, M. Catalano, and R. Phaneuf, Phys. Rev. B **66,** 155313 (2002).

[10] L. A. Coldren and S. W. Corzine, *Diode Lasers and Photonic Integrated Circuits* (Wiley, New York, 1995).

CHAPTER 5 CARRIER TRANSPORT EFFECT IN MQD LASERS

Contents:

5.1 Introduction

In the last chapter, the carrier transport effect is claimed to be responsible for generating gain inhomogeneity in MQDs, which causes deviations of the lasing characteristics of

MQD lasers from the intrinsic ones. In this chapter, we present a detailed study of the carrier transport effect.

5.2 Background

In semiconductor heterostructure devices, the carrier transport can be a serious issue that confronts the device design and characterization. The quantum structures generally used in the device active regions show characteristic transport properties pertaining to their specific quantized energy level structures. Therefore the quantum transport problem has attracted much attention since the advent of quantum structure devices.[1,2] In the variety of carrier transport aspects in heterostructure, we are interested in the carrier statistical transport, which can be either in plane with or across the heterojuntions. The in-plane transport has much to do with the lateral devices such as field-effect devices or photodetectors[3]. Experimentally the lateral carrier transport has been studied in QD-based devices, and it is revealed that carrier confinement in QDs leads to much reduced carrier diffusion length and unusual in-plane velocity-field characteristics with enhanced carrier mobility at high electrical field.[4,5] The lateral carrier transport in QDs is found to be dominated by the slow hopping process at high temperatures.[6] In the present work, we concentrate on the carrier transport across the multilayer quantum structures. The vertical carrier transport has not been studied before in QD devices. However, its importance is undoubted as MQDs prevail in devices like QD heterostructure lasers and detectors. A basic understanding of the carrier transport effect is indispensable for device characterization and design that aims to improve the device performance. In particular for MQD lasers, we would see that the carrier transport effect deeply impacts the laser dynamic behavior. This could provide a natural test bed for the study of nonequilibrium and inhomogeneous gain dynamics.

As the natural precedent, the carrier transport effects in MQW devices and particularly in MQW lasers have been studied intensively in the last decades.[7-10]The experimental investigation and theoretical modeling reveal a wide range of impacts brought about by the carrier transport effects. The impact on the dynamic properties of MQW lasers is rather profound, and attracts most of the attentions. From the carrier injection into the waveguide, through the carrier drift to and captured by the QWs, to the carrier escape and drift or tunnel to the following QWs, every step can be critical for the high speed response of MQW lasers. The bottleneck in the carrier transport chain across the MQWs would lead to non-uniform carrier injection with severe carrier accumulation, which then could limit

the laser modulation speed and cause strong dynamic broadening of lasing linewidth or frequency chirping. So the design of MQW lasers oriented to high-speed operation has become mainly a task of containing the carrier transport problems therein.

Up to date it seems that the vertical carrier transport in MQDs is the least addressed QD device property, except that the transport through a single pair of coupled dots has been investigated recently.[11] There is at least one practical reason for this status. That is the lack of high quality MQD samples till recently. The growth of well-ordered QDs in single layers has been possible for long. But it is only recently that it becomes possible to grow electronically uncoupled MQD structure with minor layer-by-layer variation in dot size and shape, and especially the growth front can be kept constantly planar up to 10 stacks. This is actually a feat of refined nanotechnology[12] and the step stone for achieving further fine control of QD structures. In this thesis work, we take advantage of the high performance lasers based on these high quality MQDs. In Chapter 4, the basic lasing characteristics of these MQD lasers have been shown to be consistent with the multilayer numbers. The state-of-the-art, high quality MQD devices prepare a good start point in materials and devices for the transport study. On one hand, it excludes the possibility of layer-by-layer non-uniformity from the material side. On the other hand, it allows exploring a large range of dot-filling factors, and helps reveal the intrinsic MQD transport phenomena that would otherwise be screened by strong state filling effect in high threshold devices.

Nevertheless, the transport study in MQD lasers is more challenging than the MQW counterpart. In MQWs, it is possible to tune the layer separation and the tunneling rate between neighboring wells without dramatic change in the energy scheme. In contrast, when the QD layer separation becomes smaller, the growth encounters problems with the QD layer-by-layer variations. Even though the MQDs may keep certain spatial correlation between multilayers, the electronic couplings between QDs in separate layers could change the whole energy scheme dramatically. The electronic properties of QDs are rather sensitive to the perturbation from the environment,[13] such as the strain. To bring QDs near to each other means not only strain engineering,[14] but also the art of controlling the electronic coupling properties.[15] The size, shape, composition and distance all can be the involving factors in determining the final state of electronic coupling. This situation reflects the challenging aspect in the device characterization and design that address transport issues in MQDs. In addition, in MQW lasers, the study of transport effects is oriented to the high-speed laser properties. [10,16] But presently, the high-speed dynamic study of QD

lasers is still in the early stage, thus prohibiting the investigation of much complex transport effects. The abovementioned factors limit the actual possibility of the carrier transport study in MQD devices. There are other aspects that may complicate the issue further. For example, in QDs, the charge neutrality condition is violated due to the electrostatic conditions.[17] With optical pumping in the barrier, charged excitons can be formed in QDs simply due to the different diffusivities of electrons and holes in the barrier, which originate not only from the difference in the effective masses of different carrier types, but also from the complex energy dependence of carrier relaxation and thermalization rate processes. This charge non-symmetry effect has been taken advantage to intentionally generate heavily charged exciton complexes in QDs for single dot spectroscopy.[18] However, for QD lasers it is a rather complicating effect. Like in QW lasers, the carrier charge imbalance near the QDs may affect the gain and waveguide properties.[19]

With the above limitation in mind, we investigate the carrier transport effect in MQD lasers by a comprehensive analysis method. It is known that the transport effects at high temperature (around RT) may become significant and detectable only at high modulation frequencies, but presently there still lack effective modeling of high speed MQD lasers as useful for the analysis of transport effects. Therefore, in this work, we avoid the high-speed modulation study, but make a temperature dependent study of spectral characteristics and the spectral transient dynamics. A series of devices are surveyed with different multilayer numbers (N = 5,6 and 10) and various device losses. Both types of QDs (1.14 μm vs. 1.3 μm) are compared concerning the role of different carrier confinement energy. It turns out that all these varied parameters have strong impact on the spectral and dynamic output of MQD lasers. The detailed analysis shows that the gain inhomogeneity incurred by the bottlenecked carrier transport plays a major role in determining these peculiar spectral features.

In the following, we first discuss the carrier transport processes and the resulting gain inhomogeneity in MQD lasers. Then we analyze the peculiar spectral features and discuss their relation to the carrier transport effect. In Section 5.4, we present the spectral transient analysis of those peculiar spectral features, in support of their origins from the carrier transport effect, and discuss the dynamic processes underlying the complex mode dynamic phenomena.

5.3 Carrier transport processes and gain inhomogeneity in MQD lasers

Now return to the basic issue. As shown by Monte Carlo modeling of steady state carrier distribution in MQW lasers, electrons and holes are distributed non-uniformly in the MQWs.[7] Holes are much affected for their larger effective masses, and electrons can diffuse fast to adapt to the holes, so that ambipolar approximation holds. In steady state lasing conditions, the carrier non-uniformity can increase with the current and optical power, leaving a hole reservoir near the p-type cladding layer. However, in high-speed case, the ambipolar approximation is found to be impropriate for the explanation of experimental results, thus it has been given up instead to treat electrons and holes separately in the dynamic transport. In MQD lasers, these situations still hold true in general, but only differ in the details and consequences.

As in the MQWs, the basic carrier transport processes are similar in the MQDs. The carriers are captured in the first dot layer, and then some of them escape from the dots and drift through the barrier toward the following dot layers, with the former processes repeated. It is interesting to compare the carrier capture in the QW and QDs. For a typical QD layer with an area density ~ 4 x $10^{10}/cm^2$, the total capture cross section amount to ~50 %, if a dot capture cross section[20] of 1.3 x 10^{-11} cm^2 is assumed. In contrast, a QW has a 100% physical cross section, though the capture probability has to be considered. In this first comparison, the QW shows advantage. But when come to carrier escape, the QW is also advantageous over the QDs, for the deep confinement of carriers in QDs. In total, the carrier transport across the QW is more efficient than across the QDs. So no wonder that the carrier in-plane diffusion length is much reduced in QDs compared to in the QW.[4] This comparison is more justified at low temperature when the carrier thermal escape from the QDs becomes quenched.

Due to different confinement energy for the electron and hole, the thermionic emission rates of electrons are much more affected by temperature. One recent temperature dependent PL study[21] particularly addressed this issue by supporting the picture of independent capture and escape for electrons and holes in QDs in a large temperature range. With slowed electron emission at low temperature, the ambipolar approximation is not justified for carrier transport. At even lower temperatures, the hole emission can be suppressed as well, leading to more severe non-uniformity for hole distribution.

From the above discussion, it can be concluded that the non-uniformity of carrier distribution in MQDs can be more severe for more dot layers, deeper confinement energy and lower temperature. At high temperatures when the electrons can move relatively fast across the dot layers, ambipolar approximation holds, and the steady state carrier distribution is characterized by the graded hole distribution across the dot layers, with more abundant holes near the p-type cladding layer. On the contrary, at lower temperature, the electrons cannot adapt to the hole distribution, so an inverse graded electron distribution could result from the bottlenecked electron transport. The unipolar non-uniformity of both electrons and holes can only increase the degree of gain inhomogeneity in the QD multilayers. Note that this type of gain inhomogeneity has nothing to do with the in plane gain distribution, which is assumed homogeneous under uniform current injection if not considering other factors.

As in MQWs, the carrier non-uniformity can change with current and optical power. A large dot-filling factor would block the carrier capture significantly due to Pauli blocking effect, and it also increases the carrier escape due to enhanced Auger escape. Both results help relieve the carrier non-uniformity by enhancing the carrier transport across the MQDs. As to optical power, below threshold the spontaneous emission lifetime (≤ 1 ns) defines the time interval in which the fast carrier transport processes can balance themselves to establish a steady state carrier distribution. Under lasing condition, the stimulated emission lifetime becomes much shorter, in tens of ps range, which is comparable to certain carrier transport processes. In this case, the lasing process would compete with the limited carrier transport, and modify the already non-uniform carrier distribution in MQDs. The carriers, gain and optical power are closely related in a complex dynamic system, so it is not guaranteed that a steady state carrier distribution will always result from this competition process. Whereas in a homogeneous single-dot-layer laser the lasing process will follow adiabatically the carrier and gain process, we may expect that in MQD lasers a kind of self-organization process could take place, with the carrier transport processes interacting with the lasing modes through gain formation and depletion in both spatial and spectral regimes. This self-organization dynamic process may be monitored in the laser turn-on transient. It is useful to note some typical values for the time constants of carrier transport processes in In(Ga)As/GaAs QD lasers:

(i) Carrier escape through thermionic emission in the order of several tens to a few of ps, depending on the temperature and confinement energy;

(ii) Electron transport in the barrier region below ps, but hole transport up to tens of ps for its larger effective mass;

(iii) Electron capture and cascaded relaxation in QDs in less than 10 ps at RT,[22] but with much fast hole processes. The time constant increases at low temperature, but can decrease to less than 10 ps at high carrier density due to carrier–carrier scattering or Auger-assisted capture and relaxation.[23]

Clearly, among these involved unit carrier processes, the electron thermal escape and hole transport in the barrier are the possible limiting steps that would finally determine the carrier distribution in the QD multilayers. So the deep carrier confinement in QDs represents an advantageous situation where we can gradually tune the rates of the limiting steps in carrier transport and the extent of gain inhomogeneity by simply changing the temperature. At low temperatures, the bottlenecked carrier transport effect then could be revealed in a laser dynamics with relatively low characteristic frequency that makes the experimental observation easier. The related spectral feature could be also enhanced due to the stronger gain inhomogeneity. In the following, we analyze the low temperature lasing spectra of MQD lasers. The peculiar spectral features are surveyed with varied temperature, device loss and confinement energy. The relation to the limited transport and the gain inhomogeneity is discussed.

5.3.1 Spectral analysis of carrier transport effects

a) Emission spectra of 1.14 μm InGaAs MQD lasers

I. The 6-fold devices

In Fig. 5-1, the amplified spontaneous emission (ASE) spectra at 50 K are shown for the 6-fold stacked 1.14 μm InGaAs QD lasers of various device parameters. First we look at the four-sided laser. Below threshold the ASE spectra from this special type of laser approximate the true spontaneous emission spectra, and for detailed discussion of this aspect we refer to Chapter 6. In Fig. 5-1, it can be seen that the true spontaneous emission spectra conform to the dot dispersion and show rather symmetric spectral profiles centered at the supposed GS center wavelength λ_0~ 1040 nm.

Now come to the two ridge lasers with different device losses. In contrast, their ASE spectra deviate strongly from the true spontaneous emission spectra. We know that this deviation is typical for the ASE spectrum of devices with strong optical feedback. So these

ASE spectra reflect the spectral gain profile in each device. At extremely low current density, 0.01 x I_{th}, the spectral gain is much lower than the device losses, so the emission spectra are less affected by the gain amplification, and both devices show similar spectral profiles but with the maximum far away from the GS center. We attribute this distortion from true spontaneous emission partly to the ES loss and exclude the possibility of strong effect from the interdot redistribution at this low temperature. In Fig. 5-1, with current, the two devices show significant difference in the region near the GS center, contrary to that as expected if assuming the spectral gain profile develops with current in a similar way in both devices. Thus the different ASE spectra indicate that the varied device losses could affect the spectral gain significantly. We may note that this effect could be the first sign indicating that the spontaneous emission can involve in the carrier distribution process along with the limited carrier transport.

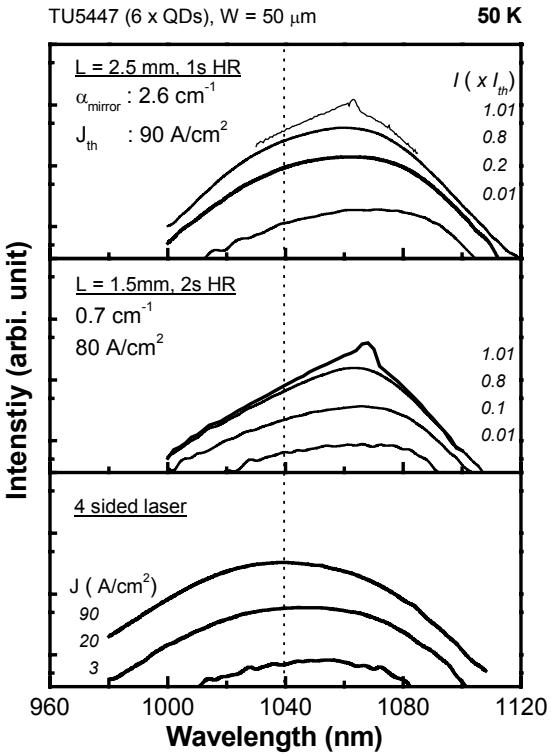

Fig. 5-1 ASE spectra of the 1.14 μm QD lasers with various device geometries. The dotted lines denote the GS maximum position.

In Fig. 5-1, the lasing spectra just above threshold are also shown for 1.01 x I_{th}. Both spectral shapes in the lasing region are rather asymmetric. Especially on the low energy side there is a distinct lasing edge that separates the lasing region from the ASE part clearly. Note that such a difference in ASE spectra and the peculiar feature in lasing spectra have never been observed at high temperatures in these devices. The lasing spectra of the above two lasers are shown in Fig. 5-2, along with those from another high loss device. As can be

seen, the lasing spectra of the high loss laser (α_m ~4 /cm) show rather symmetric spectral profile near threshold and no peculiar features as for the other two low loss devices. It is known that the symmetric spectral shape near the lasing region is a general feature of near threshold lasing spectrum as observed in QD lasers with fewer dot layers or higher losses. The symmetric spectrum property is also true for the high temperature lasing spectra of QD lasers with very low losses and more dot layers. So the abnormal spectral features only appear at low temperatures in lasers with low losses and enough number of dot layers. This correlation with the laser parameters matches exactly with the former discussion concerning the carrier transport effect, strongly suggesting that the abnormal spectral features result from the bottlenecked carrier transport in the MQDs.

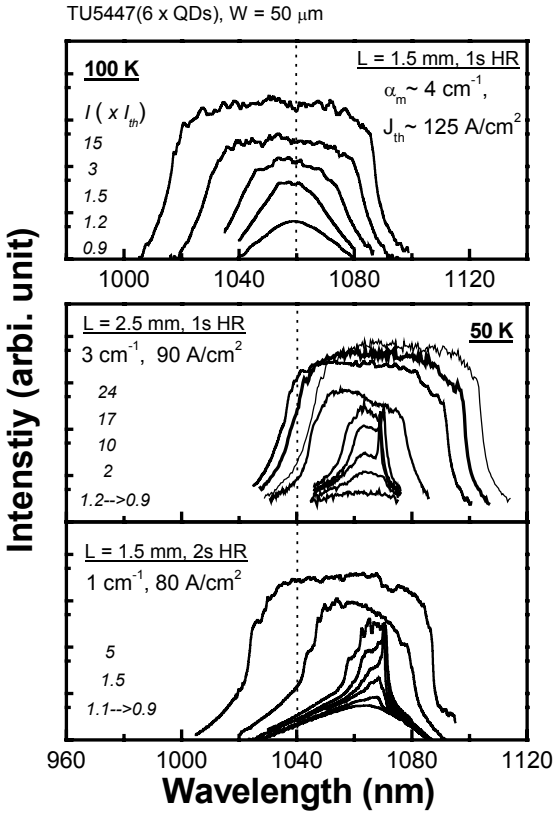

Fig. 5-2 Lasing spectra of 6-fold stacked 1.14 μm QD lasers with various mirror losses.

In Fig. 5-2, at 50 K, the spectral profiles of both low loss devices evolve with current up to 1.2 x I_{th} continually. Not only is the asymmetry apparent, but also there appears a sharp peak near the lasing edge. We can see there is slight difference in these features between the two devices. The shoulder of the sharp peak increases almost abruptly with current. At higher current, the broad spectrum gradually assumes a flattop profile, resembling the normal case as like the 100 K spectra in Fig. 5-2 for the high loss device. But differently the

flattop spectrum at 50 K is red shifting with current above 10 x I_{th}, compared to the stable spectra at 100 K of the high loss laser.

Above all, these rather abnormal spectral features are not comprehensible from the spatially homogeneous QD gain. As can be seen in Fig. 5-1 and Fig. 5-2, the ASE spectra at different current densities never show any sharp features, and all of them possess only smooth spectral profiles. This indicates that at least the lasing process is necessary for the occurrence of those peculiar features, and certain spatial inhomogeneity in spectral gain should be coupled with the optical power in an interactive way. It needs be emphasized that for the two low loss lasers, the above spectral abnormalities are absent above 150 K.

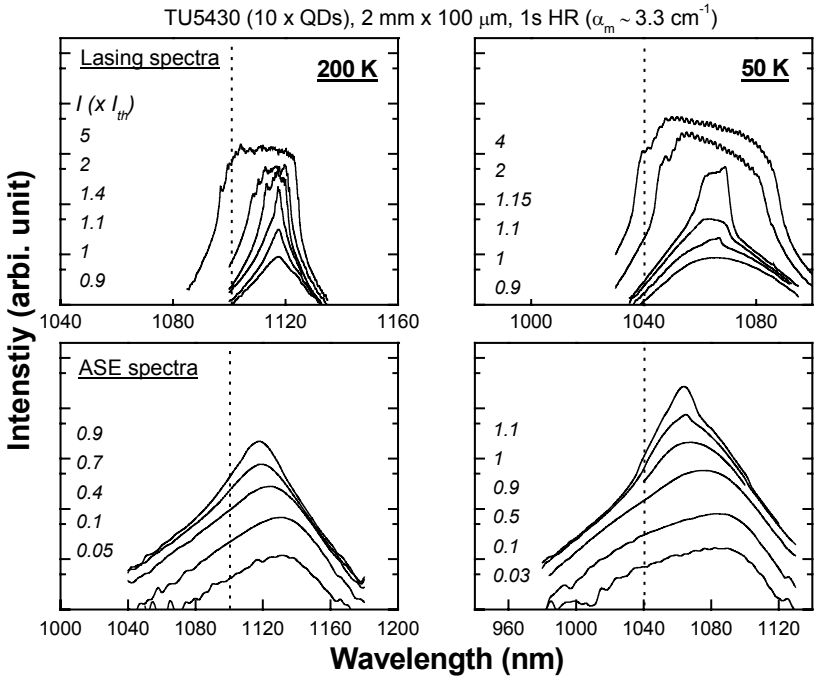

Fig. 5-3 Emission spectra of a 10-fold stacked 1.14 μm QD laser with current and temperature. The dotted lines denote the GS maximum positions respectively.

II. The 10-fold devices

In lasers with 10-fold stacked 1.14 μm QDs, we can see similar abnormal features. Fig 5-3 shows the ASE spectra and lasing spectra of one 10-fold device at 200 K and 50 K. These are only two examples. The spectra above 200 K are similar to those at 200K, and with temperature the spectral features are actually transforming gradually from the type of 50K to that of 200K. The ASE spectra at 200K show typical blue shifted gain maximum with current due to the interdot carrier redistribution. The spectral shape near threshold is rather symmetric and no skewed profile can be seen in the lasing spectra. However, at 50K the near threshold spectra show again a wedged shape, and the top profiles of high current spectra are skewed. The lasing edge is evident too in these spectra.

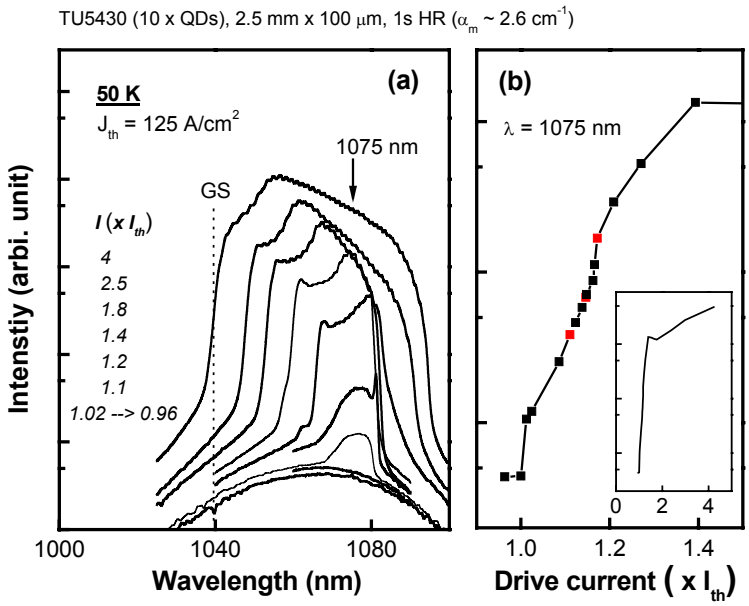

Fig. 5-4 (a) Lasing spectra of a 10-fold stacked 1.14 μm QD laser; (b) the current dependence of the emission intensity for the mode with λ = 1075 nm. The inset shows the full current range.

For a 10-fold device with slightly reduced loss, the lasing spectra are shown in Fig. 5-4a. In these spectra the abnormal features become more distinct. Above the extremely symmetric and smooth ASE spectra, the lasing action just above threshold takes place far away from the maximum of the ASE profiles, which is supposed to be also the gain maximum. In comparison, the high loss 10-fold device lases directly at the ASE maximum, as in Fig. 5-3. The fact that the lasing action seems not happening at the gain maximum is rather counterintuitive, so is the bell-like lasing peak away from the gain maximum if considering so minute current increase for such a big change. To have an idea of the spectral intensity evolution, the mode intensity change with current is shown for λ = 1075 nm in Fig. 5-4b. As shown in the inset for the whole current range, the mode intensity increases since threshold, and then saturates at high currents, similar to the most cases in QD laser spectra. However, a zoom-in into the initial stage before saturation shows detail changes with enormous anomalies. The most striking feature is the first intensity jump near threshold, where the extreme current sensitivity goes beyond the experimental current precision. Apparently this kind of lasing behavior looks totally crazy. This is still not the end.

In Fig. 5-4a, from 1.02 to 1.1 x I_{th}, the bell-like spectrum evolves with a shoulder appearing at high energy side and a sharp peak at the lasing edge. This development resembles the effect in Fig. 5-2 for the 5-fold device that has the same device geometry and loss. After the abnormal low current stage, the spectrum expands for currents above 1.2 x I_{th}. In Fig.

5-4a, we can see that on the high energy side of these spectra, the spectral profile keeps almost constant shape in the dramatic spectral expansion. This distinct feature strongly suggests that the actual gain could be composed of two or more gain components that are varying coherently with current and leading to the near constant intensity profile on the high energy side. Whereas, on the low energy side, the distinct lasing edge persists even after the expansion begins on the other side. Only since above 1.5 x I_{th}, the fixed lasing edge is replaced by spectral expansion. Note that the skewed top profiles of the high current spectra eventually will evolve into a flattop profile for much higher currents, which is not shown here but similar as those in Fig. 5-2.

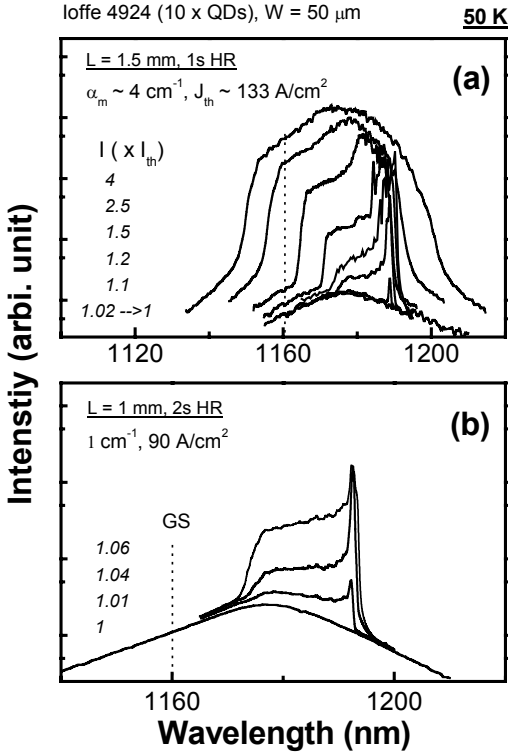

Fig. 5-5 Lasing spectra of 10-fold stacked 1.3 μm InAs QD lasers with different cavity losses.

b) Emission spectra of 1.3 μm InAs MQD lasers

After discussing the spectral features in the 1.14 μm MQD lasers, we note that the similar spectral abnormality appears in the 1.3 μm MQD devices, despite the bimodal dot distributions. For example, as in Fig. 4-9 for the 10-fold stacked 1.3 μm MQD device, the spectral features gradually change with temperature. From 200 K to 100 K, the near threshold spectra become asymmetric and the lasing peaks move away from the ASE maximum. The 100 K spectra are already very similar to those 50 K spectra of the 10-fold stacked 1.14 μm MQD laser as in Fig. 5-4a.

Note that the 1.3 μm device in Fig. 4-9 has a higher loss than that in Fig. 5-4a. But for the 1.3 μm device, the 150 K spectra already show abnormal features. In comparison, the 1.14 μm device shows the abnormal spectra only below 100 K. We attribute the different temperature threshold for the spectral abnormality to the different confinement energy of these QDs. With deeper confinement energy, the gain inhomogeneity from the bottlenecked carrier transport can take up at higher temperature due to the earlier quenched thermal escape. The deeper confinement energy also helps resist the effect of high device losses (or equivalently large dot-filling factor) in diminishing the extent of gain inhomogeneity.

In Fig. 5-5, the lasing spectra are shown for two 10-fold 1.3 μm devices with low losses. The spectra in Fig. 5-5a are almost the reproduction of those in Fig. 5-4a. They are only different in the near threshold regime. This 1.3 μm device starts lasing in a single sharp peak just above threshold, instead of the bell-like peak in the 1.14 μm device. In Fig. 5-5b, another 1.3 μm device with lower loss starts even with a broad lasing region featuring a sharp peak at the lasing edge. These varied near threshold spectra show that despite apparent difference here or there, a common set of features exist in different devices. Therefore the above comparison supports common origins for the peculiar spectral features appearing in lasers based on different QD systems. Specifically for the 10-fold 1.3 μm devices, it is to thank their low device losses that the ASE maximum is about 20 nm away from the low GS center, so that the effect of bimodal dot distribution is avoided.

It is noted that for the 5-fold 1.3 μm QDs, the concerned peculiar features can be observed only in the devices with the lowest cavity loss (~ 0.6 /cm) and below 50 K. We attribute this strict condition to the higher internal loss of the 5-fold 1.3 μm laser structure and the smaller multilayer number as compared to the 10-fold laser structure. As in Fig. 4-6, the 50 K spectra for a high loss device show rather normal features near threshold. At even higher device loss, the spectra of the 10-fold device also return to the normal state, as in Fig. 4-8.

Clearly the peculiar spectral features will be reflected in the basic lasing characteristics. The effect on J_{th}´s is not apparent, but the large $\Delta\lambda$´s at low temperature, as shown in Fig. 4-3, Fig. 4-5 and Fig. 4-7, are more or less directly affected by the varied spectral features. Like the mode intensity-current relation shown in Fig. 5-4b, the light-current characteristics may show also the jump, kinks and other irregularities, as in Fig. 5-6. The jump in these cases would lead to a nominal η_{ext} greater than 100%. This rather absurd situation can be only

understandable by taking account of the gain inhomogeneity and its dynamic aspect, as these light-current curves contain only time-averaged results. Due to these apparent abnormalities, η_{ext} is not shown in Fig. 4-7 for those low loss devices at low temperatures.

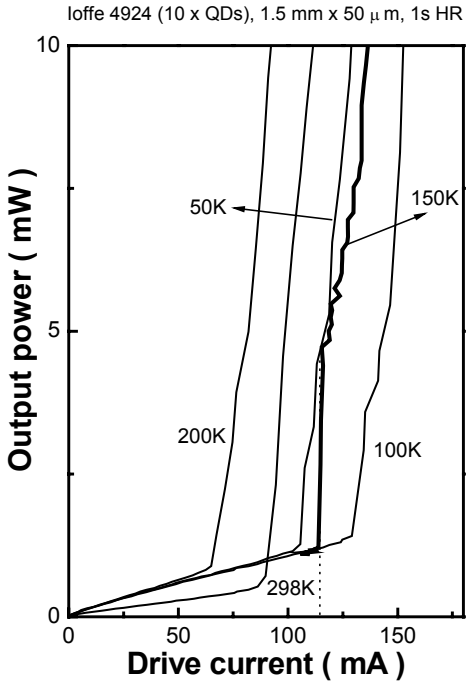

Fig. 5-6 L-I curves of a 10-fold stacked 1.3 μm QD laser at various temperatures. The dotted line indicates the abruptness of the jump section.

5.3.2 Discussion

Based on the above spectral analysis, we discuss the carrier transport effect in MQD lasers under the variations of certain parameters. As stated before, the electron escape and hole transport are the candidate of rate limiting processes for carrier transport in QD multilayers. Though the hole transport certainly has a role in determining the carrier non-uniformity, we are not concerned to discuss that, for the hole transport is supposed not to be affected significantly by the variations of the present set of parameters.

We start with the discussion of temperature effect. As the spectral analysis shows, the peculiar spectral features are totally absent at high temperatures. This indicates that the radiative recombination does not affect the carrier distribution so dramatically as at low temperature. At high temperatures, the carrier transport across the multilayers can be rather efficient due to the fast thermionic emission. Under lasing conditions, the efficient carrier transport can match the carrier depletion loss induced by the stimulated emission, thus maintain the gain stable and relatively uniform in MQDs.

At low temperatures, thermionic emission becomes quenched, and bottlenecks the carrier transport in MQDs. The inefficient carrier transport not only leads to a carrier distribution with strong *non-uniformity* across the multilayers, but also induces strong *nonequilibrium* carrier distribution in every dot layer, due to the quenched interdot carrier redistribution. Below threshold, carrier transport can still follow adiabatically the relatively slow spontaneous emission (~1 ns), so that the carrier distribution among MQDs remains intact. In this situation, the non-uniformity of carrier distribution changes little with current, and so is the gain inhomogeneity. This is reflected in the modest evolution of ASE spectra with current, without distorting the smooth spectral profile, despite the underlying strong non-uniformity of carrier distribution among MQDs.

As the threshold is approached, the stimulated emission rate overrides that of spontaneous emission, and intense carrier depletion ensues at the gain maximum region. Apparently when the carrier depletion rate goes up with optical power to the limited capacity of carrier transport, a stable lasing becomes unsustainable in the original configuration of carrier and gain distribution. In a spatially homogeneous gain, the limited carrier transport would only lead to the saturation of gain and optical power. However in a strong non-uniform carrier and gain configuration, the rearrangement of carrier distribution among the multiple dot layers is still possible. The gain then can adapt its spectral and spatial profile to the actual lasing condition. The lasing peak may deviate from the original gain maximum position for the broad spectral gain profile. It is reasonable to assume that for stronger carrier non-uniformity and nonequilibrium, the room for the carrier and gain rearrangement will be larger in both spatial and spectral dimensions, and the resulting lasing spectrum could deviate from that supposed for the original gain spectral profile in a greater manner. In reality, the spectral analysis supports the above reasoning. In all the MQD lasers investigated in this work, the lasing peak just above threshold lies either directly on the near threshold ASE maximum, as in a normal case; or red shifts from that supposed gain maximum, as shown by the peculiar features. The red-shift deviation from the ASE maximum shows strong dependence on the temperature, multilayer number, device loss and dot confinement energy. Like for a 10-fold 1.3 μm device in Fig. 4-9, the red-shift deviation increases continuously from almost zero at 200 K to near 10 nm at 100 K. It reaches about 15 nm for the 10-fold 1.14 μm device (see Fig. 5-4), and even 20 nm for other 10-fold 1.3 μm devices with lower cavity loss, as in Fig. 5-5. These results thus show that the peculiarity of spectral features is indeed related to the carrier transport effect, including the carrier and gain non-uniformity in MQDs.

As to the effect of device loss, it has been correlated to the effect of dot-filling factor. With a high dot-filling factor, the carrier capture probability in the first few dot layers is reduced and meanwhile the carrier escape is enhanced due to the Auger escape and the increased ES occupation. Thus the carrier transport problem at low temperatures can be alleviated with high dot-filling factors. For the similar device loss, the lasers with fewer dot layers will have higher dot-filling factors, and this can be the reason why it is not possible to observe the peculiar feature at low temperature in the 3-fold QD lasers. Note that for the 5-fold 1.3 μm device with relatively high loss, the feature is absent for the same reason.

Finally we consider the devices based on different QD systems that differ in the carrier confinement energy. The deeper confinement energy will make the non-uniformity of carrier distribution persist at higher temperatures and higher losses. Thus in the 1.3 μm MQD lasers, we can observe the peculiar features in a wide range of parameters.

In the end, it needs be emphasized that in the above spectral analysis we only address the time-averaged spectral features. Though the peculiar features are apparent, they are rather counterintuitive for understanding the underlying lasing processes. The same is true for the light-current characteristics. So in order to recover the dynamic information behind the peculiar features, we make transient spectral analysis in the next section.

5.4 Time-resolved study of carrier transport effects

In this section, the time-resolved lasing spectra of MQD lasers are studied to help clarify the dynamic aspects of carrier transport effect in MQD lasers. We first make detailed analysis of the spectral dynamics of the peculiar features as observed in time-averaged lasing spectra, and then discuss the underlying carrier and gain dynamics that interact with the carrier transport processes.

5.4.1 Transient spectral analysis

From the time-averaged spectral analysis, we know that the peculiar spectral features in MQD lasers vary with the temperature, device loss and dot confinement energy, as well as the multilayer number. Not to be lost in the vast variety, we take example for the 10-fold stacked 1.3 μm MQD lasers in the following time-resolved spectral analysis. These 1.3 μm lasers show distinct spectral features in an extended range of temperature, thus facilitate the analysis. The very low loss device is specifically chosen to show clear and enhanced carrier transport effects by avoiding (1) the diminishing effect of high dot-filling factor and (2) the disturbing of the bimodal dot distribution. As the similarity of the peculiar spectral features

is evident between 1.3 μm and 1.14 μm MQD lasers, the present analysis is generally applicable for MQD lasers based on both types of dots. As default case, the lasers are pumped with the electrical square pulses.

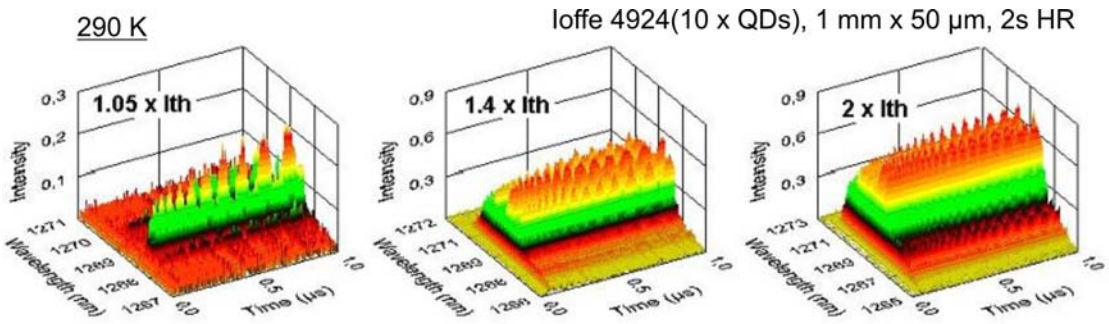

Fig. 5-7 Time-resolved spectra of the 1.3 μm QD laser. The GS maximum lies at 1260 nm for 290 K.

a) RT spectra--- a normal case

As a normal case for comparison, we begin with the RT spectra for the 10-fold 1.3 μm QD laser. The time-resolved lasing spectra are shown in color-mapped 3D plots in Fig. 5-7. The regular mode oscillations are evident, and the oscillation frequencies increase with current. Even the frequency damping effect is apparent, thus reminiscing the similar observation discussed in Chapter 3. In Fig. 5-8a, the mode resolved spectra are shown in 2D color-mapped plots. The longitudinal mode structures are well resolved with mode distances ~0.2 nm, consistent with the 1 mm cavity length. To clearly demonstrate the phase relation of mode oscillations, the mode center intensities are picked up and plotted in Fig. 5-8b. The clear check board patterns evidence antiphase oscillation relations between neighboring modes. Though the phases of a few neighboring modes are not in a perfect π relation, the spectral-integrated time trace shows that the mode oscillations compensate almost completely, leaving a constant total output intensity trace.[24] This result coincides with the case in Chapter 3, demonstrating that the typical low frequency multimode dynamics exists in lasers based on both QD systems. We note that the dynamic grating effects are critical for this type of antiphase mode dynamics. The time-averaged lasing spectra are shown in Fig. 5-9a for RT. Near threshold, the lasing peak is centered at the ASE maximum, as in the normal case.

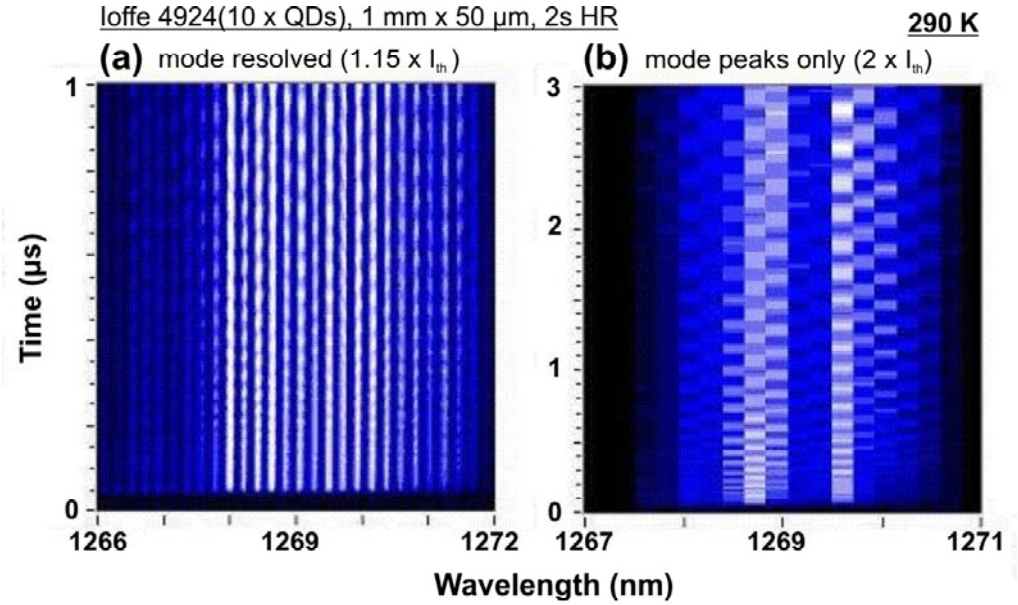

Fig. 5-8 Time-resolved spectra of the 1.3 μm QD laser as in Fig. 5-7, (a) with longitudinal mode structure resolved, (b) only the mode center peak intensity is shown.

b) Low temperature spectra---abnormal cases

The time-averaged lasing spectra are shown in Fig. 5-9b for 175 K. In contrast to the RT case, near threshold, the lasing peak red shifts ~5 nm away from the ASE maximum. Note that the red shift begins to appear since 200K, and it continuously increases with temperature decrease, as can be seen in Fig. 5-5b for 50 K.

We first make a detailed analysis of the 175 K spectral features and the dynamics. At high currents, the 175K spectra show camelback-shaped shoulder on the high energy side of the main peak, as in Fig. 5-9b. Note that near 1.7 x I_{th} the intensity of shoulder changes abruptly. The time-resolved spectra show that at low currents before the takeoff of the camelback-shaped shoulder, the lasing modes show weak intensity oscillations with similar dynamic features as at RT. However, when the shoulder takes off above 1.65 x I_{th}, the mode dynamics switches to a totally different scenario. As an example, in Fig. 5-10, the time-resolved spectra are shown for 2 x I_{th}. As can be seen clearly, both the main peak and its shoulder are now oscillating periodically at a frequency of ~140 MHz (with the period near 7.5 ns), much higher than the extrapolated one from the low current antiphase oscillation frequency. The frequency increases to 225 MHz for 2.5 x I_{th}. The mode phases are shifted almost linearly. Because the new dynamics becomes more distinct at lower temperature, we prefer to analyze its details at 100K and 75K. In Fig. 5-11, the time-integrated lasing spectra at 75 K are shown for different detection. The top spectra are measured with LN_2 cooled slow Ge detector and lock in technique, while the bottom spectra are integrated from the time traces measured with fast InGaAs detector. Except a

lower S/N ratio for the fast detector, both spectra show almost the same trend. We found the same consistent situation at 100 K. Note again that in Fig. 5-11, the shoulder takes off in a very narrow current range, similar to the 175 K case.

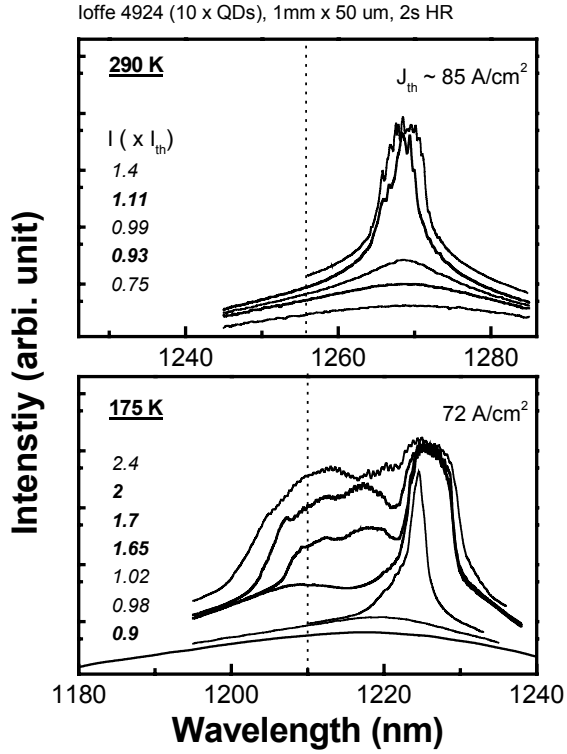

Fig. 5-9 Time-integrated spectra of the 1.3 μm QD laser as in Fig. 5-7.

For 100 K, the time-resolved spectra are shown in Fig. 5-12 for 1.06 x I_{th}. In the most left 3D plot, it can be seen that just after the laser turn-on, the lasing action is actually taking place at the ASE maximum, but it quickly red shifts to the low energy side. Thus the turn-on spectral dynamics clearly show that before lasing action the gain maximum matches the ASE maximum (λ = 1190 nm), and just after turn-on the gain adapts to the lasing process, leading to a red shift of gain maximum. This helps clarify the peculiar features in low current lasing spectra as in Fig. 5-11. However the turn-on dynamics are not just so simple as it looks like in the first 3D plot in Fig. 5-12. Clearly the lasing modes are not stable after the first run of gain adaptation process. In the second 3D plot, a zoom-in of the first 400 ns dynamics is shown. As can be also seen in the 2D plot, a regular spectral-temporal pattern is taking form evidently. The mode phase is only linearly shifted in the weak intensity region (i.e. the shoulder), whereas strong nonlinear phase shifts occur in the peak region. Note that even though the longitudinal mode structure is not visible in the shown plots, the modes show still continued phase shift relation.

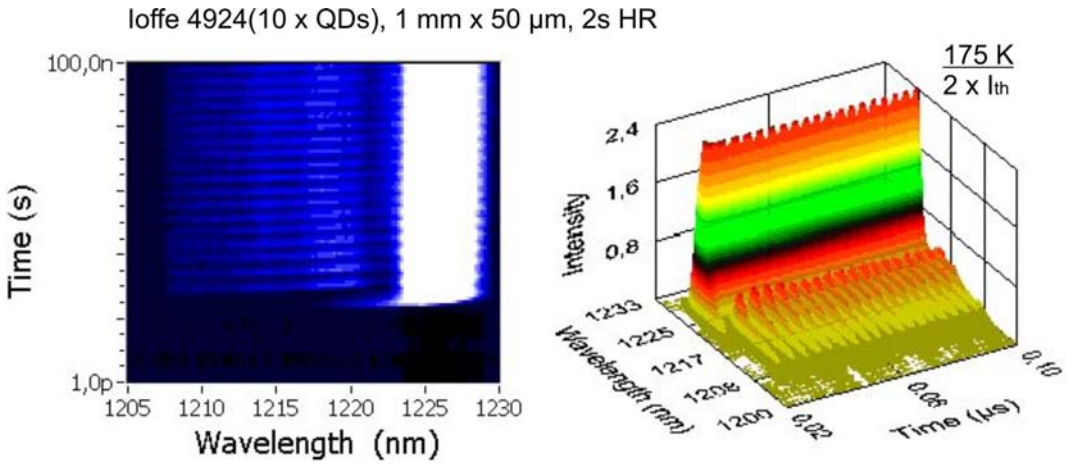

Fig. 5-10 Time-resolved lasing spectra of the 1.3 µm QD laser as in Fig. 5-7. (Left) Contour plot; (Right) 3D color mapped plot.

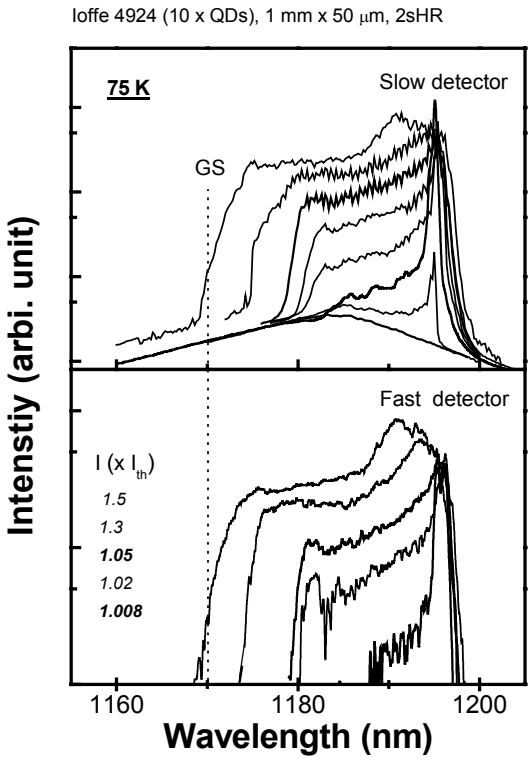

Fig. 5-11 Time integrated lasing spectra of the 1.3 µm QD laser measured by different techniques.

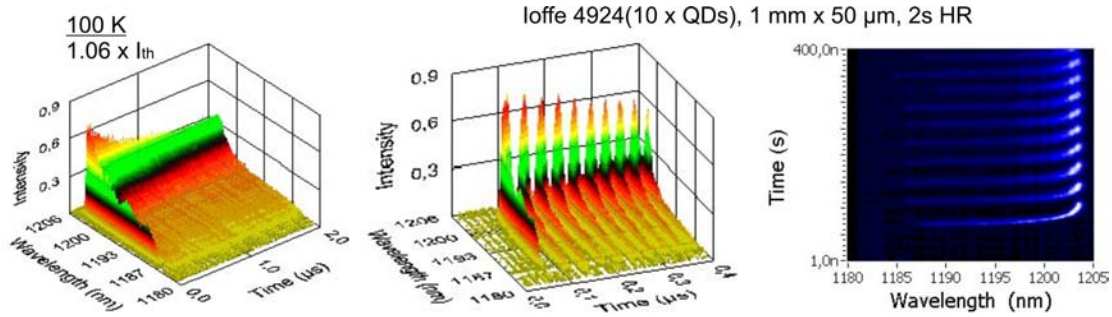

Fig. 5-12 Time-resolved spectra of the 1.3 μm QD laser, in different plots.

The spectral-temporal pattern in Fig. 5-12 may be seen from two different perspectives. From the spectral aspect, this pattern represents a spectral waving effect. As can be seen in the series of transient spectra in the left panel of Fig. 5-13, after turn-on, the broad lasing peak at the ASE maximum begins to move in the low energy direction, just like a wave surging forward. The wave is blocked at the lasing edge and forms a high tiderip, which then recedes with falling amplitude. After the first period of wave that last ~36 ns, there follows another period that has the same duration. The wave effect will continue in time. In the right panel of Fig. 5-13, another series of spectra is shown for 1.23 x I_{th}. The spectral waving effect is evident though the period is reduced to ~10 ns. It is interesting to note that the frequency increases almost 3 times with such a small current increment.

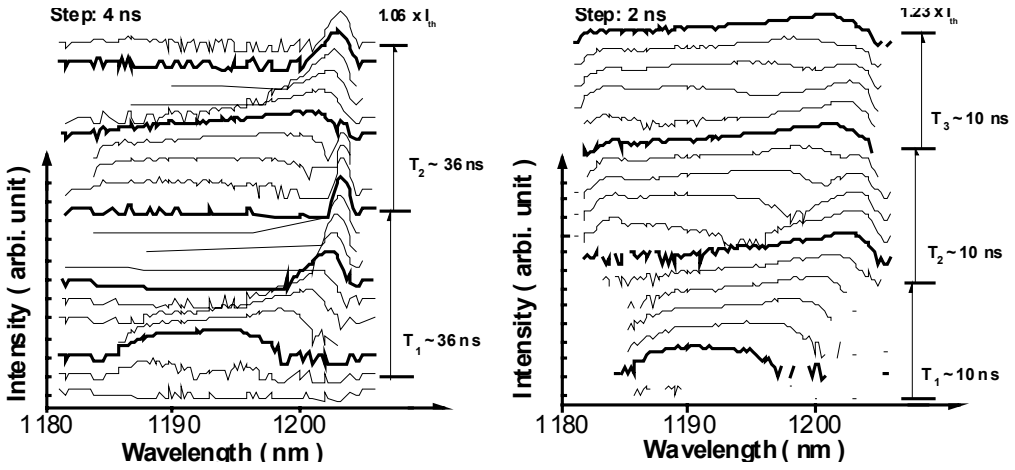

Fig. 5-13 Transient spectra at 100K of the 1.3 μm QD laser. The spectra are offset for clarity.

Now from the aspect of individual mode dynamics, we may gain a different perspective on the spectral waving pattern. As has been mentioned before, the total output intensity of the typical antiphase mode dynamics keeps constant in time, as the mode oscillations cancel each other near completely. But in the present dynamics, the total output intensity cannot be constant for no such canceling mechanisms exist. In Fig. 5-14a, the time traces of one typical mode are plotted for various currents. At 1.06 x I_{th}, the mode intensity shows rather typical damped relaxation oscillation (RO) that leads to a steady state finally. The RO

frequency increases with current. From the trend, it is expected that for 1.44 x I_{th} the RO frequency will go into GHz range, therefore beyond the limit of the detection bandwidth. Thus at this current the time trace is only an averaged trace for insufficient time resolution. From the frequency evolution with current, it can be inferred that the current RO frequency, as low as it can be, is still the main RO frequency f_1 rather than the low RO frequencies as in usual antiphase dynamics. This is further confirmed by the fact that the total output shows similar RO as the individual modes. So the present dynamics can be seen as a collective mode RO behavior, with the main RO frequency as the common oscillation frequency for all modes. It is interesting to note that the damping rate of these RO´s is extremely low, with a time constant of several hundreds ns. In Fig. 5-14a, the RO lasts almost the same length of period (> 1 μs) before the steady state. The peak intervals are analyzed in Fig. 5-14b for the two low current time traces. The RO period shows clear period damping effect, as it falls from ~36 ns to 25 ns and from 10 ns to 8 ns for 1.06 x I_{th} and 1.23 x I_{th} respectively. Apparently the time behavior of the main RO frequency is just opposite to that of low RO frequencies in antiphase mode dynamics.

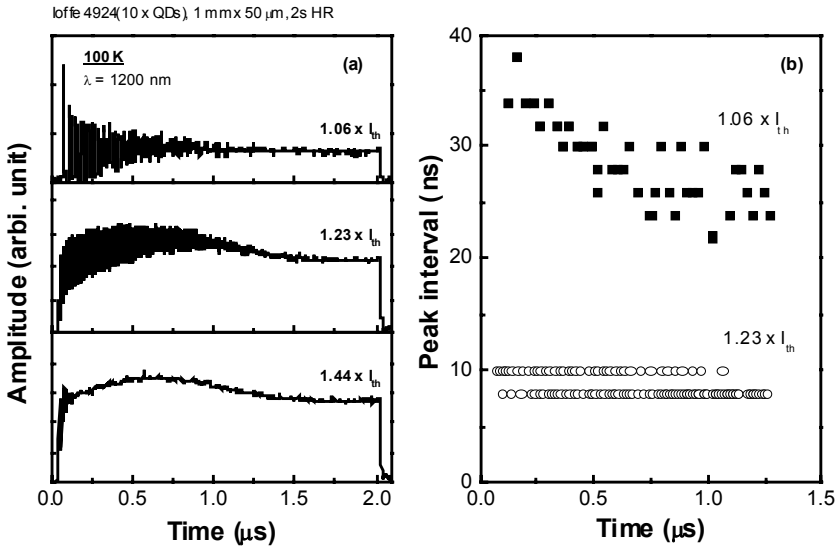

Fig. 5-14 (a) Time traces of the 1.3 μm QD laser, (b) temporal behavior of oscillation peak intervals.

The spectral dynamic features are similar for both 75 K and 100 K. So we analyze the evolution of the dynamics with current for 75 K as an example. In Fig. 5-15, the 3D plots of the time-resolved spectra are shown for various currents. The turn-on dynamics is the same as discussed before, with the lasing starting at the ASE maximum and the following red shift, the same for all the currents. At 1.005 x I_{th}, as in Fig. 5-15a, the shoulder region is too weak to see any effect, but at 1.01 x I_{th}, the spectral waving pattern begins to be visible, with the main peak at the lasing edge oscillating slightly. With current, the mode

oscillations intensify, and from 1.02 x I_{th} on, the spiking behavior becomes clear. To see the mode dynamic evolution, we plot the typical time traces in Fig. 5-16. A similar RO behavior is observed as for 100 K in Fig. 5-14a. But look at the time traces for 1.01 x I_{th}. While the spiking behavior in the two shoulder modes is visible, we can see in the peak mode (λ ~ 1196.4 nm) there appears mode oscillation that is in low frequency and experiences frequency damping. More importantly, the peak mode is in antiphase relation with the mode at 1195 nm. This shows that at this current two type of mode dynamics coexist. Above that current, the RO dynamics prevail, whereas below that current, antiphase dynamics dominate. Note again that for the current above 1.26 x I_{th} the RO frequencies approach and go beyond the detection limit, so the RO envelope becomes irregular and then only averaged time traces are taken as for 1.5 x I_{th}.

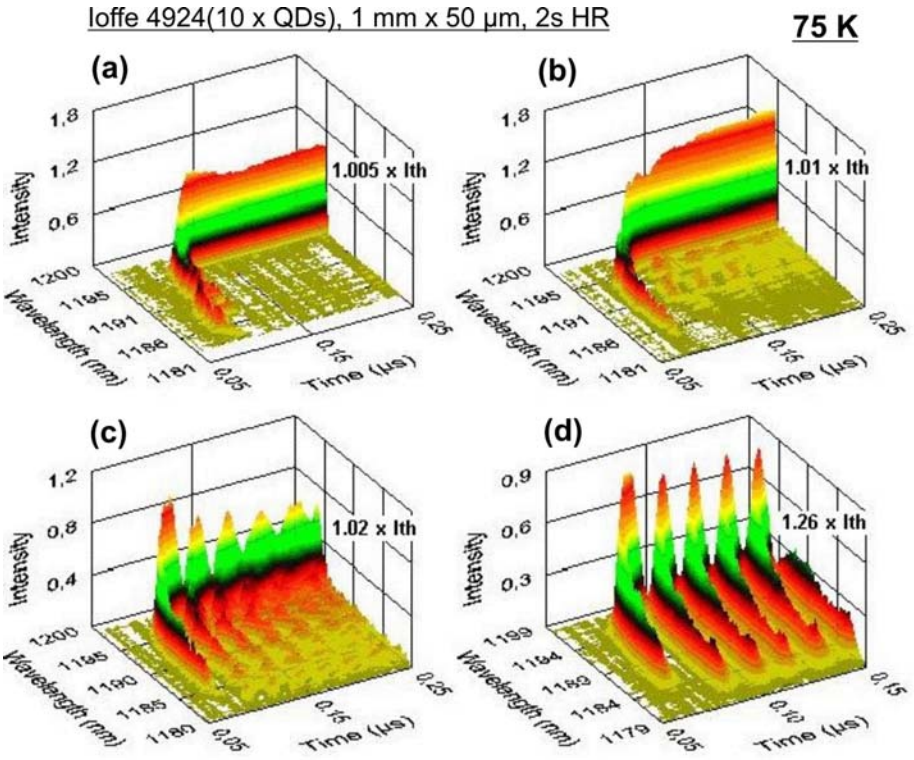

Fig. 5-15 Time-resolved lasing spectra of the 1.3 μm QD laser. Note that the apparent intensity is not consistent with current, due to different slit widths used

5.4.2 Discussion and conclusion

In MQD lasers, the bottleneck effect in carrier transport results in non-uniform carrier distribution and gain inhomogeneity in MQDs. By assuming uniform carrier injection in the junction plane, the non-uniformity and inhomogeneity both refers to the multilayer effect. As first approximation, we ignore the possible non-uniformity within each layer. This is more or less justified in wide stripe devices, like w = 50 or 100 μm in this study, because the non-uniformity can be usually treated as the edge effect. But in narrow stripe

lasers this approximation does not hold, and its impact will be discussed in Section 5.5. The in-plane carrier transport may become important at high optical power when the optical density is not uniform in the longitudinal direction, especially near the facets, or when the lateral spatial hole burning effect assumes significance. However, the main spectral features in discussion here occur for the current near threshold, so we assume the non-uniformity or inhomogeneity within each layer is not significant.

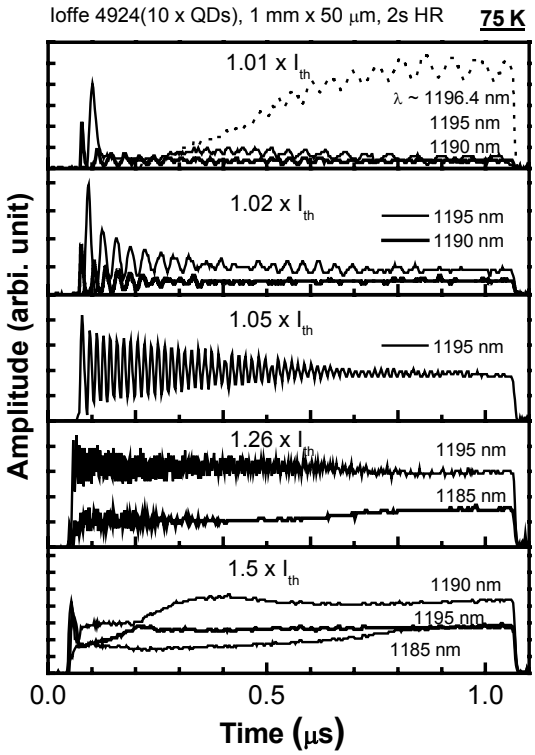

Fig. 5-16 Time traces of the 1.3 μm QD laser at various current and wavelengths

As have been discussed in Section 5.3, at high temperature the carrier transport can match the carrier depletion from the lasing process, and the non-uniformity of carrier distribution is relatively low. So at high temperature, the laser dynamics are governed by the dynamic grating effect, that is the gain inhomogeneity induced by the longitudinal mode intensity. This is known to induce antiphase mode dynamics as demonstrated by the RT case in this section. The spectral features at RT are thought as normal. With temperature decrease, we meet abnormal spectral features. These peculiar features are generally attributed to the bottlenecked carrier transport at low temperature. The ensuing non-uniformity in carrier distribution and gain inhomogeneity are the necessary conditions for the appearance of the abnormal features, as can be deduced from the analysis of the relation between the spectral features and various device parameters.

a) Laser dynamic processes and self-organization mechanisms

From the viewpoint of nonlinear dynamic system,[25] the MQD laser composed of spatially homogeneous carrier and gain distribution is a simple dynamic system that can only generate spectral variations, due to inhomogeneous broadened spectral gain, but with the dynamics similar to that of a single mode laser. When the dynamic grating effect is considered, the dynamic system then includes gain inhomogeneity. This new dynamic system may demonstrate periodic, quasi-periodic or chaotic multimode dynamics after various bifurcations. The antiphase mode dynamics at RT belongs to this set of dynamic effects.[24] Now at low temperature, when the carrier transport is bottlenecked, strong non-uniform carrier distribution among MQDs ensues, and this would add another term of spatial gain inhomogeneity in the dynamic system. At first thought, it seems that the system complexity does not change so much except increased degree of gain inhomogeneity. However, the later added gain inhomogeneity, unlike the dynamic grating, is intimately related to the carrier transport processes. Under lasing condition, the carrier and gain dynamics are not only related to the optical power, but also committed to the strongly limited carrier transport processes. The greatly increased complexity will lead to complex structure including pattern formation, due to higher bifurcations in the resulted dynamic system. It is worthy to note that the MQD lasers contain a multiple of dynamic dimensions, not only spectral and temporal, but also spatial ones. In this study we address only the spectral-temporal behavior by analyzing the time-resolved spectra. As in other strongly nonlinear dynamic systems,[25] the formation of complex structure is anticipated in the laser dynamics of MQD lasers with limited carrier transport. In the following, we continue to discuss the dynamic mechanisms underlying the observed intriguing spectral dynamic features at low temperatures.

As the turn-on dynamics shows, the laser action actually starts at the ASE maximum, which is the gain maximum before the optical power takes off. After start, the lasing peak red shifts continually. This spectral red shift process reflects the same process for the spectral gain. Due to the gain inhomogeneity, the actual gain process underlying the red shift is the adaptation of the QD layer gains to the optical power and the carrier transport processes. Considering the asymmetrical distribution of electrons and holes between n- and p-type cladding layers in MQD lasers, as illustrated in the following schematics:

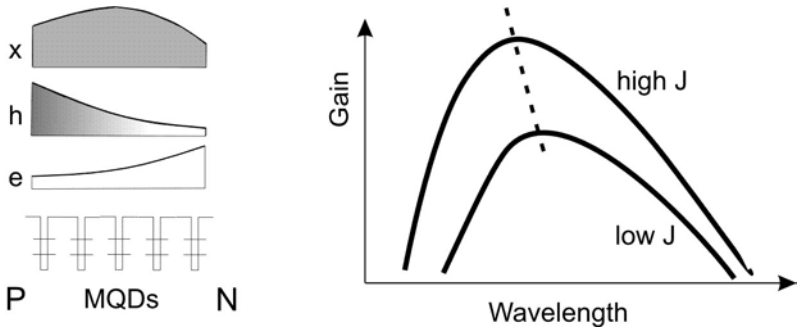

The electrons and holes tend to accumulate in the dot layers on the n- and p-side respectively when the carrier transport becomes bottlenecked. The gain profile is approximately proportional to the exciton (x) density, so it has a maximum in the middle dot layers. The dot layers on both sides have relatively low gain, in so far as the carrier non-uniformity is strong and the threshold is low enough. The excess carriers in these dot layers may not contribute gain but can help reduce loss. The representative spectral gain profiles are illustrated with the high J curve corresponding to the gain from the middle dot layers and the low J curve for the side layers. Note that the gain maximum blue shifts with carrier density, and this can be inferred from the ASE spectra as in Fig. 5-1. Apparently the larger the layer gain, the higher the stimulated emission rate, and so is the carrier depletion rate. In this case, the middle dot layers have larger gain, so the carriers will be depleted from these layers relatively fast. One important aspect in the carrier dynamics is that the carrier depletion in the middle layers actually helps block the minority carrier transport to the side layers. This carrier blocking effect is most severe when the carrier transport to the middle layers has been bottlenecked due to the decreased carrier escape rate. When the sum gain of all dot layers reaches the threshold, the optical power builds up, and lasing begins. With the laser turn-on, the optical power builds up and the gain of the middle layers becomes suppressed for the *spectral hole burning* effect. But due to the carrier blocking effect, the side layer gain is deeply suppressed for the *reduced carrier density*. That means the low J gain curve in the above illustration will retreat with a red shifted maximum. The combined gain spectrum then red shifts in the lasing process. With the optical power, the gain begins to saturate and in turn the optical power stops to increase. This also stops the increase of carrier depletion rate and carrier blocking effect. So the low J gain curve stops the red shift. All these developments are reflected in the later formation of the lasing edge, as in Fig. 5-15a. So in the whole, the gain adaptation process comes with a non-uniform carrier distribution, and is facilitated by the slowed carrier transport that enhances the carrier blocking effect among QD multilayers. Apparently, the carrier transport effect plays a critical role in this self-organization process typical for a complex dynamic system.

In general for MQD lasers, the gain variation in each dot layer is determined locally by the *gain suppression* and *differential gain*. The former is related to the spectral hole burning by the optical power, and the latter concerns the variation of carrier density in the specific dot layer. The carrier density and gain variations in different dot layers are correlated through the carrier transport processes. The resulting sum gain then determines the optical power. So under the conditions of a constant injection current and threshold gain, the carrier, gain and optical power is interwoven in a network of strong nonlinear dynamic processes. The system is driven far away from equilibrium, when the carrier transport is bottlenecked. The main characteristic of such a nonequilibrium nonlinear dynamic system is the self-organized structure formation in its dynamic behavior. In the following, we discuss the observed spectral waving pattern in the MQD lasers as an example for the self-organization effect in MQD laser dynamics.

Continued in Fig. 5-15 (b, c), with a minute current increment, the spectral waving pattern is taking shape and fully developed. We turn to Fig. 5-13 for a more distinct waving pattern (left panel). In contrary to low current case like in Fig. 5-15a, after the formation of lasing edge peak, a broad lasing peak turns up in the shoulder region, and it repeats the similar red shift dynamics as the lasing start peak. This new period indicated that the gain in the middle dot layers recovers after the black out. It can be seen that the new shoulder peak is anticorrelated with the lasing edge peak. So the gain in the side layers also recovers and this can happen fast for the reduced carrier blocking. It will be easier to understand the gain recovery process from the perspective of mode dynamics. As in Fig. 5-14a, the individual modes show damped RO´s, and so is the total output. Thus the sum gain of MQDs is oscillating around the threshold for all lasing modes. The first spike in the RO´s shows that the overshoot of the optical power at these slightly higher currents deeply suppresses the laser gain, leading to a sudden drop of optical power. This supports the former assumption that all dot layer gains are recovering in the black out, for they are all deeply suppressed not only due to the spectral hole burning effect but also for the carrier blocking. Note that the MQD laser dynamics show phase transition with current. At low current, the antiphase mode dynamics prevails, as in Fig. 5-15a and in Fig. 5-16 for 1.01 x I_{th}. With current, the damped RO begins to dominate. The coexistence of both types of dynamics, as shown in Fig. 5-16 for 1.01 x I_{th}, show that the mode coupling effect of dynamic grating still works in a strong non-uniform carrier distribution. This is understandable for the dynamic grating occurs in the longitudinal direction whereas the MQD layer gain inhomogeneity concerns only the vertical direction. Thus both gain inhomogeneity effects, dynamic gratings and

MQD layer gain inhomogeneity, can induce their characteristic dynamics. However, depending on the current and carrier transport rate processes, the RO dynamics can dominate and kill the antiphase dynamics. That is, when the spiking behavior in the RO intensifies, the optical power is turned up and down so frequently and forcefully that other dynamics cannot develop. As observed, the RO´s are damped to steady state, so it can be inferred that the carrier and gain dynamics in the present system can damp any further mode oscillations and help stabilize the laser output. That also facilitates the phase transition.

Note that the observed RO´s in MQD lasers can have a period over 30 ns, as in Fig. 5-14b. Considering the general relation for the main RO frequency $f_1 \propto \text{Sqrt}\,(\tau_p \cdot \tau_e)$,[26,27] with the photon lifetime $\tau_p \sim 25$ ps, it would suggest a carrier lifetime τ_e much longer than 1 ns. This long effective carrier lifetime reflects the complex carrier and gain dynamics that are impacted by the limited carrier transport across QD multilayers. Actually the effective carrier time constants have been generally used in the QW laser dynamic study to account for the transport effect.[7,28] In the modeling of antiphase dynamics in QD lasers, it is also found that an effective carrier lifetime larger than 1 ns is necessary,[24] but in that case it is the carrier capture process, rather than the transport issue, that matters.

b) Nonequilibrium carrier effects

Now we discuss the role of nonequilibrium carrier distribution in the laser dynamics. At low temperature, the quenched interdot carrier redistribution leads to the carrier nonequilibrium among the dots of different confinement energy within every dot layer. This could extend the effective carrier lifetime, for the carriers are mostly affected by the QD localization effect and separated from the lasing dots. The nonequilibrium distribution could be also responsible for the long damping time and the period damping effect in the RO´s, as in Fig. 5-14b. In the RO process, the carrier distribution will be continually adjusted and adapted to the gain and optical spectrum. The adjustment thus improves the time response of the carrier distribution to the processes of both lasing and carrier transport. That then leads not only to periodic mode oscillations, but also to the synchronization of mode phases, as shown in the 2D dynamic patterns in Fig. 5-12.

c) Conclusion

Finally in the above discussion, we demonstrate only the spectacular pattern formation in MQD laser dynamics. This serves as an example to clarify the basic laser processes and

possible self-organization mechanisms related to the carrier transport processes. With varied laser parameters and conditions, the dynamic output of the MQD lasers can vary greatly, as reflected in the diversity of abnormal features in time-averaged spectra. To account for such a weird range of dynamics, it is necessary to address the trivial details of carrier processes and gain nonlinearity, which are know to be rather complicated in QD system. In this work, we can only be satisfied with the consistency obtained in the lasing behavior analysis in a wide range of parameters and in certain reprehensive examples.

In summary, the time-resolved spectral study shows that the carrier transport effects strongly impact the spectral dynamic characteristics of MQD lasers. The limited carrier transport at low temperature is responsible for the peculiar spectral features and the underlying dynamic structure formation. The strong quantum confinement effect and gain nonlinearity pertaining to QD systems make QD lasers attractive for the study of nonlinear laser dynamics. Coupled with the carrier transport effect, the MQD lasers can be useful model systems for the study of nonequilibrium nonlinear dynamics far away from equilibrium. The great flexibility in tailoring the QD and laser parameters by advanced growth technique offers QD lasers a particular advantage, among many other merits of semiconductor lasers.

5.5 Dynamics variations in narrow stripe MQD lasers

In this section we investigate the spectral dynamics of narrow stripe MQD lasers. First we discuss the particular laser parameters and properties that are specifically affected by the narrowing of stripe widths. Then we analyze the time-resolved lasing spectra of a narrow stripe MQD laser. In the end, we discuss the dynamic instability mechanisms and a variety of dynamic effects as induced by carrier transport effect.

5.5.1 Narrow stripe effects

We discuss the narrow stripe effects in shallow-mesa ridge waveguide lasers.

Narrow stripe lasers are intended for obtaining low threshold current and better control of lateral modes.[29] With the narrowing of stripe widths, the current injection area decreases, and the edge effects become important.[30] The first edge effect is *current spreading*. The large serial resistance of narrow stripe devices could enhance the lateral current flow and increase the ratio of current spreading. By adjusting the ridge mesa depth the current spreading effect can be minimized. The second edge effect would be *carrier diffusion*. The carrier confinement effect of QDs helps reduce the effective diffusion length.[4] It is

anticipated that in QD lasers the carrier diffusion range is suppressed outside the ridge region. Both edge effects smear the gain/loss zone interface at the edge, so they can affect the lateral mode confinement in the gain-guided shallow-mesa devices, leading to strong mode sensitivity to current variations.

In the narrow stripe devices, when the stripe width is larger than the carrier diffusion length, the lateral carrier distribution in the active region has a bell-shaped profile due to the carrier diffusion. Under laser conditions, the mode spatial hole burning effect will suppress the carrier density in the central region, resulting in a double-lobed carrier profile. With the carrier-induced refractive index change, the distorted carrier profile can significantly affect the lateral mode confinement. In conventional semiconductor lasers, the refractive index decreases with carrier density at a coefficient[31] of ~ - 10^{-20} /cm^3, so in these lasers the carrier-induced anti-guiding effects dominate, which may cause typical mode instability phenomena, such as kinks and beam steering with current variations.[29] However, recently both theoretical and experimental study[32,33] shows that anomalous carrier-induced dispersion occurs in QDs. In contrary to the plasma dispersion that works in bulk and the QWs, the coulomb interaction with the carriers in the wetting layer may lead to very low or even negative linewidth enhancement factor[32] for QD GS gain, which indicates that the carrier-induced refractive index change can be reversed in contrary to the conventional case. At high carrier density, the refractive index will increase with current and the carrier guiding effect ensues. In QD lasers, the carrier density is not sufficiently clamped above threshold. This could result in a continuous change of mode guiding conditions with current, and increase the mode sensitivity to current variations, especially at high carrier density. In lasers with stripe widths comparable to the effective carrier diffusion length, the carrier diffusion can counter the spatial hole burning effect, and the carrier profile remains in one peak, which would cause strong anti-guiding effect and increase the mode loss and laser threshold. The extremely low or negative linewidth enhancement factors of QD gain could help limit the mode width, thus reduce the modal loss and lead to extremely low threshold current for such narrow QD devices.

It is known that the inherent high serial and thermal resistance of a narrow stripe laser can cause stronger junction heating than in wide stripe devices. The non-uniform temperature distribution in the active region may affect the mode guiding due to the temperature dependence of refractive index. The thermal guiding effect becomes stronger at higher current density.

Finally the above-mentioned narrow stripe effects have their dynamic aspects that could have impact on the dynamic characteristics of narrow stripe lasers. The temporal development of carrier density profile is closely related to that of the mode field profile through the spatial hole burning and the carrier-induced index change. The carrier diffusion in and out of the active region can significantly slow down the dynamic response.[34] The junction heating effect will cause continuous temperature increase after current switch-on. In the lasers with high temperature sensitivity, the temporal change of temperature and its distribution can induce dramatic dynamic variations of lasing properties.

In the following, we analyze the temporal behaviors of a narrow stripe MQD laser, and discuss their relation to the above narrow stripe effects.

5.5.2 Transient spectral analysis

a) Sample description

The narrow stripe lasers here investigated have the same laser structure (Ioffe 4924) as the wide stripe devices in Section 5.4. The lasers are processed with shallow-mesa ridge waveguide, with a mesa etch depth of 1.5 μm, smaller than the total thickness of the p-doped GaAs contact layer and AlGaAs upper cladding layer of about 2.4 μm, so we expect that the lateral cavity effect[35] would be too weak to be visible in the lasing spectrum. In fact, we have similar devices but with a mesa etch depth of 2.2 μm, and there the lateral cavity effects are indeed strong enough to induce spectral intensity modulations.

The stripe width is set at 8 μm to show enough narrow stripe effects while avoiding the high scattering loss that would occur in devices with narrower stripe. The laser performances remain constant for the stripe width down to 8 μm.[36] For such a shallow mesa, the induced shallow index step will cut off high order modes for relatively larger widths.[30] So this 8 μm wide laser will emit mainly in the lateral fundamental mode, if the other guiding effects, like carrier and thermal effects, are not considered.

b) Stable lasing cases --- high temperature and low current

In Fig. 5-17, the RT time-resolved spectra are shown for the narrow stripe laser. The mode structures, in Fig. 5-17a, are well resolved with distance at 0.2 nm for 1 mm cavity length. The check board pattern is also apparent in the mode peak spectrum as in Fig. 5-17b. So the antiphase mode dynamics here is rather similar to that in Fig. 5-8 for the wide stripe laser. The 270 K spectrum with a full spectral range is shown in Fig. 5-18a, and the coarse

spectrum in Fig. 5-18b shows clearly that the neighboring modes cancel their oscillations rather completely. The frequency damping effect is also present in these spectra, suggesting that it does not depend on the multi-lateral-mode operation. The only obvious difference here is the significant red shift of modes with time for the narrow stripe laser, as in Fig. 5-17a. This evidences the strong junction heating effect in narrow stripe devices.

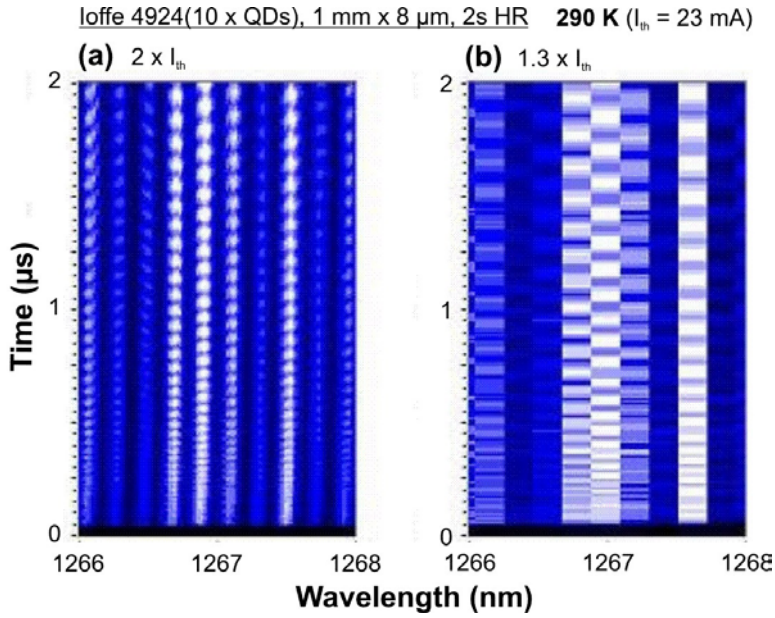

Fig. 5-17 Time-resolved spectra of the narrow stripe 1.3 µm QD laser, (a) with longitudinal mode structure resolved; (b) only the mode centre intensities are shown.

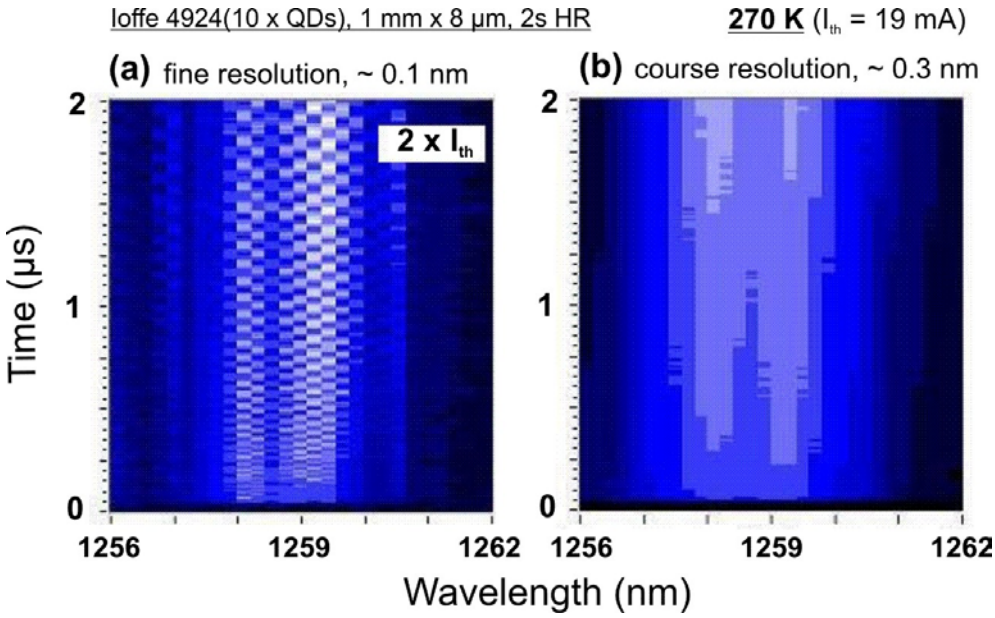

Fig. 5-18 Time-resolved spectra of the narrow stripe 1.3 µm QD lasers. Mode center intensities at different spectral resolutions are shown.

c) Dynamic instability cases --- high temperature but high current

I. Time-resolved spectra

The above shown spectra are rather regular as those of wide stripe lasers. However at higher currents, the temporal behavior of lasing spectra differs. As shown in Fig. 5-19, strong destabilization gradually sets in with current, and it comes up earlier for higher current. Because no such instability effects are observed in wide stripe devices at the similar current density, we attribute this instability effect to the narrow stripe effect. As in Fig. 5-19, for 3.5 x I_{th}, the mode dynamics show increased frequency compared to the former low current spectra, and the spectrum is in regular form except the strong red shift induced by the junction heating at this high current. Note that in the spectrum for 3.5 x I_{th}, there are apparent patterns that seem indicating spectral intensity modulation and blue shift of peaks against the red shift of the spectrum center. But these patterns are not the real spectral features, rather a visual display effect. For a full view of the dynamic instability, we have plotted these spectra in a wide spectral window, so the mainstream parts of the high-resolution spectra are pressed in a narrow spectral region. That then induces the misleading interference pattern effect. Be careful that the similar situation may occur in a few of the following 3D spectra.

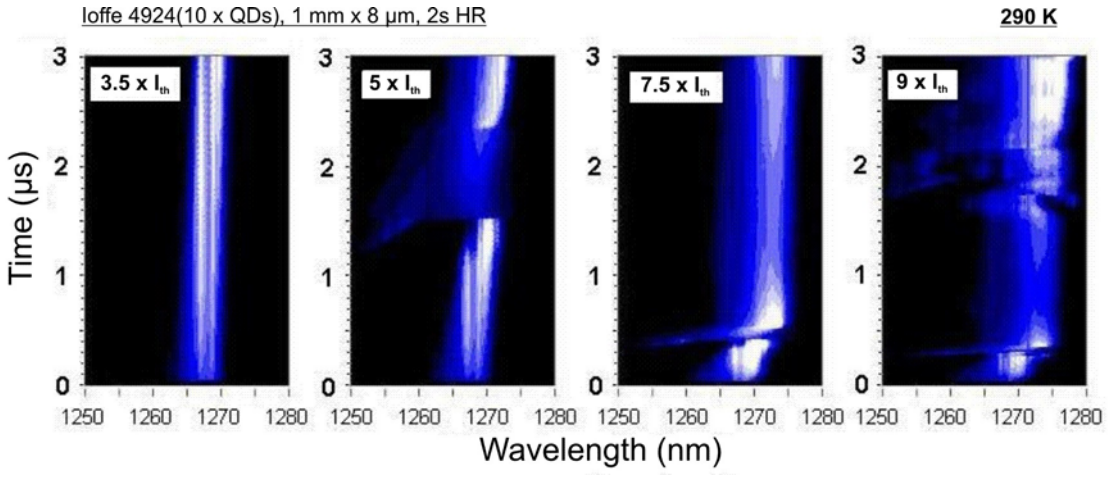

Fig. 5-19 Time-resolved spectra of the narrow stripe 1.3 μm QD laser at high currents. I_{th} = 23 mA.

With current, the instability effect begins to appear first in the end of the 3 μs pulse, and then moves gradually to the beginning of the pulse. At 5 x I_{th}, the destabilization occurs in the middle way with a new peak appearing far away at the high energy side. A clear view of the whole course can be seen in the 3D plot of a similar spectrum at 270 K in Fig. 5-20a for 4 x I_{th}. At the pulse beginning, there are double mainstream peaks that show antiphase mode oscillations. Since near 0.8 μs, a new peak at the high energy side begins to grow up

at the expense of one of the original peaks, and it gradually red shifts back to the mainstream. In between the original main peak collapses, with another new peak borne at its high energy side. Near the pulse end, one peak comes up on the same position as the collapsed main peak, and the lasing spectrum is resuming the intensity and position as would be expected from a stable lasing case, as in Fig. 5-19. Note that after the main peak collapse, the antiphase mode dynamics also disappear from the scene.

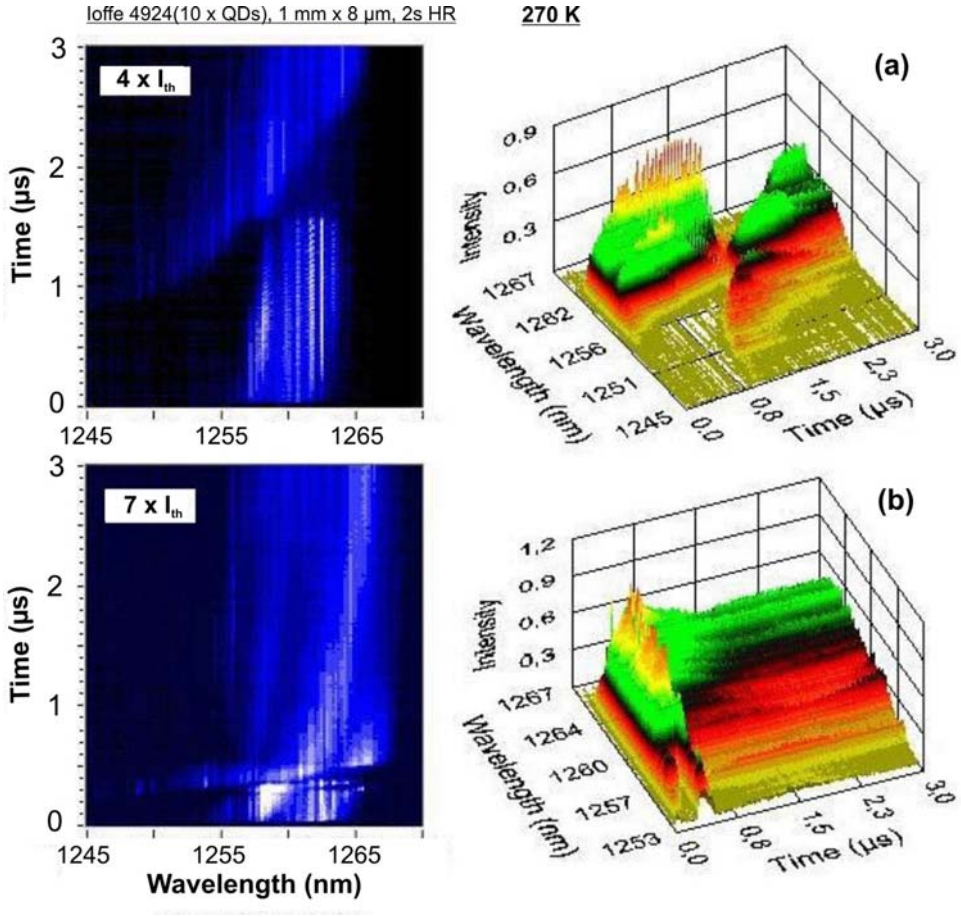

Fig. 5-20 Time-resolved spectra of the narrow stripe 1.3 µm QD laser at high currents in different plots.

As can be seen in Fig. 5-19, with further current increase, the instability processes start earlier and return to the stable lasing course even quicker. Up to 9 x I_{th} a chaotic lasing process follows. Before the instability process begins, the red shifts intensify with current, indicating stronger junction heating effect. Now we analyze the total output time traces of these lasing processes.

II. Total output power

In Fig. 5-21a, the time traces of the total output power are shown for various currents. As noted before, for relatively low currents, the modes oscillate in antiphase relation before the instability occurs. Apparently the present smooth total output time traces evidence the

antiphase mode dynamic at low currents. In these time traces, the dynamic instability processes are reflected in the power reduction regions just before the strong singularity point, after which the power retreats continuously. For 9 x I_{th}, the second run of dynamic instability induces a strong power boost at its beginning. It should be emphasized that the driving electrical square pulse has an amplitude variation within 1% for 5 x I_{th} and 0.22% for 7.5 x I_{th}, so the big variations in the total output power are supposed not due to the current change, but rather originate from the dynamic instability effects characteristic of narrow stripe devices. It may be possible that a large current uncertainty or noise could help trigger the dynamic instability process.

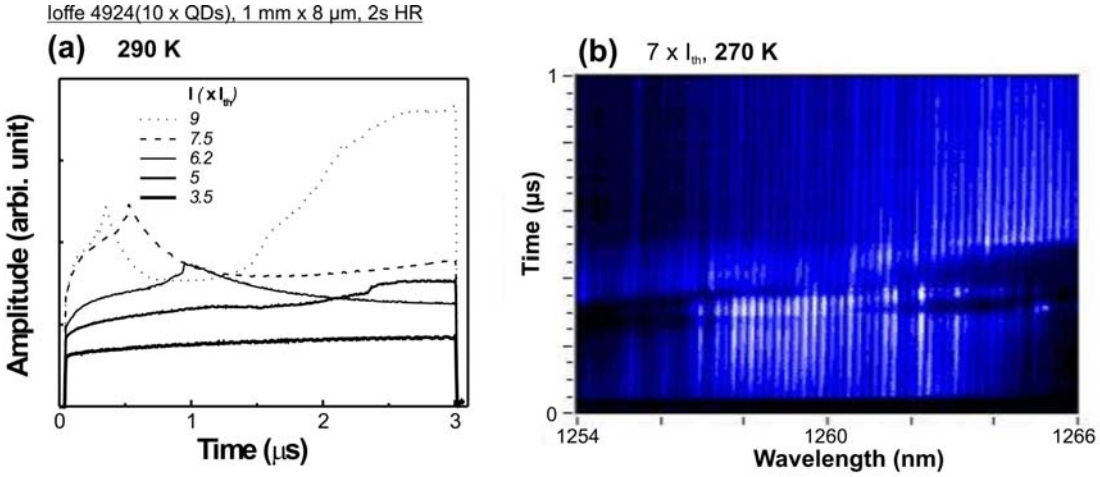

Fig. 5-21 (a) Total output time traces of the narrow stripe 1.3 µm QD laser at various currents. (b) Time-resolved spectrum with longitudinal mode structure resolved.

III. Mode structure

The above analysis shows that in the dynamic instability process, both the transient spectrum and the total output power vary dramatically. What about the mode fine structure? In Fig. 5-21b, the mode resolved fine spectrum is shown, which is a zoom-in for the first µs period of the spectrum as in Fig. 5-20b. A universal mode red shift pattern is recognizable in the whole 1 µs period, and as before it is attributed to the junction heating effect. During the instability process around t=0.4 µs, it can be observed that the mode red shift rate increases. In the whole instability process all modes are displaced about half of the mode distance from the original red shift course as determined by the junction heating effect. This mode displacement is equivalent to a variation of the effective refractive index $\Delta n_{eff} \sim +6 \times 10^{-4}$. The mode red shifts afterwards become normal, implying that the changed mode guiding condition is stable against the junction heating effect. With current, such as at 9 x I_{th} as in Fig. 5-19, a second time of destabilization near t=1.5 µs first reverts the mode guiding, and then chaotic instability appears with unpredictable mode behavior.

IV. Time-averaged spectra

From RT down to 200 K, the dynamic features are rather similar, with stable lasing at low currents and instability processes at high currents that finally lead to chaotic instability. The RT time-averaged lasing spectra are shown in Fig. 5-22. Low current spectra show single peaks direct above the ASE maximum, and only at high currents like above 8 x I_{th}, the lasing instability causes a shoulder at the high energy side. It has been clear that this shoulder is mainly present during the instability process. So it is totally different from the spectral intensity modulations as caused by the lateral cavity effect. Moreover, in Chapter 3, it has been shown that the lateral cavity effect is rather stable lasing feature, as in Fig. 3-15. It is interesting to note that in a deep mesa laser, where the lateral cavity effect is active, the lateral mode is confined through at least weak index guiding, due to the inherent step index profile. The index-guided mode is robust against the variations of current, carrier density and temperature, so no dynamic instability effects like above can be observed in the narrow stripe deep mesa devices. This guarantees that the spectral intensity modulation features from the deep mesa devices have a stable temporal behavior.

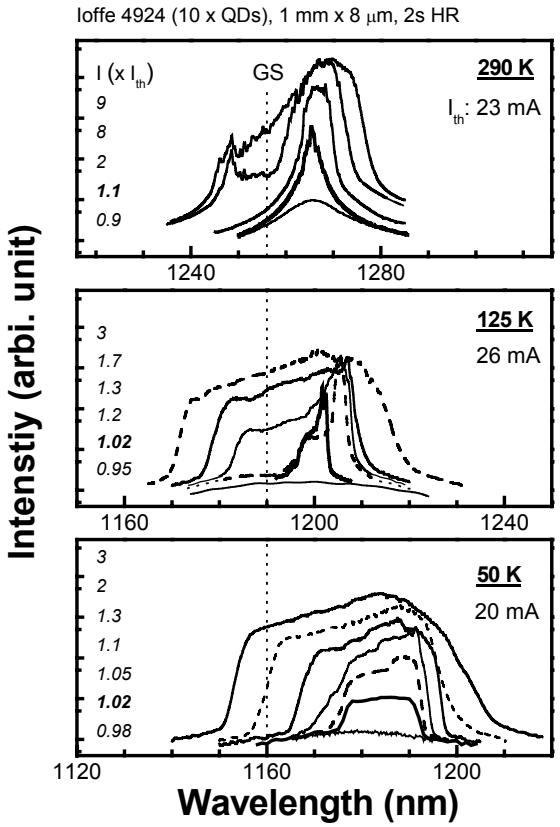

Fig. 5-22 Time-integrated lasing spectra of the narrow stripe 1.3 μm QD laser.

d) Low temperature spectra and dynamics

For temperatures below 200 K, the near threshold lasing spectra show abnormal features like in the wide stripe devices. The time-averaged spectra are shown in Fig. 5-22 for 125 K. Typical abnormal features include the nonsymmetrical near threshold spectral profile, red shift from the ASE maximum, the distinct lasing edges, and sharp lasing peaks with broad shoulder. All these features have been observed in wide stripe devices, and attributed to the carrier transport effects. In the following we analyze the spectral dynamics underlying these abnormal features, with emphasis on the peculiarity in narrow stripe lasers.

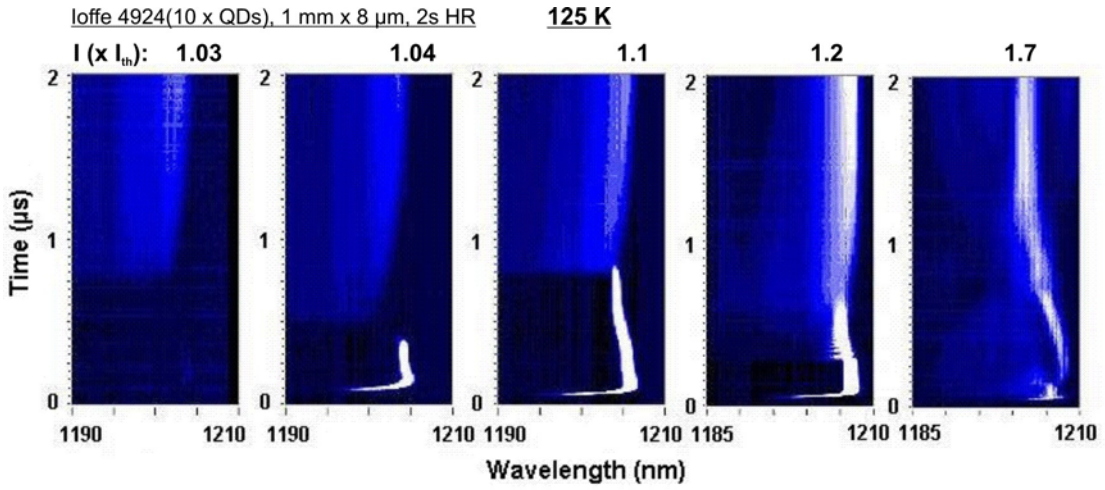

Fig. 5-23 Time-resolved spectra of the narrow stripe 1.3 μm QD laser at various currents.

For 125K, Fig. 5-23 shows a series of time-resolved spectra with increasing currents. Some of them are plotted in Fig. 5-24 in 3D to enhance the perspectives. The dynamics are astounding. For $I < 1.7 \times I_{th}$, two time zones with distinct spectral features can be identified. The *first* is just after laser turn-on, and its transient behaviors are pretty similar to that observed in the wide stripe devices for currents very near threshold. The lasing action begins at the ASE maximum, and the lasing peak red shifts quickly with time to the lasing edge, above which no lasing modes exist. The lasing edge peaks correspond to the sharp peaks in Fig. 5-22, where the spectrum is averaged for only the first half μs period. The dynamics near the lasing edge vary with current from stable lasing to spectral waving effect, as in Fig. 5-25(a, b, d). Note that in Fig. 5-23, at $1.03 \times I_{th}$, there is a similar turn-on dynamics as that for $1.04 \times I_{th}$, though the former is not so far way from the ASE maximum and has rather weak intensity, as suggested by the time-averaged spectrum in Fig. 5-22 (middle).

The *second* time zone follows almost directly after the collapse of the peak in the first one. It features a broad lasing range that may expand at the low energy side. Apparently the mode

intensity is stronger for longer wavelength, though the average mode intensity is much lower than the former peak intensity.

As known, the above two-time-zone dynamics is not observed in wide stripe devices. In Fig. 5-23, at 1.7 x I_{th}, the dynamics are rather chaotic, and the two time zones are not so distinct as before, as can be seen in Fig. 5-24c. For even higher currents, a typical spectrum is shown in Fig. 5-25 for 2.7 x I_{th}. The chaotic lasing dominates in the first time zone, whereas in the second zone one the dynamics is surprisingly stable with gradually increasing intensity.

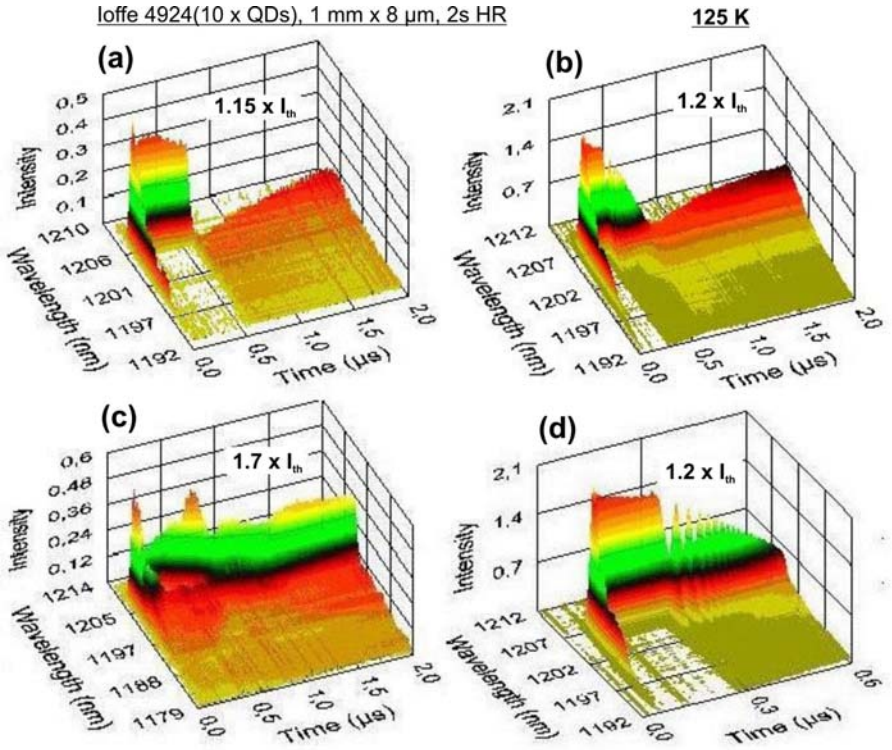

Fig. 5-24 Time-resolved spectra of the narrow stripe 1.3 µm QD laser. Note the different time scales for 1.2 x I_{th}.

Finally, we can see that for even lower temperatures like 50 K, the time-averaged spectral features are different from the former 125 K ones only for currents near threshold, as in Fig. 5-22. The lasing dynamics, as shown in Fig. 5-26 and Fig. 5-27, are not so much different, except that the first time zone shows more distinct variations of spectral waving patterns.

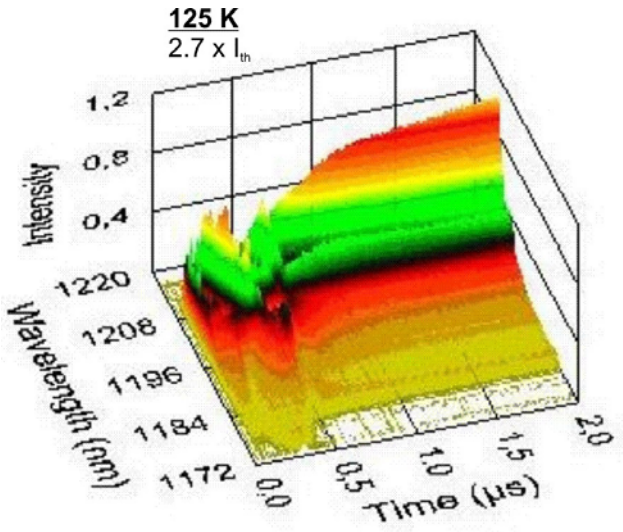

Fig. 5-25 Time-resolved lasing spectrum of the narrow stripe 1.3 μm QD laser at 2.7 x I_{th} and 125K.

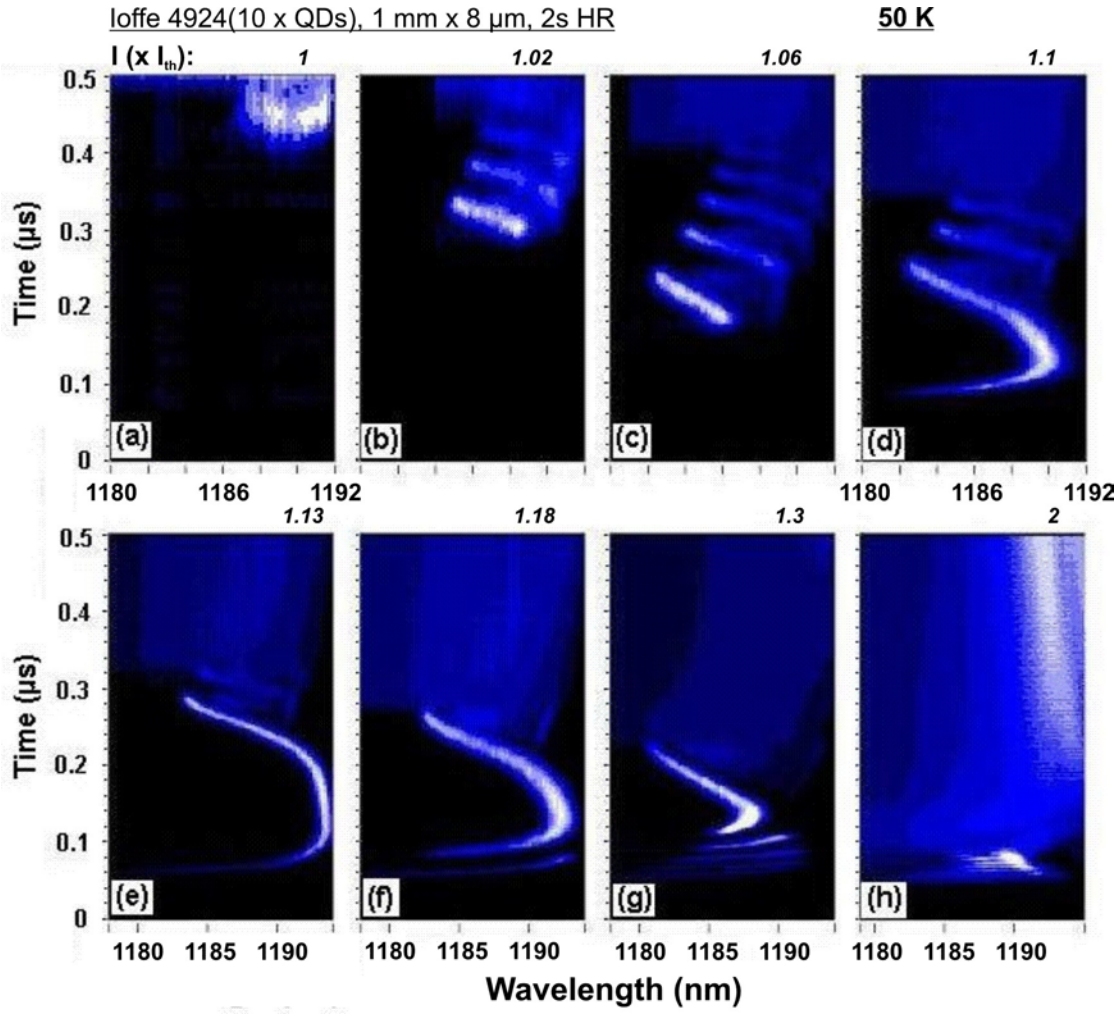

Fig. 5-26 Time-resolved spectra of the narrow stripe 1.3 μm QD laser at various currents.

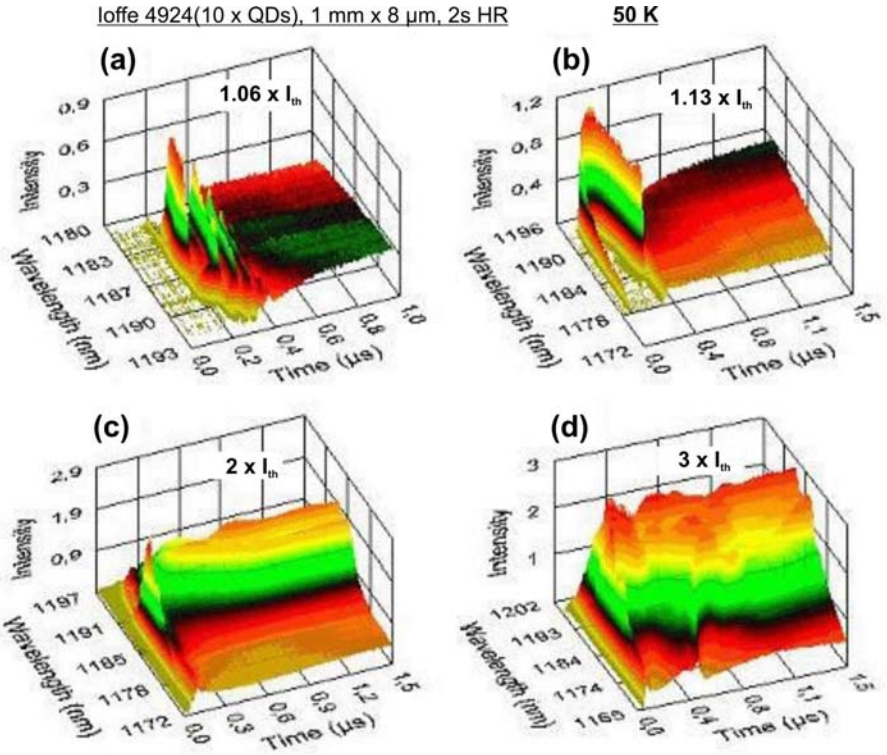

Fig. 5-27 Time-resolved spectra of the narrow stripe 1.3 μm QD laser at various currents.

5.5.3 Discussion and conclusion

After the above spectral analysis, we discuss the possible mechanisms underlying these laser dynamics processes, with the dynamic instability at first.

a) Dynamic instability mechanism in narrow stripe lasers

I. Non-uniform lateral profiles

As noted, the dynamic instability phenomena at high temperatures are characteristic of narrow stripe lasers that are mainly gain-guided in the lateral direction. In these lasers the mode guiding conditions can be varied at the change of current and temperature, especially due to the narrow stripe effects as discussed in Section 5.5.1. The narrow stripe effects lead to a considerable contribution from the non-uniform lateral distributions of gain, carrier density, and temperature to the mode confinement in narrow stripe devices. This basically brings the mode guiding dynamic effects into the lasing process, and prepares for the possible dynamic consequence.

II. Total output power and mode losses

It has been observed that the dynamic instability process is accompanied with the dramatic change of spectrum, total output power and mode structure. Under the constant injection current, it is hardly possible that only the junction heating can induce these changes

without significant variation in the mode field profile. The change of the total output power can be related to that of mode loss, just like in the traditional Q-switching case. The reduction of mode loss will lead to the enhancement of total output power. As the mirror loss is supposed to be relatively constant for the supported lasing modes, the possible source for the change of loss would be the absorption loss, scattering loss and propagation loss, all of which depend on the mode field profile. In the gain-guided devices, the increase of mode loss can result from the mode expansion in its lateral extension, or it can occur when high order lateral mode is switched on and enhanced. For the current 8 μm stripe width, both situations would be possible.

III. Mode self-focusing

In Fig. 5-21a, before the onset of dynamic instability, the total output power is continuously increasing and the trend is relatively stronger for higher currents. This implies that the mode loss is decreasing with time. The thermal guiding effect should contribute to the loss reduction, for the temperature gradient increases with time due to the junction heating. With increasing optical power, the lateral spatial hole burning effect is enhanced that then can suppress the carrier density. In a normal carrier-induced dispersion case, the carrier density suppression will lead to the refractive index increase, thus enhance the mode guiding. The thermal guiding and the following carrier guiding effects accelerate each other so that the mode is *self-focusing*, which could cause destabilization eventually. Note that, QD gain can have stronger spatial hole burning effect than any conventional laser gain, due to the weak linked carriers between isolated dots.

IV. Lateral spatial hole burning and high order modes

Now we consider the temporal behavior of the lasing mode spectra. At the beginning of every instability process there appears always a new lasing spectral region at the high energy side, far away from the mainstream spectrum. This implies that at least for these new lasing modes the gain is excited by higher carrier density. Considering the spatial hole burning effect as illustrated in the following schematics:

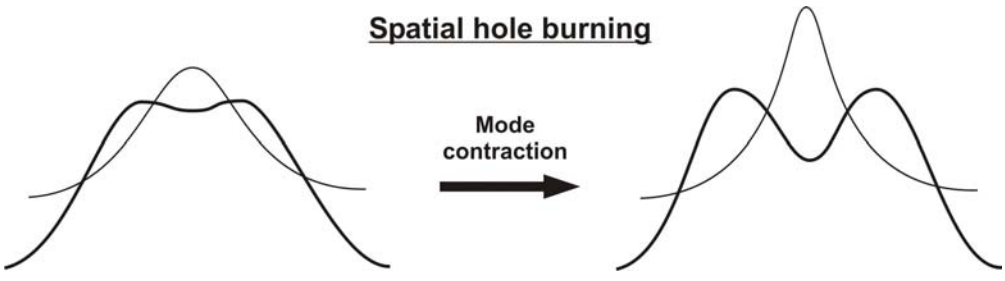

it can be seen that with the contraction of *lateral mode profile (thin line)*, the hole burning in the *carrier density profile (thick line)* becomes intense, and the double lobed carrier profile ensues. The carriers accumulated at the double lobe regions are less consumed by the fundamental mode, so they could support higher order modes. As the fundamental mode is self-focusing, the overlap of mode with the double lobes continues decreasing, thus the possibility for the switch-on of high order modes increases. As in Fig. 5-21a, at 5 x I_{th}, the destabilization finally occurs near the middle of the 3 μs pulse. The optical power is actually reduced within the instability stage. This results from the high loss for the high order modes. The high order new lasing modes consume mainly the gain at the double lobe regions, where the carrier density is much higher than the middle region, so they should appear at the high energy side of the original spectral modes. However, the fundamental mode does not contract so much at this current, so it is also in strong need of the gain in the same region. This gain competition effect may help explain the spectral development at the beginning of the instability process as in Fig. 5-20a, where the new spectral modes at the high energy side appear at the cost of the original peaks, and their further red shift and enhancement lead to the collapse of the main peak. The red shift of high energy spectral modes can be related to the decrease of carrier density at the double lobe regions. After the mode and carrier adaptation in the instability process, the stable lasing is being resumed, and near t=2.4 μs the power jumps to a higher level, which is due to the turn-off of the high loss higher order modes.

At higher currents, the total optical power increases since the laser turn-on, and the instability process appears earlier and lasts shorter, as reflected in the power reduction region before the apparent maximum point, as in Fig. 5-21a. Except the shorter duration, the spectral development is similar to the low current case. So it can be assumed that high order modes appear in the instability process due to the spatial hole burning effect, as in the former low current case. At high currents, the mode adaptation is hastened by the large intensity of high order modes due to higher carrier density. It is interesting to note that in the short instability process, there is an anomalously large mode red shift, which would be equivalent to $\Delta n_{eff} \sim + 6 \times 10^{-4}$, as in Fig. 5-21b. In the normal carrier dispersion case, such positive index change means a decrease of effective carrier density. This is consistent with the assumption that high order modes are switched on to consume the excess carrier density at the double lobe regions. In Fig. 5-21b, from t=0.2 to 0.5 μs, the mode spectra change dramatically with some modes turning on and off many times, in contrast with that

in Fig. 5-20a. This shows that the mode gain competition at high current and high optical power level intensifies, which is presumably due to the better mode confinement for all modes at higher temperature and even stronger spatial hole burning effect that helps feed high order modes with preferable gain distribution. The spatial hole burning is the crucial mechanism for the dynamics of switching between the fundamental modes and high order modes.

Note that even in the low current case as for 5 x I_{th} in Fig. 5-21a, the background of the total output power is still increasing continuously with time, and the power reduction due to the instability only reduces the absolute power level but not changes the trend. This indicates that even after the turn-on of high loss high order modes, the mode confinement is still in improvement. We attribute the improvement to the change of carrier density and index profile. As the high order lasing modes reduce the carrier density near the double lobe regions, the refractive index there is increased that helps improve the mode confinement wholly. Here the simultaneous increase of power and refractive index in the instability regime indicates a normal carrier dispersion relation at the carrier density level in the investigated QD devices, presumably due to the low threshold current density. It is anticipated that the anomalous carrier dispersion would appear at higher carrier density, and then the increase of carrier density will induce guiding effect, rather than the carrier anti-guiding effect, as is the case for conventional lasers.

The above discussion shows consistent relations among the mode confinement, total output power, and mode wavelength during the instability process. It indicates that the strong non-uniformity in the carrier profile, as induced by the spatial hole burning effect, is critical for the understanding of such a complex dynamic process. In contrast, for wide stripe lasers, multi-lateral-mode lasing prevails from the laser turn-on, and no significant spatial hole burning effect occurs that can cause strong non-uniformity in the carrier profile, therefore the dynamic instability is prevented. For index-guided narrow stripe lasers, the carrier non-uniformity can be significant due to the spatial hole burning effect, but the mode confinement is not particularly affected due to the inherent dominant index guiding mechanism, which helps greatly delay the occurrence of destabilization to much higher current and optical power regime.[29]

V. Junction heating effects, current focusing and thermal guiding

Now we discuss what happen after the instability stage. As in Fig. 5-21b and Fig. 5-28, the mode red shift afterwards shows no anomalous index change. For the long term up to 3 μs as in Fig. 5-20b and Fig. 5-28, the red shift rate of the mode wavelengths is gradually slowing down, indicating that the temperature begins to saturate. In this device, the response time of junction heating effect decreases quickly with current and is within a μs for the two highest current cases in Fig. 5-19. In these cases, the spectra just after the instability process are red shifted significantly, but after that they only show slight red shift, consistent with the temperature saturation.

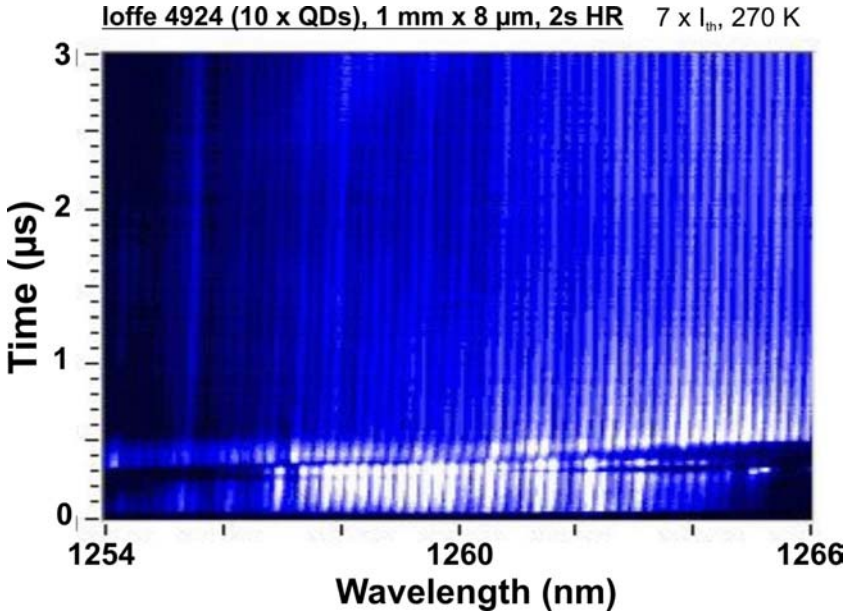

Fig. 5-28 Time-resolved lasing spectrum similar as that in Fig. 5-21b, but with longer pulse duration.

In Fig. 5-21a, it can be seen that at low current, the power reduction after the maximum point continues to the end of the pulse; with current, the power begins to increase again near the pulse end, such as for 7.5 x I_{th} and higher current. This current dependent trend suggests that the thermal effect is still there after the maximum power, and because the temperature becomes saturated with time, it needs more time than at the beginning of the pulse to help resume the trend of power increase, though the time can be shorter for higher currents. Similarly, the power decreases after the maximum point, and it takes shorter time at higher currents to retain the stable power level, especially for low currents at the pulse end the power is still decreasing. This current dependence indicates that the power drop is still a thermal effect, but it seems to have a trend exactly reversed from that at the beginning of the pulse. We may exclude the possibility of temperature decrease, which would cause the mode blue shift even after considering the power drop effect. The

power drop leads to increased carrier density and reduced index, which would result in a mode blue shift on its own. So apparently the temperature is increasing continuously in the power drop stage, as indicated by the continuous mode red shifts in Fig. 5-28.

To reconcile the above apparent contradiction between the temperature increase and power drop effects, we need to consider more carefully the functions of junction heating. The junction heating can have two effects. First it can generate a *temperature distribution* in the active region, so that a thermal guiding effect ensues. Second it can heat up the whole device and increase the *background temperature*. The first effect usually has a fast response time than the second one. Apparently, a more focused current profile will generate a larger temperature difference in the temperature distribution, though the whole heating power is still the same. The mode confinement is mostly affected by the temperature difference that results in index change, whereas, the modal gain and effective index is mostly determined by the averaged temperature. So even without changing the background temperature, the temperature distribution can be in change due to the varied current profile. The uniform current profile will generate the least temperature difference for the same current.

After the laser turn-on, the fundamental modes dominate, so the current flows mostly to the center region of the mode profile, where the carrier depletion is strongest. With time, both the background temperature and temperate difference increases, thus leading to both the mode red shift and thermal guiding effect. In the power drop regime, the temperature is still increasing with time, but there lacks the thermal guiding effect. The latter means that the temperature difference changes little. We attribute the less significant temperature difference to the particular current profile. As discussed before, the instability process introduces high order modes into the lasing process, and leaves a low carrier density as indicated by the anomalous red shift of mode wavelengths. In the whole instability stage, the modes and carrier density profile adapt to each other intensely, and the fundamental modes also balance with high order modes through the spatial hole burning effect. In the end of this chaotic mode competition process, a rather stable configuration of modes and carrier density profile is reached, that will stop the instability and return the laser to stable lasing stage. The low carrier density and stable lasing indicate that both the fundamental modes and high order modes are present and they cooperate to make a rather flat carrier density profile, for otherwise, one type of modes will be favored and that can lead to instability again through the spatial hole burning effect. Therefore, through the instability process, the carrier density profile is switched from a strongly distorted, double lobed one

to a rather flat top profile. Simultaneously the current profile is also switched to a more uniform profile. Clearly this resulting current profile is less efficient in generating temperature difference, and the thermal guiding effect is taken out of functioning. By the thermal response time, the power will begin to decrease for the deteriorated mode confinement condition.

The power drop causes the increase of carrier density and the reduction of effective refractive index. So the mode guiding condition is changing due to the carrier anti-guiding effect. The mode intensity ratio has to adapt to the new situation. The power drop also means a weakened spatial hole burning effect, which makes the mode interaction less intense and a mild mode adaptation can occur without instability. The high order modes will be affected earlier by the varied mode guiding condition than the fundamental modes, so it is anticipated that the mode intensity ratio becomes to favor the fundamental modes. To this point, it is clear that the thermal guiding effect will come into function, for the reduction of high order mode ratio will cause a more focused current profile that can enhance the temperature difference. But up to this time, the background temperature has been raised after a long period of continued increase, so it will be harder to generate temperature difference. This is why we see that the power recovery process needs much longer time to have a significant power increase that at the beginning of pulse. The higher current helps shorten the recovery time. As can be seen in Fig. 5-19 and Fig. 5-21a, for 9 x I_{th}, the mode self-focusing after the power drop leads to another run of destabilization. This time the mode guiding conditions are different from the first time, and the instability process becomes chaotic.

VI. Conclusion

In conclusion, the transient dynamics of shallow-mesa narrow stripe MQD lasers are strongly impacted by the inherent weak mode guiding mechanism. The variations in the non-uniform distribution of gain, carrier density and temperature can perturb the mode guiding conditions and lead to significant change in the laser output. The junction heating effects are the driving force in generating the transient dynamics. The temporal change of thermal guiding condition induces the change of total output power and carrier density, and the interplay of these processes may cause the mode self-focusing effect. A significant spatial hole burning effect will lead to dynamic instability that is characterized by the switch-on of high order lateral modes and the ensuing mode and gain adaptation processes. Intense mode competition can occur between the fundamental modes and high order

modes, as mediated by the spatial hole burning effect. The dynamic instability process ends with a rather stable lasing condition characterized by low carrier density and balanced mode components. It is found that the formation of thermal guiding depends on the current injection profile. A more focused current profile helps generate large temperature difference and enhance the thermal guiding effect.

Due to the anomalous carrier dispersion property in QDs,[32] it is expected that, for devices working at higher carrier density, the above dynamic instability may be avoided by the canceling effect of thermal guiding and *carrier-induced guiding* mechanisms, or at least delayed to higher power regime.

b) Low temperature spectral dynamics

The above discussion shows that, at high temperatures, the transient dynamics of shallow-mesa narrow stripe MQD lasers are impacted by their sensitive mode guiding mechanism. The non-uniformity in the lateral profiles of gain, carrier density and temperature is the crucial factor that induces various transient dynamics. At low temperatures, these factors still exist, and continue to affect the transient mode guiding conditions.

In Section 5.4, we have discussed the low temperature transient spectral dynamics of the wide stripe MQD lasers. There it has been shown that their dynamics are impacted by the carrier transport effect, and determined by the gain inhomogeneity among the QD multilayers and the bottlenecked carrier transport processes. The peculiar dynamic features appear at low currents near threshold and in the first μs. After the first 1 μs the laser output becomes stable and so is at high currents. Similarly, in narrow stripe MQD lasers, we found also certain dynamic features characteristic of the carrier transport effect. Like in Fig. 5-23 and Fig. 5-24, the turn-on transient dynamics within the first 1 μs are rather similar to those in Fig. 5-15 from the wide stripe device. The dynamics in Fig. 5-26 are just the variations of spectral waving patterns as in Fig. 5-15.

In narrow stripe devices, the lateral non-uniformity of gain and carrier density will add to the gain inhomogeneity as induced by the limited carrier transport across the MQDs. That modifies the sum gain in narrow stripe devices. However, the rate limiting processes in the gain and carrier dynamics are still those vertical carrier transport processes, which are not affected by the variation of stripe widths. Therefore, the major laser dynamic features based on carrier transport effects should remain the same for wide or narrow stripe devices, as is the case.

On the other hand, the particular transient effects in narrow stripe devices are driving by the junction heating, and these thermal effects are characterized by their slow response and only become relatively fast at high currents. So the typical dynamic time constants of carrier transport effects are much faster than the thermal one. This makes the carrier transport dynamic features less vulnerable to the transient effects in narrow stripe lasers, especially at low currents and in the laser turn-on regime.

The two-time-zone behaviors, as in Fig. 5-24 and Fig. 5-27, can be attributed to the sensitivity of the carrier transport effect to the variations of the dot layer spectral gain profiles that determine the sum gain. In narrow stripe devices the lateral non-uniform gain profiles can vary with the mode profile, and the typical narrow stripe transient effects are the temporal variations of mode guiding conditions. So the dot layer spectral gain profiles can vary in the transient, and this leads to the particular variations of carrier transport dynamic features in narrow stripe devices.

As stated before, the carrier transport specific dynamics occur at low currents and in the laser turn-on regime. After the turn-on dynamics or at high currents, the narrow stripe transient effects would dominate the laser dynamics. As can be seen in Fig. 5-27, from 2 x I_{th} to 3 x I_{th}, the stable lasing after the short period turn-on dynamics is destabilized to a chaotic one. This shows again that the dynamic instability is characteristic of the transient laser dynamics in narrow stripe MQD lasers, especially for the gain-guided ridge waveguide devices as in the present case.

5.6 Summary

In this chapter, the carrier transport effects in MQD lasers are explored. First, we study the time-averaged spectral features of MQD lasers under the variations of different parameters, such as temperature, device loss, dot layer number and the dot confinement energy. The peculiar spectral features are consistently attributed to the gain inhomogeneity that is caused by the limited carrier transport across the MQDs.

In the next, the spectral dynamics pertaining to the peculiar spectral features are analyzed. The underlying basic laser dynamics processes are discussed, including the possible self-organization mechanisms that lead to the characteristic turn-on dynamics and spectral waving patterns. It is found that the limited carrier transport at low temperature is crucial for a consistent laser dynamics system analysis. From the mode dynamics aspects, the spectral waving patterns are equivalently to the mode phase shifted relaxation oscillations.

These damped relaxation oscillations are identified to be the main relaxation oscillations that have much reduced frequencies due to the carrier transport effect. With current, phase transition of mode dynamics is observed from the antiphase mode oscillations to the collective damped relaxation oscillations.

Then, the dynamic instability processes in the transient dynamics are studied in shallow-mesa narrow stripe MQD lasers. They are related to the weak mode guiding conditions that are perturbed by transient junction heating effects. Multi-lateral-mode dynamics are introduced by spatial hole burning effect. The non-uniform lateral profiles of gain, carrier density and temperature are discussed with relation to different mode guiding mechanisms and their interplay. The formation and extent of thermal guiding is found to depend on the current injection profile. A more focused current profile favors thermal guiding for the enhanced temperature gradients. In addition, the low temperature spectral dynamics of narrow stripe MQD lasers are analyzed. The variations of carrier transport related dynamic features are related to the narrow stripe transient effects.

Finally, based on the above studies, we note that the strong quantum confinement and gain nonlinearity pertaining to QD systems make QD lasers rather attractive for the study of nonlinear laser dynamics. Coupled with the carrier transport effect, the MQD lasers can be useful model systems[37] for the study of nonequilibrium nonlinear dynamics far away from equilibrium. The great flexibility in tailoring the QD and laser parameters by advanced growth technique offers QD lasers a particular advantage, among many other merits of semiconductor lasers, over other types of laser systems. Specifically, in the future, the spatial-temporal patterns of the optical near field[38] in the MQD lasers can be explored, in addition to the spectral-temporal patterns. These will provide the information of spatial mode dynamics in support of the present study of dynamic instability in MQD lasers.

References:

1 *Theory of transport properties of semiconductor nanostructures*; *Vol. 4*, edited by E. Schöll (Chapman & Hall, London, 1998).

2 D. K. Ferry and S. M. Goodnick, *Transport in nanostructures*, Vol. 6 (Cambridge University Press, Cambridge, 1997).

3 S.-Y. Lin, Y.-J. Tsai, and S.-C. Lee, Appl. Phys. Lett. **83,** 752 (2003).

4 J. K. Kim, T. A. Strand, R. L. Naone, and L. A. Coldren, Appl. Phys. Lett. **74,** 2752-2754 (1999).

5 B. Kochman, S. Ghosh, J. Singh, and P. Bhattacharya, Electron. Lett. **38,** 752 -753 (2002).

6 B. KOCHMAN, et al, J. Phys. D, Appl. Phys. **35,** L65–L68 (2002).

7 Optical and quantum electronics **26,** S647-S855 (1994).

[8] J. Piprek, P. Abraham, and J. E. Bowers, Appl. Phys. Lett. **74,** 489-491 (1999).
[9] P. Vasil´ev, in *Ultrafast diode lasers: fundamentals and applications* (Artech House, Boston, 1995), p. 190.
[10] K. A. Williams, P. S. Griffin, I. H. White, B. Garrett, J. E. A. Whiteaway, and G. H. B. Thompson, IEEE Journal of Quantum Electronics **30,** 1355-1357 (1994).
[11] T. Ota, T. Hatano, S. Tarucha, H. Z. Song, Y. Nakata, T. Miyazawa, T. Ohshima, and N. Yokoyama, Physica E **19,** 210-214 (2003).
[12] V. Shchukin, N. N. Ledentsov, and D. Bimberg, *Epitaxy of Nanostructures* (Springer-Verlag, Heidelberg, 2003).
[13] L. Banyai and S. W. Koch, *Semiconductor Quantum Dots*, Vol. 2 (World Scientific, Singapore, 1993).
[14] F. Guffarth, R. Heitz, A. Schliwa, O. Stier, N. N. Ledentsov, A. R. Kovsh, V. M. Ustinov, and D. Bimberg, Phys. Rev. B **64,** 085305 (2001).
[15] M. Colocci, A. Vinattieri, L. Lippi, F. Bogani, M. Rosa-Clot, S. Taddei, A. Bosacchi, S. Franchi, and P. Frigeri, Appl. Phys. Lett. **74,** 564-566 (1999).
[16] R. Nagarajan, M. Ishikawa, T. Fukushima, R. S. Geels, and J. E. Bowers, IEEE J. Quantum Electron. **28,** 1990-2008 (1992).
[17] L. V. Asryan and R. Suris, IEEE Journal of Selected Topics in Quantum Electronics **3,** 148-160 (1997).
[18] E. S. Moskalenko, K. F. Karlsson, P. O. Holtz, B. Monemar, W. V. Schoenfeld, J. M. Garcia, and P. M. Petroff, Phys. Rev. B **64,** 085302 (2002).
[19] V. I. Tolstikhin, J. Appl. Phys. **87,** 7342-7348 (2000).
[20] J. M. R. Cruz, F. V. d. Sales, S. W. d. Silva, M. A. G. Soler, P. C. Morais, M. J. d. Silva, A. A. Quivy, and J. R. Leite, Physica E **17,** 107-108 (2003).
[21] E. C. L. Ru, J. Fack, and R. Murray, Phys. Rev. B **67,** 245318 (2003).
[22] T. Müller, F. F. Schrey, G. Strasser, and K. Unterrainer, Appl. Phys. Lett. **83,** 3572-3574 (2003).
[23] J. Feldmann, S. Cundiff, M. Arzberger, G. Böhm, and G. Abstreiter, J. Appl. Phys. **89,** 1180-1183 (2001).
[24] D. Ouyang, submitted to PRL (2003).
[25] E. Schöll, *Nonlinear spatio-temporal dynamics and chaos in semiconductors*, Vol. 10 (Cambridge University Press, Cambridge, 2001).
[26] G. P. Agrawal and N. K. Dutta, in *Long-wavwlength semiconductor lasers* (Van Nostrand Reinhold, New York, 1986), p. 221.
[27] A. Sudbo and L. Bjerkan, IEEE Journal of Quantum Electronics **19,** 1542- 1551 (1983).
[28] K. Y. Lau, in *Quantum well lasers*, edited by J. Peter S. Zory (Academic Press, Boston, 1993), p. 217-275.
[29] N. Chinone and M. Nakamura, in *Part C, Secmiconductor injection lasers, II / Light-emitting diodes*; *Vol. Lightwave communications technology*, edited by W. T. Tsang (Academic press, Orlando, 1985), p. 61-91.
[30] R. J. Nelson and N. K. Dutta, in *Part C, Secmiconductor injection lasers, II / Light-emitting diodes*; *Vol. Lightwave communications technology*, edited by W. T. Tsang (Academic press, Orlando, 1985), p. 1-59.
[31] J. Manning, R. Olshansky, and C. Su, IEEE J. Quantum Electron. **19,** 1525- 1530 (1983).
[32] H. C. Schneider, W. W. Chow, and S. W. Koch, Phys. Rev. B **66,** 041310(R) (2002).
[33] S. Schneider, P. Borri, W. Langbein, U. Woggon, R. L. Sellin, D. Ouyang, and D. Bimberg, CLEO (2002).

[34] K. Petermann, *Laser diode modulation and noise*, Vol. 3 (Kluwer Academic Publishers, Dordrecht, 1988).
[35] D. Ouyang, R. Heitz, N. N. Ledentsov, S. Bognar, R. L. Sellin, C. Ribbat, and D. Bimberg, Appl. Phys. Lett. **81,** 1546-1548 (2002).
[36] D. Ouyang, N. N. Ledentsov, D. Bimberg, A. R. Kovsh, A. E. Zhukov, S. S. Mikhrin, and V. M. Ustinov, Semicond. Sci. Technol. **18,** L53 - L54. (2003).
[37] K. Otsuka, *Nonlinear Dynamics in Optical Complex Systems*, Vol. 7 (Kluwer Academic Publishers, Dordrecht, 1999).
[38] C. Tamm, L. A. Lugiato, M. Brambilla, A. B. Coates, C. O. Weiss, and R. McDuff, in *Nonlinear Dynamics and Quantum Phenomena in Optical Systems, Proceedings of the third international workshop on nonlinear dynamics and quantum phenomena in optical systems*; *Vol. 55*, edited by R. Vilaseca and R. Corbalan (Springer-Verlag, Berlin, 1990), p. 225.

CHAPTER 6 FOUR-SIDED LASERS

Contents:

6.1 Introduction

The two-dimension (2D) optical cavities with regular or tailored geometries[1-8] have attracted much attentions in recent years. On one hand, there is interest in the study of the fundamental ray optics and wave propagation dynamics in these cavities. For example, 2D polygonal cavities including square-shaped ones are subjects of study in renowned billiard problems, concerning the chaotic dynamic properties.[9] The optical counterpart of these billiard problems is the study of mode or orbit dynamics in the polygonal optical cavities, for the specular reflection of the billiard at the sidewalls resembles the optical reflection at the cavity boundary. The study on the optical cavities with basic geometrical shapes, such as circle and square, is fundamental for the understanding of those with much complex geometry. On the other hand, the 2D optical cavities have great potentials for applications in the area of optoelectronics, integrated optics and optical communications. They are compatible with the current planar waveguide and processing technology so that large-scale cost-effective implementation and large scale integrations becomes possible. The flexibility in tailoring the optical functions by adjusting the cavity geometry would be another advantage. It is shown that, by fine-tuning the geometry, stadium-shaped microlasers based on quantum cascade structure can emit efficiently in strongly directional far field profiles,

in contrast to the round shaped lasers with whispering-gallery-modes, which have extremely low light output efficiency.[2,9,10] In this respect, the geometrical factors play a critical role in affecting the basic cavity optical functions, such as the cavity transmission and emission properties. Among the most basic 2D geometrical shapes, the circle or round shapes have been addressed for long due to their highest symmetrical properties. However, square-shaped cavities are only addressed till recently. For square-shaped cavities, recent studies mainly concern the high-Q, high-finesse cavity resonance modes confined by total internal reflection (TIR),[11] because these modes provide strong and stable mode selectivity and particularly the long side area of the square cavity allows a stronger evanescent wave overlap[12] for out-coupling, compared to the very limited overlap point in the round cavity. The square micro-resonators has been shown to be able to potentially act as efficient add-drop filters in compact integrated optic devices.[7,11] In addition to these cavity transmission properties, recently large progress has been made in understanding the emission properties of vertical cavity surface emitting lasers (VCSELs) with oxide-confined square-shaped apertures. The diamond-scarred near field patterns are successfully imaged and they are in excellent agreement with the results of theoretical calculations based on 2D quantum billiard models.[13,14] The modes confined by total internal reflection (TIR) can be clearly observed for the first time experimentally. The results of the above studies provide a strong base for the further exploration of the emission properties of square cavities.

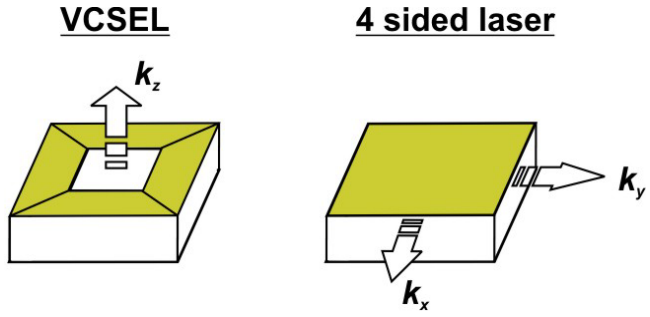

Fig. 6-1 Schematics of VCSEL and four-side lasers.

In this chapter, we study the emission properties of the four–sided lasers that possess near-square-shaped laser cavity. The four–sided lasers belong to edge emitting lasers, in contrast to the VCSELs with square apertures. As illustrated in Fig. 6-1, the wave vectors of confined modes in the square VCSEL have finite transversal component k_z (Z is normal to the 2D cavity plane), which allows the direct observation of TIR modes, whereas, in the four-sided lasers, the mode wave vectors have both lateral components (k_x, k_y) in finite size, but the transversal component k_z is negligible. The latter fact means that the TIR modes in four-sided lasers are totally confined in 3 dimensions, and contribute no output. The

emission of the four-sided lasers comes from those modes that are not or only partially confined by TIR´s. In Fig. 6-2a, the typical ray trajectories of TIR modes are shown in the square cavity. The total confinements by TIR´s ensue when both the reflection angles are larger than the critical angle for TIR; otherwise, the modes will emit in either pair of opposite boundaries. In Fig. 6-2b, the mode emits in the upper and lower sides due to the partial reflection, meanwhile it is totally reflected in the other two sides.

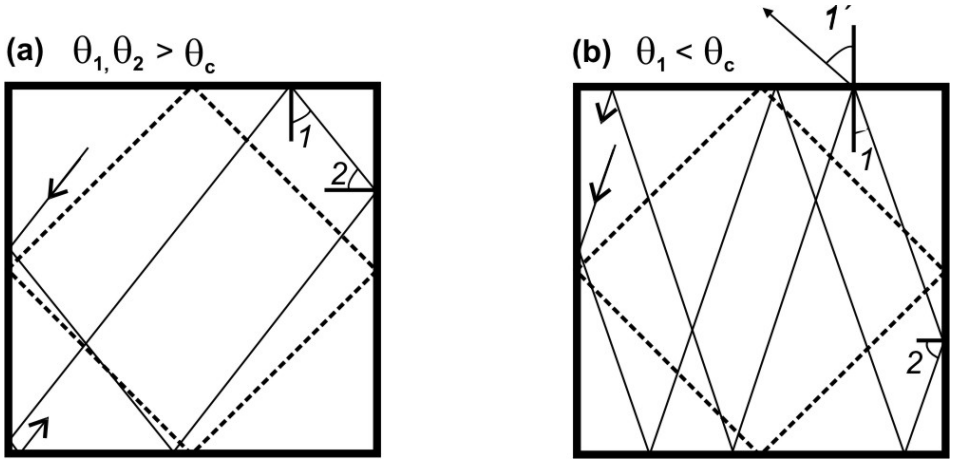

Fig. 6-2 (a) Total internal reflection modes. (b) Leaky modes. The dashed lines denote a closed orbit mode.

The four-sided lasers investigated in this work are fabricated from the similar laser structures as used for the stripe geometry lasers. The stripe definition lithographical step is left out, and the wafer thinning and p- and n-side metallization are the only steps to process the laser die. For the formation of near-square-shaped cavity, the laser die is cut in 4 sides. The as-cleaved 4 facets are perfect cavity boundaries endowed by the nature. As gain media, the QDs support emission in a wide spectral band, owing to their broad spectral gain profile. This facilitates the observation of resonance mode wavelengths in a wide range. The superior lasing parameters of the used QD laser structures, like low threshold current density, high internal quantum efficiency and low internal loss, help minimize the complication from the non-uniform thermal and carrier distributions, so that the intrinsic spectral and azimuthal mode properties can be revealed.

In the following, we first investigate the far field emission profiles of the four-sided lasers, and then discuss their basic lasing characteristics including the light-current and spectral ones. In the next, the spectrally resolved far field profiles are investigated to reveal the characteristics of azimuthal modes in the four-sided lasers. Finally, by ray trace simulation, the corner diffraction effect on the azimuthal modes is studied for the near-square-shaped cavity, and is compared to the former experimental results. Note that the emission

wavelength (~1-1.3 μm) is much smaller than the cavity dimension (~500 μm), so it is justified to use ray optics in this work.

6.2 Far field emission profiles

6.2.1 Ray optics in the four-sided lasers

In the four-sided laser diodes, the thin waveguide structure provides for a single-traverse-mode optical confinement, similar to that in stripe geometry lasers. So it can be treated as a 2D optical cavity, with the four as-cleaved facets as boundaries. When the light rays meet the boundary, they are reflected totally or partially depending on the incidence angle. Here we consider only the TE mode (i.e. the electric field parallel to the incidence plane), for the intensity of TM mode is found to be one order of magnitude lower generally, presumably due to the low reflectivity for TM modes, similar as in stripe geometry lasers. The reflectivity for the TE mode at the semi-infinite semiconductor (GaAs) - ambient interface is given by the following Fresnel´s formula:[15]

$$R_p = (n_i\cos\theta_0 - n_0\cos\theta_i)^2/(n_0\cos\theta_i + n_i\cos\theta_0)^2 \qquad (6\text{-}1)$$

Where $n_i = 3.3$, $n_0 = 1$ and θ_i is the incidence angle, θ_0 the outgoing far field angle. The reflectivity curve is shown in Fig. 6-3.

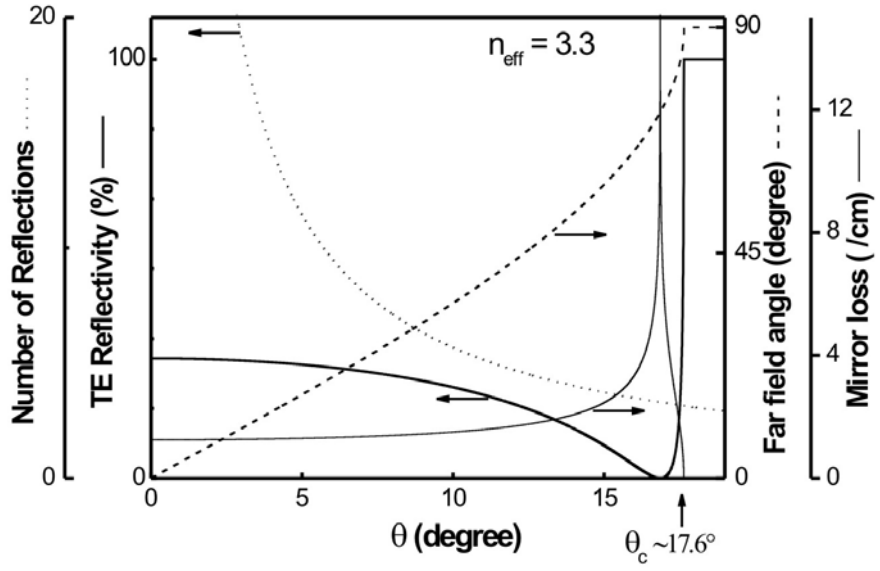

Fig. 6-3 Angular dependence of reflectivity of TE modes, mirror loss, and number of reflections in a roundtrip. The incidence angle θ is also converted to the far field angle.

For the ray traces with incidence angles $\theta_c < \theta < 90°-\theta_c$, the light is totally confined by TIR´s at all boundaries, as illustrated in Fig. 6-2a. Null reflection loss makes these modes of high Q, but that also means that they have no contribution to the cavity emission. One possible way of damping these modes is through the corner diffraction, which may couple out part of the mode intensities, but this emission should provide no angular features at first hand. For the incidence angle is complementary in 90° for the consecutive reflection of the same ray trace, light emission through reflection loss is only possible through the opposite two boundaries in either one edge direction, and for one incidence angle $\theta < \theta_c$. as illustrated in Fig. 6-2b. It is generally conceivable that a typical ray trace will plough the whole cavity after a definite number of round trips, except those of periodic orbits like the dashed one in Fig. 6-2. In the present lasers, θ_c = arcsine $(n_0/n_i) \sim 17.6°$, so for all the emitting modes, the ray trace will bounce many times between two opposite boundaries within one round trip, as illustrated by the solid ray trace in Fig. 6-2b.

In Fig. 6-2a, it can be seen that with only a minor change of incidence angle, the ray trajectory shows significant variations from the periodic orbit (in dashed line). This is characteristic of discrete ray dynamics. The ray trace can even hit the corner after one roundtrip. Here the corner represents a singularity point for the ray optics. We assume the corner diffraction produces no far field profile, or to say the light is isotropic in the 2D plane after the corner diffraction. So the corner diffraction becomes an important loss mechanism for all kinds of rays that have a chance to meet the corner in their lifetime. In Section 6.4.2, we will explore the corner diffraction as a critical mode selection for the azimuthal modes.

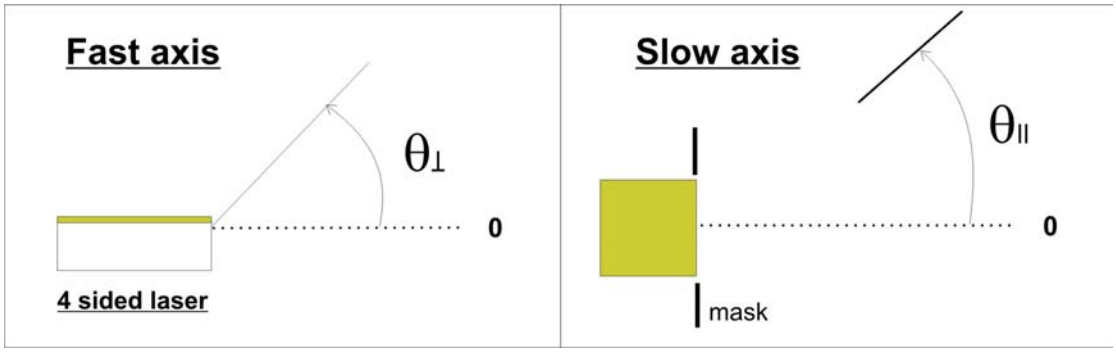

Fig. 6-4 Far field measurement setup.

6.2.2 Far field profiles

As a gross characteristic of emission from the four-sided lasers, we start with the far field emission profiles; here concentrating on the spectrally integrated profiles and in later

sections spectral-resolved ones will be addressed. As for the experimental set-up, the laser diode is seated on the centre of a rotating stage composed of two stepping motors, which is controlled by computer. A LN_2 cooled Germanium detector with Lock-in technique is used to collect light on a distance of 1 meter from the laser diode, providing for ~1° angular resolution. Both fast and slow axes are scanned as schematically shown in Fig. 6-4. For the slow axis, we use the mask to stop the emission light from both side facets in order to measure the emission profile form the single front facet. The laser diodes are fabricated from the laser structure (TU3623) with 3-fold stacked 1 μm InGaAs QDs.

a) Fast axis profile

In the fast axis (i.e., vertical to the laser diode junction plane), a single-lobed profile (Fig. 6-5a) is observed for all the currents, which is consistent with the single-transverse-mode confinement. The tilt of the emission maximum to the substrate direction can be attributed to the non-symmetry of the waveguide in the fast axis. Note that the intensity above threshold stays in the same order of magnitude as that below threshold. This is a characteristic feature of the four-sided lasers, because the high-Q TIR modes lase only inside the cavity without out-coupling to the far field emission, whereas the far field emitting lasing modes are those of long lifetime against reflection and other losses, so their threshold losses are higher than the TIR modes, and their emission intensity is suppressed by the lasing TIR mode. The short-lived modes with large losses will contribute only to the spontaneous emission.

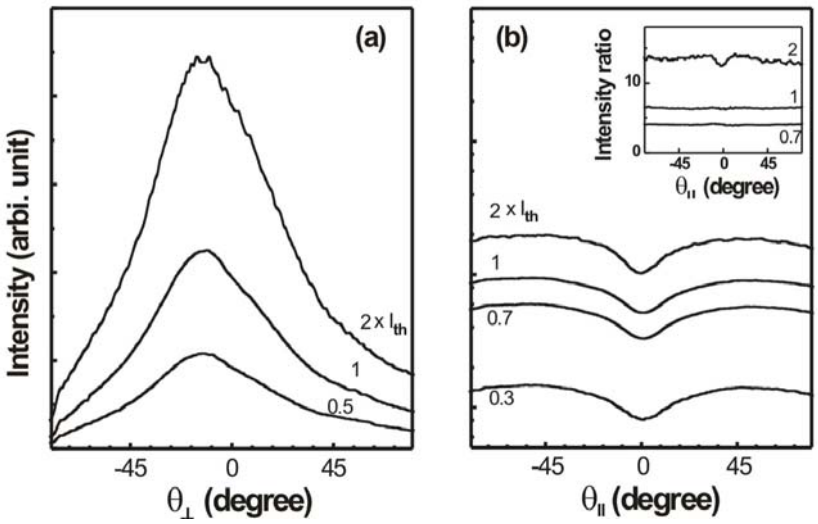

Fig. 6-5 (a) Fast axis far field profile. (b) Slow axis far field profile. The insets show the intensity ratio of various profiles to the lowest current profile.

b) Slow axis profile

Along the slow axis, the far field profile without the mask is shown in Fig. 6-5b. All the profiles show double-wing patterns. The intensity ratio to the lowest current profile is shown in the inset of Fig. 6-5b. Below threshold, the intensity increases at a common rate for all directions, so the ratio remains constant for all the angular range. Above threshold, a shallow dip in the intensity ratio shows up for the directions near the facet normal (0°), indicating that the normal emission is slightly suppressed. However, the difference is rather minor in the whole angular range.

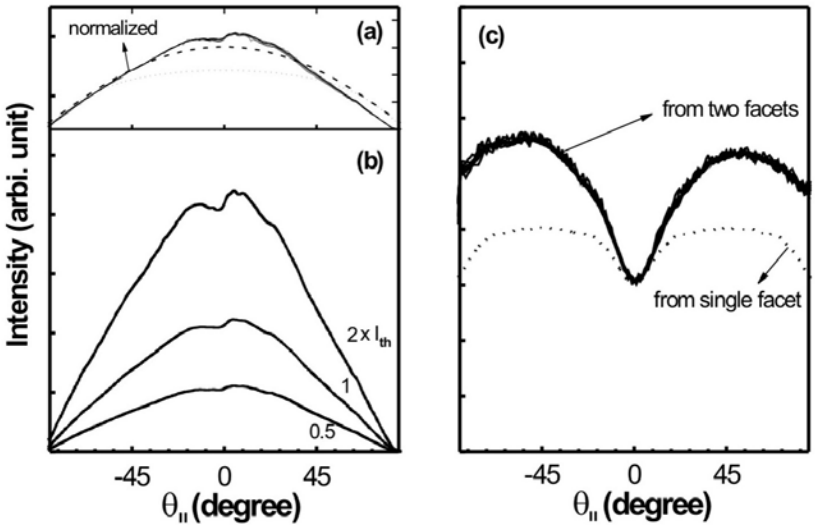

Fig. 6-6 (a) and (b) Slow axis profiles from single facet with (a) normalized. (c) Normalized slow axis profiles from two facets. The dashed and dotted profiles are calculation results. See the text.

The former slow axis profile actually includes not only the front facet emission, but also those from the two side facets. We use the mask in Fig. 6-4, to block the side facet emissions, and get the single front facet emission. As in Fig. 6-6b, the single facet profile is single lobed, and near the facet normal (0°) a strong non-symmetric profile appears that is common for all currents. The normalized profiles for all currents are shown in Fig. 6-6a, and it is striking to see that they coincide with each other. This shows that the lasing action makes almost no impact on the far field distribution. The irregularity near the facet normal (0°) can be attributed to the incomplete masking of the side facet emission.

Now we discuss the origin of these slow axis profiles. The emission profile is directly associated with the angular intensity distribution of light that incident on the facet within the laser cavity. The light is refracted into the far field according to Snell law:

$$n_i Sin\theta_i = n_0 Sin\theta_0 \qquad (4\text{-}2)$$

where n_i ~ 3.3, n_0 = 1 are the refractive index of laser cavity and air respectively.

We first ignore the angular dependence of reflectivity, and will add its effect later. For $I(\theta_0)\Delta\theta_0 = I(\theta_i)\Delta\theta_i$, and considering a uniform angular distribution inside cavity, i.e. assuming I (θ_i) = Constant, the far field profile can be calculated as follows:

$$I(\theta_0) = \frac{I(\theta_i)\Delta\theta_i}{\Delta\theta_0} = I(\theta_i)\frac{n_0 Cos\theta_0}{\sqrt{n_i^2 - n_0^2 Sin\theta_0^2}} \qquad (4\text{-}3)$$

The calculated far field profile is plotted in Fig. 6-6a in the dashed line. Its intensity is normalized like the normalized experimental profiles in reference to the angle of - 45°. In the next, we add the angular dependence of the reflectivity to the calculation.

$$I'(\theta_0) = I(\theta_0)\, T_p = I(\theta_0)\,(1 - R_p) \qquad (4\text{-}4)$$

The result is shown in Fig. 6-6a in the dotted line. It is clear that the discrepancy lies mainly in the central angular region. This indicates that the angular distribution inside cavity is enhanced near the normal incidence, compared to a uniform angular distribution.

With the single facet profile, we can synthesize the full facet profile without masking. The synthesized profile is shown in Fig. 6-6c in the dotted line, along with the normalized experimental curves of those full facet profiles (see Fig. 6-5b). Apparently the characteristic double-wing pattern originates from the overlap of the emissions from the neighboring facets. The intensity maximum at 45° is evident in all the profiles. The experimental curves coincide well with each other, indicating again the negligible impact of the laser action. The discrepancy between the experimental curves and the synthesized profile can be attributed to the uncertainty of the measurement near the facet normal, which significantly modifies the intensity near 0° and 90°.

Based on the above study, the four-sided laser can be treated as a special stripe-geometry laser with ultra broad emission area. For the loose mode confinement in the lateral direction, the slow axis profile is rather broad, ~90° (see Fig. 6-6b), as compared to the narrow Gaussian profile of the narrow stripe laser that has a typical FWHM of only ~10–20°.

Here the far filed profile shows no significant impact of laser action. Later we will see that the lasing output power of the four-sided lasers is rather limited, even compared to the spontaneous emission. So without screening out most of the spontaneous emission, it is difficult to see any fine structures as related to the emitting lasing modes. In later sections, we will use spectral filtering to measure the spectrally resolved far field profiles, and discuss the distinct angular dependence therein.

6.3 Basic lasing characteristics of four-sided lasers

In this section, we discuss the lasing characteristics of the four-sided QD lasers, including light-current (L-I) curves and spectral properties.

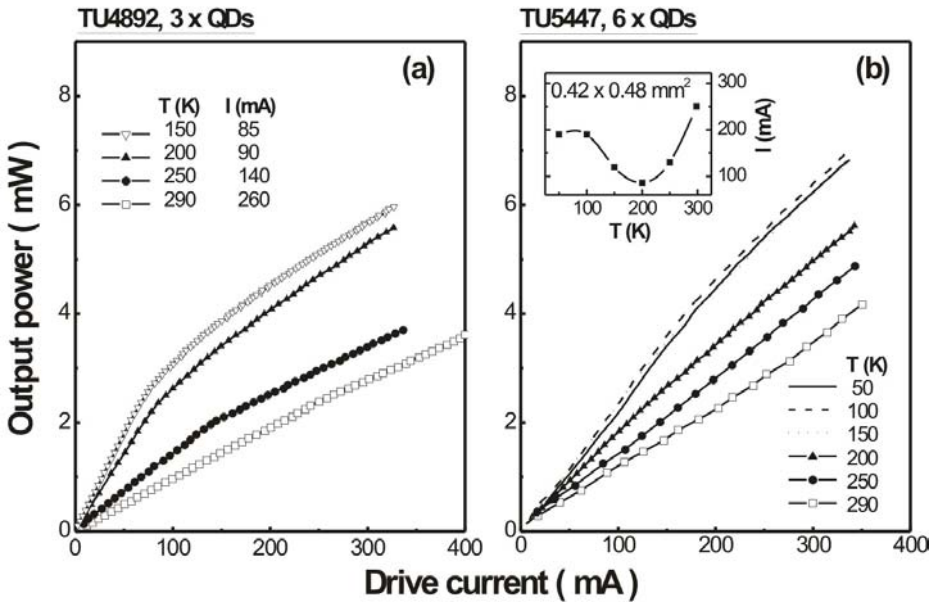

Fig. 6-7 L-I curves of two four-sided QD lasers at various temperatures.

6.3.1 Light-current characteristics

The L-I curves of a four-sided QD laser with 3-fold stacked InGaAs QDs are shown in Fig. 6-7a. They feature two linear sections with distinct slope efficiency. The transition points are found to coincide with the appearance of sharp peaks in the emission spectra, so they can be assigned as the thresholds of the four-sided laser. Apparently these L-I curves are totally different from those of stripe geometry lasers. Here the L-I section before the transition point should be spontaneous emission. After the transition or above threshold, the slope efficiency even decreases, instead of taking up in stripe geometry lasers. This indicates that the spontaneous emission is suppressed above threshold, implying a clamped carrier density above threshold. But the output power of the emitting lasing modes is so limited that it is even lower than that supposed for spontaneous emission. Apparently this

low lasing mode emission cannot make any significant impact on the carrier density as such. We can readily attribute the suppression of carrier density to the TIR lasing modes. As is, the TIR modes are always totally confined in the cavity without any contribution to the far field emission. They have the lowest losses among all possible lasing modes, so above threshold, they start lasing, and lead to the suppression of spontaneous emission. The emitting lasing modes have higher losses due to the reflection and diffraction, so their intensities amount to only a minor portion of the total lasing power, compared to the TIR lasing modes. That makes the slope efficiency of lasing action look very low, and can be even lower than that of spontaneous emission.

Now we discuss the lasing principle in the four-sided lasers. The four-sided lasers belong to the traveling wave lasers in principle. There are very few TIR modes having closed periodic orbits like the dashed one as shown in Fig. 6-2. But these few numbered modes are highly competitive for their lowest loss levels. In comparison, other TIR modes may be damped by the additional corner diffraction losses. The emitting lasing modes, or to say leaky modes, have higher losses than any TIR modes, so they are, at first hand, inhibited to lase aside the TIR lasing modes. Above threshold, the TIR modes with the lowest losses start lasing, followed by the other TIR modes. In a traveling wave assumption, there will be no chance for other leaky modes to lase at all. But in reality, the TIR modes with closed orbits can form standing wave patterns, that is, the spatial hole burning effect is in action. This eventually leaves a chance for the leaky modes to obtain enough gain for laser action. Apparently among the leaky modes, those with longer lifetime will be favored in the lasing process.

Because the TIR modes consume the main part of gain and current, they determine the average gain levels by gain compression. The emission of long-lived leaky modes reflects the gain compression levels. To demonstrate the gain compression effect, the L-I curves from another four-sided laser with 6-fold stacked InGaAs QDs are shown in Fig. 6-7b. The 6-fold one has higher gain saturation level, so the gain compression is less efficient than in the 3-fold QD laser. This makes more gain margin for the leaky modes and increases the slope efficiency for the 6-fold laser. Due to the stronger gain compression, the L-I curves of the 3-fold laser shows more distinct turning points. Note that the sublinear or superlinear behavior near the turning point is determined only by the relative difference between the lasing slope efficiency and the spontaneous emission efficiency.

As can be seen in Fig. 6-7, the temperature dependence of the four-sided lasers is rather similar to that of the stripe geometry lasers. It is mainly determined by the temperature dependence of QD gain properties. The waveguide effects are more reflected in the suppressed emission output and the following spectral characteristics.

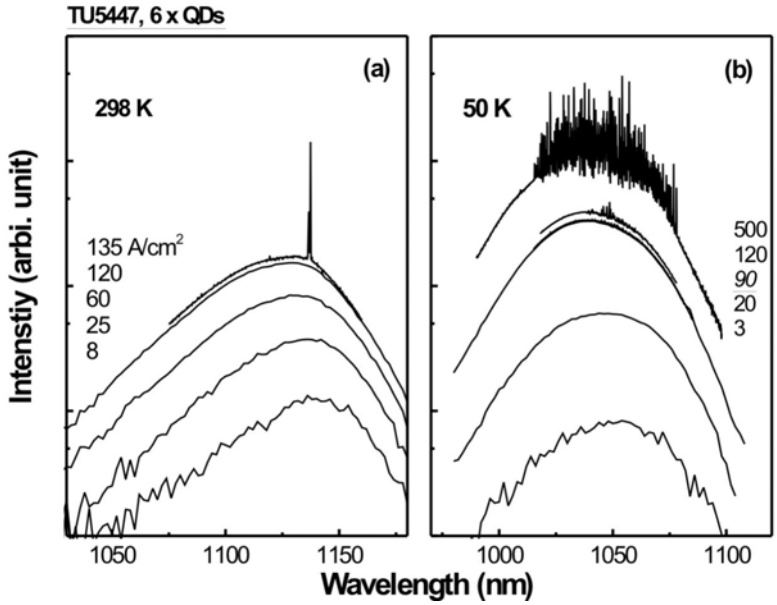

Fig. 6-8 Emission spectra of the four-sided QD laser.

6.3.2 Spectral characteristics

a) True spontaneous emission

In the following we investigate the emission spectra of the four-sided QD lasers. As in Fig. 6-8, the below threshold spectra show little change in the spectral profiles and the maximum position. This is characteristic of the four-sided lasers, because the modes that experience strong gain effect are mainly confined inside cavity. These spectra thus can be used as true spontaneous emission spectra. As can be seen, the low temperature spectra are much broader than the RT ones, reflecting the quenched interdot carrier redistribution.

b) Lasing spectrum characteristics

Above threshold, sharp lasing peaks appear in the RT spectrum in Fig. 6-8a. Apparently the peak is not at the maximum of the spontaneous emission spectra. As a usual case in stripe geometry lasers, the lasing peak should appear first at the maximum of amplified spontaneous emission (ASE) spectrum. But as discussed, here the below threshold spectra are true spontaneous emission ones, so their maxima are not the maximum gain positions. In Fig. 6-8b, the low temperature spectra show more peaks just above threshold but with low intensity, and only at high currents, more dense and stronger peaks appear. The high

current lasing peaks are distributed symmetrically around the narrow range lasing peak of the low current spectra, indicating that the gain increases steadily at both directions with current. It is noted that at both temperatures, the integrated lasing power is apparently much lower than the integrated power of spontaneous emission. This is consistent with the low slope efficiency of the L-I curves.

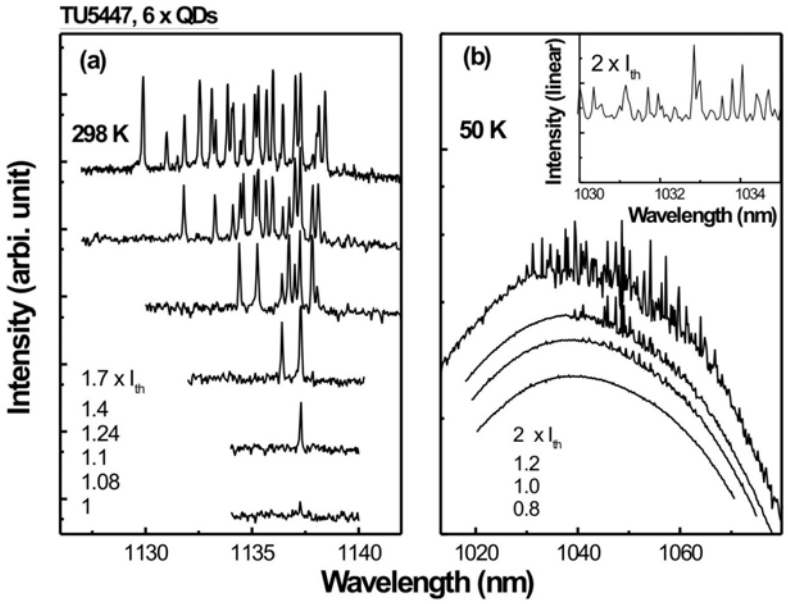

Fig. 6-9 Lasing spectra of the four-sided QD laser. In (a) the spectra are offset for clarity.

The evolution of lasing spectra with current is shown in Fig. 6-9. At RT, sharp and strong peaks appear consecutively with current, and the spectra become broad at high currents. The latter reflects the broadband characteristics of QD gains. At low temperature, as in Fig. 6-9b, the lasing peaks are scattered in a wide range and generally low in intensity. This reflects the reduced homogeneous broadening and the broadened gain spectrum. The spectral hole burning effect due to the finite homogeneous linewidth at RT actually induces lasing at a single sharp peak with a resolution-limited linewidth (~ 0.1 nm). This is rarely achievable in the Fabry-Perot QD laser because the spatial hole burning effect induces multi-longitudinal-mode lasing, but in the four-sided laser, the emitting leaky modes are actually traveling wave modes, so they are free from the interference effect of spatial hole burning effect.

It is recognizable that, in Fig. 6-9b, the background level of these small lasing peaks is slightly reduced and shows corrugated structures, strongly suggesting that similarly scattered lasing peaks from the TIR modes are suppressing the gain around this wide spectral range, though the TIR lasing peaks are invisible to the outside. On the contrary,

the whole background level of spontaneous emission is continuously increasing with current. At low temperature this trend is slightly stronger than at RT. This shows clearly that the gain compression is stronger at RT, presumably due to the large homogeneous linewidth; but for all temperatures, the gain compression does not clamp completely the carrier density. The latter fact makes it possible for the leaky modes to lase. Normally for a traveling wave laser, the mode gain compression will clamp completely the carrier density, if without the nonlinear gain effect. However, in the four-sided lasers, the traveling wave modes are actually dispersed spatially, not like in the stripe geometry traveling wave lasers. This significantly reduces the gain compression effect. The QD gain adds to this reduction further, due to the weak spatial cross relaxation induced by the weakly linked carriers between spatially isolated QDs.

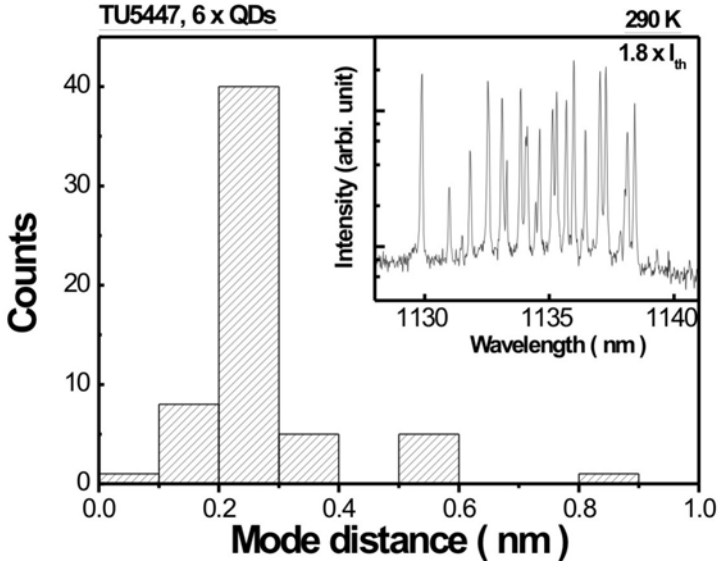

Fig. 6-10 Histogram of most-neighboring-mode distances for the lasing spectrum in the inset.

As shown in the inset of Fig. 6-9b, the lasing peaks always show discrete structure. This is further explored in Fig. 6-10 for the spectrum in the inset. The histogram shows that the interval between the most neighboring peaks has a major distribution around 0.25 nm, which is consistent with the mode distance of roundtrip resonance modes[11] for this four-sided laser cavity of edge dimension ~ 0.45 mm. In Fig. 6-11, more lasing spectra are shown for various lasers and temperatures. As in Fig. 6-11a, the lasing just above threshold is not necessarily single-mode, and there is mode competition as certain modes are turned on and off with current. We note that the four-sided QW lasers are also studied, and they share the similar L-I and spectral characteristics as those of QD lasers, except that the QW lasers show more intense mode competition. This can be attributed to the stronger spectral and spatial cross relaxation in the QWs that facilitates the gain suppression in the current

traveling wave laser. At low temperature, like in Fig. 6-11b, the mode competition is rarely seen, indicating reduced gain suppression.

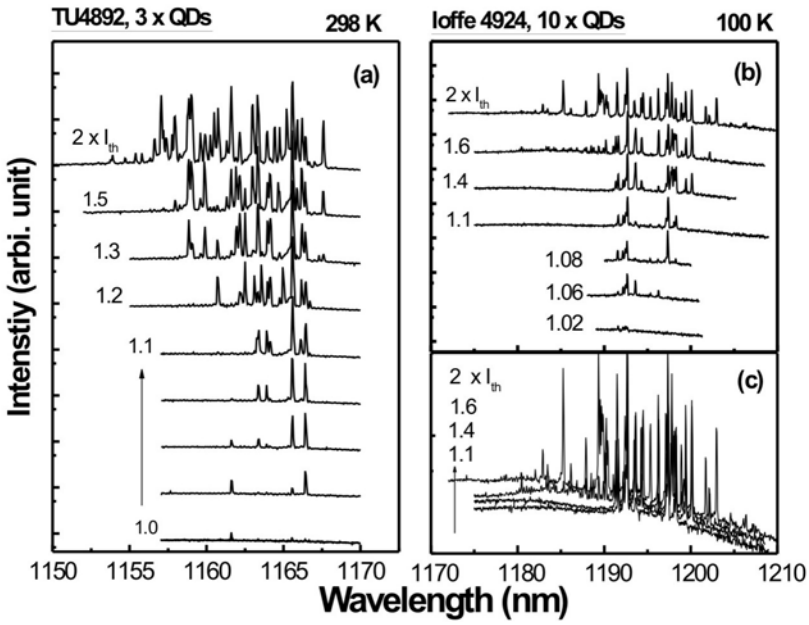

Fig. 6-11 Lasing spectra of other four-sided QD lasers. The spectra are offset for clarity, except in (c)

It is noted that, in all the shown lasing spectra of the four-sided lasers, it can be frequently observed that the discrete lasing peaks are somehow clustered, not confirming with the continual spectral profile of QD gain spectrum. This aspect is rather complicated issue. Here there is no apparent spectral modulation period such as those in Chapter 2, except the roundtrip resonance mode distance that is comparable to the longitudinal mode distance in the stripe geometry lasers. But we definitely cannot exclude the cavity effect. The four-sided cavity geometry can only complicate the cavity effect. The mode interaction is less known in this special cavity than in the Fabry-Perot lasers, due to the complex discrete ray dynamics. The hidden TIR modes inside the cavity make the experimental study of them almost impossible. A further study may be done with reduced cavity dimension so that the resonance mode distance can be tuned. Near field optical study of TIR lasing modes is also important.

Finally, it is emphasized that the abovementioned lasing characteristics are not limited to specific QD systems, indicating that they are characteristic features of the four-sided laser. In general, the four-sided lasers based on 1.3 μm InAs QDs show similar L-I and spectral characteristics. But there are also certain peculiarity pertaining to the gain media. For example, in Fig. 6-11c, we plot together the 100 K lasing spectra of the 10-fold 1.3 μm QD laser to compare their background levels. At the high energy side, it can be seen that the

background level shows abnormal change with current. This can be related to the gain inhomogeneity due to the carrier transport effect pertaining to the multi-stacked QDs, as explored in Chapter 5. Possible dynamics underlying this anomalous effect may be investigated in the future to find the peculiarity affected by the laser cavity.

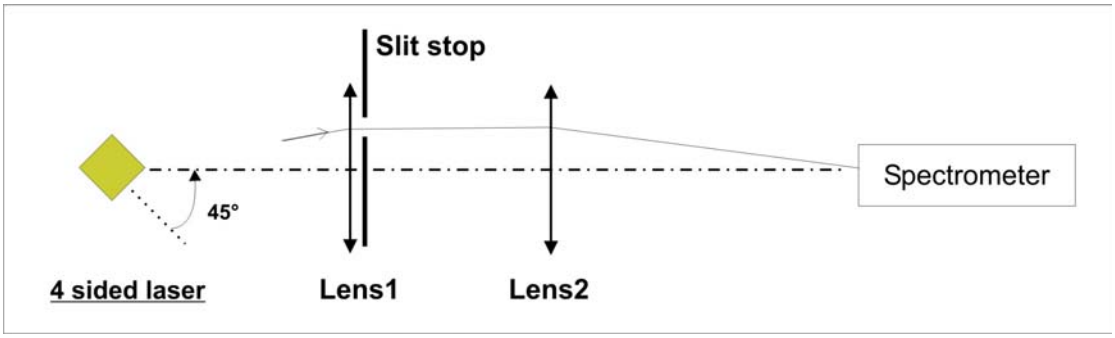

Fig. 6-12 Far-field-resolved spectrum measurement setup. The slit stop is moved in vertical direction.

6.4 Far-field-resolved emission spectra

In this section we first study the far-field-resolved emission spectra of the four-sided lasers. Then the corner diffraction effect is proposed as a selection mechanism for the azimuthal modes in the near-square-shaped laser cavity. A ray optical analysis is done to test the proposal.

6.4.1 Experiments

To measure the far-field-resolved emission spectra of four-sided lasers along the junction plane, we use the experimental setup as shown in Fig. 6-12. The laser diode is fixed here, and the emitting facet is imaged to the slit of the spectrometer. The far field is resolved by using the narrow slit stop behind the first lens. The slit stop has an aperture width ~ 2 mm, equivalent to an angular resolution of ~ 2.8° in the current setup. With the laser cavity fixed at 45° to the optical axis, we can measure an angular range about ± 17° around the optical axis, which corresponds to the far field angles in between ~ 28° to 60°.

As known from the previous lasing spectra of the four-sided lasers, the discrete lasing peaks are resolution limited and have low integrated intensity compared to the spontaneous emission background. Therefore it is necessary to use the highest spectral resolution (~ 0.1 nm) to resolve them from the background. That means a narrow slit width ~ 10 μm needs be set for the current spectrometer (BM50 0.5 meter). Such a narrow slit cannot tolerate any sizable transverse movement of the image of the emitting laser facets. The advantage of the setup in Fig. 6-12 lies in that it avoids the movement of laser

diodes, so the uncertainty in mechanical movement of image is eliminated. The angularly resolved spectrum is obtained by measuring the spectrum with the slit stop scanned in the direction parallel to the junction plane of the laser diode. For every azimuthal angle, the spectrum would include the emission from the two facets.

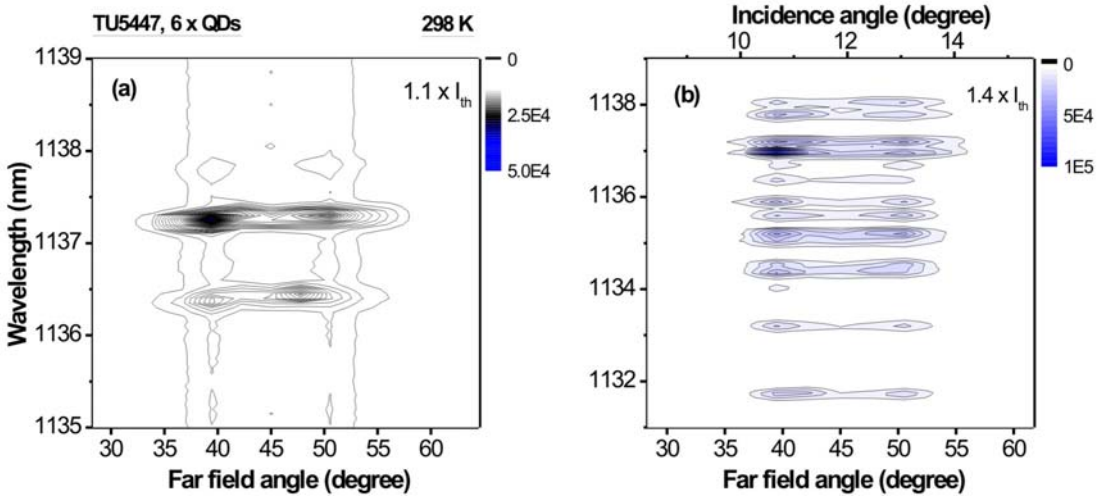

Fig. 6-13 Far-field-resolved lasing spectra of the four-sided QD laser at various currents.

6.4.2 Results

The angularly integrated spectra are already shown in Fig. 6-9a. Here we present the angularly resolved spectra for the same device.

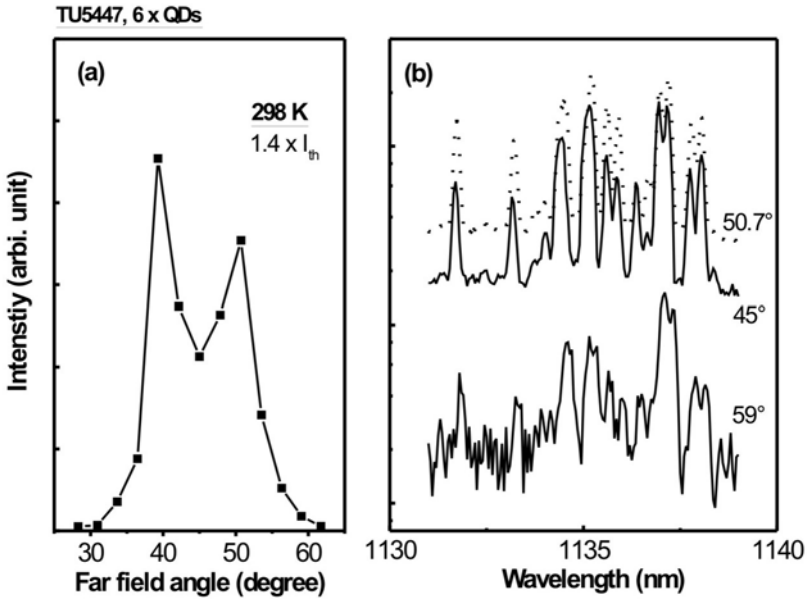

Fig. 6-14 (a) Far field profile obtained by spectrally integrating the spectrum in Fig. 6-13b. (b) The spectra at various far field angles.

The lasing spectra are shown in Fig. 6-13 for different currents. The contour plots are centered around 45°. The lasing spectral modes generally show double-lobed non-

symmetrical profiles. In Fig. 6-13a, at 1.1 x I_{th}, there are only two spectral peaks that have concentrated angular dependence. At 1.4 x I_{th}, more spectral peaks appear as in Fig. 6-12b, but the angular dependence is not so much different from the former one. Most peaks concentrate near two azimuthal angles, and the peaks near 40° are apparently stronger than those near 50°. As mentioned before, the emission from both the front laser facets contribute to the spectrum at each azimuthal angle, thus the current non-symmetrical angular profiles indicate that at least there exists certain difference in the angular dependence between the two facets. The spectra in Fig. 6-13b are integrated to get the far field profile, as shown in Fig. 6-14a. The big dip near 45° is evident in the far field profile, which indicates that there is also strong angular dependence in the far field profile from each single facet, at least within ± 10° around 45°. The angularly resolved spectra at three azimuthal angles are compared in Fig. 6-14b. The spectral mode structures are rather similar for all angles. This suggests that the azimuthal mode structure in the far field profile could be related to the geometry factor.

6.4.3 Discussion

At first, it is interesting to compare the present far field profile in Fig. 6-14a with those in Section 6.2.2. The previous far field profiles are measured without spectral filtering, so they integrate all the spontaneous emission output, whereas the present far field profile only integrates the very limited part of the spectrum where there are lasing peaks. As the lasing power is comparable to or even lower than the integrated spontaneous emission, the far field profile without spectral filtering would just smear out the impact of lasing action. With spectral filtering, most part of spontaneous emission is screened out, so the structures in the far field profile as brought about by the laser action can be revealed. In this aspect, the spectrally resolved far field measurement is critical for the study of lasing azimuthal modes in the four-sided lasers.

Secondly, from the nonsymmetrical far field profile in Fig. 6-14a, it can be inferred that the far field profiles of the two neighboring facets are different, and both could have sharp features. The two facets are different in nothing except their edge dimensions, as reflected in the device dimension, 0.42 x 0.48 mm^2. By denoting the cavity dimension as L x L´, and L´= L x (1 - δ), then the *rectangular level* δ of this near square laser cavity is ~ 0.125, with L = 0.48 mm. If considering the single-facet far field profile like in Fig. 6-6b, it is hardly possible to understand the present far field profile featuring a sharp selection of lasing azimuthal modes. Then the question is: what kind of mechanism can be responsible for

the sharp selection of azimuthal modes? Does it have any relation to the current edge size difference of 12.5 %? In the next, we try to answer this question.

6.4.4 Corner diffraction effect in near-square-shaped cavity

In the following, we examine the corner diffraction effect as the possible selection mechanism for the azimuthal modes. As the above experimental results suggest that the geometry factor of the laser cavity could be important for the azimuthal mode selection, we first analyze the loss mechanisms associated with the cavity geometry.

The selection of the far field azimuthal modes is equivalent to the selection of the corresponding leaky modes inside cavity. For the leaky modes, the mirror loss is one of the mode loss mechanisms that differ for different azimuthal modes. The roundtrip mirror losses for modes with different azimuth angles can be calculated for the square cavity in a similar way as for the Fabry-Perot lasers. As shown in Fig. 6-3, the mirror loss is a continuous function of incidence angles in the angular region of interest, which is below 17° here. Apparently the mirror loss solely cannot select the azimuthal modes in a sharp angular region. In the laser cavity, the internal loss and scattering loss are both distributed losses and should be no difference for different azimuthal modes, so they can be excluded. The only left loss mechanism then is the *corner diffraction*. As illustrated in Fig. 6-15, when the ray traces run into the very corners of the cavity, they will be diffracted, and the ray intensity will be damped instantly. If the mode can travel for a long time (compared with its lifetime) without running into the corners, then it will be advantageous in the competition with other leaky modes in contributing to the far field emission. Compared to other loss mechanisms, the corner diffraction is different in that it is related to the singularity points of the laser cavity, so the azimuth angles of the modes actually matter. This suggests the corner diffraction can be the potential mechanism for the azimuthal mode selection. For different azimuth angles, the probability of corner diffraction before a certain number of roundtrips can be calculated as follows.

We do ray tracing in the near square cavity for the incidence angles that correspond to the leaky modes. As in Fig. 6-15, the starting points for ray tracing are sampled uniformly from the left side of cavity. For each angle, one run of ray tracing is initiated for each of the starting points. The roundtrip number before the ray trace meets the corner is registered for each run of ray tracing. In this way, a statistical distribution of the roundtrip number can be found for each angle. We can set a *threshold roundtrip number*, and count the above

threshold probability as the *mode survival probability*, which means the probability of the specific azimuthal modes surviving the corner diffraction before the threshold roundtrip number.

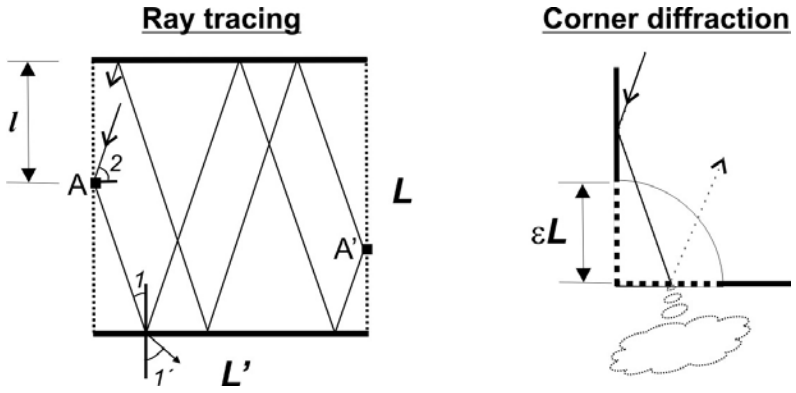

Fig. 6-15 Ray tracing schematics and corner diffraction effect.

In the ray tracing, we take advantage of the symmetrical property of the near square cavity. The ray tracing can be done easily by the mapping method. As in Fig. 6-15, one roundtrip can be, for example, from point A to point A´ and from A´ back to the left side. For each angle, one look-up table for the mapping can be generated at first, and the following ray tracing is equivalent to looking up in the table for the consecutive mapping points.

In the following we first analyze the calculated angular dependence of mode survival probability, and compare the result based on the actual cavity dimension with the experimental angular dependence of the emission spectrum.

Before the ray tracing, we need define some parameters. The *rectangular level* δ has been defined before as $L' = L \times (1-\delta)$ for the cavity dimension $L \times L'$. The actual laser has $\delta \sim 0.125$ with $L = 0.48$ mm. In addition to the rectangular level, another critical parameter is the *tolerance* ε for the corner diffraction, that is, the corner diffracts the ray only if the ray hits on a point within εL from the corner apex, as illustrated in Fig. 6-15. The corner diffraction is basically a wave optic effect, so the characteristic dimension should approach the wavelength inside cavity. In the present cavity, the tolerance ε can be approximated by $\lambda/(n_{eff}L)$, i.e. ~ 0.002. In practice, we found that a maximum roundtrip number of 10^4 is enough, because after this number, almost no modes can survive from the corner diffraction. The threshold roundtrip number is chosen to show more or fewer survived modes. In the following, the mode survival probability is first calculated as a function of

the incidence angle and for the different laser facets, and these results are converted to the far field profile.

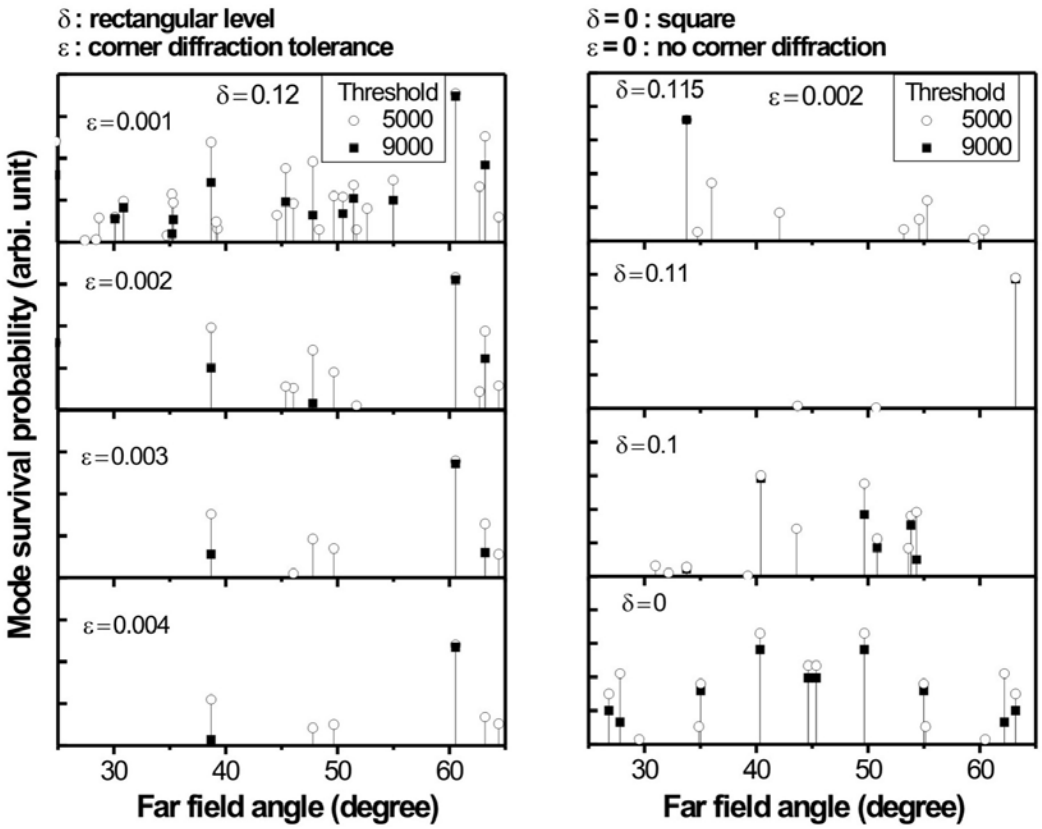

Fig. 6-16 Mode survival probability at various rectangular levels and tolerances for corner diffraction.

The typical calculation results are shown in Fig. 6-16 With increasing corner diffraction tolerance ε, the number of survived azimuthal modes decreases dramatically, and finally only a few of widely separated modes survive. This indicates that the corner diffraction can actually select the azimuthal modes. Apparently high threshold roundtrip number leads to high mode selectivity. In Fig. 6-16, with increasing threshold, the mode survival probability is reduced, and only those most long-lived modes can survive with finite probability. In the four-sided lasers, the threshold roundtrip number may be related to the available gain level. With a lower gain level, a mode is required to have higher survival probability in order to reduce the corner diffraction loss to match the gain for laser action. As discussed before, in the four-sided lasers, the emitting lasing modes have rather low gain margin as pinned by the non-emitting TIR lasing modes inside cavity, thus it is expected that the corner diffraction effect will lead to a strong selection of the azimuthal modes. It can be seen that in Fig. 6-16, for a rectangular level $\delta = 0.12$, the calculated far field profiles for the tolerance $\varepsilon \geq 0.002$ are rather similar, and in good agreement with the experimental far

field profile in Fig. 6-14a. The used rectangular level value is within the error range of the device dimensions, which amounts to ± 10 μm for a length of 0.48 mm.

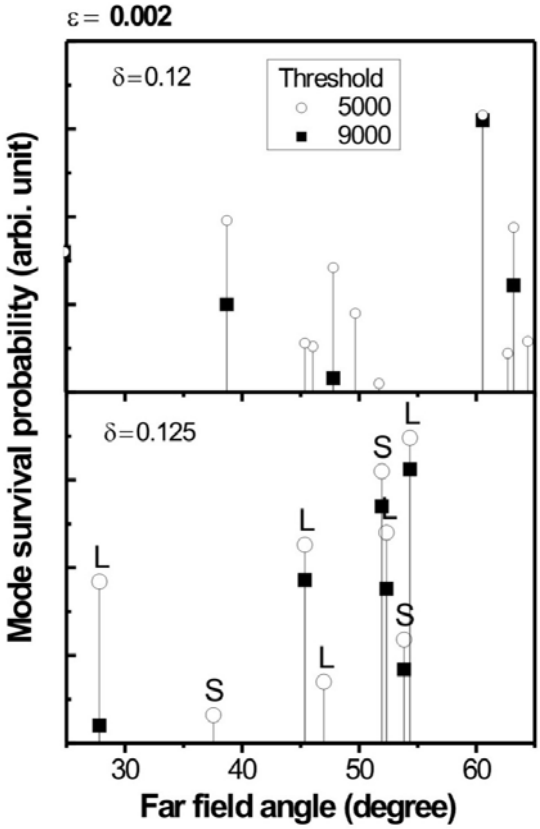

Fig. 6-17 Continued from Fig. 6-16.

In the near-square-shaped laser cavity, the discrete ray dynamics is not affected by the scaling of the cavity dimension, but it can be rather sensitive to the cavity shape variations, and this could have great impact on the far field profile. In Fig. 6-16, for a typical corner diffraction tolerance $\varepsilon = 0.002$, the calculated far field profiles for various rectangular levels are shown. We can see a symmetrical profile for the exact square cavity ($\delta = 0$), but with the introduction of rectangular deviation, i.e. the rectangular level $\delta \neq 0$, the symmetry about 45° is broken, and the far field profiles originating from the different facets are quite different. The very sensitivity to the rectangular level is shown by the totally different far field profiles for $\delta = 0.1$ and 0.11. An increase of δ to 0.115 leads to another different profile. This behavior reminds of chaotic one. In Fig. 6-17, further increase of rectangular levels leads to still different profiles, indicating that a large parameter change also result in unpredictable behaviors. For $\delta = 0.125$, the azimuthal modes emitted from both the long (L) and short (S) cavity sides are labeled respectively to indicate their origins. The non-

symmetry is evident in both the single-facet profiles and the total profile. The symmetry breaking occurs for all $\delta \neq 0$ cases.

The above calculation results give us a good appreciation of the strong azimuthal mode selection effect by the corner diffractions in the four-sided lasers. This is characteristic of the discrete ray dynamics in the near-square-shaped cavities. It is believed that this discrete dynamics could not only lead to a selectivity for spatial modes, but also a strong discrimination for spectral modes, as evidenced by the varied lasing spectra of the four-sided QD lasers. For such spectral mode discrimination, both factors, cavity geometry and gain, i.e. the passive and active cavity properties, need be considered. Ideally, there are always a group of spectral modes belonging to each selected azimuthal mode. These spectral modes can scatter with each other and compete for the distributed gain, thus they will be dispersed in the cavity space to avoid the full overlap of ray trajectories. As these different ray trajectories have different corner diffraction losses, the associated spectral modes then could be discriminated due to their different losses. However, the mode scattering and competition is not limited to the spectral modes within one spatial azimuthal mode. The spectral modes from different azimuthal modes can scatter each other as well because they need share gain and carriers in the overlapped ray path region. The scattering probability of each spectral mode is bound to the cavity gain distribution, cavity geometry and its discrete ray dynamics. The internal TIR lasing modes are in the same situation except that they are dark to the outside. When the gain is limited, these mode scattering effects can be critical in determining the fate of most spectral modes. The resulting strong spectral mode discrimination is evidenced in the discrete single-mode or few-mode lasing spectra just above threshold. With current, more spectral modes begin to lase for the available gain. The mode scattering can help rearrange the mode gain, thus we can see that certain spectral modes are turned on or off frequently with current. The more significant spectral mode competition in the four-sided QW lasers than in the QD ones shows that the gain suppression through spectral hole burning effect is a crucial mode interaction mechanism. At high current, the mode interaction helps distribute the gain rather evenly among the spectral modes. This is reflected in the converging mode distance and mode intensity with current. The fluctuation of mode intensity can be related to the statistic properties of the mode scattering processes.

6.5 Summary

In this chapter, we investigated the emission properties of the four-sided lasers for the first time. The spectrally integrated far field profiles are measured in both fast and slow axis. The fast axis profile is similar to that of the usual stripe geometry lasers. But the slow axis profile from the single facet shows much broad far field width (~ 90°), due to the loose mode confinement in the junction plane. From the slow axis profile it can be inferred that the angular distribution of the spontaneous emission intensity inside the cavity is not isotropic, but rather concentrates near the facet normal. The laser action has almost no impact on the far field profile, due to the weak integrated intensity of the lasing modes compared to that of the background spontaneous emission.

The L-I characteristics of the four-sided lasers show distinct turning points at the threshold, but the output slope efficiency of the laser action is comparable to or even lower than that of spontaneous emission, indicating that the major part of the injection current is consumed by the high-Q TIR lasing modes, which, though, are totally confined inside the cavity and make no contribution to the far field emission. The lasing spectra show continuously increasing *true spontaneous emission* background with current, indicating that the gain and carrier density is not completely clamped by the laser action. The spatial hole burning effect of the TIR modes with closed orbits and the insufficient gain compression provide gain for the emitting leaky modes. The emitting leaky modes are rather weak in intensity for their higher loss than that of TIR modes, and the lasing spectra show sharp and discrete spectral mode structures. The far-field-resolved lasing spectra are measured, and through spectral filtering, large part of the spontaneous emission is screened out, that helps reveal distinct spectral and azimuthal mode structure. The observed strong selection of azimuthal modes in the four-sided laser is attributed to the corner diffraction effect. Taking account of the corner diffraction effect, the ray tracing calculation result is in good agreement with the experimental far field profile. In the end, we discuss the discrete ray dynamics characteristic of the four-sided laser cavity. The mode scattering and gain suppression are identified as important mechanisms for the spectral mode discrimination in the four-sided laser.

Reference:

[1] T. Harayama, P. Davis, and K. S. Ikeda, Phys. Rev. Lett. **90,** 063901 (2003).

[2] J. U. Nöckel and A. D. Stone, Nature **385,** 45 (1997).

[3] R. K. Chang and A. J. Campillo, *Optical Processes in Microcavities* (World Scientific, Singapore, 1996).

[4] H.-J. Moon, Y.-T. Chough, and K. An, Phys. Rev. Lett. **85,** 3161 (2000).
[5] J. Wiersig, Phys. Rev. A **67,** 023807 (2003).
[6] S. V. Boriskina, T. M. Benson, P. Sewell, and A. I. Nosich, Optical and Quantum Electronics **35,** 545-559 (2003).
[7] M. Lohmeyer, Optical and Quantum Electronics **34,** 541-557 (2002).
[8] D. Rafizadeh, J. P. Zhang, S. C. Hagness, A. Taflove, K. A. Stair, S. T. Ho, and R. C. Tiberio, Opt. Lett. **22,** 1244 (1997).
[9] W. P. Reinhardt, in *Mathematical analysis of physical systems*, edited by R. E. Mickens (VanNostrand Reinhold, New York, 1985).
[10] C. Gmachl, F. Capasso, E. E. Narimanov, J. U. Nöckel, A. D. Stone, J. Faist, D. L. Sivco, and A. Y. Cho, Science **280,** 1556-1564 (1998).
[11] A. W. Poon, F. Courvoisier, and R. K. Chang, Opt. Lett. **26,** 632 (2001).
[12] F. de Fornel, *Evanescent Waves* (Springer-Verlag, Berlin, 2001).
[13] K. F. Huang, Y. F. Chen, H. C. Lai, and Y. P. Lan, Phys. Rev. Lett. **89,** 224102 (2002).
[14] Y. F. Chen, K. F. Huang, and Y. P. Lan, Phys. Rev. E **66,** 046215 (2002).
[15] J. Lekner, *Theory of Reflection* (Martinus Nijhoff Publishers, Dordrecht, 1987).

ACKNOWLEDGEMENT

1. I would like to thank Prof. Dr. D. Bimberg for his hospitality in my stay in Berlin. His continuous support and encouragement are invaluable and make the study pleasant and stimulating. I appreciate the freedom in research and enjoy the adventure that is indispensable for the maturity in the scientific research. His excellence in both research and management makes the workgroup excel as well.

2. I would like to thank Prof. Dr. N. N. Ledentsov for his support and expertise. Many discussions and advices provide insights and broaden the perspective. It is a pleasant experience to work with him together.

3. I would like to thank Prof. Dr. D. Zimmermann for his understanding and I am happy to have him chair the examination.

4. I would like to thank Priv. Doz. Dr. R. Heitz for his valuable contributions to the work. His fine expertise in experimental physics and specifically spectroscopy is indispensable for the lab operation. I would like also to thank Prof. Dr. M. Grundmann for the stimulating discussions, and critical help with experiments. Particularly I would emphasize the contributions from Dipl. Phys. S. Bognar. For many years his cooperation lays down the stepping-stone towards the possible scientific output.

5. I would like to thank all the other members of this workgroup for their readiness in lending their help to me. I always feel they are at hand and sometimes forget they are also busy with their own tasks. I dare to name you by all because it is a good feeling for us to be or have been in one workgroup, if not because I may fail anyone miserably. Anyway it is my pleasure to keep you busy. I would like also to thank the visiting members from Ioffe institute, Russia, for their generous sharing of experience and expertise, and particularly they are also representatives of the new generation of Russian scientists.

6. I would like to thank Herr W. Kaczmarek and his team in mechanical workshop. Both their skills and warm hearts inspire us in love of work and life. I believe their

fundamental works are the combination of exactness and art, but their intuitive designs make every article a masterpiece. I would like also to thank many other TU personnel who are willing to help me in many ways and for many years. I particular appreciate the friendship relation between TU Berlin and many institutions in China.

7. I would like to thank Dr. P. Borri and her colleagues for their crucial contributions to the QD dynamics.

8. I would like to thank Dr. E. A. Viktorov and Prof. P. Mandel for their genuine cooperation and help.

9. I would like to thank Prof. Lide Zhang and Prof. Chimei Mo for their candid recommendation and advices. The financial support from Volkswagen Stiftung and DAAD is greatly appreciated. I am grateful for the assistance of the personnel from both institutions and their representatives in TU Berlin.

10. I would like to thank my family and friends for their tolerance.

BIOGRAPHY

Birth:

26. 12. 1970, *Dong Zhi County, Anhui Province, PR China*

Education:

- 9.1976 – 7.1981 *Gao Shan elementary school*
- 9.1981 – 7.1987 *Dong Zhi second high school*
- 9.1987 – 7.1992 *University of Science and Technology of China (USTC, Hefei), Department of Physics and Materaials Science and Engineerings (MSE),* Materials Physics (Bachelor of Science degree)
- 9.1992 – 7.1995 *USTC, MSE department,* Condensed Matter Physics (Master of Science degree)
- 9.1995 - 1996 *Institute of Solid State Physics (ISSP, Hefei), Academia Sinica, PR China,* Nanomaterials group (Doctorate candidate)
- 5.1997 *Goethe Institut Berlin*, *Germany*. Two step German courses
- 1998 - 2003 *Technische Universitaet Berlin, Germany. Institut fuer Festkoerperphysik, AG Prof. Bimberg,* Semiconductor QD lasers group, partly funded by Volkswagen Stiftung and DAAD Fellowship (Dr. rer. nat.)